Frontispiece

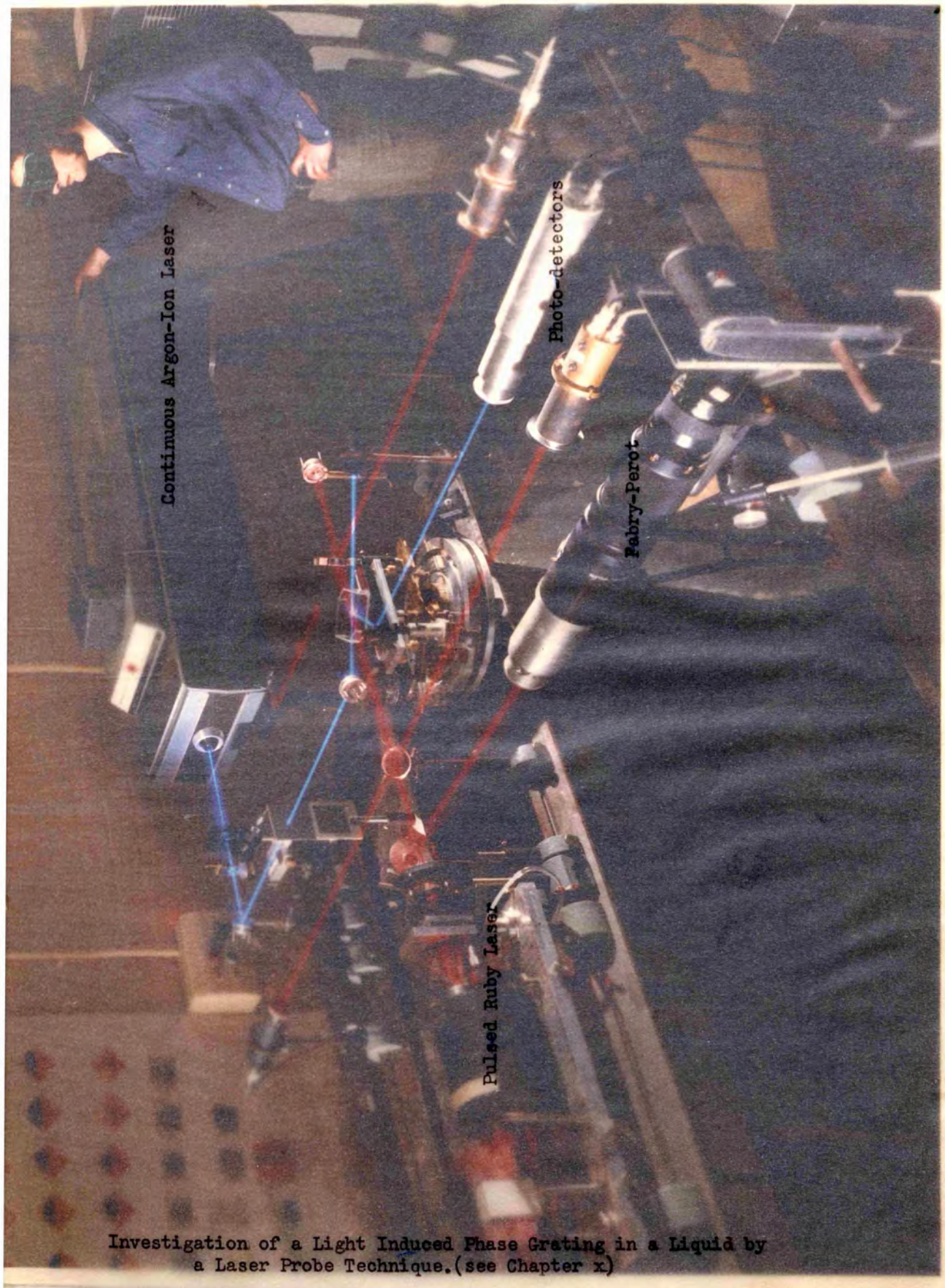

Investigation of a Light Induced Phase Grating in a Liquid by a Laser Probe Technique.(see Chapter x)

Nil Desperandum

NON-LINEAR OPTICAL EFFECTS IN LIQUIDS

by

ROBERT GRAHAM HARRISON

Thesis presented for the
Degree of Doctor of Philosophy
in the University of London

July, 1970

Department of Physics,
Royal Holloway College

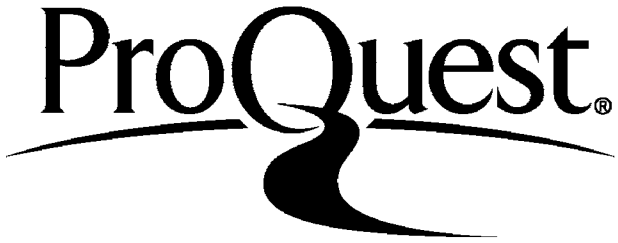

A B S T R A C T

Recent advances in the field of non-linear optical phenomena are reviewed in which particular reference is made to those effects induced within liquid media.

Several aspects of this field of study were experimentally investigated. In particular, direct quantitative examinations were made of the intensity dependent refractive index modulations (associated with the phenomena of stimulated light scattering) induced in both absorbing and non-absorbing liquids by the intense light fields from a pulsed ruby laser. A probe technique, which facilitated both spatial and temporal analyses of this induced non-linearity, was developed, in which the output from a continuous argon ion laser was Bragg reflected off the induced structure within the liquid. The experimental and theoretical results are shown to be consistent and values for the thermal relaxation time of liquids are determined.

Qualitative aspects of the non-linear phenomena of self trapping and de-focusing of laser light are considered with particular emphasis placed on the effects of self-bending and the interaction of self-trapped light beams.

Studies were conducted into the effect of intense laser light on saturable absorbers. The intensity dependent blue fluorescence observed from these absorbers when excited by ruby laser light resulted from excited state absorption to the second singlet state. The intensity dependence also indicated the power density required to saturate the first excited singlet state for each dye. A similar fluorescence due to two photon absorption was observed in certain solvents.

The residual population inversion characteristics of ruby were examined using a stimulated light scattering feedback technique. The results of these investigations are shown to be in qualitative agreement with current theories.

C O N T E N T S

C O N T E N T S

C O N T E N T S
(continued)

C O N T E N T S
(continued)

CHAPTER I

GENERAL INTRODUCTION TO NON-LINEAR OPTICS

It is the purpose of this thesis to study some of the effects that high intensity radiation, emitted by a laser, may have on the optical properties of any system illuminated by it. The response of bulk material to the radiation emitted by conventional sources is linear in the sense that all effects can be adequately explained in terms of induced electric and magnetic polarizations which are proportional to the applied field. However, such a linear relationship is only a first order approximation of a more general relationship, which can be expressed as:

$$P = \chi_1 E + \chi_2 E^2 + \chi_3 E^3 , \qquad \ldots (1.1)$$

where the χ's may be complex, and are strictly tensor qualities as the polarization is not necessarily co-linear with the field.

The above series is generally rapidly convergent, but at sufficiently high electric fields the second and third order terms are not trivial. That lasers can produce fields of sufficient strength for these non-linear terms to be of significance is not surprising when it is realized that the electric field strength in the beam emerging from a ruby laser is at least two or three orders of magnitude greater than the field strength available from conventional sources.

Considered from a purely academic point of view, the uniqueness of many of these non-linear phenomena pose quite unexpected and at first sight, very puzzling problems. For example, a parallel beam of highly intense laser light focused in a liquid will propagate forward from this focal region as an extremely fine pencil of light, and in the backward direction there can be generated a highly intense light beam of shifted frequency from the incident light. In addition a density modulation is

induced in the liquid which oscillates at the difference frequency of the two light waves. For the propagation of high powered laser light through certain crystalline solids it is found that a certain proportion of the emergent light is frequency doubled with respect to the incident light frequency. Hence a quantity of red ruby laser light traversing the crystal will emerge as blue light. A final illustration of these phenomena is that of the de-focusing, an effect which induces a parallel beam of laser light propagating through an absorbing media to emerge as a divergent cone. These problems together with many others, will be discussed in detail in the subsequent chapters of this thesis.

The interest taken in such conundrums over the last few years has, of course not been solely that of scientific curiosity. Let us now briefly consider some of the reasons for, and uses derived from, the study of these phenomena.

Such non-linear effects can be generally classified into the following two groups:

(a) Interaction and self-action of light waves, and
(b) Stimulated scattering.

In classification (a) the non-linear effects are generally considered to take place without participation of the internal bulk motion of the medium. The interacting wave phenomenon in classification (a) include such effects as frequency doubling[1-4], mixing[5,6], and parametric amplification[7-10], all these effects involve waves having widely different frequencies. Such processes have been extensively investigated during the last nine years as they have great potential importance in providing a means of extending the frequency range in which intense monochromatic sources are available.

The phenomenon of 'self-action' includes such effects as self-focusing[11-15], and de-focusing of laser light[16,17]. In both these processes the high intensity laser light perturbs the refractive index of the medium through which it passes. Hence a phase change is induced across the laser beam profile which results in a convergence or divergence of the laser beam depending on whether there is an increase or a decrease of refractive index.

These two effects have also been the source of considerable interest and research recently as it is believed that it is precisely the self-action that determines the main feature of the behaviour of powerful light beams in material media[18,19]. The non-linear phenomenon of stimulated scattering (classification b), another effect arising from high power light fluxes, has, with the advent of the laser, attracted considerable attention[2,7,20-25]. It is now generally accepted that every spontaneous scattering should transform into a stimulated scattering at sufficiently high intensities of incident radiation. Thus spontaneous scattering processes such as Rayleigh wing, Brillouin and Raman scattering will each have an associated stimulated scattering effect providing the probe light fluxes are of sufficiently high intensity.

In each of these stimulated processes there is generated, at and above a critical incident laser intensity, an intense backward (and sometimes forward) scattered light wave which is, for the backward wave, usually shifted down in frequency (Stoke) and, for the forward wave, shifted up in frequency (anti-Stokes) with respect to the frequency of the incident exciting laser light. In the medium there is simultaneously generated another wave which is, for Rayleigh scattering thermal, for Brillouin scattering acoustic, and for Raman and Rayleigh wing scattering a wave produced by molecular oscillations and re-orientations.

These waves within the medium constitute a periodic polarization which enables coupling and modulation of other light components present. Such stimulated scattering processes have several markedly different characteristics from their spontaneous counterparts. For example, as has been previously stated, the stimulated processes give rise to extremely intense scattered light waves in contrast to the low power scattering achieved from the spontaneous effects. Also, for some stimulated scattering phenomena, the stimulated wave has a different frequency from the corresponding spontaneous scattered wave. Examples of the value of the study of such properties in the fields of laser development and solid and liquid state physics include:

(i) Stimulated Brillouin scattering (S.B.S.) facilitates high precision measurements of hypersonic velocities[26,27].

(ii) The use of S.B.S. as a passive Q-switch[28,29,32].

(iii) The study of transient relaxation effects in liquids in the time range of 10^{-7} - 10^{-12} secs[30,31,33,37].

A further very important reason for the study of such effects arises from the potentially serious problems imposed by stimulated light feedback in the laser amplifier system, resulting in a subsequent limitation of the maximum output power. To date most conventional laser systems have output powers below the threshold power required for stimulated scattering, so the problem is of no real significance. However, it can be foreseen that the future development of very high powered systems will be seriously limited by such processes.

An additional problem arising from these stimulated effects is that of laser amplifier damage caused by high pressure gradients arising from stimulated acoustic wave generation in the medium[34,35]. Two other non-linear effects attributed to high intensity light fields are those of multi-photon and excited state absorption.

In the process of multi-photon absorption[7,24,36] energy levels in a medium having energy gaps equal to multiples of an incident photon energy are directly excited by such photons from a highly intense laser beam. Two photon absorption[38-41], which is one type of multi-photon process, has been of great practical benefit in detecting picosecond laser light pulses.

The excited state absorption process[40,42,43] occurs as a result of the saturation of the first singlet state of a material by high intensity laser radiation excitation, of photon energy corresponding to the first singlet energy level. Subsequently, due to this saturation, the second singlet state is forced into a condition of excitation. Such a process has been used by the author to determine the laser light power thresholds at which saturation of various liquid dyes occur[40].

Of the many aspects of non-linear optics considered in this thesis significant attention will be given to the stimulated scattering processes. Consequently, to facilitate a better understanding of these effects, a brief survey will be given, (in the next Chapter) of their counterpart spontaneous scattering processes.

CHAPTER II

SPONTANEOUS SCATTERING

2.1 INTRODUCTION

In all liquids the spontaneous scattering spectrum can be considered to be made up of the Rayleigh triplet, i.e. Brillouin doublet together with an unshifted central component which has superimposed on itself a continuous depolarized spectrum which extends to 180 cm^{-1} (see Plate 3.1). In addition to these spectra there can exist additional contributions from other scattering processes such as Raman scattering. Each of these contributing affects will now be considered separately.

2.2 BRILLOUIN SCATTERING

This effect was first comprehensively considered by Brillouin in 1914[44]. His theory was based on the Einstein-Rayleigh theory of scattering from density fluctuations of elastic waves in a homogeneous medium[45], the elastic waves being of thermal origin. The change in mass density due to the elastic waves gives rise to a proportional variation in the dielectric constant of the medium. Thus the elastic waves effectively constitute a continuous spatial grating which provides a mechanism for Brillouin scattering. In this theory a doublet in the spectrum of the scattered light is predicted (see Plate 3.1). This doublet derives from Doppler shifts of frequency of the incident light when the light is reflected by the refractive index variations produced by the propagating elastic waves.

Classically, light reflected from the moving wave crest of one of the thermally induced sound waves at an angle θ experiences a Doppler frequency shift given by:

$$\Delta\nu = \pm 2\,\nu_i \left(v_p \frac{n}{c}\right) \sin\frac{\theta}{2} \quad \text{for} \quad v_p \ll c \,. \qquad \ldots\ (2.1)$$

The light is reflected from a succession of wave crests and these light rays interfere constructively at the observation point only if the path length traversed by each successive ray differs by a light wavelength. This puts a condition on the wavelength of the sound contributing to significant light scattering at a given angle θ .. This condition is:

$$\lambda_1 = 2\,\lambda_p \sin\frac{\theta}{2} \quad \text{or} \quad \nu_p = 2\nu_1\, v_p \frac{n}{c} \sin\frac{\theta}{2}\ , \qquad \ldots (2.2)$$

where v_p is the sound or phonon velocity, ν_p is its frequency, $\frac{c}{n}$ is the velocity of light in the medium, and ν_1 is the light frequency.

Comparison of equations (2.1) and (2.2) show that:

$$\Delta\nu = \pm\,\nu_p\ , \qquad \ldots (2.3)$$

that is, the difference in frequency between the incident and scattered light at an angle θ is precisely the frequency of the sound from which the light is scattered.

Quantum mechanically one envisages the interaction of an incident photon (energy $= h\nu_1$, momentum $= \hbar k_1$), a scattered photon ($h\nu_s$, $\hbar k_s$), and a phonon ($h\,\nu_p$, $\hbar k_p$). The phonon is either created or annihilated in the interaction. That is the incident photon splits into a scattered photon and a phonon or the incident photon combines with a phonon to produce the scattered photon.

Conservation of energy and momentum in the two cases yield:

$$\left.\begin{aligned} h\,\nu_1 &= h\,\nu_p + h\,\nu_s \\ \hbar\,k_1 &= \hbar\,k_p + \hbar\,k_s \end{aligned}\right\} \qquad \text{Creation} \qquad \ldots (2.4)$$

$$\left.\begin{aligned} h\,\nu_1 + h\,\nu_p &= h\,\nu_s \\ \hbar\,k_1 + \hbar\,k_p &= \hbar\,k_s \end{aligned}\right\} \qquad \text{Annihilation} \qquad \ldots (2.5)$$

The vector momentum equation (2.5) corresponds to equation (2.1) and the energy conservation equation corresponds to equation (2.2). Besides velocity, spontaneous Brillouin scattering yields another important acoustic parameter, the acoustic absorption α_p. Since the scattering

sound waves are decaying because of absorption, there will be an uncertainty in their frequency. This will be evidented as a broadening of the Brillouin line[46]. This line width is related to the absorption by:

$$\alpha_p = \frac{\Gamma_b}{v_p} , \qquad \ldots (2.6)$$

where Γ_b is the frequency halfwidth of the Brillouin component after the width of the exciting radiation has been taken into account.

2.3 CENTRAL RAYLEIGH SCATTERING

From the very beginning, workers investigating the Brillouin spectrum found, in addition to the Brillouin doublet components, a central or unshifted component in the spectrum of the scattered light. Landau and Placzek[47] proposed that the quasi-elastic scattering was produced by non-propagating density fluctuations, i.e. isobaric entropy fluctuations.

As stated previously, Brillouin had suggested that light is scattered by thermal sound waves. Because sound propagation is an adiabatic process, density fluctuations should be decomposed into pressure fluctuations at constant entropy and entropy fluctuations at constant pressure[48]. The pressure fluctuations at constant entropy produce the Brillouin scattering which has already been considered, and the light scattered by the fluctuations at constant pressure produce the central Rayleigh line. Although this line is unshifted in frequency it is broadened somewhat due to thermal dissipative processes which damp out these fluctuations.

2.4 RAYLEIGH WING SCATTERING

The Rayleigh wing spectrum, which is a continuous depolarized background spectrum to the Rayleigh triplet (see Plate 3.1) is considered to be due to anisotropic fluctuations in the liquid. First observations of the wing were made by E. Gross in 1930[49].

Recent treatises on this aspect of scattering[50-53] consider the capability of elastic (rather than viscous) resistance of liquids to shearing stress connected with temporary equilibrium positions of atoms. The concept was put forward by Frenkel in 1925[48].

In this theory the liquid atoms are considered to perform a large number of oscillations about some equilibrium position during a time τ, after which each atom of liquid can jump to a new equilibrium position. Thus during short time intervals, smaller than the lifetime of the atom or molecule τ_p in an equilibrium position, the motion of the molecules may be regarded as elastic vibrations. In terms of the frequency distribution of the wing, this corresponds to $\omega > 1/\tau_p$. Suppose that on average, during the time interval $t \sim \tau_p$, a transition of the molecule from one equilibrium position to another takes place. Then during intervals $t \gg \tau_p$, aggregates of these transitions may perhaps be regarded as rotational diffusion, neglecting for such intervals the small vibrations of the molecules between transitions. Again, in terms of the frequency distribution of the wing, this will correspond to $\omega \ll 1/\tau_p$.

The transition from the rotational process to the vibrational process must get closer to the unshifted line with an increase in the viscosity since τ_p here plays the role of the lifetime of the molecule in an equilibrium position and $\tau_p \propto \mu$. At very high viscosities the diffusion wing will contract towards the centre and there will be left only the wing of the elastic oscillations.

Recent experimental investigations[50-53] have confirmed these theories, and anisotropic and viscosity (vibrational) relaxation times have been determined. Typically, they are $\sim 10^{-12}$ secs for anisotropic relaxation and 10^{-14} secs for viscosity relaxation.

2.5 BRILLOUIN SCATTERING FROM SHEAR WAVES

Another contributing scattering effect can be produced from thermal shear waves which are considered to be derived from the thermal motion of anisotropic molecules. More specifically, this is a Brillouin type scattering off the transverse component of the translational motion of the molecules, the translational motion being accompanied by an angular motion of the molecule. The transverse component has a frequency in the hypersonic range (10^{10} c.p.s.) and so in liquids will be strongly damped since this frequency is of the order of the relaxation time of the liquid.

The scattering effect, which is depolarised, has been recently discovered and subsequently investigated using the continuous output from gas lasers as a source of excitation[54-56]. Such investigations should yield values of the transverse sound velocity, the high frequency shear modulus and the shear relaxation times for liquids.

2.6 RAMAN SCATTERING

In 1928 a new form of scattering was discovered by Raman[57,58]. This scattering consisted of a series of discrete frequency components shifted from the incident radiation frequency. The shifts were so great that it was impossible to explain them as the modulation of scattered light by thermal elastic waves (see Plate 3.1). Classically the Raman effect is explained as a result of the interaction of the polarization induced by the incident light with the internal motion of the molecules. Both rotational and vibrational motions should be considered. In the case of rotation, the polarizability of the molecule may be dependent on the orientation of the molecule with respect to the incident wave; in the case of vibration, the polarizability may be a function of the intermolecular distance. These molecular motions are slow compared with the variation of the electromagnetic vectors in the optical region.

The modulation of the polarization p at the rate ν_i of the molecular motions causes the generation of radiation at frequencies $\nu_p \pm \nu_i$, where ν_p is the frequency of the incident radiation. Thus Raman lines are produced when the molecular vibrations change the polarizability of the molecules.

Quantum mechanically the Raman process can be depicted as shown in the energy diagram .

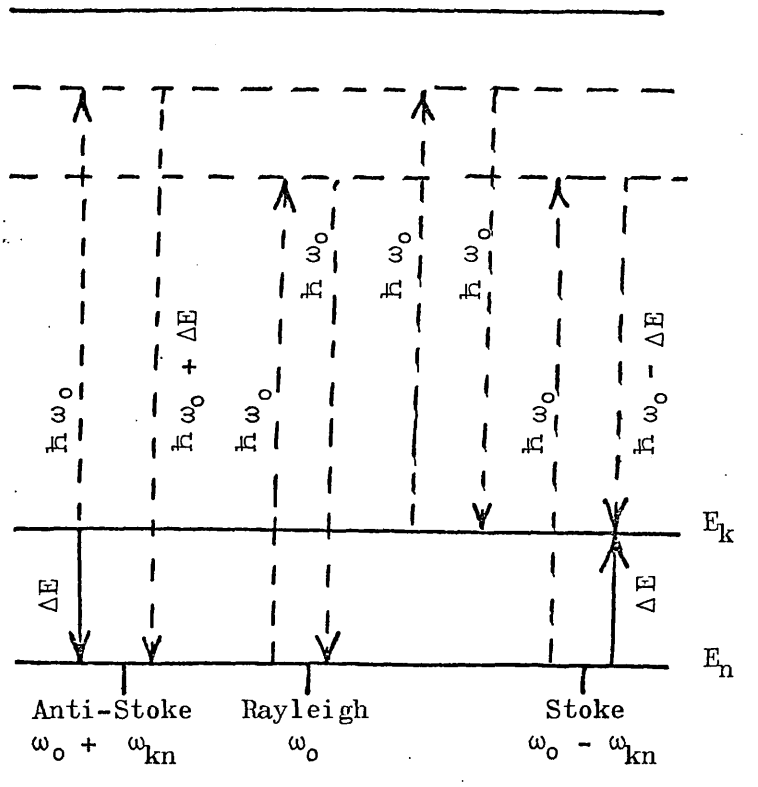

When a light quantum frequency ω_o and energy $\hbar\omega_o$ interacts with a molecule in its ground state n, or in any of its excited states (stationary states k) the energy of the system is increased to $\hbar\omega_o + E_n$ or $\hbar\omega_o + E_k$. If the molecule does not possess a stationary state with the energy, the light quantum will be instantaneously scattered in any direction and the molecule either returns to its original state or goes to a different state. (By a stationary state is meant a state with the energy $\hbar\omega_o + E_n$ or $\hbar\omega_o + E_k$, in which the incident light quantum is absorbed, raising the molecule to the excited state from which some time later a quantum can re-emit. This process is called fluorescence.) If the molecule returns to its original state, no energy has been taken from the light quantum and no energy has been given to it. Therefore the frequency of the quantum remains

unchanged and we have Rayleigh scattering. If the molecule goes over to another stationary state, it has either taken energy from the light quantum or given up part of its energy and the frequency of the light quantum is changed. As a consequence the frequencies $\omega_o - \omega_{nk}$ and $\omega_o + \omega_{nk}$ appear in the scattered light and we have the Raman effect. A recent extremely comprehensive review of this effect has been published by Loudon[59].

CHAPTER III

THEORETICAL REVIEW OF NON-LINEAR OPTICS

3.1 INTRODUCTION

If a dielectric medium is subjected to an optical electric field E which is small, it sets up a polarization in the medium that is linear in the field:

$$P = \chi_1 E \, . \qquad \ldots (3.1)$$

The relationship, however, is approximate and at high field strengths one considers the polarization expressed in the power series:

$$P = \chi_1 E + \chi_2 E^2 + \chi_3 E^3 \, , \qquad \ldots (3.2)$$

where the susceptibility tensors χ are complex.

The second order non-linear coefficient χ_2 exists for materials that possess no inversion symmetry[2,7,60], and leads to effects such as second harmonic generation, parametric process, i.e. generation of sum and difference frequencies, and optical rectification[1-8]. The third order susceptibility tensor χ_3 exists for materials possessing inversion symmetry[2,7,60], i.e. isotropic media such as liquids. The processes in liquids derived from this non-linearity will be the principal field of study in this thesis.

In the case of a lossless medium the susceptibility coefficients are real and in this case the primary non-linear effects are the generation of new frequency components, and the intensity dependent changes in the refractive index for the existing frequency components. For actual material systems the non-linear coefficients are complex, and it is this imaginary component of χ_3 that leads to stimulated Raman, Brillouin, Rayleigh and Rayleigh wing scattering, and to multi-photon, and excited state absorption of the light beam.

In general the non-linear polarization can arise in several ways, viz. electronic polarization, induced by forced anharmonic motion of the valence electrons in atoms by the electric field; electric field induced changes in the bulk properties of the material such as density and temperature changes; and finally field induced molecular re-orientation and redistribution for both isotopic and anisotropic molecules.

Consideration will first be given to effects arising from the electronic polarizability.

3.2 NON-LINEAR POLARIZATION DUE TO ELECTRIC FIELD-DEPENDENT ELECTRONIC POLARIZABILITY

This electronic polarizability may be understood from a consideration of the simple classical model of Lorentz for an anharmonically bound valence electron[23,60]. When an electric field is applied to the dielectric, the electron moves according to the equation of motion:

$$\frac{d^2r}{dt^2} + 2a\frac{dr}{dt} + \omega_o^2 r - br^2 - cr^3 = -\frac{e}{m}\cdot E \ , \qquad \ldots (3.3$$

where the notation in this equation and throughout this theoretical chapter are as defined in Section 3.19.

The solution of this equation for a time dependent electric field of the form $E = E(\omega)\, e^{-j\omega t} + E^*(\omega)\, e^{j\omega t}$ where $E(\omega) = A\, e^{jkz}$ is:

$$r = -\frac{e}{m} E(\omega) \frac{e^{-j\omega t}}{(\omega_o^2 - 2ja\omega - \omega^2)}$$

$$+ \frac{e^2}{m^3} bE^2(\omega) \frac{e^{-2j\omega t}}{(\omega_o^2 - 4ja\omega - 4\omega^2)(\omega_o^2 - 2ja\omega - \omega^2)^2}$$

$$+ \frac{e^2}{m^3} bE(\omega)\, E^*(\omega) \frac{1}{\omega_o^2\,(\omega_o^2 - 2ja\omega - \omega^2)(\omega_o^2 + 2ja\omega - \omega^2)} + \text{c.c.}$$

$$+ \ldots\ldots \text{(higher order terms)} \qquad \ldots (3.4)$$

Now the polarization density of the medium is generally given by:

$$P = Ner \ .$$

Thus the contributions to the induced polarization density proportional to the first and second powers of the electric field are:

$$P_1 = \chi_1(\omega)\ E(\omega)\ e^{-j\omega t} + c.c. \qquad \ldots (3.5)$$

where:

$$\chi_1(\omega) = \frac{Ne^2}{m}\ \frac{1}{(\omega_0^2 - 2ja\omega - \omega^2)} = \frac{Ne^2}{m} F(\omega)$$

$$P_2 = \chi_2(\omega,\omega)E^2(\omega)\ e^{-2j\omega t} + \chi_2(\omega,-\omega)\ E(\omega)\ E^*(\omega)\ , \qquad \ldots (3.6)$$

where $\chi_2(\omega,\omega)$ and $\chi_2(\omega,-\omega)$ are obtained from the general function

$$\chi_2(\omega_1\omega_2) = -\frac{N b e^3}{m^2} F(\omega_1)F(\omega_2)\ F(\omega_1 + \omega_2)\ ,$$

by setting $\omega_1 = \omega$ and $\omega_2 = \pm\ \omega$.

It can therefore be seen that a field oscillating at the single frequency ω can induce in the system a polarization having components oscillating not only at frequency ω but at frequencies 2ω, as well as one which is constant in time. These polarizations radiate to give rise to radiation field containing second harmonics of the applied field. If these calculations are carried forward to values of field higher than the second order, one will obtain higher harmonics of the fundamental frequency such as 3ω, 4ω stc.[20]. However, harmonics greater than 3ω have proved to be too weak to be observed.

From this discussion it is also implied that, if the original source field contains, instead of a single frequency, a whole series of frequencies then radiating fields of sum and difference frequencies will be generated. So in general for:

$$E = \sum_n E(\omega_n)\ e^{-j\omega_n t}\ ,$$

the sum being over all pairs of $\pm\ n$:

$$P_1 = \sum_n \chi_1(\omega_n)\, E(\omega_n)\, e^{-j\omega_n t} \qquad \ldots (3.7)$$

$$P_2 = \sum_{n,m} \chi_2\,(\omega_n,\omega_m)\, E(\omega_n)\, E(\omega_m)\, e^{-j(\omega_n+\omega_m)t}$$

$$P_3 = \sum_{n,m,\ell} \chi_3\,(\omega_n,\omega_m,\omega_e)\, E(\omega_n)\, E(\omega_m)\, E(\omega_e)\, e^{-j(\omega_n+\omega_m+\omega_e)t}\ ,$$

the sum over n, m and ℓ all running over the same required pairs of positive and negative values.

3.3 CONSERVATION OF ENERGY AND MOMENTUM - PHASE MATCHING

An important condition that governs the efficiency of many non-linear processes in a dielectric, arises from the optical dispersion of the medium.

Consider a three frequency interaction:

$$\omega_3 = \omega_2 + \omega_1 . \qquad \ldots (3.8)$$

Then this describes the energy conservation of the photons involved in the interaction, i.e.

$$\hbar\omega_3 = \hbar\omega_1 + \hbar\omega_2 \ .$$

Energy conservation is a well defined quantity in the sense implied by the uncertainty principle, i.e. $\Delta E \cdot \Delta t \gtrsim \hbar$. Δt is large so the uncertainty in the energy is small and so E must be conserved.

In a similar way, being particles, conservation of momentum of the photons must be considered. By de Broglies relation momentum $= \hbar k$ where k is the wave vector. Thus:

$$k_3 = k_2 + k_1 \qquad \ldots (3.9)$$

in as much as k is a well defined quantity in the sense of the uncertainty relation $\Delta(\hbar k)\, \Delta z \gtrsim \hbar$ where Δz is the uncertainty in position of the photon. As the photon location is somewhere within a block of dielectric many wavelengths thick, Δz must be large and so $\Delta k \ll k$.

Thus the wave vector is a well defined quantity and so the conservation equation (3.9) is satisfied.

The simultaneous satisfaction of equation (3.8) and (3.9) constitute what is called phase matching, and the coupling of these waves gives phase velocity, viz: $\frac{\omega_1}{k_1} = \frac{c}{n_1}$, etc., where c is the velocity of light and n_1 the refractive index of the dielectric at each frequency. In general, media are dispersive and the n's are not equal. It is this, that makes the simultaneous satisfaction of the energy and momention conservation rules so difficult. As example for second harmonic generation $\omega_3 = 2\omega$, $k_3 = k_{2\omega}$ and $\omega_1 = \omega_2 = \omega$; $k_1 = k_2 = k_\omega$. Thus equations (3.8) and (3.9) give the matching condition $2\omega/k_{2\omega} = \omega/k_\omega$, i.e. equal phase velocities at the primary frequency and at the second harmonic.

In the next section we will consider in general what effect a non-linear polarization in a medium will have on an electromagnetic wave travelling through that medium.

3.4 PROPAGATION OF E.M. WAVES IN A NON-LINEAR DIELECTRIC

The propagation of electromagnetic radiation in a dielectric material whose magnetic polarizability is negligible can be derived from, Maxwell's equations to be:

$$\text{curl curl } \underline{E} + \frac{1}{c^2} \frac{\partial^2}{\partial t^2} \underline{E} = -\frac{4\pi}{c^2} \frac{\partial^2}{\partial t^2} \cdot \underline{P} , \quad \ldots (3.10)$$

if $\underline{E}$ and $\underline{P}$ are now expressed in terms of their frequency components.

$$\underline{E} = \sum_n \underline{E}(\omega_n)\, e^{-j\omega_n t} \quad \text{and} \quad \underline{P} = \sum_n \underline{P}(\omega_n)\, e^{-j\omega_n t} \quad \ldots (3.11)$$

Equation (3.10) becomes for each component:

$$\text{curl curl } \underline{E}(\omega_n) - \frac{\omega_n^2}{c^2} E(\omega_n) = \frac{4\pi\omega_n^2}{c^2} \cdot \underline{P}(\omega_n) . \quad \ldots (3.12)$$

For a medium whose response is linear:

$$\underline{P}(\omega_n) = \underline{P}_1(\omega_n) = \underline{\chi}^{(1)}(\omega_n) \cdot \underline{E}(\omega_n) \ , \qquad \ldots (3.13)$$

equation (3.12) then becomes the familiar wave equation:

$$\text{curl curl } \underline{E}(\omega_n) - \frac{\omega_n}{c^2} \underline{\mathcal{E}}(\omega_n) \cdot \underline{E}(\omega_n) = 0 \ , \qquad \ldots (3.14)$$

where the dielectric tensor is defined as:

$$\underline{\mathcal{E}}\ (\omega_n) = \underline{1} + 4\pi\ \chi^{(1)}\ (\omega_n).$$

For a medium whose response is non-linear, the polarization field can be expressed as:

$$\underline{P}(\omega_n) = \underline{P}_1(\omega_n) + \underline{P}^{NL}(\omega_n) \ , \qquad \ldots (3.15)$$

where:

$$\underline{P}^{NL}(\omega_n) = \underline{P}_2(\omega_n) + \underline{P}_3(\omega_n) + \ldots$$

$\underline{P}^{NL}\ (\omega_n)$ is that part of the field which depends on the electric field in a non-linear fashion as described by equation (3.2). Equation (3.12) now becomes:

$$\text{curl curl } \underline{E}(\omega_n) - \frac{\omega_n^2}{c^2} \underline{\mathcal{E}}(\omega_n) \cdot \underline{E}(\omega_n) = \frac{4\pi\omega_n^2}{c^2} P^{NL}(\omega_n) \qquad \ldots (3.16)$$

which is the linear equation (3.14) with an additional source or driving term.

As the interactions in non-linear optics are very weak, giving rise to only small contributions, P^{NL} to the induced dipolar field, equation (3.16) can be solved by treating the non-linear term on the right hand side as a perturbation. Thus a solution may be expressed in the form:

$$E(\omega_n) = A_{\omega_n}(z) \cdot \underline{a}_{\omega_n}\ e^{jk_n z} \qquad \ldots (3.17)$$

where the amplitude factor $A_{\omega_n}(z)$ is regarded as a slowly varying function of z and $\underline{a}_{\omega_n}$ is a unit vector in the direction of the polarization of the wave. The solution of equation (3.16) is, for each component of field:

$$\frac{dA_{\omega_n}}{dz} = j\ \frac{2\pi\omega_n^2}{\kappa_n c^2} \cdot \underline{a}_{\omega_n} \cdot \underline{P}_{NL}(\omega_n)\ e^{-jk_n z} \ . \qquad \ldots (3.18)$$

This expression shows that the various field components E_{ω_n} are coupled together through the assumed dependence of $\underline{P}_{NL}(\omega_n)$ on the various field amplitudes.

3.5 NON-LINEAR POLARIZATION IN LIQUIDS

It has been stated earlier that the lowest order non-vanishing non-linearity in media with inversion symmetry is due to a polarization which is a cubic function of the electric field. Consider a polarization at the sum frequency created by the simultaneous presence of three electromagnetic waves with frequencies ω_1, ω_2 and ω_3 and wave vectors k_1, k_2 and k_3 respectively.

The non-linear polarization at frequency:

$$\omega_p = \omega_1 + \omega_2 + \omega_3$$

has a spatial distribution characterised by a wave vector:

$$k_p = k_1 + k_2 + k_3$$

and a component of it may be defined from equations (3.2), (3.7) and (3.11) as:

$$P_3(\omega_p) = \chi_3(\omega_1,\omega_2,\omega_3)\, E(\omega_1)\, E(\omega_2)\, E(\omega_3) \; . \qquad \ldots (3.19)$$

In practice P and E are strictly vectors and χ is a tensor. However, in an isotropic medium such as a liquid the physical principles of the various interactions to be considered here can be quite clearly demonstrated by considering scalars. In this way presentation is simplified considerably.

In the next two or three sections we will discuss some of the effects that arise from the third order polarization associated with electronic polarizability. The physical processes will be distinguished from one another according to the special relationship between the four frequencies, or whether the non-linear susceptibility is real or imaginary.

3.6 TWO-PHOTON ABSORPTION

Consider an electric field consisting of two frequencies ω_1 and ω_2. The electric field of each of these frequencies will be governed by the polarization that oscillate at each end of these frequencies. Hence, from equation (3.19):

$$P_{NL}(\omega_1) = \chi_3\ (\omega_2, -\omega_2, \omega_1)\ E(\omega_2)\ E^*(\omega_2)\ E(\omega_1) \qquad \ldots (3.20)$$

$$P_{NL}(\omega_2) = \chi_3\ (\omega_1, -\omega_1\ \omega_2)\ E(\omega_1)\ E^*(\omega_1)\ E(\omega_2)\ ,$$

since in general $E(\omega) = A\ e^{jkz}$ it follows:

$$P_{NL}(\omega_1) = \chi_3\ (\omega_2, -\omega_2, \omega_1)\ |A_2|^2 A_1\ e^{jk_1 z}\ ,$$

$$P_{NL}(\omega_2) = \chi_3\ (\omega_1, -\omega_1, \omega_2)\ |A_2|^2\ A_2\ e^{jk_2 z}\ . \qquad \ldots (3.21)$$

Since the polarizabilities are complex, they can be separated into real and imaginary parts. Due to the overall symmetry of the polarisabilities (treated as tensors) appearing in equation (3.21) their real parts are equal, as are the imaginary components at a resonance[7,23,63,64], i.e. $\omega_1 + \omega_2 \sim \omega_0$. In addition $\mathrm{Im}\ \chi\ (= \chi_I)$ will be positive under normal conditions but will become negative under conditions of population inversion[60]. The polarizability in equation (3.21) can then be expressed as $\chi_R + j\chi_I$ and with the expression of equation (3.21) substituted into the general equation (3.18), we obtain:

$$\frac{dA_1}{dz} = \left(\frac{2\pi\ \omega_1^2}{k_1\ c^2}\right)(j\ \chi_R - \chi_I)\ |A_2|^2\ A_1$$

$$\frac{dA_2}{dz} = \left(\frac{2\pi\ \omega_2^2}{k_2\ c^2}\right)(j\ \chi_R - \chi_I)\ |A_1|^2 A_2 \qquad \ldots (3.22)$$

It should be noted from these equations that no exponential factor appears as in equation (3.18), which depends on the propagation constants k_1 and k_2. Therefore the problem of phase matching does not arise. If these expressions are summed, multiplied by their complex conjugate, and finally integrated, one arrives at the Manley & Rowe relation[61]:

$$N_{\omega_1} - N_{\omega_2} = \text{constant} \qquad \ldots (3.23)$$

where N_{ω_1} and N_{ω_2} are the fluxes and are given by :

$$\frac{k_1}{\omega_1^2} \cdot |A_1|^2 \quad \text{and} \quad \frac{k_2}{\omega_1^2} |A_2|^2 .$$

This relation shows that any gain or loss of photons by the radiation at frequency ω_1 must be accompanied simultaneously by an exactly equal gain or loss of the photons at frequency ω_2.

Consider now only the χ_I terms of equation (3.22). These expressions show that, under normal conditions, when χ_I is positive, both A_1 and A_2 will decrease with increasing z at a rate proportional to the strength of the other field and to χ_I. The waves at frequencies ω_1 and ω_2 are attenuated by the non-linear medium when their sum approximates to a transition frequency of the medium. Neither wave is attenuated on its own but when both are present the attenuation arises from simultaneous absorption of two photons, one from each wave, whose total energy is just sufficient to cause an excitation of the medium. The energy lost by the two waves thus appears as excitation energy in the medium. Two photon absorption was first observed by Kaiser and Garrett[62], who found evidence, from the detection of fluorescence, for the excitation by ruby laser radiation of a level of Eu^{2+} in CaF_2 whose transition frequency from the ground state was of the order of twice the ruby laser frequency. In such a process the incident frequencies are the same, i.e. $\omega_1 = \omega_2$, and so equation (3.22) takes the form:

$$\frac{dA_1}{dz} = -\frac{2\pi\omega_1^2}{k_1 c^2} \chi_I |A_1|^2 A_1 \qquad \ldots (3.24)$$

where χ_I is now of the form $\chi_I(\omega_1, -\omega_1, \omega_1)$ and is positive. Subsequently this process has been reported by several research workers including the author [62,38-41].

It should be added in passing that the imaginary terms in equation (3.2), i.e. $j\chi_R$, result in modifying the propagation constant of each wave in a way that is proportional to χ_R and to the intensity in the other wave.

3.7 STIMULATED RAMAN EFFECT

In this process, unlike the process for two photon absorption, it is the difference instead of the sum of the frequency of the two components of the radiation field that is close to a resonance frequency of the medium, i.e. $\omega_2 - \omega_1 = \omega_o$. Using the same development as before, the completed equation becomes:

$$\frac{dA_1}{dz} = \left(\frac{2\pi\,\omega_1^2}{k_1\,c^2}\right)(j\chi_R + \chi_I)\,|A_2|^2\,A_1$$

$$\frac{dA_2}{dz} = \left(\frac{2\pi\,\omega_2^2}{k_2\,c^2}\right)(j\chi_R - \chi_I)\,|A_1|^2 A_2 \qquad \ldots (3.25)$$

Here again χ_I can be shown to be positive under normal equilibrium, (references 7,23,63). Note also that again no phase matching conditions control the solution of these equations. The difference in sign in the equations arises because at a resonance for the medium $\omega_2 - \omega_1 \approx \omega_o$, the polorization for the two frequencies are equal but opposite in sign, i.e, $\chi_I = \chi_I(\omega_1, -\omega_1, \omega_2) = -\chi_I(\omega_2, -\omega_2, \omega_1)$. The corresponding Manley Rowe relation will now be:

$$N_{\omega_1} + N_{\omega_2} = \text{constant} . \qquad \ldots (3.26$$

Thus any gain or loss of photons by the radiation field at frequency ω_1 must be accompanied by an exactly equal loss or gain of photons at frequency ω_2. Hence one component is amplified and the other attenuated. For χ_I positive there will be amplification of the Stokes frequency component and an attenuation of the fundamental component. It should be

mentioned in passing that it is also possible to amplify the Anti-Stoke component. The process is one of parametric amplification in which the fundamental and Stoke components together set up a modulation in the medium which produces side-bands on any radiation present[65].

The process of stimulated Raman scattering is explained quantum-mechanically in the same way as the spontaneous Raman scattering process (see Chapter II). The point to notice is that the process involved is one of emission. Such a process can either take place spontaneously (spontaneous Raman scattering), or be induced or stimulated to take place by the presence, in the vicinity of the medium, of radiation of exactly the same type that is emitted. It is the latter mechanism that applies to stimulated Raman scattering. Thus if radiation at frequency ω_2 is incident on a medium, some of it disappears and reappears as scattered radiation at frequency ω_1 which is lower than ω_2 by the transition frequency of the medium. However, it is seen from equation (8.25) that the rate at which radiation at frequency ω_1 builds up is proportional to the amount of radiation present at the same frequency. This process is therefore one in which the medium is induced to emit radiation at ω_1 , i.e. stimulated Raman effect. As this effect is a third order effect, one would expect it to be negligible small compared with the spontaneous process. However this is not always true for, by using an intense laser beam to provide the incident radiation at ω_2 , enough spontaneous Raman scattering can take place to provide scattered radiation intense enough to stimulate the process still further, i.e. the induced effect can build up from noise. Further enhancement of the effect is achieved by confining the radiation inside a cavity. The Raman maser has been a subsequent development of this principle.

The stimulated Raman effect was first observed by Woodbury and

Ng[66], Eckhardt et al[67], and Terhune[68]. It has subsequently been extensively investigated by many research workers[7,20,23,60-74].

Finally it is pointed out that, although the discussion developed in this section has attributed the Raman effect to vibrated motion of the atoms and molecules by way of an electronic polarizability, the stimulated Raman effect also arises from molecular orientation. This process is analogous to that producing stimulated Raleigh wing scattering (to be discussed in a later section).

3.8 SATURABLE ABSORPTION

If a material is normally absorbing at ω_1 due to a transition be between levels g and n, the rate of absorption may become so great at high intensities that a sizable population N_n builds up in the excited level n. Since the absorption rate is proportional to the population difference $N_g - N_n$, the absorption coefficient will decrease at high intensities. This process is governed by equation (3.24), viz:

$$A_1 \approx \exp\left[\left(\frac{2\pi\ \omega_1^2}{k_1\ c^2}\right)\ |A_1|^2\ \chi_I\right] z \qquad \ldots (3.27)$$

where χ_I, which is of the form $\mathcal{I}m\chi(\omega_1 - \omega_1, \omega_1)$ is now negative[7,23,63]; this accounts for the positive exponential as compared with the negative one for the two photon process of equation (3.24). In addition to this exponential, there must be added an expression for linear absorption, viz: $e^{-\alpha z}$. Thus:

$$A_1 \cong \exp\left[\left(\frac{2\pi\ \omega_1^2}{k_1\ c^2}\right)\ |A_1|^2\ \chi_I - \alpha\right] z \ . \qquad \ldots (3.28)$$

At optical frequencies this phenomenon is used in saturable absorbers which absorb at low intensities but become transparent if the low intensity becomes very high. This technique is used for Q-switching lasers[75-79].

3.9 INTENSITY DEPENDENT INDEX OF REFRACTION

The real part of the polarizability used in the previous section on saturable absorbers, namely $\chi(\omega_1,-\omega_1,\omega_1)$, describes the in-phase component of the polarizability. This type of real non-linear coupling parameter, as briefly discussed earlier, modifies the propagation constant of the wave by an amount that is proportional to χ and to the intensity of the wave. This modification is detectable as a change in the effective refractive index of the medium; this change being proportional to the square of the amplitude of the wave causing the change.

Thus, from equations (3.22) and (3.25), considering only the imaginary parts, and setting $\omega_1 = \omega_2$, then:

$$A_1 \sim \exp j\left[\left(\frac{2\pi\,\omega_1^2}{k_1\,c^2}\right)\chi(\omega_1,-\omega_1,\omega_1)\;|A_1|^2\right] z. \quad \ldots (3.29)$$

In this situation, the total refractive index may be written as:

$$n_{total} = n_o + n\,|A_1|^2, \quad \ldots (3.30)$$

where the polarization is related to the index by the usual expression:

$$4\pi P = \left(n_{total}^2 - 1\right) E \simeq \left(n_o^2 - 1\right) E + 2\,n n_o\,|A_1|^2\,E\,. \quad \ldots (3.31)$$

The last term is the non-linear polarization and the relationship between the intensity dependent index of refraction and the non-linear susceptibility is consequently:

$$n = 2\pi\,n_o^{-1}\,\chi(\omega_1,-\omega_1,\omega_1)\,. \quad \ldots (3.32)$$

Important manifestations of this intensity dependent index of refraction are those of self-focusing, self-trapping, and de-focusing. Before considering these topics in more detail, we will consider in the next few sections how the non-linear polarization arising from the bulk properties of media (in contrast to the electronic polarization discussed so far), gives rise to additional, and usually dominant, intensity dependent refractive index changes accompanied by stimulated scattering processes.

3.10 INTRODUCTION TO STIMULATED SCATTERING AND INTENSITY DEPENDENT NON-LINEAR REFRACTIVE INDEX MODULATION

In all the non-linear processes discussed so far, the induced non-linear polarization has been associated with an electronic polarizability of the type described in section 3.2.

In this section we will consider polarizations that arise from the effect of the electric field intensity of light radiation on the bulk properties of the medium through which it passes. Such polarizations will be shown to give rise to the stimulated scattering effects and refractive index modulators briefly discussed in Chapter I. The related theory, developed by the author, follows similar lines to the work of Herman and Gray[80]. In addition this present theory has been extended to include other non-linear effects such as refractive index modulation and stimulated entropy scattering (from the electrocaloric effect). The intensity dependence of refractive index in a non-absorbing medium is attributed to the optical Kerr effect, electrostriction, the electrocaloric effect, and electronic polarizability. In absorbing media an additional refractive index change occurs which is due to density changes resulting from absorption of the light radiation. In the first of these effects, the optical Kerr effect, refractive index changes are caused by variations in the orientational distribution of the molecules and by induced molecular re-distribtuion. The counterpart spontaneous processes have been discussed in Chapter II, in the section on the Rayleigh wing scattering. Typical values for the induced refractive index are 10^{-13} to 10^{-11} e.s.u.[87] and the 90^{0} out of phase component of this refractive index change leads to the stimulated Rayleigh wing scattering, (references 25,81-86).

In the second effect, electrostriction, pressure changes are induced in the medium by the electrostrictive force of the light radiation on the medium through which it passes. The electrostrictive pressure is related to the energy of the light[88] by the expression:

$$P_{el} = \left(\frac{\gamma}{8\pi}\right) E^2$$

where γ is the electrostrictive constant $\rho\, \partial\varepsilon/\partial\rho$.

For non-absorbing media the effect will give rise to stimulated Brillouin scattering (S.B.S.)[80], and for absorbing media, the additional processes of stimulated thermal Rayleigh(scattering (S.T.R.S.)[80], and stimulated thermal Brillouin scattering[80] are induced. The analogous spontaneous scattering associated with S.B.S. and S.T.R.S. effects are Brillouin and central Raleigh scattering described in Chapter II. Typical values of the induced real refractive index[87] are $\sim 10^{-11}$ e.s.u. The electrocaloric effect[89], the third of these intensity dependent processes, arises from entropy changes induced by the radiation field. The phenomenon consists of intense temperature waves, produced when an intense exciting giant probe of laser light and a weak initial light scattering, caused by entropy fluctuations, interact with the medium.

The associated stimulated scattering arising from this effect is the stimulated entropy scattering (S.E.S.)[90]. This effect is defined[91] by the expression:

$$\Delta S = \frac{1}{4\pi}\left(\frac{\partial\varepsilon}{\partial T}\right)_P E\,\Delta E ,$$

where S is the entropy and ε the dielectric constant.

The last effect, that of electronic polarization, is an effect associated with anharmonic vibrations of electrons within atoms induced by high electric fields. The induced refractive index changes are typically $\sim 10^{-15} \sim 10^{-14}$ ~~e.s.u.~~ It is the effect which results in the many phenomena discussed in the previous sections. The associated

stimulated effect is that of stimulated Raman scattering (S.R.S.), which has also been previously discussed.

Apart from electronic polarizability all the other intensity dependent refractive index effects described here are dependent on the bulk properties of the medium. It is for this reason that, relative to the electronic process, these latter processes are slow and can only follow the low frequency components of the stimulating electric fields.

The non-linear polarization P^{NL} arising as a result of these effects may be written as:

$$P^{NL} = \left[\left(\frac{\partial \chi}{\partial \rho}\right)_T \Delta\rho + \sum_{m=1,2} \left(\frac{\partial \chi}{\partial \alpha}\right) \Delta\alpha_m + \left(\frac{\partial \chi}{\partial T}\right)_P \Delta T \right] E \ , \qquad \ldots (3.33)$$

where $\Delta\rho$, $\Delta\alpha$, and ΔT are in general sinusoidal varying functions of the electric field.

The first term is associated with density variations due to electrostriction; the second term with molecular redistribution ($m = 1$) and orientational distribution ($m = 2$) effects; and the third term with absorptive heating and the electrocaloric effect.

From equation (3.32) χ is related to the non-linear refractive index n by:

$$\chi = \frac{n\, n_o}{2\pi} \ . \qquad \ldots (3.34)$$

Now in the following theory, temperature (T) and density (ρ) are regarded as the independent variables. Hence we may re-express the last term of equation (3.33) from equation (3.34) and using thermodynamics[92] as:

$$\frac{n_o}{2\pi}\left(\frac{\partial n}{\partial T}\right)_P \Delta T \ ,$$

for which

$$\left(\frac{\partial n}{\partial T}\right)_P = \left(\frac{\partial n}{\partial \rho}\right)_T \left(\frac{\partial \rho}{\partial T}\right)_P + \left(\frac{\partial n}{\partial T}\right)_\rho .$$

The term $\left(\partial n/\partial T\right)_\rho$ may be neglected since it is assumed that the temperature dependence of the refractive index is caused by thermal expansion (and

resultant density changes) and not by the intrinsic temperature dependence at constant density. Hence:

$$\left(\frac{\partial n}{\partial T}\right)_P = \left(\frac{\partial n}{\partial \rho}\right)_T \rho\beta \quad ,$$

also

$$\Delta T = \left(\frac{\partial T}{\partial \rho}\right) \Delta\rho = \frac{\Delta\rho}{\rho\beta} \quad ,$$

and therefore

$$\left(\frac{\partial n}{\partial T}\right) \Delta T = \left(\frac{\partial n}{\partial \rho}\right)_T \Delta\rho \quad .$$

This term is the same as that for electrostrictive. Therefore the non-linear polorization expression may be re-written as:

$$P^{NL} = \frac{n_o}{2\pi}\left[\left(\frac{\partial n}{\partial \rho}\right)_T \Delta\rho + \left(\frac{\partial n}{\partial \alpha}\right) \Delta\alpha\right] E \cdot \qquad \ldots (3.35)$$

Also for future reference define:

$$\frac{n_o}{2\pi}\left(\frac{\partial n}{\partial \rho}\right) = \frac{\gamma}{4\pi\rho_o} \quad \text{and} \quad \frac{\partial n}{\partial \rho} \Delta\rho = \Delta n \qquad \ldots (3.36)$$

where γ is the electrostrictive coefficient.

Consideration will first be given to the first term of equation (3.35) which includes electrostriction, thermal absorption, and the electrocaloric effect.

Both density $\Delta\rho$ and temperature ΔT variations can be determined from the linearized hydrodynamic equations derived by Hunt[93]. See also the treatment of R. Mountain[94].

After modification to include the effects of electrostriction and absorptive heating[80] and entropy fluctuations, these equations are:

$$\frac{\partial^2}{\partial t^2}\rho - \frac{v^2}{\gamma}\nabla^2\rho - \frac{\eta}{\rho_o}\frac{\partial}{\partial t}\nabla^2\rho - \frac{v^2\beta\rho_o}{\gamma}\nabla^2 T = -\frac{\gamma}{8\pi}\nabla^2 E^2 \qquad \ldots (3.37)$$

$$\rho_o C_v \frac{\partial T}{\partial t} - \lambda\nabla^2 T - \frac{C_v(\gamma-1)}{\beta}\frac{\partial}{\partial t}\rho = \frac{1}{4\pi}\left(n_o c\alpha E^2 + T\gamma\beta\gamma \cdot E\frac{\partial E}{\partial t}\right) \qquad \ldots (3.88)$$

where the electrocaloric expression is expressed from equation (3.36) now in terms of γ , where ρ = the density of the medium, v the velocity of sound, γ the ratio of principal specific heats = C_p/C_v , β, the coefficient of thermal expansion, λ the thermal conductivity, n_o the refractive index, α the absorption coefficient, T the temperature, E the electric field and η the bulk viscosity. γ is the electrostrictive coefficient.

Consider the electric field E to consist generally of two waves of the form:

$$E_1 = A_1(z)e^{j(k_1 z - \omega_1 t)} + \text{c.c.} \quad \text{and} \quad E_2 = A_2(z)\ e^{j(k_2 z - \omega_2 t)} + \text{c.c.}, \qquad \ldots (3.39)$$

where $A_1(z)$ and $A_2(z)$ are complex amplitudes that vary with z. Then the square of the electric field is given by

$$E^2 = (E_1 + E_2)^2 = \sum_{m,n} A_m(z)\ A_n(z)\ e^{j[(k_m+k_n)z - (\omega_m+\omega_n)t]} \ldots, \qquad \ldots (3.40)$$

where m and n run over all values of ± 1 and ± 2 such that $\omega_{-1} = -\omega_1$; $k_{-2} = -k_2$; and $A_{-1} = A^*_1$.

The density wave, and the temperature wave are defined as

$$\rho_{total} = \rho_o + \rho(z)\ e^{j(kz - \omega t)} + \text{c.c.}, \qquad \ldots (3.41)$$

where

$$\Delta\rho = \rho_{total} - \rho_o ,$$

and

$$T_{total} = T_o + T(z)\ e^{j(kz - \varphi t)} + \text{c.c.} \qquad \ldots (3.42)$$

where

$$\Delta T = T_{total} - T_o .$$

and where the abreviation $k = k_m + k_n$ and $\omega = \omega_m + \omega_n$ has been used. $\rho(z)$ and $T(z)$ are both complex amplitudes that vary with z.

Substituting equation (3.40 → 3.42) - where only one component in equation (3.40) has been taken - into the hydrodynamic equations (3.37) and (3.38), and eliminating T, we arrive at an expression for $\Delta\rho$ of

the form:

$$\Delta\rho = \frac{1}{4\pi} \frac{\left[\frac{\gamma k^2}{2}(\lambda k^2 - j\rho_o c_v \omega) - \frac{k^2 v^2 \beta \rho_o}{\gamma}\left(n_o c\,\alpha - j\frac{\gamma T_o}{2}\beta\gamma\omega\right)\right] A_m A_n e^{j(k_z - \omega t)}}{\left(-\omega^2 + \frac{v^2 k^2}{\gamma} - j\frac{k^2 \eta \omega}{\rho_o}\right)\left(\lambda k^2 - j\rho_o c_v \omega\right) - jk^2 v^2 \rho_o c_v \left(\frac{\gamma - 1}{\gamma}\right)\omega} \quad \ldots (3.43)$$

where it has been assumed that the amplitudes of the light, acoustic and thermal waves are only slowly varying compared with the wave vectors, i.e. $kA \gg \partial A/\partial z$; $k\rho \gg \partial\rho/\partial z$, and $kT \gg \partial T/\partial z$. Also only the steady state is considered, i.e. E, ρ, and T are considered to be only functions of distance z.

By imposing the necessary frequency conditions on equation (3.43) we can simplify this expression and can so study each individual effect arising from this equation separately.

3.11 STIMULATED BRILLOUIN SCATTERING (S.B.S.)

Consider α , λ, and β^2 as being negligible. These conditions are easily satisfied in experiments. Taking the imaginary parts of $\Delta\rho$:

$$j\Delta\rho_{Im} = \frac{j \cdot (\gamma/8\pi)(\omega_B^2/v^2)\,\Gamma_B\,\omega}{(\omega^2 - \omega_B^2) + (\Gamma_B\omega)^2} \cdot A_1 A_2^* e^{j(kz - \omega t)}, \quad \ldots (3.44)$$

where $\omega_B = vk$, $\Gamma_B = \left(\frac{\eta k^2}{\rho_o}\right)$ and is the spontaneous Brillouin line-width. Note that for $\Delta\rho$ to be significant $\omega(=\omega_m + \omega_n) \approx \omega_B$. As $\omega_B(= vk)$ is relatively small the only component of the electric field in equation (3.40) that satisfies this condition is the difference frequency $\omega_1 - \omega_2$. In equation (3.44) we are also considering two electric waves propagating in opposite directions such that $k_1 - k_2 = |k_1| + |k_2|$.

From equations (3.35, 3.36 and 3.44) the non-linear polarization will be:

$$P^{NL} = \left(j\frac{\gamma}{4\pi\rho_o}\Delta\rho_I\right)E \; . \quad \ldots (3.45)$$

The effect of this non-linear contribution on the electric field

amplitudes is as usual given by equation (3.18) giving:

$$\frac{\partial A_1}{\partial z} = - g_B k_1 |A_2|^2 A_1(z) - \alpha_o A_1(z) \qquad \ldots (3.46)$$

$$\frac{\partial A_2}{\partial z} = - g_B k_2 |A_1|^2 A_2(z) + \alpha_o A_2(z) \qquad \ldots (3.47)$$

where:

$$g_B = \left(\frac{\gamma^2 k_L^2}{32\pi n_o^2 \rho_o}\right) \frac{\Gamma_B \omega}{(\omega^2 - \omega_B^2)^2 + (\Gamma_B \omega)^2} \qquad \ldots (3.48)$$

where A_1 and A_2 refer to the forward going laser wave (pump wave) and backward wave (signal wave). The approximation has been made that $k = |k_1| + |k_2| \sim 2k_1$. The additional terms $\alpha_o A$ have been added to take account of optical loss due to linear absorption. Thus the primary forward wave (laser beam) will suffer a net loss and the backward travelling Stokes wave will suffer a gain. Equation (3.47) shows that the rate of change of the Stokes amplitude in the $-z$ direction, or the direction of propagation of the Stokes wave, contains an optical loss term and a gain term. The gain which is due to stimulated Brillouin scattering is proportional to the product of the intensities of the primary and Stokes waves.

The resonant denominator in the gain coefficient equation (3.48) shows the finite band-width of the amplification process. The gain coefficient has a maximum for $\omega \simeq \omega_B$:

$$\left(g_B\right)_{max} = \frac{\gamma^2 k_L^2}{32\pi n_o^2 \rho_o} \cdot \frac{1}{\Gamma_B \omega_B} \qquad \ldots (3.49)$$

Note that for $\omega \simeq - \omega_B$ there is an equal and opposite loss, i.e. attenuation of the anti-Stoke component. Plate (3.1) shows the gain characteristics of this effect (together with the gain characters of all other stimulated scattering processes) as a function of frequency[95]. For $\omega \sim 0$ there will be no gain. From equations (3.46) and (3.47) it can be shown by converting these expressions into photon fluxes (as

Plate 3.1

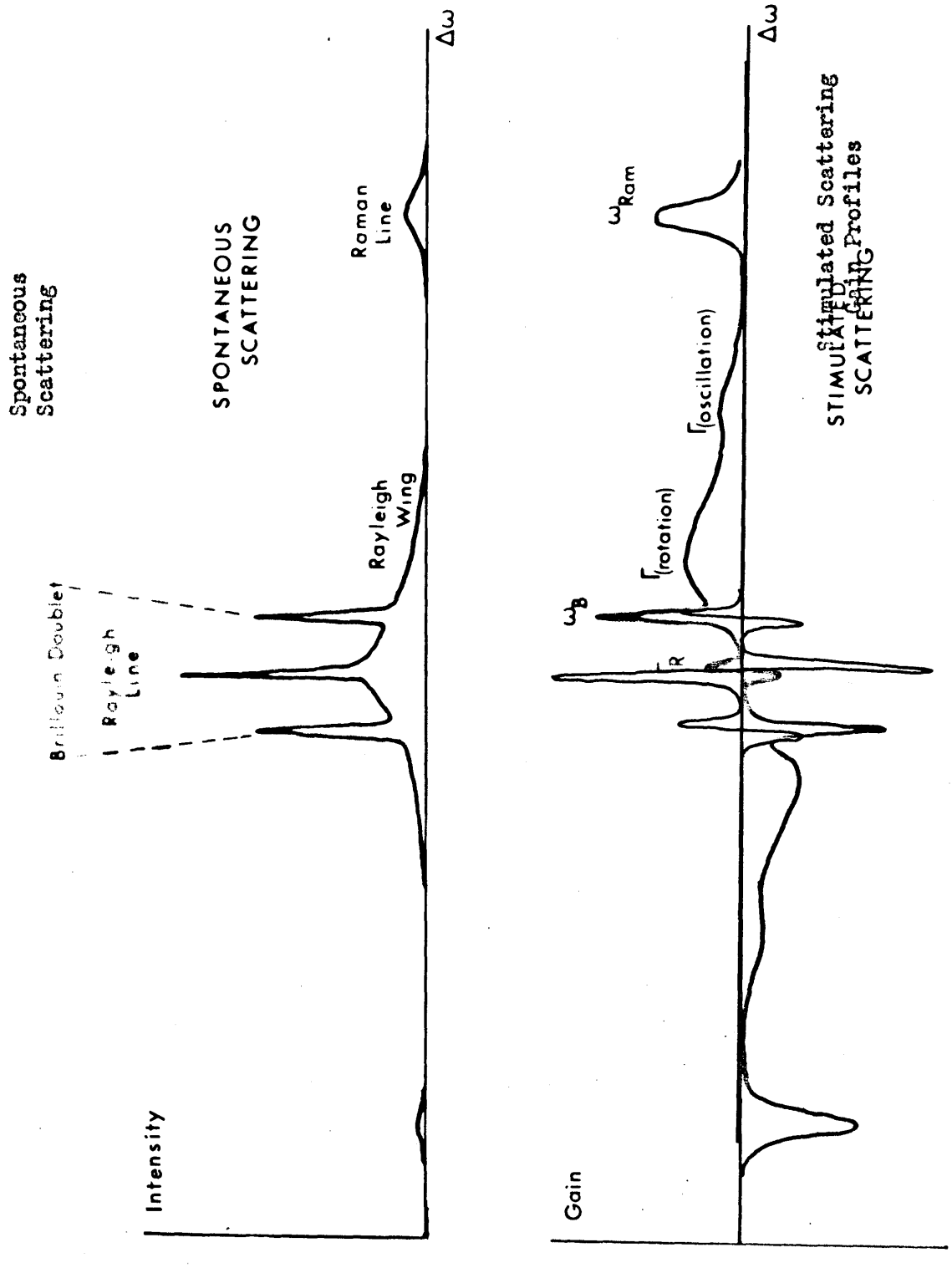
Spontaneous Scattering
SPONTANEOUS SCATTERING
Brillouin Doublet
Rayleigh Line
Rayleigh Wing
Raman Line
Intensity
Δω
STIMULATED SCATTERING
Stimulated Gain Profiles
ω_Ram
Γ(oscillation)
Γ(rotation)
ω_B
Γ_R
Gain
Δω

Plate 3.1

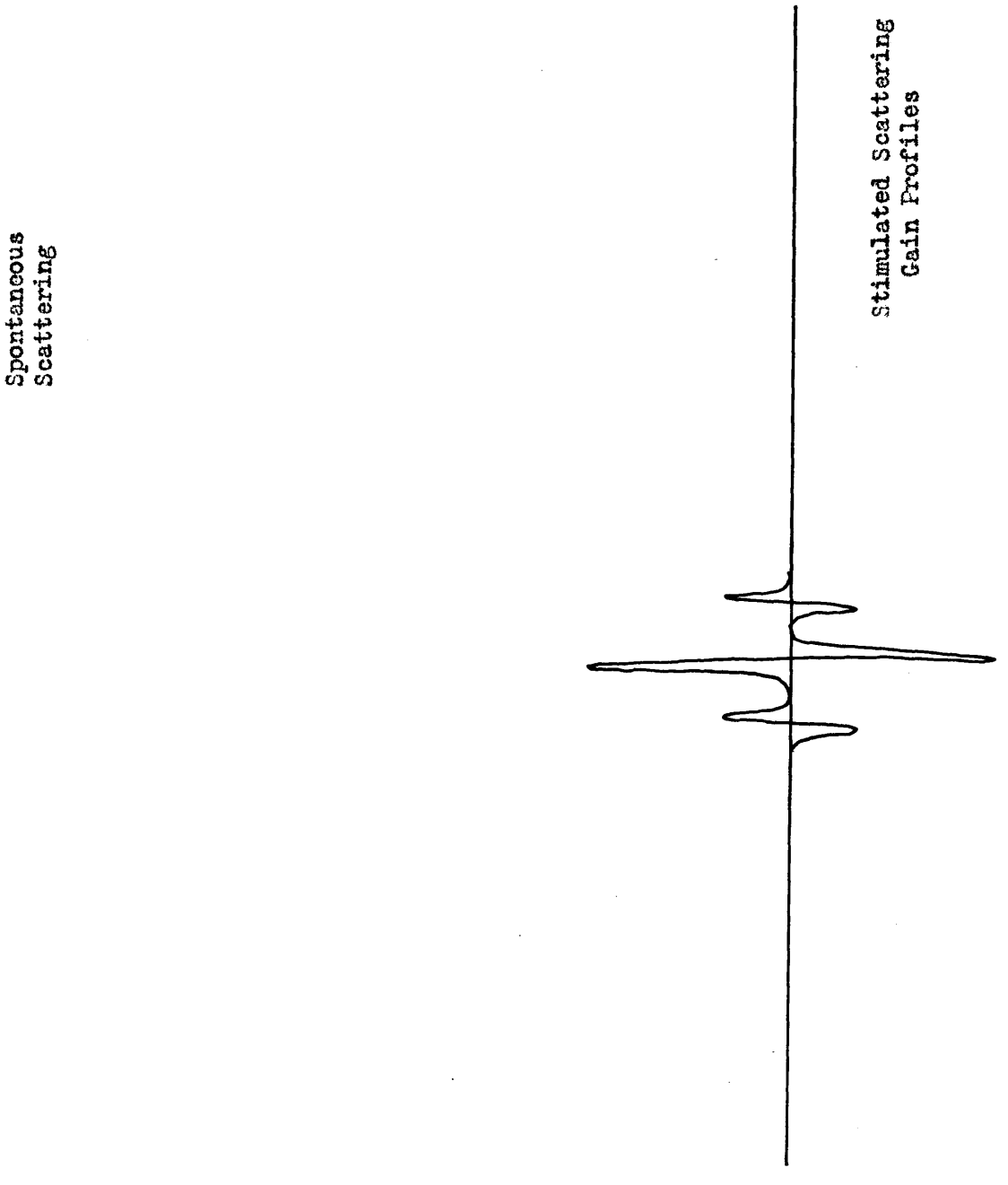
Spontaneous
Scattering
Stimulated Scattering
Gain Profiles

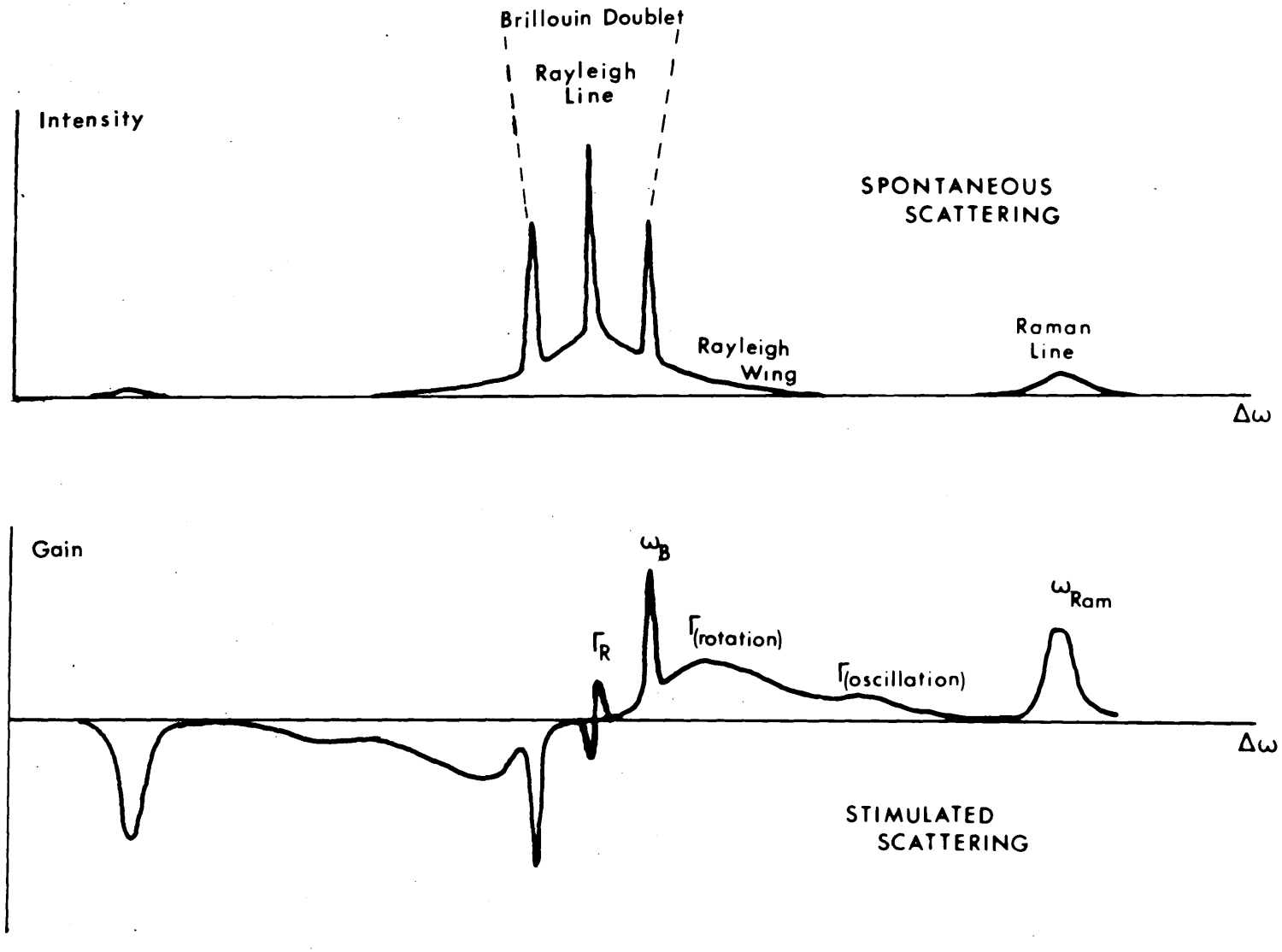
Brillouin Doublet
Rayleigh Line
Intensity
SPONTANEOUS SCATTERING
Rayleigh Wing
Raman Line
Δω
Gain
ω_B
ω_Ram
Γ_R
Γ(rotation)
Γ(oscillation)
Δω
STIMULATED SCATTERING

has been previously done for the Raman effect etc.) that the rate of decrease of primary photon flux in the + z direction due to S.B.S. is precisely that of increase of the Stokes photon flux in the backward direction due to the same process, i.e. Manley and Rowe relation.

When acoustic loss in the medium is sufficiently large to prevent absolute temporal photoelastic instability from developing, in the absence of any externally applied coherent Stokes signal, the Stokes output must be due to stable spatial amplification of noise at the Stokes frequency. In the case of stimulated scattering of ruby laser light at room temperature by far the greatest contribution to noise is due to normal Brillouim scattering of the laser photons by forward travelling thermally excited phonons throughout the medium.

From equation (3.47) it can be seen that the threshold requirement for amplification is $g_B k_2 |A_1|^2 \geq \alpha_0$. Typically for absorption coefficients of the sound and light being $\sim 10^{-1}$ cm^{-1}, and 10^{+2} cm^{-1} respectively, the laser power required to meet the threshold condition(96) $\sim$ 1 MW/cm. The maximum energy which can be fed into acoustic waves is the fraction ω_B/ω_1, given by the ratio of phonon-to-photon energies, or the order of 10^{-4} of the input energy. Substantial build-up of the acoustic waves and scattered light during the short pulse of a giant pulse laser requires, of course, light intensities which are appreciably above threshold, and only under these conditions can the acoustic wave or the scattered wave be easily detected. Such powers are achieved by focusing the laser beam to give powers $\sim 10^5$ MW/cm. Typical frequency shifts for the Stoke wave are ~ 1 cm^{-1} corresponding to an acoustic wave of frequency 3×10^{10} c.p.s.

Further references to this work are (20,23,97-104).

Consider now the real part of $\Delta\rho$ in equation (3.43) returning still the restrictions of small λ, α, and β^2. Then:

$$\Delta\rho_R = -\frac{\gamma k^2}{8\pi} \cdot \frac{\omega^2 - \omega_B^2}{(\omega^2 - \omega_B^2)^2 + (\Gamma_B\omega)^2} \cdot A_1 A_2^* \; e^{j(kz - \omega t)} \quad \ldots (3.50)$$

where again we consider one forward and backward travelling wave and that $k = |k_1| + |k_2|$ and $\omega = \omega_1 - \omega_2$.

It is seen by substituting the resultant non-linear polarization term into the amplitude equation (3.18) that like the previous case of the Raman effect, the real part, or in phase component of the acoustic wave will only modify the propagation constant of the wave.

Generally from equations(3.34, 35, 36 and 52) the refractive index will be modulated in such a way that

$$\Delta n_R = -\frac{\gamma^2 k^2}{16\pi\rho_o n_o} \cdot \frac{\omega^2 - \omega_B^2}{(\omega^2 - \omega_B^2) + (\Gamma_B\omega)^2} \cdot A_1 A_2^* \; e^{j(kz-\omega t)} \quad \ldots (3.51)$$

At $\omega = o$, i.e. $\omega_1 = \omega_2$; then:

$$\Delta n_R = +\frac{\gamma^2 A_1 A_2^* \; j2kx}{16\pi \; n_o \; \rho_o \; v^2} \quad \ldots (3.52)$$

Thus a periodic refractive index charge is produced in the medium by an electric field standing wave.

At $\omega_1 = \omega_2$ and $k = k_o - k_o = 0$, i.e. two waves of the same frequency and travelling in the same direction the change in refractive index is:

$$\Delta n_R = +\frac{\gamma^2}{16\pi n_o \rho_o v^2} A_1 A_2^* \quad \ldots (3.53)$$

This expression is in agreement with that derived by Shen[104]. This dependence of the refractive index of the medium on the electric field produces the effect of self-focusing that will be discussed later.

Note also from equation (3.51) that the refractive index charge will increase (be positive) only from $\omega \leq \omega_B$.

3.12 STIMULATED THERMAL BRILLOUIN SCATTERING (S.T.B.S)

Consider the general expression for $\Delta\rho$ given by equation (3.43) for frequencies $\omega \sim \pm \omega_B$ where $\omega_B = kv^2$. The resultant imaginary component will then be; neglecting small terms:

$$\Delta\rho_I = \frac{\omega_B^2}{4\pi} \cdot \frac{\left[\frac{\gamma\Gamma_B\omega}{2v^2} - \frac{\beta^2 T_o \Gamma_B \gamma\omega}{2c_v} + \frac{\beta n_o c\alpha}{c_p}\left(\frac{\omega^2 - \omega_B^2}{\omega}\right)\right]}{\left(\omega^2 - \omega_B^2\right)^2 + \left(\Gamma_B \omega\right)^2} A_1 A_2 e^{j(kz - \omega t)} \quad \ldots (3.54)$$

where again for two waves travelling in opposite directions $k = |k_1| + |k_2|$ and $\omega = \omega_1 - \omega_2 \approx \pm \omega_B$.

The first term gives the normal S.B.S. discussed already, and the second term gives the electrocaloric effect to be discussed later. (Note this term may also be neglected for $\omega \approx \pm \omega_B$ since it is very small in comparison with other contributions.) The last term gives rise to stimulated thermal Brillouin scattering (S.T.B.S) which, was first theoretically investigated by Herman and Gray[80].

This term has a positive maximum in the vicinity of $\pm \omega_B$ giving rise to a Brillouin-Stokes - Anti Stokes Doublet (Plate 3.1). The effect on the electric waves can be shown in a similar way to the previous treatment to be:

$$\frac{\partial A_1}{\partial z} = - g_{TB} k_1 |A_2|^2 A_1 \quad \text{and} \quad \frac{\partial A_2}{\partial z} = - g_{TB} k_2 |A_1|^2 A_2 \quad \ldots (3.55)$$

where

$$g_{TB} = \frac{\gamma\beta c \alpha}{8\pi \rho_o n_o c_p} \cdot \frac{\omega_B^2}{\omega} \cdot \frac{(\omega^2 - \omega_B^2)}{(\omega^2 - \omega_B^2)^2 + (\Gamma_B \omega)^2} \quad \ldots (3.56)$$

Thus the backward travelling wave will experience amplification and be

both Stoke and anti-Stoke shifted in frequency, the maximum gain occurring for $\omega = \pm \omega_B + \frac{1}{2} \Gamma_B$, such that:

$$(g_{TB})_{max} = \frac{\gamma \beta c \alpha}{16\pi \rho_o n_o c_p} \cdot \frac{1}{\Gamma_B} . \qquad \ldots (3.57)$$

Hence this contribution associated with the heating will give two maxima one each lying in the lower frequency wing of both the Stokes and anti-Stokes Brillouin lines. In accordance with Herman and Gray's theory a comparison of the gains of this effect to the stimulated thermal Rayleigh effect (to be discussed in the next section) shows that the latter is twice that of the Brillouin doublet arising from absorptive heating. This effect has been experimentally verified by Pohl et al[106].

The real term for $\Delta\rho$ in equation (3.43) for $\omega \sim \pm \omega_B$, will be for two electric waves travelling in opposite directions:

$$\Delta\rho_R = -\frac{1}{4\pi} \frac{\left[\frac{\Gamma_B \omega_B^2 \beta n_o c \alpha}{c_p} - \frac{\omega^2 (\omega_B^2 - \omega_B^2)}{2}\left(\frac{\gamma}{v^2} - \frac{\beta^2 T_o}{c_v} \gamma\right)\right]}{(\omega^2 - \omega_B^2)^2 + (\Gamma_B \omega)^2} A_1 A_2^* e^{j(kz - \omega t)} \qquad \ldots (3.58)$$

The second term has been dealt with in the previous section and the third component due to the electrocaloric effect will be discussed later.

The refractive index modulation produced by the first term, will then be:

$$\Delta n_R = -\gamma \frac{\Gamma_B \omega_B^2 \beta c \alpha}{8\pi \rho_o c_p} \frac{A_1 A_2^*}{(\omega^2 - \omega_B^2)^2 + (\Gamma_B \omega)^2} e^{j(kz - \omega t)} \qquad \ldots (3.59)$$

This refractive index will therefore <u>decrease</u> with the applied electric field amplitudes.

3.13 STIMULATED THERMAL RAYLEIGH SCATTERING (S.T.R.S.)

Consider now the general expression for $\Delta\rho$ of equation (3.43) near $\omega \approx 0$:

$$\Delta\rho = \frac{\beta}{4\pi\gamma c_v} \cdot \frac{\left[\left(-\frac{n_o c\,\alpha\Gamma_R}{2} - \frac{T_o\,\gamma\,\beta\,\gamma\omega^2}{2}\right) - j\left(n_o\,c\,\alpha - \frac{\Gamma_R T_o \gamma\,\beta\,\gamma}{4}\right)\omega\right]}{\left(\omega^2 + (\tfrac{1}{2}\,\Gamma_R)^2\right)} \cdot A_m A_n\, e^{j(kz-\omega t)}, \qquad \ldots (3.60)$$

where the numerator term $(\lambda k^2 - j\rho c_v\omega)$ in equation (3.43) has been neglected as it is far off resonance. $\Gamma_R = (2\lambda k^2/\rho_o \gamma c_v)$, is the spontaneous Raleigh line-width which is usually very narrow, thus implying that for large $\Delta\rho$, ω must again be a difference frequency.

Hence the imaginary component will be for $\omega \approx 0$ and $k = |k_1| + |k_2|$

$$\Delta\rho_I = -\frac{\beta}{4\pi\gamma c_v} \cdot \frac{\left[n_o\,c\,\alpha - \frac{\Gamma_R \gamma T_o \beta\gamma}{4}\right]}{\omega^2 + (\tfrac{1}{2}\,\Gamma_R)^2}\, \omega\, A_1 A_2^*\, e^{j(kz-\omega t)} \qquad \ldots (3.61)$$

Hence $\Delta\rho_I$ has a maximum for $\omega \sim \left|\Gamma_R/2\right|$.

If the electrocaloric effect is disregarded for the time being, then the effect of the absorptive heating term is

$$\Delta\rho_I = -\left(\frac{\beta\, n_o\, c\alpha}{4\pi\,\gamma\,c_v}\right) \cdot \frac{\omega}{\omega^2 + (\tfrac{1}{2}\,\Gamma_R)^2} \cdot A_1 A_2^*\, e^{j(kz-\omega t)} \qquad \ldots (3.62)$$

which gives rise to electric field amplitude variations of the form:

$$\frac{dk_1}{dz} = -\,g_R\,k_1 |A_2|^2 A_1 \quad \text{and} \quad \frac{\partial A_2}{\partial z} = -\,g_R\,k_2\,|A_1|^2 A_2 \qquad \ldots (3.63)$$

where

$$g_R = -\left(\frac{\gamma\beta c\,\alpha}{8\pi\rho_o\,\gamma\,c_v n_o}\right) \frac{\omega}{\omega^2 + (\tfrac{1}{2}\,\Gamma_R)^2}\,. \qquad \ldots (3.64)$$

This gain has a positive maximum for $\omega(=\omega_1 - \omega_2) = -\,\tfrac{1}{2}\,\Gamma_R$ such that:

$$g_{R\max} = \left(\frac{\gamma^{\wedge}\ \beta\, c\, \alpha}{8\pi\ \rho_o\ \gamma c_v\ n_o}\right) \frac{1}{\Gamma_R} \qquad \ldots (3.65)$$

(see Plate 3.1).

Therefore the backscattered wave travelling in the -z direction is amplified and anti-Stokes shifted by an amount $\frac{1}{2}\Gamma_R$. However in actual practice because of the narrowness of Γ_R it is necessary to convolve this function with the laser line[80] resulting in, a frequency broadening of $\frac{1}{2}(\Gamma_L + \Gamma_R)$, ($\Gamma_L$ being the linear linewidth), and a lowering of the gain. This anti-Stoke shift is in sharp contrast to the cases of S.B.S. and stimulated Raleigh-wing scattering in which laser photons are converted to lower energy photons the excess energy appearing in the liquid excitations. In the present process, laser photons are converted into higher energy photons, the extra energy being supplied by the thermal fluctuations, which in turn, are created through prior absorption of electromagnetic energy. The anti-Stoke shift can be traced to the fact that in absorptive heating, liquid molecule tend to migrate away from light field regions (provided $\beta > 0$) thus lowering the index of refraction - in contrast to the situation for the electrostrictive and molecular alignment effects responsible for S.B.S. and Rayleigh-wing scattering.

It should be noted that this stimulated process is distinguished from its spontaneous counterpart (see Section 2.2) for in the latter no frequency shift occurs in the scattered light (see also Plate 3.1). To observe a particular process when two or more competing non-linear processes exist in a medium, it is necessary that the corresponding non-linear gain be larger than or equal to other existing gains. A comparison of gains per unit length for S.T.R.S. and S.B.S. leads to the following condition for the absorption coefficient of the medium α, with which S.T.R.S. may be observable[80].

$$\alpha \geq \alpha_{cr} = \frac{\gamma c_v \omega_B}{\beta n_o^2 v^2 c} \cdot \frac{\Gamma_L + \Gamma_R}{\Gamma_L + \Gamma_B} \qquad \ldots (3.66)$$

where α_{cr} is the critical absorption coefficient.

Recent experimental work on this effect in both liquids[106,107] and gases[108,109] have generally confirmed the theoretical predictions. Typically a laser power of $\sim$ 20 MW focused by a 10 cm lens into an absorbing liquid with $\alpha_{cr} \sim 0{\cdot}4$ cm^{-1} will produce S.T.R.S. with an anti-Stoke frequency shift[108] $\gtrsim 0{\cdot}01$ cm^{-1}. It should be noted that $\Gamma_R \ll \Gamma_L$ so that the anti-Stokes shift corresponds approximately to the half-width of the laser line. The total backscattered power as observed by Rank et al[107] was approximately 10% of the incident power. It was also found that the line-width of the S.T.R.S. line was about 85% of that of the incident light with no measurable change in polarization.

Consider now the contribution to the induced real refractive index (in phase part) of equation (3.60). Hence:

$$\Delta\rho_{Re} = -\left(\frac{\beta}{4\pi\gamma c_v}\right) \frac{(\frac{1}{2} n_o c \alpha \Gamma_R + \frac{1}{2} T_o \gamma \beta \gamma \omega^2)}{\omega^2 + (\frac{1}{2}\Gamma_R)^2} \times A_1 A_2^* e^{j(kz-\omega t)} \qquad \ldots (3.67)$$

For two waves travelling in opposite directions.

For $\omega_1 \approx \omega_2$ and considering for the moment only the absorptive heating term, the refractive index modulation will be

$$\Delta n_R = -\frac{\gamma c \alpha \beta}{8\pi \rho_o \gamma c_v} \cdot \frac{(\frac{1}{2}\Gamma_R)}{\omega^2 + (\frac{1}{2}\Gamma_R)^2} A_1 A_2^* e^{j(kz-\omega t)} \qquad \ldots (3.68)$$

Note that the refractive index <u>decreases</u> with the electric field for all frequencies.

For $\omega = 0$, i.e. for a forward and backward wave of the same frequency:

$$\Delta n_R = -\frac{\gamma \beta c \alpha}{4\pi\lambda k^2} A_1 A_2^* e^{j2k_1 z} \qquad \ldots (3.69)$$

This expression is in agreement with that derived by Letokhov et al[111]. As in the previous case of electrostriction discussed earlier there will be no gain for the back-scattered wave by the in-phase component of this thermal absorptive effect.

Again for two forward travelling waves of the same frequency there will be an intensity dependent charge of refractive index. However unlike the similar case arising from electrostriction there will be in general no contribution to self-focusing of pulsed laser light. This is so because generally most liquids suffer a decrease in refractive index for an increase in temperature; an effect that contributes significantly to the defocusing of continuous laser light. The general properties of this absorptive effect are studied in detail in this thesis. Further references can be made to a paper published by the author and his co-workers[37] (see enclosed papers) and to Letokhov[111].

3.14 STIMULATED ENTROPY SCATTERING (S.E.S.)

Referring back to equation (3.61) it can be seen that:

$$\Delta\rho_I = + \frac{\beta}{4\pi\gamma c_v} \cdot \frac{\frac{1}{4} \cdot \Gamma_R \gamma T_o \beta \gamma \omega}{\omega^2 + (\frac{1}{2}\Gamma_R)^2} \cdot A_1 A_2^* e^{j(kz - \omega t)} , \qquad \ldots (3.70)$$

where the term due to absorptive heating has been omitted. This expression describes the out of phase component of the electrocaloric effect and can be shown in the usual way to modify the electric fields as:

$$\frac{\partial A_1}{\partial z} = - g_c k_1 |A_2|^2 A_1 \quad \text{and} \quad \frac{\partial A_2}{\partial z} = - g_c k_2 |A_1|^2 A_2 , \qquad \ldots (3.71)$$

where:

$$g_c = \frac{\gamma^2 \beta^2 T_o}{16\pi \rho_o c_v n_o^2} \cdot \frac{(\frac{1}{2}\Gamma_R)\omega}{\omega^2 + (\frac{1}{2}\Gamma_R)^2} . \qquad \ldots (3.72)$$

Thus it can be seen that the Stoke shifted backward travelling wave, travelling in the -z direction will be amplified and the forward travelling pump wave will be attenuated in a similar way to that described for

the S.B.S. process. This expression is in agreement with that recently obtained by Starunov[90]. Maximum gain will occur for $\omega \sim \frac{1}{2}\Gamma_R$, Stoke-shifted in contrast to the maximum gain of S.T.R.S. at $\omega \sim \frac{1}{2}\Gamma_R$ anti-Stoke shifted (Plate 3.1). At $\omega \sim 0$ there is zero gain.

First experimental observations of this effect were made by Zaitsev et al[112] using a ruby laser giving an output power of up to 90 MW focused by a 2.5 cm focal lens into Benzene which has a large $(\partial\varepsilon/\partial T)$ value. Further discussion and theory can be found in references 113 and 114.

Consider now the in-phase contribution to the refractive index. From equation (3.67) this is for two waves travelling in opposite directions and with approximately the same frequency:

$$\Delta n_R = -\frac{\beta^2 T_o \gamma^2}{16\pi \rho_o n_o c_v} \frac{\omega^2}{\omega^2 + (\frac{1}{2}\Gamma_R)^2} A_1 A_2^* e^{j(k_1 z - \omega t)} \quad \ldots (3.73)$$

Δn_{Re} will be a maximum for $\omega \propto (\frac{1}{2}\Gamma_R)$ and is zero for $\omega = 0$.
Note again that Δn_R decreases with field intensity for all frequencies.

3.15 STIMULATED RAYLEIGH WING SCATTERING (S.R.W.S.)

As stated earlier in the theoretical introduction to stimulated scattering processes the stimulated Rayleigh wing scattering arises from the re-orientation and re-distribution of anisotropic molecules and the resultant induced polarization can be expressed from equation (3.33) considering now only orientation processes as:

$$P^{NL} = \left(\frac{\partial\chi}{\partial\alpha}\right) \Delta\alpha \cdot E \,. \quad \ldots (3.74)$$

Again in the presence of an electric field $E_1 + E_2$ the only possible field components that the orientational process can follow will be those in expressions (3.40) that have a difference frequency.

Derivation of this non-linear polarization will not be given here; the result will instead be taken from the treatment given by

Bloembergen[20,86]. Hence the non-linear polarization parallel to the electric field arising from the imaginary component of the polarizability $(\partial\chi/\partial\alpha)\Delta\alpha$ is:

$$P_{\parallel}^{NL}(\omega^2) = + \frac{j\, n_o'}{2\pi} \quad \frac{(\omega)\,\tau_c}{1 + \omega^2\,\tau_c^2} \quad |E_1|^2\, E_2 \qquad \ldots (3.75)$$

where τ_c is a characteristic time for molecular re-orientation and given by $\tau_c = 8\pi\,\eta a^3/6k_2T$; a is the radius of a spherical molecule and η the viscosity n_o' is given by the expression:

$$n_o' = \left(\frac{n_o + 2}{3}\right)^4 \quad \frac{(\alpha_{\parallel} - \alpha_{\perp})^2}{45\ kT}\ N\ ,$$

N being the number of molecules/cc; $\alpha_{\parallel}$ and $\alpha_{\perp}$ are the polorizabilities, for anisotropic molecules with axial symmetry, along and perpendicular to the axis respectively.

From equation (3.18) it can be seen that the electric field will be again modified such that:

$$\frac{dA_1}{dz} = -\, g_W\, k_1 |A_2|^2 A_1 \quad \text{and} \quad \frac{dA_2}{dz} = -\, g_W\, k_2 |A_1|^2 A_2\ , \qquad \ldots (3.76)$$

where:

$$g_W = \left(\frac{n_o'}{n_o}\right) \frac{\omega\,\tau_c}{1 + \omega^2\tau_c^2}\ . \qquad \ldots (3.77)$$

Thus a backward travelling wave moving in the -z direction will be amplified providing $\omega_2 < \omega_1$, i.e. Stoke shifted (Plate 3.1) . This gain has a maximum for $(\omega_1 - \omega_2) = 1/\tau$ (see Plate 3.1). The polarization perpendicular to the applied electric field is $\frac{3}{4}$ that for polarization parellel to the applied field for molecules having axial symmetry which are the ones considered here[20,86]. At $\omega_1 = \omega_2$ equation (3.77) gives zero gain.

As the temperature is varied the stimulated Raleigh line shifts in frequency since $\omega_1 - \omega_2 = 1/\tau$ where τ is a function of temperature and viscosity and is typically 10^{-10} to 10^{-13} sec. Further reference to this work can be found in the references 25,81-86.

The expression for the real (in phase) part of the refractive[20] index is :

$$\Delta n_R = n_0' \frac{1}{1 + \omega^2 \tau_c^2} A_1 A_2^* \, e^{j(kz - \omega t)} \qquad \ldots (3.78)$$

3.16 SUMMARY OF INTENSITY DEPENDENT NON-LINEAR REFRACTIVE INDEX CHANGES

In conclusion to these sections on stimulated scattering and their associated intensity dependent refractive index modulations a summary will be made of the contributions of the total refractive index amplitude charges induced by such effects, i.e. from both the in-phase and out-phase components. (Note that the out of phase component is that given by the gain expressions multiplied by n_0 .)

S.B.S. Plus In-Phase Component

$$n_a = \frac{\gamma^2 k^2}{16 \pi \rho_0 n_0} \left(\frac{1}{(\omega^2 - \omega_B^2)^2 + (\Gamma_B \omega)^2} \right)^{\frac{1}{2}} A_1 A_2$$

S.T.B.S. Plus In-Phase Component: (for $\omega \sim \pm \omega_B$)

$$n_a = \frac{\gamma \beta c \alpha}{8 \pi \rho_0 c_v \gamma} \left(\frac{1}{(\omega^2 - \omega_B)^2 + (\Gamma_B \omega)^2} \right)^{\frac{1}{2}} \cdot \frac{\omega_B^2}{\omega} A_1 A_2 .$$

S.T.R. Plus In-Phase Component; (for $\omega \sim 0$)

$$n_a = \frac{\gamma c \alpha \beta}{8 \pi \rho_0 c_p} \left(\frac{1}{\omega^2 + (\frac{1}{2} \Gamma_R)^2} \right)^{\frac{1}{2}} A_1 A_2 .$$

S.E.S. Plus In-Phase Component; (for $\omega \sim 0$)

$$n_a = \frac{\gamma^2 \beta^2 T_0}{16 \pi \rho_0 c_v n_0} \left(\frac{1}{\omega^2 + (\frac{1}{2} \Gamma_R)^2} \right)^{\frac{1}{2}} \omega \cdot A_1 A_2 .$$

S.R.W. Plus In-Phase Component;

$$n_a = n' \left(\frac{1}{1 + (\omega \tau_c)^2} \right)^{\frac{1}{2}} A_1 A_2 ,$$

where:

$$\omega = \omega_1 - \omega_2 \quad ; \quad \Gamma_B = \left(\eta \, k^2 / \rho_0 \right) \quad ; \quad \Gamma_R = \left(\frac{2 \lambda k^2}{\rho_0 \gamma c_v} \right) .$$

Hence it is seen that by a judicious choice of liquids, and frequency for the backward travelling light wave, i.e. such that $\omega(= \omega_1 - \omega_2)$ satisfies the conditions imposed by one of the above effects; any of these non-linear effects above can, to varying degrees, be isolated from the others. From a subsequent measurement of the magnitude of the refractive index change induced by such effects, information, such as relaxation times, and any of the other parameters appearing in the above expressions, may in principle be determined. This in fact has been the object of a substantial amount of the experimental research to be presented in this thesis , (see Chapters IX and X).

The method employed in these investigations was that of probing the structure using a collimated light source, i.e. laser, at the Bragg angle, and measuring the reflectivity of the induced structural grating (see Chapter X). It would appear, from the literature, that such direct probe investigations of non-linear induced refractive index structures within liquids have not been adopted before. In fact, to date, serious attention has only been given to the stimulated light scattering from these effects.

The underlying theory of this Bragg reflection probe technique is given in the next section.

3.17 BRAGG REFLECTION OF LIGHT OFF AN INDUCED NON-LINEAR STRUCTURE IN A MEDIA - FOUR PHOTON INTERACTION

The non-linear effects discussed in the previous sections on stimulated scattering, as we saw, produced, for two electromagnetic waves of similar frequencies and travelling in opposite directions, an electric field intensity dependent refractive index modulation. Such a modulation can in principle be probed and detected by Bragg reflection of an independent light beam off the structure (see Chapters IX and X).

This process may be regarded as a four photon interaction since a two photon stimulated effect interacts with the incident and reflected photon from the probe. Consider the schematic diagram below representing the induced modulation probed by a light beam at an angle θ_1 :

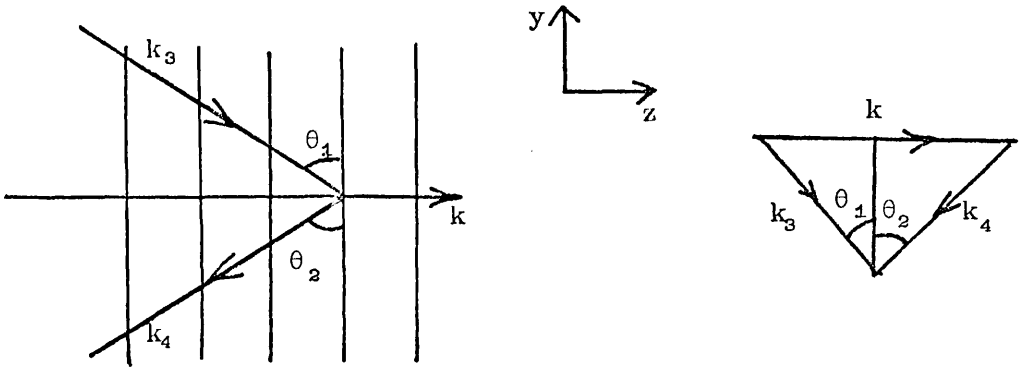

where the structure is defined as before in the shorthand notation for the frequency and wave vectors (ω,k) where:

$$k = |k_1| + |k_2| \quad \text{and} \quad \omega = \omega_1 - \omega_2$$

(k_1, ω_1) and (k_2, ω_2) describe the forward and backward laser light beams inducing the structure in the medium. Now in general $\omega \neq 0$ and so the standing modulations is moving and so produces a Doppler shift in the reflected probe beam.

Hence following similar arguments to those given by Quate et al[115] in their treatment of reflection off a sound wave, the forward and backward probe beams are defined such that:

$$E_f = A_3(z)\ e^{j(k_3 z \sin\theta_1 + k_3 y \cos\theta_1 - \omega_3 t)}$$
$$E_b = A_4(z)\ e^{j(-k_4 z \sin\theta_2 + k_4 y \cos\theta - \omega_4 t)} \qquad \ldots (3.79)$$

From conservation of energy and momentum considerations, the phase matching conditions are (see diagram)

$$\omega_3 = \omega_4 + \omega \quad \text{and} \quad k_3 = k_4 + k\ .$$

written in vector components the momentum relation becomes:

$$k_3 \sin\theta_1 + k_4 \sin\theta_2 = k$$

$$k_3 \cos\theta_1 = k_4 \cos\theta_2 \quad .$$

Since: $$\frac{\cos\theta_1}{\cos\theta_2} = \frac{k_4}{k_3} \approx 1 \quad \text{then} \quad \theta_1 \approx \theta_2 \ ,$$

and so

$$(k_3 + k_4) \sin\theta = k \ . \qquad \ldots (3.80)$$

The probe light is coupled to the induced non-linear polarization (equations (3.35) and (3.36) to give:

$$P^{NL} = \frac{n_o}{2\pi} \Delta n E \ .$$

where it is remembered that Δn is the refractive index modulation equation (3.36), which is a function of the laser light fields that induce the modulation. The various expressions for Δn arising from the non-linear effects such as electrostriction, absorptive heating, etc. have all been derived previously in the sections on stimulated scattering (see Chapter III, Sections 3.11 to 3.17)

Substituting this expression together with the expressions for the electric fields given by equation (3.79) into equation (3.18) , two coupled differential equations are obtained, describing the amplitude variations of the probe light such that:

$$\frac{\partial A_3}{\partial z} = + j \frac{k_3}{n_o \sin\theta_1} \cdot n_a A_4(z)$$

$$\frac{\partial A_4}{\partial z} = - j \frac{k_4}{n_o \sin\theta_2} \cdot n_a^* A_3(z) \qquad \ldots (3.81)$$

where, it will be remembered, n_a is the electric wave intensity dependent amplitude of Δn (Chapter III, Section 3.16). Assuming an exponential solution to these equations of the type[114] $e^{\pm \Gamma z}$, an expression for Γ is readily found from equations (3.81) to be :

$$\Gamma = \frac{k_3}{n_o \sin\theta_1} \left(\frac{\omega_4}{\omega_3}\right)^{\frac{1}{2}} n_a n_a^* \ .$$

Using equation (3.81) with the boundary conditions $A_4(L) = 0$ (L is the length of the interaction region) then:-

$$A_3 = A_3(0) \frac{\cosh \Gamma(z-L)}{\cosh \Gamma L}$$

and

$$A_4 = - j A_4(0) \left(\frac{\omega_4}{\omega_3}\right)^{\frac{1}{2}} \left(\frac{n^*}{n}\right)^{\frac{1}{2}} \cdot \frac{\sinh \Gamma(z-L)}{\cosh \Gamma L} \ .$$

Thus at the input $z = 0$, the ratio of the backward travelling wave to the forward travelling wave is:

$$\frac{A_4(0)}{A_3(0)} = j \left(\frac{\omega_4}{\omega_3}\right)^{\frac{1}{2}} \tanh \Gamma L \ .$$

For small values of ΓL this becomes,

$$\frac{P_4(0)}{P_3(0)} = \frac{|A_4(0)|^2}{|A_3(0)|^2} \approx (\Gamma L)^2 \ ,$$

when the approximation $\omega_2 \sim \omega_4$ and $\theta_1 \sim \theta_2 \sim \theta$ have been used.

Hence finally the ratio of the reflected light to the incident light, i.e. reflectivity R, is:

$$R = \frac{P_4(0)}{P_3(0)} = \left(\frac{k_1 L}{n_o \sin\theta}\right)^2 |n_a|^2 \qquad \ldots (3.82)$$

The variation of the reflectivity with angle of incidence is given by reference 115) as:

$$R \approx (\Gamma L)^2 \frac{\sin^2\left(\frac{\Delta\theta}{\sin\theta_1} \cdot \frac{kL}{2}\right)}{\left(\frac{\Delta\theta}{\sin\theta_1} \cdot \frac{kL}{2}\right)^2} \qquad \ldots (3.83)$$

3.18 SELF-FOCUSING, SELF-TRAPPING AND DE-FOCUSING

In this final section of the theoretical chapter we will consider, in a fairly general way, the effects on a highly intense light beam, of the non-linearities induced within a medium by this light beam, i.e. self-action effects. One finds that, within such effects as self-trapping and self-focusing, there exist a large range of non-linear phenomena all of which contribute to the appearance of these effects. This is not surprising when it is realized that the intensity of laser light arising from such effects is extremely high, and well above the power threshold for the onset of many non-linear phenomena, i.e. stimulated scattering. To attempt to analyze the relative significance of these non-linearities within such effects is extremely complicated and not altogether necessary in obtaining a general conception of the underlying principles of these effects. Hence the following discussion will be of a purely qualitative nature.

The self-action effects are derived from the intensity dependent non-linear refractive index changes discussed in the previous sections. such index changes are generally defined from equation (3.30) as:

$$n_{total} = n_o + n\,|A|^2 + \text{higher order terms} \qquad \ldots (3.84)$$

These effects give rise to the physical effect of non-linear refraction of the light rays since for the field of a bounded light beam, a medium which is initially homogeneous becomes optically inhomogeneous by virtue of equation (3.84); the refractive index of the medium is now determined by the distribution of the intensity of the propagating wave.

The character of the non-linear refraction is determined by the sign of n (contributions from higher order terms being neglected as they are much less than the first order non-linear term $n\,|A|^2$). For $n > 0$ the regions of maximum intensity are simultaneously also the

optically densest regions. In this case the non-linear refraction should lead, to a concentration of the energy - the peripheral rays are deflected in a region where the field is a maximal.

To clarify the principle of self-focusing and trapping consider the propagation of a cylindrical laser beam, of rectangular distribution of amplitudes, through a medium with $n_o > 0$ and where $\text{Im } n_0 = 0$. Then the refractive index outside the beam is $n = n_0$ and inside the beam $n = n_0 + n\,|A|^2$. The rays travelling from the optically denser area of the beam to the less dense region outside the beam will at this boundary suffer total internal reflection providing φ (see diagram) is large enough.

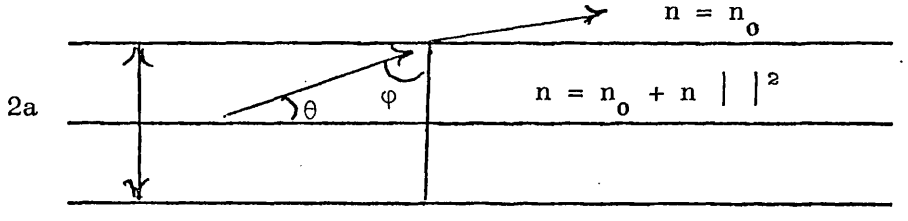

The critical angle corresponds to a ray whose inclination θ_0 to the beam axis is

$$\theta_0 = \cos^{-1}\left(\frac{n_0}{n_0 + n\,|A|^2}\right) \qquad \ldots (3.85)$$

Rays with $\theta > \theta_0$ emerge to the outside, and rays with $\theta < \theta_0$ return to the axis. In a beam whose phase front at the entrance to the non-linear medium is plane, the angle θ is determined by diffraction:

$$\theta_d = \frac{0.61\,\lambda_0}{n_0\,2a} \qquad \ldots (3.86)$$

The relative contributions of the non-linear refraction and diffraction to the behaviour of such a beam can be estimated by comparing the angles θ_0 and θ_d:

(a) When $\theta_0 < \theta_d$, the beam spreads, but the rate of this spreading is smaller than in a linear medium.

(b) When $\theta_o = \theta_d$ (non-linear refraction compensates for the diffraction spreading completely) the dimensions of the propagating beam remain unchanged. The beam produces for itself a unique optical waveguide, in which it propagates without divergence. This phenomena is called self-trapping of the wave beam.

The critical power for self-trapping for equations (3.85 and 3.86) can be shown to be

$$P_{cr} = \frac{\lambda_o^2 \, c \, (1.22)^2}{n \quad 64} \quad \text{and} \quad \frac{\theta_d^2}{2} = \frac{n \, |A|^2_{cr}}{n_o}$$

(c) When $\theta_o > \theta_d$ (and consequently $P > P_{cr}$ the rays are deflected towards the beam axis — self-focusing takes place. In this case the non-linear medium acts as a positive lens of focal length[11].

$$R = \frac{a}{2} \sqrt{\frac{n_o}{n \, |A|^2}} \; .$$

Theoretical treatments of self-focusing were first considered by Askaryan[116], Talanov[117] and Chiao, Garmire and Townes[12,118]. First experimental studies were made by Pilipetskii and Rustamov[119] and Chiao, Garmire and Townes[12,118]. In the experiment of Chiao et al it was found that the self-focused light was in fact formed of a number of thin filaments of width $\sim 30 \sim 50 \; \mu$. Such filamentry structure has been observed by many workers[119-122]. In addition, it has been found[123-124] that these self-focused filaments have a fine structure which consists of hyperfine filaments typical widths $\sim 3-5 \; \mu$ of very short lifetime $\lesssim 1$ nsec.

The length of propagation for these self-trapped filaments is governed usually by dissipative processes such as multi-photon[14] absorption and heating[123]. With such a conversions of the light energy the light power in the filaments drops below the threshold value and so the self-trapping ceases.

For media where the non-linear refractive index is less than zero non-linear refraction leads to defocusing of a powerful laser beam. The causes of appearance of this effect are quite varied, but the most important of them is heating of the medium, connected with dissipation of the energy of the light beam as described in the previous section on S.R.S. Although thermal effects can apparently play a definite role also in the propagation of short pulses their action is strongest on a light beam in the steady state, when a stationary temperature gradient is established. The time of establishment of the stationary state is $\tau \propto a^2/\lambda$ where λ is the coefficient of thermal conductivity and is usually $> 10^{-1}$ sec. References to this effect can be found in references (15-17).

3.19 GLOSSARY OF SYMBOLS

E , A	electric field and amplitude
P , P^{NL}	linear and non-linear polorization
χ	susceptibility tensor
r	electron displacement from its equilibrium position
m	electron mass
ω_o	electron natural frequency
a	damping factor
b , e	coefficients associated with anharmonic motion
N	electron density
ω_m	wave frequency of light wave (where m = 1,2,3 etc.)
k_m	wave vector of light wave
ω	$= (\omega_1 - \omega_2)$ (for sections 3.10 to 3.18)
k	$= (k_1 - k_2)$ (for sections 3.10 to 3.18)
c .	velocity of light
v	velocity of sound
n_o	index of refraction

n	non-linear refractive index
ρ_o	unperturbed density
T_o	unperturbed temperature
$\Delta\rho$	induced density wave
ΔT	induced temperature wave
$\Delta\alpha$	induced molecular re-orientation and re-distribution wave
Δn	induced refractive index wave
p	pressure
β	coefficient of thermal expansion
λ	coefficient of thermal conductivity
γ	coefficient of electrostriction
η	coefficient of bulk viscosity
α	coefficient of light absorption
c_p, c_v	specific heats at constant pressure and volume respectively
γ	ratio of specific heats
Γ_B	spontaneous Brillouin linewidth
Γ_R	spontaneous Raleigh linewidth
Γ_L	laser linewidth
g_B	gain coefficient of S.I.S.
g_{TB}	gain coefficient of S.T.B.S.
g_T	gain coefficient of S.T.B.S.
g_c	gain coefficient of S.E.S.
g_w	gain coefficient of S.R.W.S.
ω_B	Brillouin line shift = vk
τ_c	characteristic time for molecular re-orientation
λ_o	wavelength

CHAPTER IV

DESIGN AND USE OF APPARATUS

4.1 LASER HEAD

The Laser head assembly is shown in Plate 4.1. This system comprised the reflector cavity, which contained the laser rod and a high energy flash tube; front and rear mirrors, one of which could be replaced by a mode selecting device as shown; and two Q-switching cells.

The reflector cavity was an aluminium cylinder of elliptical cross-section which had a highly polished and anodised internal surface to give high reflectivity.

The laser rod was mounted along one focus of the reflector ellipse and the flash tube along the other focus. Thus practically all light radiation from the flash tube would, by this arrangement, find its way to the ruby rod.

Both the ruby rod and the flash tube were water cooled, each being enclosed by concentric silica tubes through which water continually flowed. For the ruby rod, quartz optical flats (flatness $\sim \lambda/10$) were used as seals at the end of the tube; these were mounted in aluminium annular casings and could be tilt adjusted by three screws.

The ruby rod used in the cavity was $6\frac{1}{2}$" length and $\frac{5}{8}$" diameter. For laser emission that was plane polorized, the rod had its optical axis at 60° inclination to its length. The ends of the rod were ground and polished flat to within 0.2 λ and were parallel to within a few seconds of arc. Such rods are cut from a single crystal of aluminium oxide doped with 0·04% of chromium oxide and produce a light output at a wavelength of 6943 Å .

Ruby Laser Head

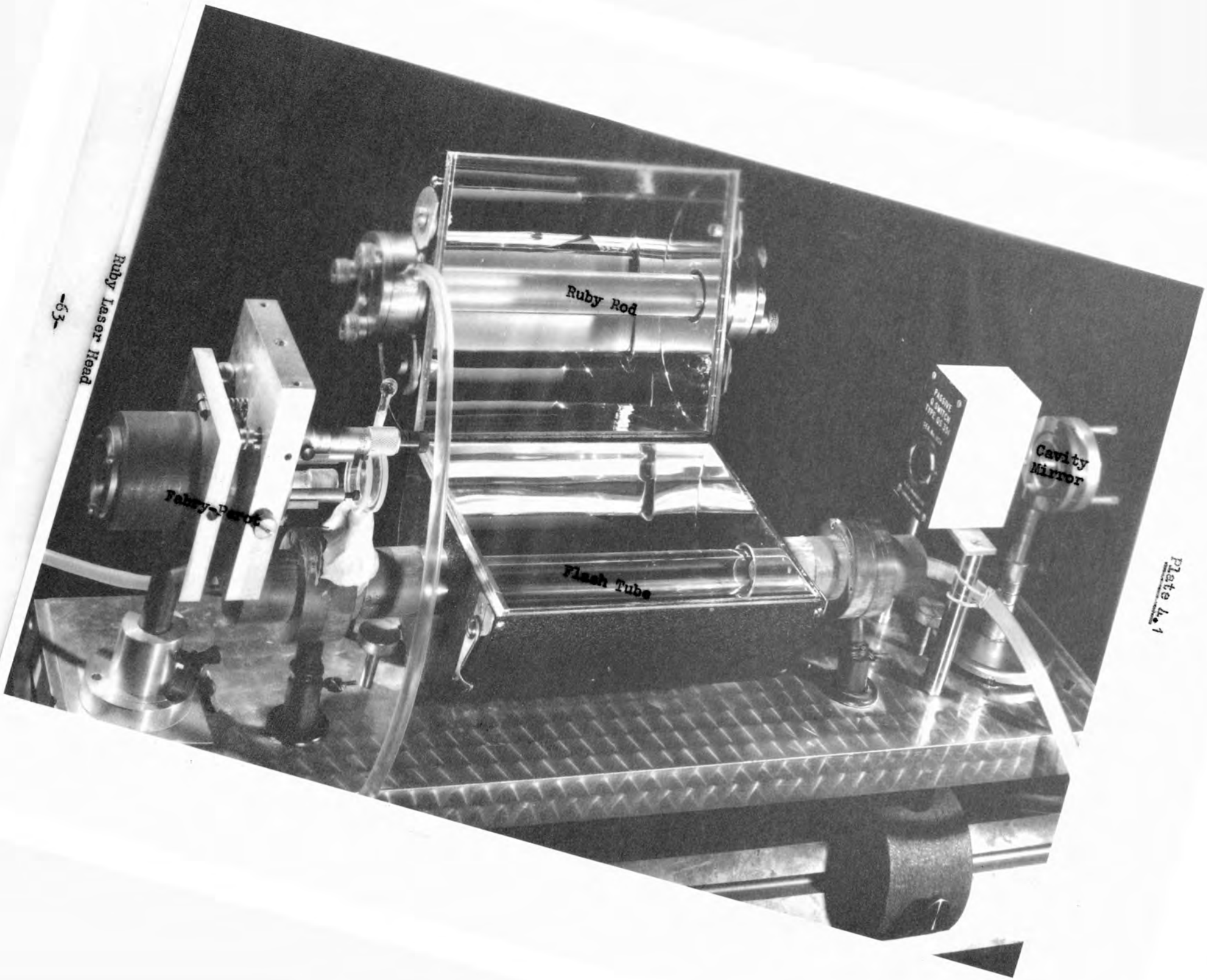

Plate 4.1

The flash tube consisted of a quartz envelope filled with Xenon gas at a pressure of 45 cm of mercury and was fitted with sealed electrodes at each end separated by some $6\frac{1}{2}$ inches. Discharge was initiated by a pulsed trigger voltage of some 15000 V from the secondary of a transformer having an amplification factor of ten (see Plate 4.2). The subsequent rapid electrical discharge from the power bank into the tube produced an intense pulse of radiation having a typical duration of from 2 to 3 milliseconds and an energy of up to 9000 joules. The power bank consisted of six capacitors in parallel giving a total capacitance of $\sim$ 2400 μF and charging voltages were up to $\sim$ 3 kV.

Cavity Mirrors The rear mirror was a dielectrically coated fused quartz plate having a reflectivity of better than 99·5% at the operating wavelength.

The front mirror, when fitted, was a dielectrically coated fused quartz plate having a typical reflectivity of 10%. However, in order to facilitate longitudinal mode selection, a more sophisticated arrangement was used in which this front mirror was replaced by a Fabry-Perot etalon (Plate 4.1). This etalon consisted of two uncoated fused quartz plates with such a spacing as to give a spectral resolution of $\sim$0.01 cm^{-1}. This corresponded approximately to the longitudinal mode separation in the cavity, the latter being about 50 cm in length. Hence, any modes having frequencies lying in the band for which the etalon gives highest reflectivity would experience further gain in the ruby, whereas other frequencies would be transmitted with very little amplification. The etalon as a whole was mounted in a vertical table which could be sensitively controlled using two micrometer screws. The mount for the back mirror was removable from the laser table to facilitate alignment of the optical system. In position, three symmetrical V-shaped radius

Plate 4.2

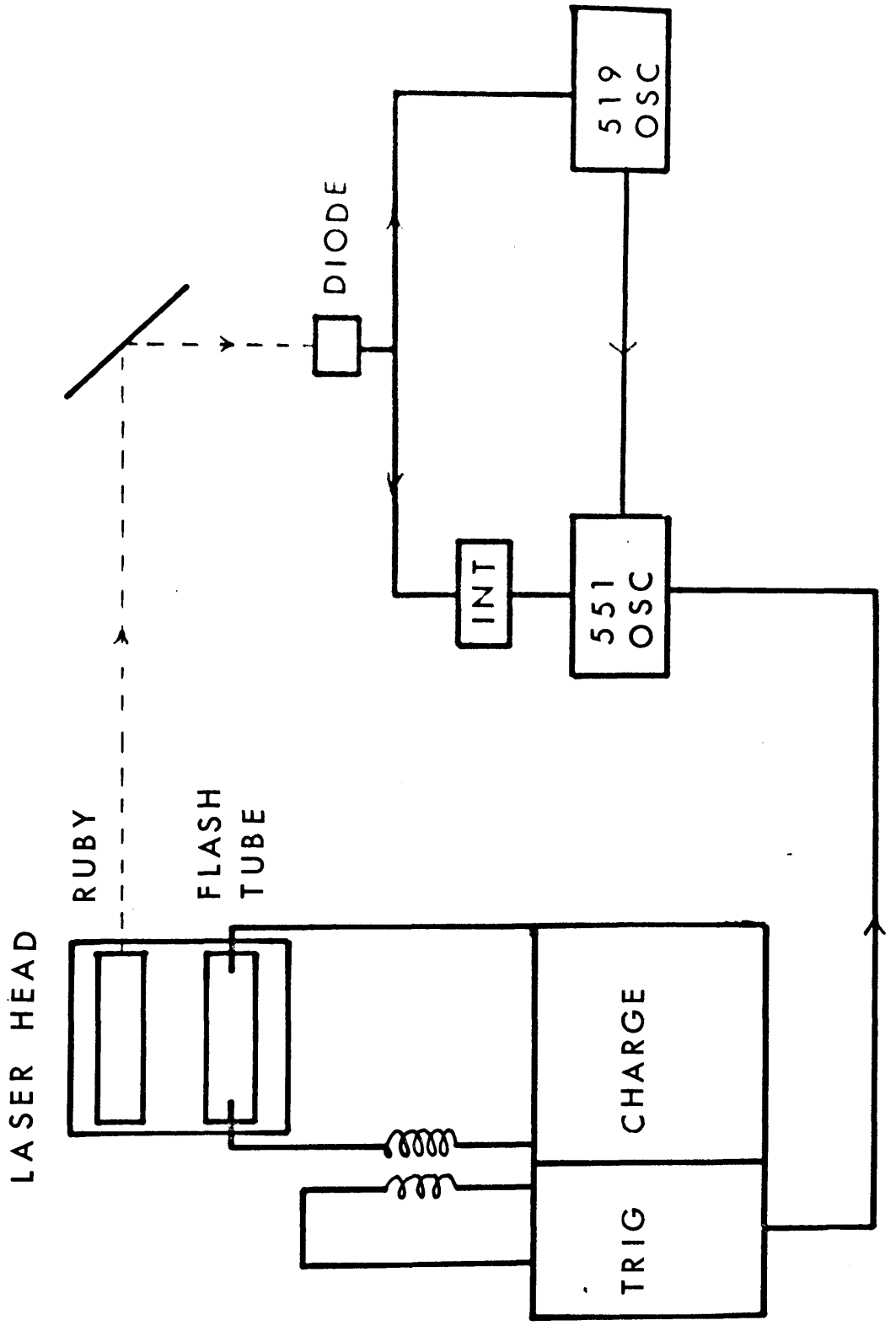

Ruby Laser Detecting System

grooves cut in the underside of the base of the mirror mount rested on three ball bearings half countersunk into the laser table. In this way one had in principle a kinematic mount.

The laser table was mounted on a base-plate in such a way as to allow vertical, lateral, and rotational motion of the table as a whole by means of four screws.

Ruby Laser Detection. A portion of the output radiation from the ruby was directed, be means of a beam splitter, into a photo-diode type EMI 9648. The signal from the diode was then monitored simultaneously on two Tektronix oscilloscopes, one of which was a type 519 and the other a type 551, the latter having an integrating circuit coupled to it (see Plate 4.2). The diode used had an S.10 cathode and, at a voltage of about 500 V, gave a quantum efficiency of about one in a hundred. Uniform illumination of the diode face was ensured by using a ground glass screen fixed over the aperture of the diode housing. The 551 oscilloscope, which has a relatively slow rise time of ~ 0.012 μsec, was used to monitor the number of laser pulses emitted by the ruby. Because of this slow rise time in comparison with the laser pulse duration ~ 20 nsec, an integrating circuit with a time constant $\sim 10^{-6}$ was used consisting simply of a resistance in parallel with a capacitor. This oscilloscope was triggered by the triggering circuit of the flash tube. In this way no doubt arose as to whether all laser pulses had triggered the 551 scope. By contrast, the 519 scope has a very fast rise time of <0·35 nsec. For this reason it was used for the temporal analysis of the laser pulses. However, because of the finite recovery time of the oscilloscope sweep, not all the laser pulses were necessarily recorded. Because of this a link was made to the 551 oscilloscope through which the signal from the 519 oscilloscope passed. The signal

was recorded on the upper trace of the 551 oscilloscope so that it could be instantly identified from its actual position on the trace relative to other pulses as recorded on the lower trace of the 551 oscilloscope. This can be seen in Plate 5.4 where the traces on the left side are from the 519 oscilloscope and the traces on the right side are from the 551 oscilloscope.

Absolute energy measurement of the laser output was recorded on a Laser Associates Calorimeter - Model 42, which had an energy range of from 20 millijoules to 300 joules.

4.2 ARGON ION LASER

The argon ion laser used was a Spectra-Physics Model 140 Induction Ion Laser as shown in the frontispiece. The design was based on the r-f induction excitation of an ion laser discharge. The continuous output gave eight different wavelengths, any one of which could be tuned in by adjustment of a prism type back reflector. However, only wavelengths of 4880 Å and 5145 Å were of significant intensity, each giving an output of about 1 watt. The laser beam diameter was $\sim 1{\cdot}6$ mm at $1/e^2$ intensity points and had a divergence of $\sim 0{\cdot}7$ milliradians. The beam polorization was plane to better than 1 part in 1000 and had its electric vector orientated vertically. The overall Doppler broadened line-width was $\sim 5 \times 10^9$ hertz. To the laser tube was attached a gas reservoir which had an automatic gas pressure valve. An axial magnetic field confined the lasing action to the centre of the tube, thus minimizing wall contamination.

The output power was continuously recorded on calibrated photodiode by way of a beam splitter. In the experiment for which this laser was used (illustrated in the frontispiece), the argon beam was used as a probe for detecting induced refractive index changes in a liquid. The

resulting small reflected signal was recorded on a photo-multiplier type 56 AVP. Such a photo-multiplier has an S-11 cathode and, at an anode voltage of 2200 V, gives a gain of 10^8. The rise time of the 56 AVP was 2 nsec. The photomultiplier housing was designed with a screw-in front holder into which could be inserted a diffusing screen (for uniform illumination of the cathode) and any number of required filters. Extraneous light scatter from the ruby system was eliminated by using narrow band filters which only transmitted the argon wavelength.

4.3 FABRY-PEROT SYSTEM

This system which is illustrated in Plate 4.3 incorporated a filter and diffusing screen holder, shutter, Fabry-Perot etalon, telescopic lens (focal length 76 cm), forward–backward beam discriminator and a camera, and was designed to be totally self-contained. The whole system was mounted on a table which could be tilt-adjusted about directions both along, and at right angles to, the length of the system. As shown in the frontispiece the table was fixed to the optical bench by means of a saddle.

The Fabry-Perot etalon had a stainless steel housing into which were slotted the optical flats, one at each end of an annular spacer. The spacer made contact with the inner face of each optical flat at three positions, which corresponded with the positions of contact on the outer face of one of the flats of the three adjusters. The adjusters each (see Plate 4.3) consist of a screw housed in a cylindrical tube, the latter being fixed to the etalon casing. Within this tube the screw pressed against a spring which in turn made contact with a point on the periphery of the flat by means of a small metal end-piece attached to the spring. The optical flats used in the etalon were flat to $\lambda/100$

Plate 4.3

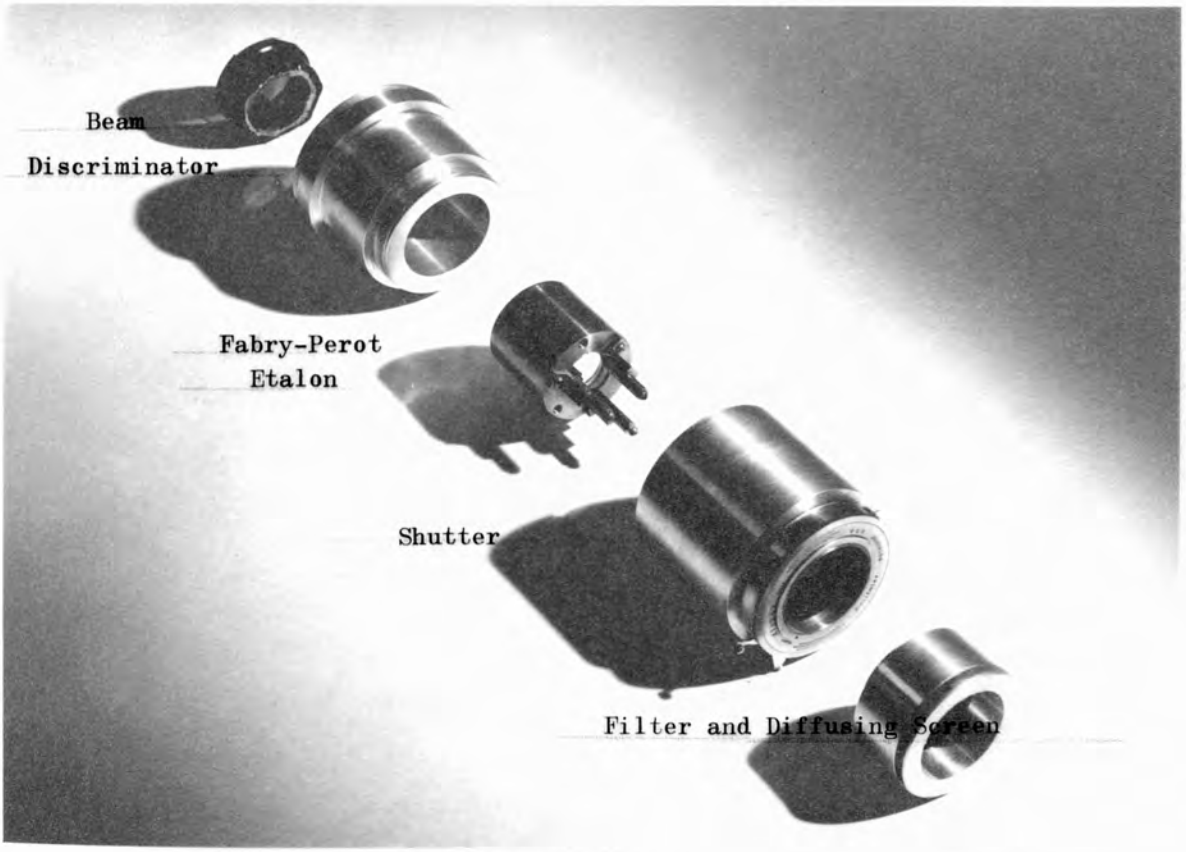

Fabry-Perot System

and were either silver, aluminium or dielectric coated. The spectral resolution of this system was $\sim 0.01\ cm^{-1}$.

Before assembling the system the Fabry-Perot etalon was independantly aligned using the output from a low power continuous helium neon laser.

The forward - backward beam discriminator was placed in the entrance aperture of the camera housing, the latter being rigidly fixed to the telescopic lens by means of the ratchet plate. The ratchet plate allowed the poloroid camera to be moved so that two or three photographs could be taken on one piece of film.

The forward - backward beam discriminator consisted simply of four quadrants of poloroid, one pair of symmetrically opposed poloroid quadrants having the same polorization which was arranged to be at right angles to the polorization of the other pair of quadrants. The principle of this discriminator is shown in Plate 4.4. The forward travelling light beam with its plane of polorization perpendicular to the plane of the paper, passed twice, via a beam splitter and mirror, through a $\lambda/4$ plate, thus experiencing a 90^{o} change in its polarization direction. The light then passed through the Fabry-Perot etalon to the camera where only the poloroid quadrants with their plane of polorization in the same direction as the polorization of the beam would transmit light. The backward travelling beam (which, in the experiments for which it was used, was derived from the forward beam) suffered no polorization change and so was transmitted to the camera through the other pair of quadrants. The lower portion of Plate 4.4 shows some typical results obtained using this system. The ring patterns resulting from the forward - backward travelling beams are shown separately and together in the photographs. Such discrimination was important since quite often the backward

Plate 4.4

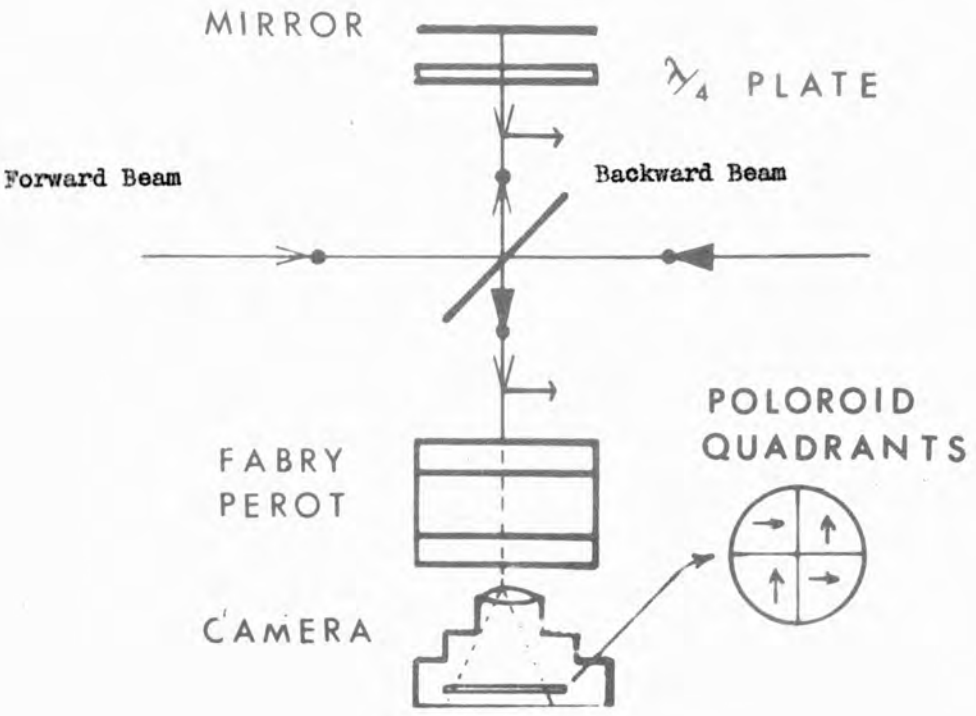

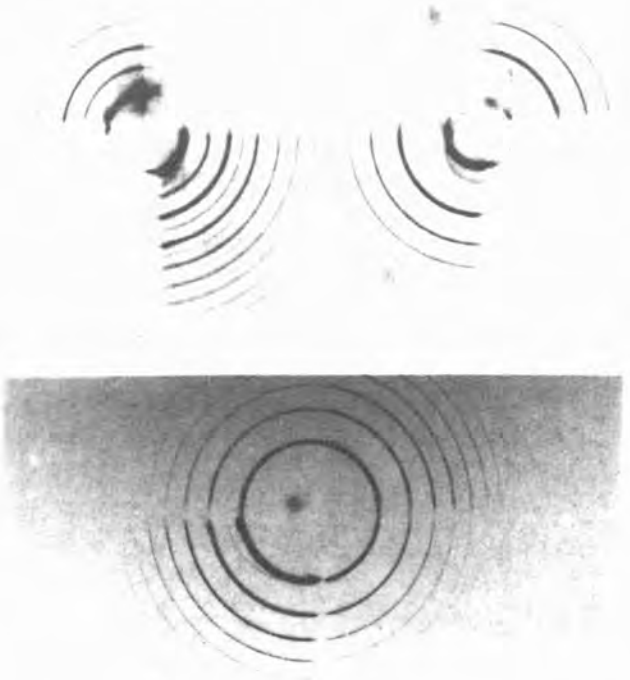

Forward and Backward Beam Discriminator

travelling beam had additional frequency shifted light, arising from stimulated scattering processes induced in a liquid through which it passed.

A comparison of the ring structure produced by the backward travelling beam with that produced by the forward travelling beam gave an indication of the effects that had been induced by the media.

4.4 KINEMATIC OPTICAL TABLE

A versatile spectrometer table with removable arms was designed using kinematic principles, (Plates 4.5 and 4.6). The movable arm has two ball bearings rigidly fixed to its underside. These rest in a circular groove of V-shaped cross-section cut into the base-plate. A third ball bearing, fixed to the upper face of the arm and positioned at its end, makes contact with the underside of a flange machined parallel to the base-plate. Thus five points of contact are made between the arm and the fixed part of the instrument leaving one degree of freedom, i.e. rotation about a central axis. When the balls are correctly located as shown in the diagram, the system is in neutral equilibrium provided the centre of mass of the arm lies outside the V-groove circle. A number of arms may be positioned simultaneously, and arms may easily be interchanged.

Angular displacements of an arm were estimated by using a vernier scale attached to the arm and a circular scale engraved on the base-plate. A micrometer screw was adapted to the system and used to achieve more precise adjustments.

The precision with which changes in the angular position of an arm could be made where governed by the accuracy with which the groove and flange were machined. Hence it was estimated that a displacement of

Plate 4.5

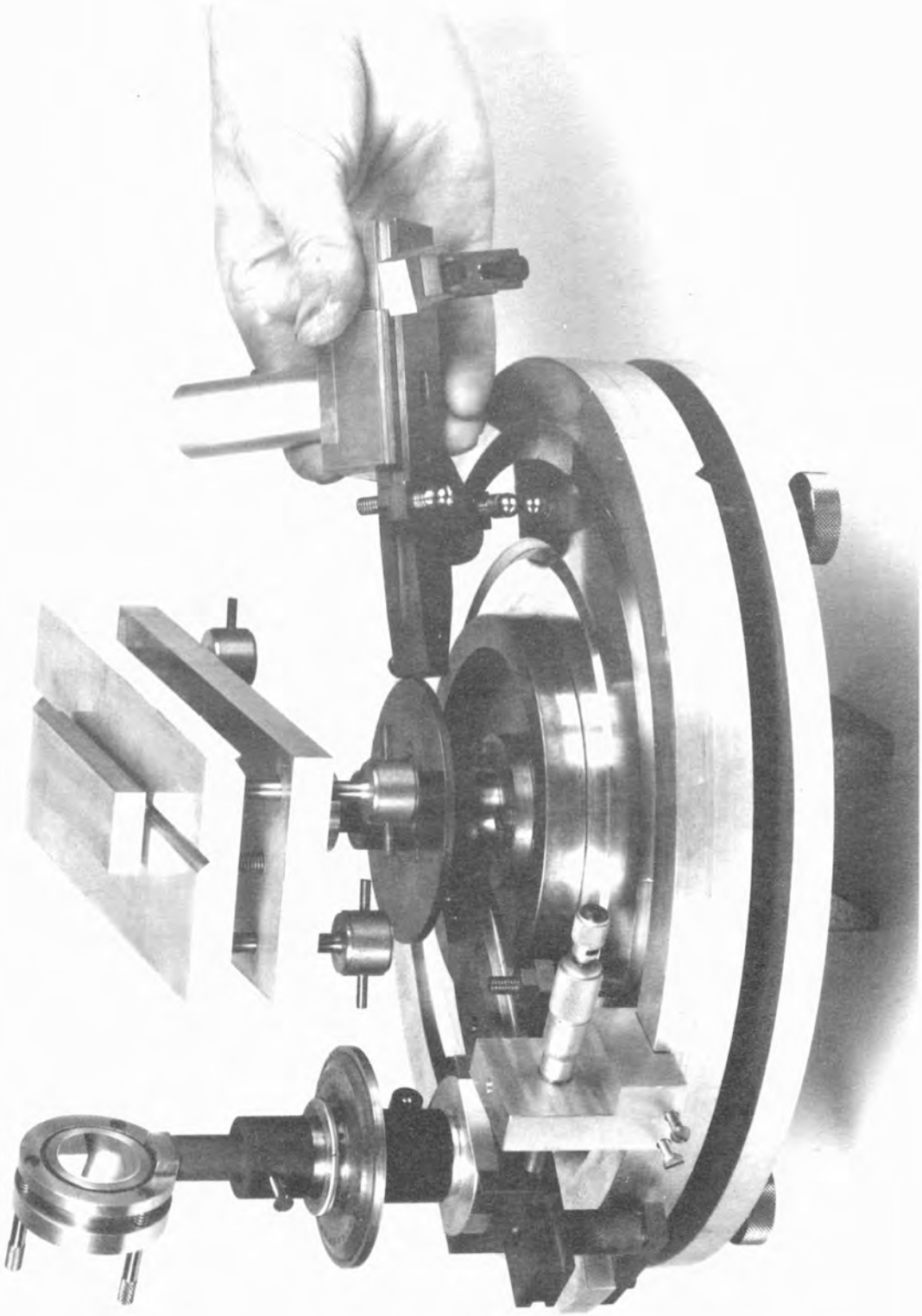

Kinematic Table

Plate 4.6

Side Elevation

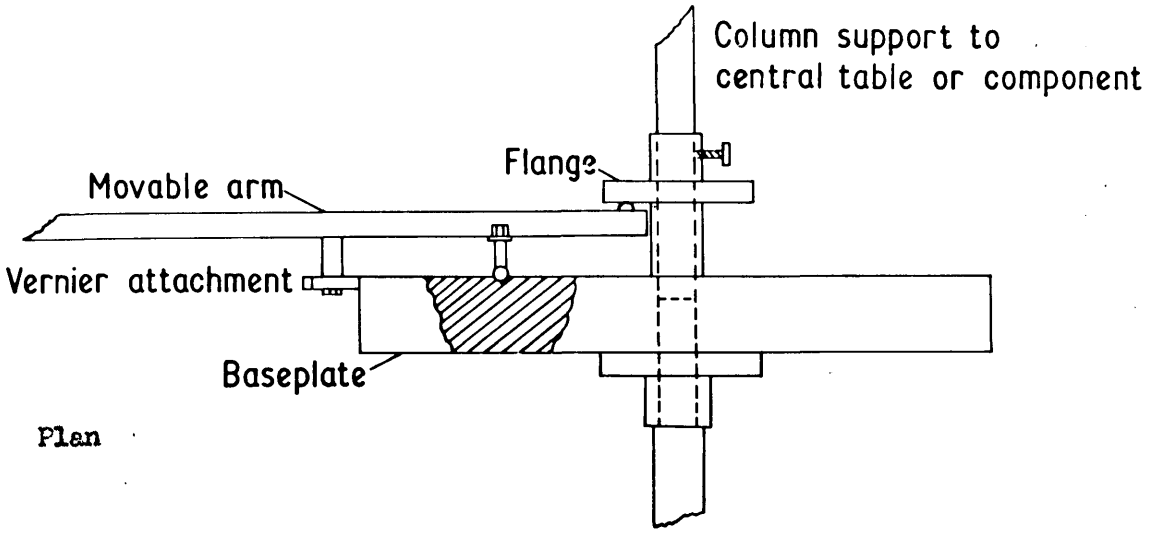

Plan

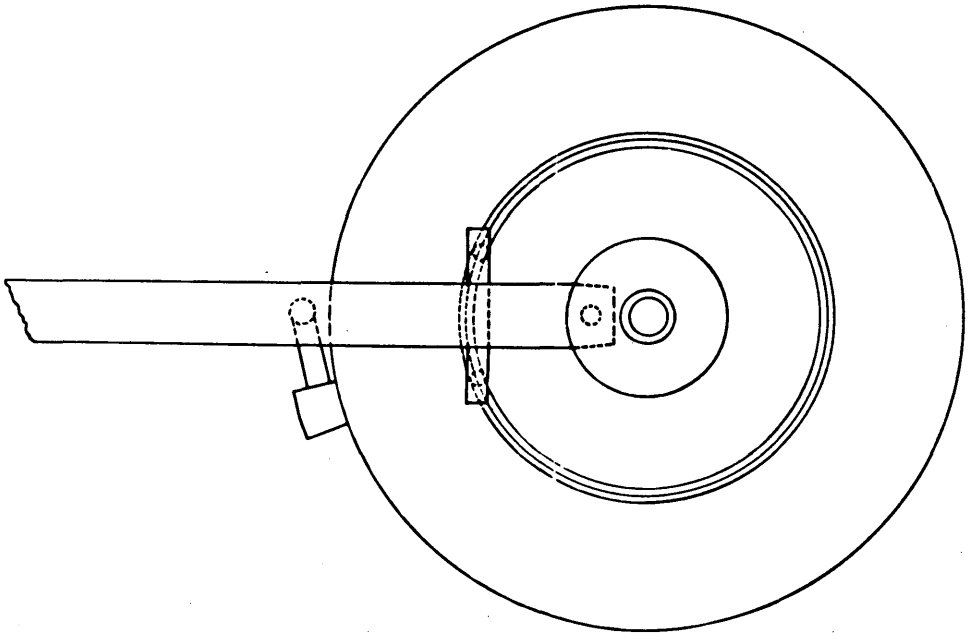

Kinematic Optical Table

the order of 10^{-1} radians would be subject to an angular error of not greater than 10^{-5} radians.

A note was published by the author and co-workers on the design and principle of such a table [127].

4.5 ADDITIONAL OPTICAL COMPONENTS

Mirror Holders: The mirror holders were generally of the type shown in Plate 4.1. The mirror was held by countersunk grub screws in an annulus casing made of aluminium. By means of three symmetrically placed spring-loaded screws the casing was held to, and could be adjusted about, the main stand holder. The front face of the mirror was usually arranged to protrude from the aluminium annulus of the main stand, in order that maximum surface area of mirror could be used when placed at an angle to the incident laser beam.

Optical Tables: A variety of optical tables were used throughout the experiments. For experiments in which high precision and sensitive control were required, tables were used which were designed on kinematic principles[128]. Such a table was used to obtain phase matching in an A.D.P. crystal where sensitive control over a range of a few minutes was required.

Filters: Light attenuation of low powered light sources was achieved using neutral density filters.

Powerful light sources, such as the ruby output, were attenuated using either glass impregnated filters such as the Wratten 18 A, or a $CuSO_4$ solution of the required concentration. At no time could gelatine filters be exposed to the direct ruby or argon beam so they suffered almost immediate damage.

Noise due to the flashlight from the ruby cavity was minimised by use of a Wratten 29 filter. For discriminate detection of the argon beam, narrow band filters were used with an additional Jena BG 18 filter to eliminate the scattered ruby laser light and generally any emission in the red.

4.6 ALIGNMENT OF RUBY LASER AND OPTICAL COMPONENTS

Alignment of all optical systems throughout the experiments was obtained by using a low power continuous helium neon laser in single mode operation giving an output power of <3 mW at a wavelength of 6328 Å. Because of the closeness in wavelength of this line to the ruby wavelength of 6943 Å any dispersion effects could be neglected. The beam divergence of this system was < 3 milliradians so reasonable accuracy could be achieved in alignment.

Alignment of a typical optical system as shown in the frontispiece was carried out in the following manner. The helium neon laser was clamped to the optical bench at one end by means of two saddle mounts (both of which had sensitive vertical and lateral adjustment) and in such a way that its beam was directed approximately along the length of the bench. With all optical components removed from the bench the gas laser was accurately aligned to two identical pointers which were placed one at each end of the bench. The ruby laser system with its back mirror mount removed was then placed in position on the optical bench. The gas laser beam, passing through a small hole in a white card, travelled through the ruby system and the reflections from the various optical components were recorded on the card as a number of 'light points'.

The first alignment requirement for the ruby system was that of a vertical plane of polorization for the ruby rod. Two pieces of poloroid were mounted in vertically rotating holders, one at each end of the ruby;

it was found in practice that the poloroid near the gas laser end was redundant as the polorization of the gas laser output was vertical within the limits of accuracy of this method. With the ruby cavity opened (see plate 4.1) the gas laser light passed uninterrupted from one piece of poloroid to the other. Light extinction was then arranged by rotating the second piece of poloroid. The ruby was then put in place and rotated until extinction was again achieved, thus obtaining a plane of vertical polorization for the ruby.

By adjustment of the laser table as a whole the gas laser beam was arranged to pass symmetrically through the centre of the ruby. With the two optical flats at the end of the ruby misaligned, and the front mirror blanked off, accurate ruby alignment was made by further adjustment of the table so that reflections from both the front and back face of the ruby coincided with the aperture in the white plate. The front mirror (or Fabry-Perot system) was then aligned by its micrometer screw adjustments to give the same coincidence between the aperture and the reflected beam.

Any additional optical components were then put in place on the optical bench and each in turn, proceeding from the ruby position , were aligned in a similar way to that described for the laser mirror. Finally the back mirror of the ruby cavity was replaced and its back face was used for alignment purposes.

It should be noted that additional optical components within the laser cavity such as Q-switch cells and the quartz water seals were misaligned to prevent inter-cavity laser build-up.

CHAPTER V

RUBY LASER OUTPUT CHARACTERISTICS

5.1 NORMAL MODE OF OPERATION

Ruby consists of aluminium oxide in which a small proportion (~ 0·5 mole percent) of the $A\ell^{3+}$ ions have been replaced by Cr^{3+} ions. The ruby laser system is essentially a three level one. Excitation occurs by absorption of broad bands in the green region of the spectrum, which results in a transitory population in the $^4F_2$ levels, followed by rapid, phonon-assisted transitions to a pair of sharp fluorescent levels[129,130]. These have a long lifetime (~ 5 msec) so that, if pump power is supplied at a sufficiently high rate, an inversion of population is produced between one of these ^2E levels and the ground state, the decay of the fluorescence from this level being predominantly radiative.

In the normal un-Q-switched mode of operation the light output from the ruby consists of a long train of randomly positioned spikes. The train of pulses lasts for about 1 or 2 milliseconds and the duration of each spike is ~ 1 μsec[129-131]. This relaxation oscillation effect results from the fact that when oscillation occurs, the rate of depletion of the population of the ^2E level exceeds that at which the levels are populated from the excitation process. The population ratio thus drops below the critical value required to sustain oscillation until the necessary inversion is re-established, when a further discharge occurs. The power emission during the emission spikes is extremely high — of the order of megawatts.

5.2 HYPOTHESIS CONCERNING THE MODE STRUCTURE

The light output from solid state lasers consists generally of a large number of frequencies. The nature of this multi-frequency production is to this day still not clear. The first proposed mechanism was that of spectral 'hole burning'[131,132]. According to this model, laser action at the frequency with the highest gain at any given time depletes the inverted populations at the corresponding location in the flourescent line, thus 'burning a hole' in the line. Therefore, the position of highest gain shifts to another location in the line and the laser is forced to oscillate in a different mode. This process continues while the pump and the relaxation tend to restore the population at the 'hole' location. However it seems that this hypothesis is untenable since such a process would require a relatively slow spectral relaxation time. In ruby the contrary is true since the homogeneously broadened line of ruby has a relaxation ($\sim 12^{-12}$ sec).

In view of these difficulties recent proposals[134-136] attribute the presence of multi-frequency components to the lack of sufficiently rapid spatial relaxation of population inversion within the active region of the laser crystal. It is visualized in the hypothesis, that when the laser oscillates in a certain mode, the active ions are de-excited at the antinodes for this mode and remain inverted at the positions of the nodes. Thus the population inversion becomes spatially modulated. Because of the lack of spatial relaxation, this modulation persists for a sufficiently long time that the laser tends to shift the frequency of oscillation to a mode which has at least some of its antinodes at the maxima of the population inversion. Experimental justification for such a mechanism has been reported by Boersch et al[137].

5.3 Q-SWITCHING BY A SATURABLE ABSORBER

In the Q-switched mode of operation the light output consists predominantly of one giant pulse, of power up to 200 MW and duration ~ 20 nsec. The underlying principle of this mode of operation is that of reducing the Q of the resonator until a substantial inversion is achieved; then it is possible to release a much larger amount of energy in a single pulse.

The Q-switching device used in this work was a saturable absorber in the form of a cryptocyanine solution in either isopropyl, alcohol or methanol (see theoretical Chapter III, Section 3.8 on saturable absorbers). Initially the dye content of the cryptocyanine solution presents an opaque path through the cavity between the laser rod and the rear mirror. This reduces the effective reflectivity of the rear mirror and hence the gain of the cavity, increasing the threshold at which laser emission occurs and allowing excess energy to build-up within the laser rod. Once the threshold condition is reached, stimulated emission developes and laser radiation commences. The cryptocyanine solution absorbs energy in the red region of the spectrum from the initial emission, (Plate 5.1) causing the dye to bleach instantly and become transparent (Plate 5.2, Fig.(a)). As a result the reflectivity of the rear mirror is restored, raising the gain of the cavity. The excess energy in the laser rod is emitted as a single giant pulse (Plate 5.2, Fig.(d)) or as a number of pulses; depending upon the concentration of the dye solution. Once laser action ceases, the cryptocyanine solution reverts to its original opaque condition[75-79].

Plate 5.1

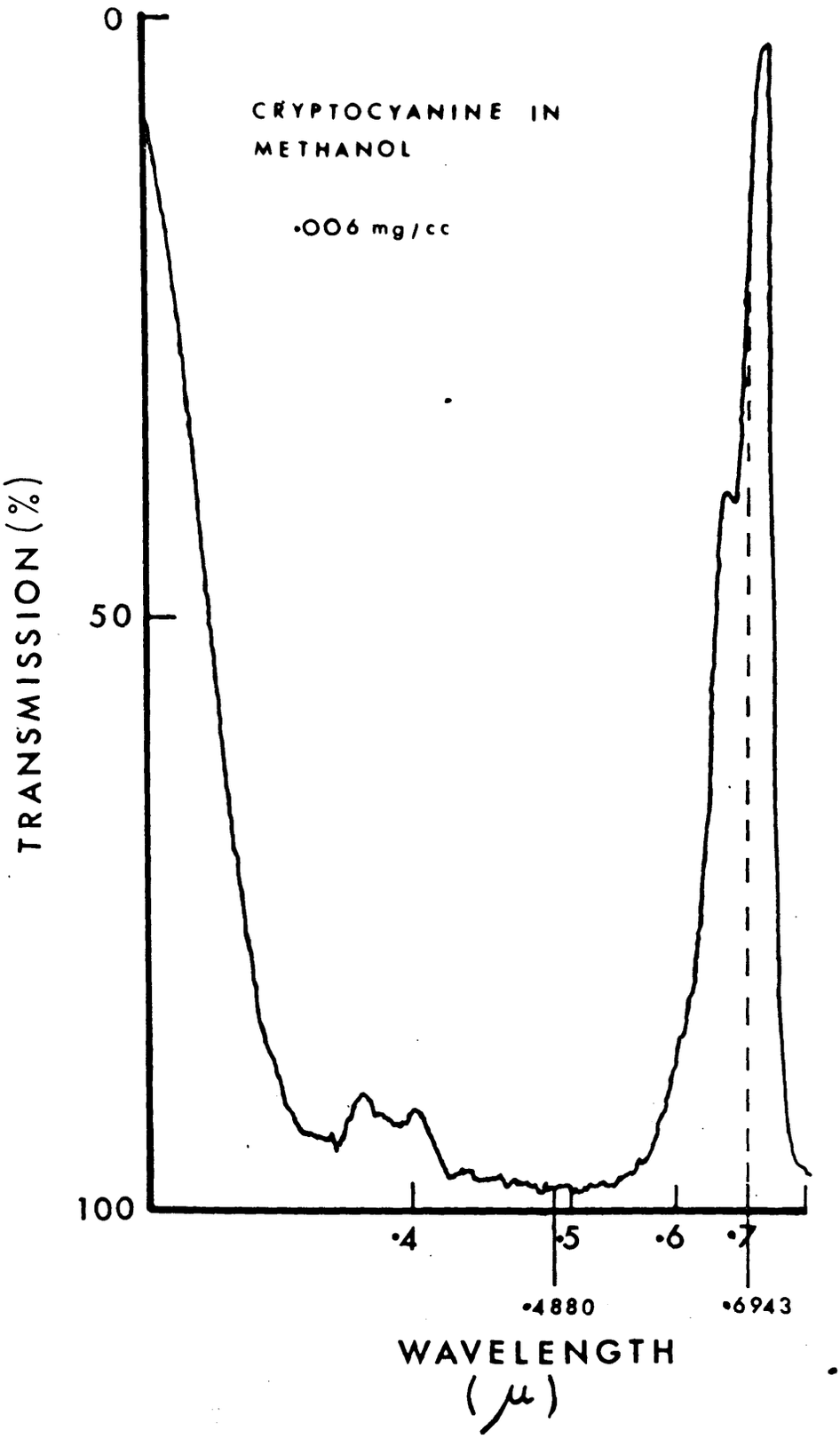

Spectrophotometer Recording of the Transmission Curve for a Solution Of Cryptocyanine in Methanol

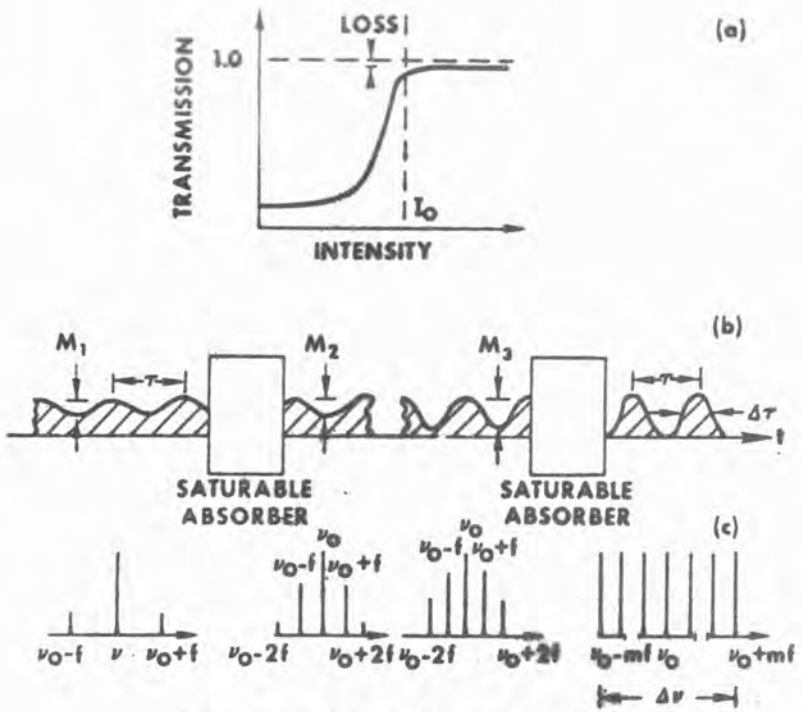

Operation of a saturable absorber in the time and frequency domain.

Plate 5.2

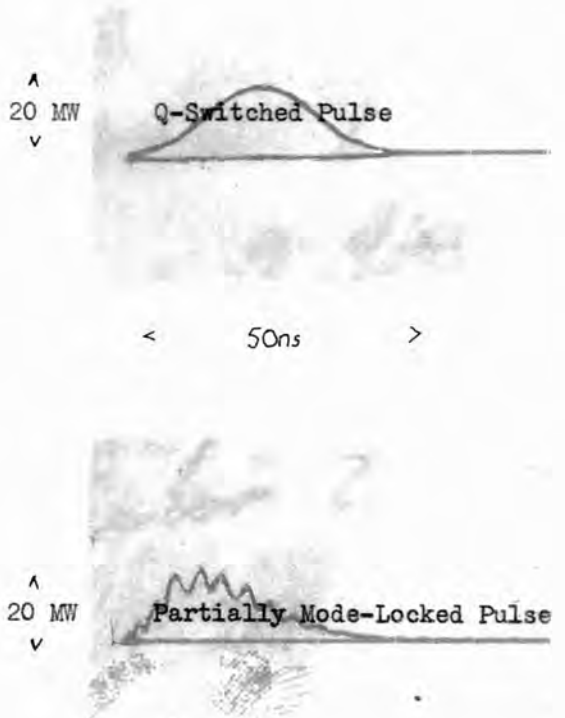

5.4 MODE LOCKING

An interesting consequence of the saturable absorber is that of mode locking of the laser cavity modes. Consider Plate 5.2, Fig.(b), which shows an amplitude modulated wave train of frequency Δf comprised of three laser frequencies, ν_o and $\nu_o \pm f$ (where f is the axial mode separation and is equal to Δf) entering the saturable absorber. Because of the absorber action the high amplitude components will suffer less attenuation than the low amplitude components. Hence the signal leaving the absorber will have an enhanced modulation. After many circuits through the dye the modulation will be sharpened to the steady state limit of being a pulse travelling back and forth through the cavity with a period equal to the loop time of the cavity and with a harmonic content equal to the overall bandwidth of the system. This repetitive output pulse train will have discrete spectral components defined by the Fabry-Perot resonances of the cavity extending to $\pm mf$ on either side of ν_o for a bandwidth $\Delta\nu$ as shown in Plate 5.2, Fig.(c). This result is to be expected since from Fourier's theorem, and repetitive pulse train can be represented by a series of discrete sinusoidal functions having integrally related frequencies and fixed phase relationships. The frequencies are all multiples of Δf and the narrower the pulse width $\Delta\tau$, the larger the bandwidth required to reproduce the repetitive pulse. The requirement for the saturable absorber are (a) that it has an absorption line at the laser wavelength; (b) that it has a linewidth equal to or broader than the laser linewidth; and (c) that the recovery time of the dye is shorter than the loop-time delay of the laser. Cryptocyanine satisfies all these requirements.

Partial mode locking, in which only two or three modes were locked is shown in Plate 5.2, Fig.(e). This was obtained using a Brewster

angled ruby rod in conjunction with a cryptocyanine Q-switch. The trace was scanned on a 519 oscilloscope. For good production of mode locking, the fine structure amplitude of the pulse should range from zero to a maximum; typically, a pulse-width of 9×10^{-11} seconds and a repetition rate of 2×10^{-9} seconds, will give a power of $\sim$ 20 MW. It is essential for the achievement of such mode locking that no mode selecting optics exist within the cavity, such as optical flats and laser rod ends which have their faces parallel to the cavity mirrors; such a system restricts the number of available oscillating modes because of the additional boundary requirements imposed by the mode selectors. Detailed analysis of mode locking can be found in references (138-142).

5.5 MODE SELECTION

It could be inferred from the above discussion that, in order to obtain efficient longitudinal selection, a number of good quality optical flats should be aligned in the cavity as described above. This however does not necessarily afford the most efficient output since it is possible that the frequencies corresponding to the maximum gain of the ruby emission may not satisfy the boundary conditions imposed by the flats.

The method employed by the author was that of using two saturable absorber Q-switches, one at either end of the ruby, in conjunction with the exit mirror Fabry-Perot system described in the previous chapter. As implied in the discussion on saturable absorbers, the laser emission frequencies with the highest gain will oscillate first in the cavity and so, by discriminate amplitude bleaching set up an amplitude grating of bleached and non-bleached regions with an intensity dependent real refractive index modulation (see theoretical Chapter III). This bleaching mechanism was originally suggested by J. Katzenstein et al[143] and subsequently experimentally verified by the author and co-workers using a Bragg

reflection probe technique. The details and results of this investigation are given in Chapter IX, and were also published[144]. Such a refraction index modulation will reflect most efficiently light waves of a frequency corresponding to that which induced the modulation. For other frequencies there is mismatch resulting in a loss of intensity for these frequencies due to interference effects. The associated modulated bleaching effect also enhances mode selection since the absorption is effectively removed for those modes with frequencies close and equal to the inducing light frequency of the structure. Other frequency components off the peak of the gain profile of the laser, which have consequently lower initial amplitudes, will experience absorption loss in the absorber due again to their mismatch with the bleached modulation.

If such a composite grating is produced in two relatively widely separated regions, i.e. an absorber at each end of the ruby, the frequency restrictions imposed by the grating for the building of waves of frequencies other than the initially exciting one are quite stringent. In this way there is a preferential amplification of only the frequencies with the high gain. The simultaneous satisfaction of this Q-switch requirement together with the frequency requirements imposed by the Fabry-Perot exit system produces fairly consistent single longitudinal laser mode outputs.

Transverse mode selection was not considered necessary in these experiments as the mode separation was considerably shorter than that for longitudinal modes. However such selection could have been obtained using a two lens and aperture arrangement inside and at one end of the cavity such that only the modes travelling exactly along the length of the cavity could pass through the aperture[145,146]. In conclusion, it is seen from these discussions that a saturable absorber has

the novel property of either mode selecting or mode locking, the first of these two effects producing a large frequency distribution and the latter effect producing a single frequency emission. Preference is given to one or the other effect by the choice of optical design and components for the laser cavity. In general for mode selection two long Q-switching cells in conjunction with the Fabry-Perot exit system are required as discussed. For mode locking a thin Q-switching cell is used and all optical components within the cavity are Brewster angled to prevent mode selection.

5.6 CALIBRATION AND DISCUSSION OF THE RUBY LASER OUTPUT

The experimental arrangement for this calibration is shown in Plate 5.3. As described in the section on laser detection, (Chapter IV, Section 1) the output from the laser was fed to a 519 oscilloscope for shape analyses and simultaneously to the 551 oscilloscope via an integrator to determine (a) the number of laser pulses and (b) the position of the pulses, recorded on the 519, relative to the train of pulses emitted by the laser.

The results of the calibration are shown in Plate 5.4 and 5.5, where all measurements and scales are recorded on the covers of the photographs.

The results shown in Plate 5.4 were taken for various dye concentrations but with constant high input energy to the discharge tube. The left hand scope traces in these plates are from the 519 oscilloscope and the right hand traces are from the 551 oscilloscope, the top trace recording the number of pulses that triggered the 519 and the bottom trace recording the actual number of pulses emitted by the laser. At low dye concentrations the laser threshold requirements were so low that multiple

Plate 5.3

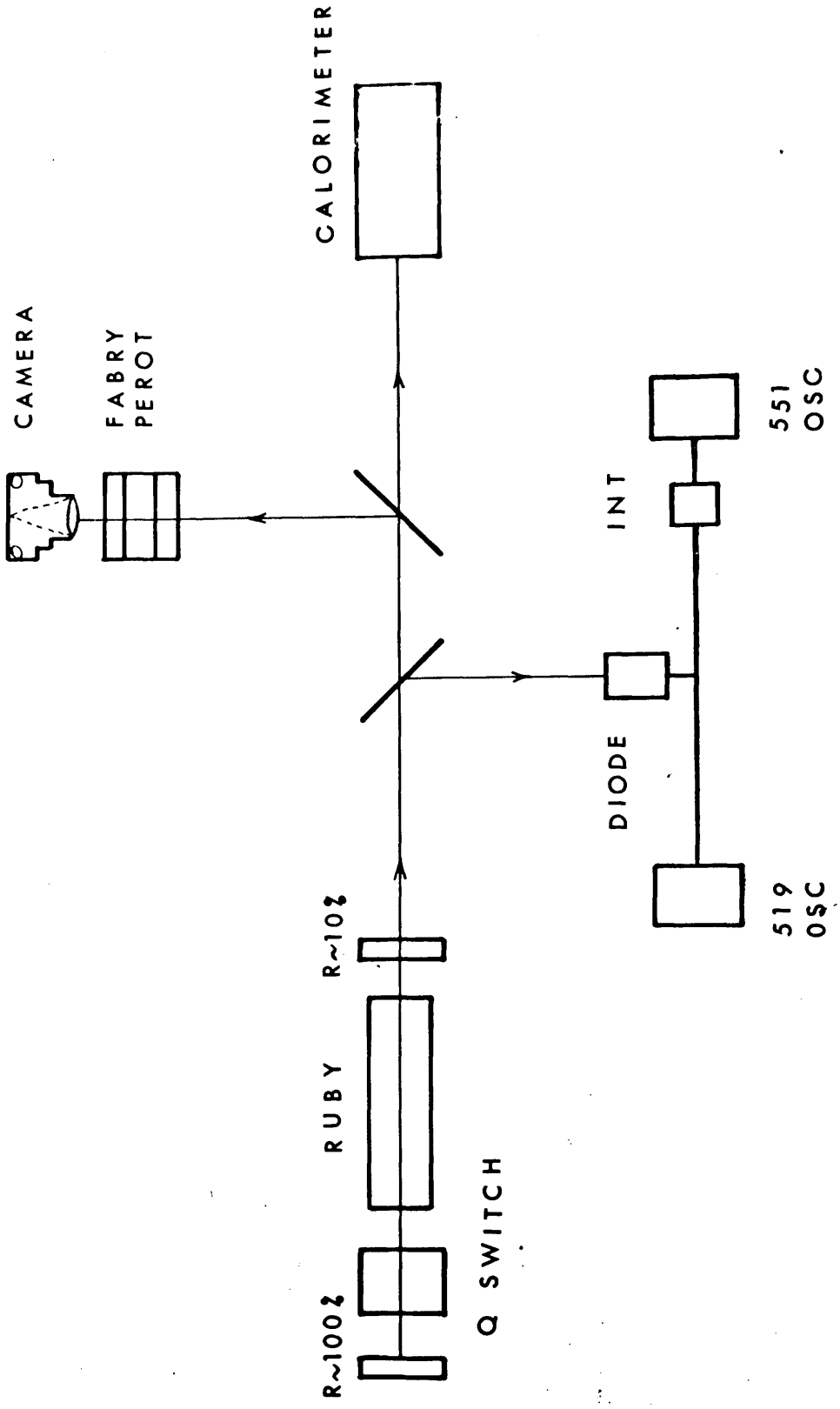

Experimental Arrangement for Calibration of the Ruby Laser Output

Plate 5.4

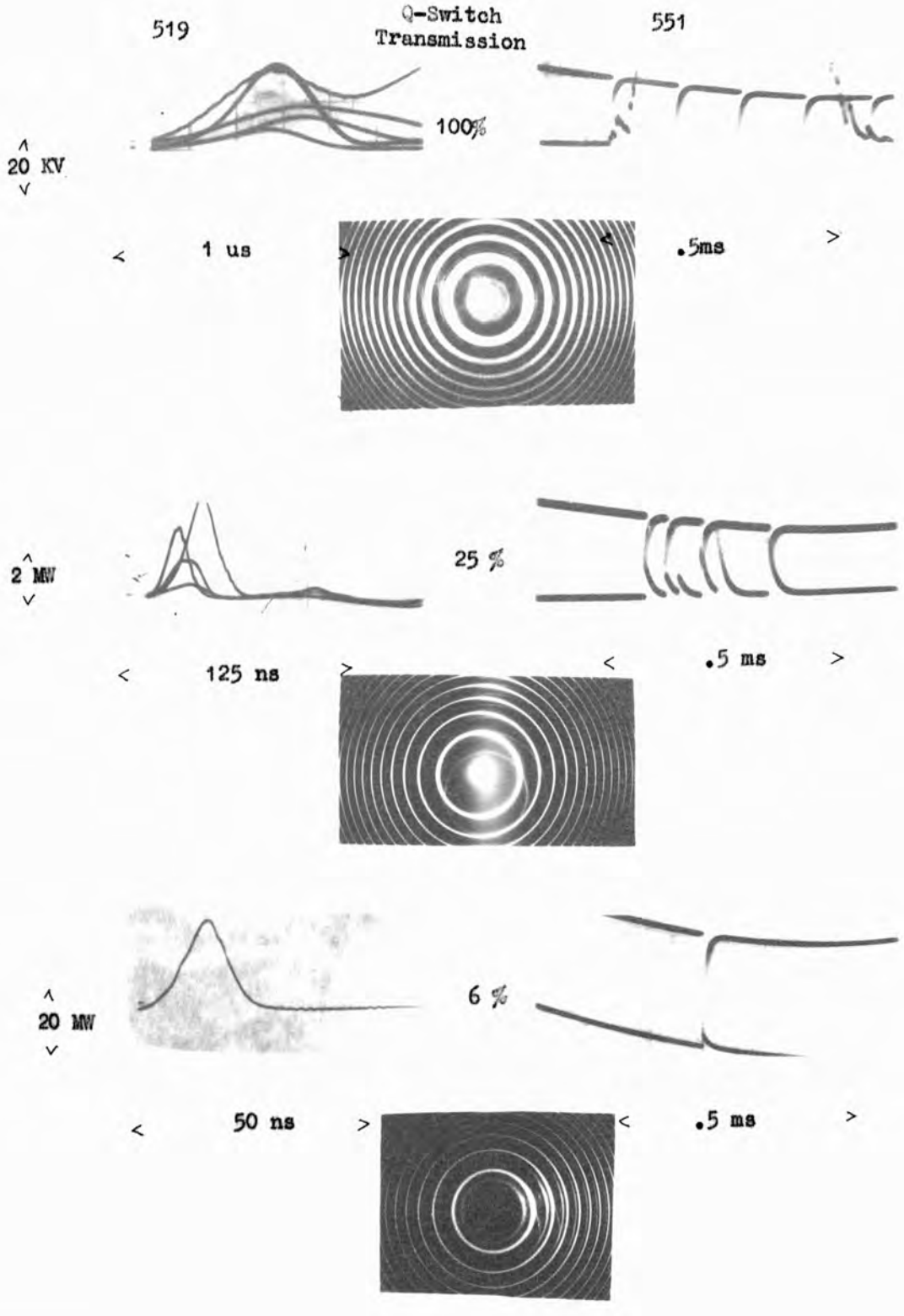

Laser Output Characteristics for Variable Q-Switch Concentration and Constant Input Energy

Plate. 5.5

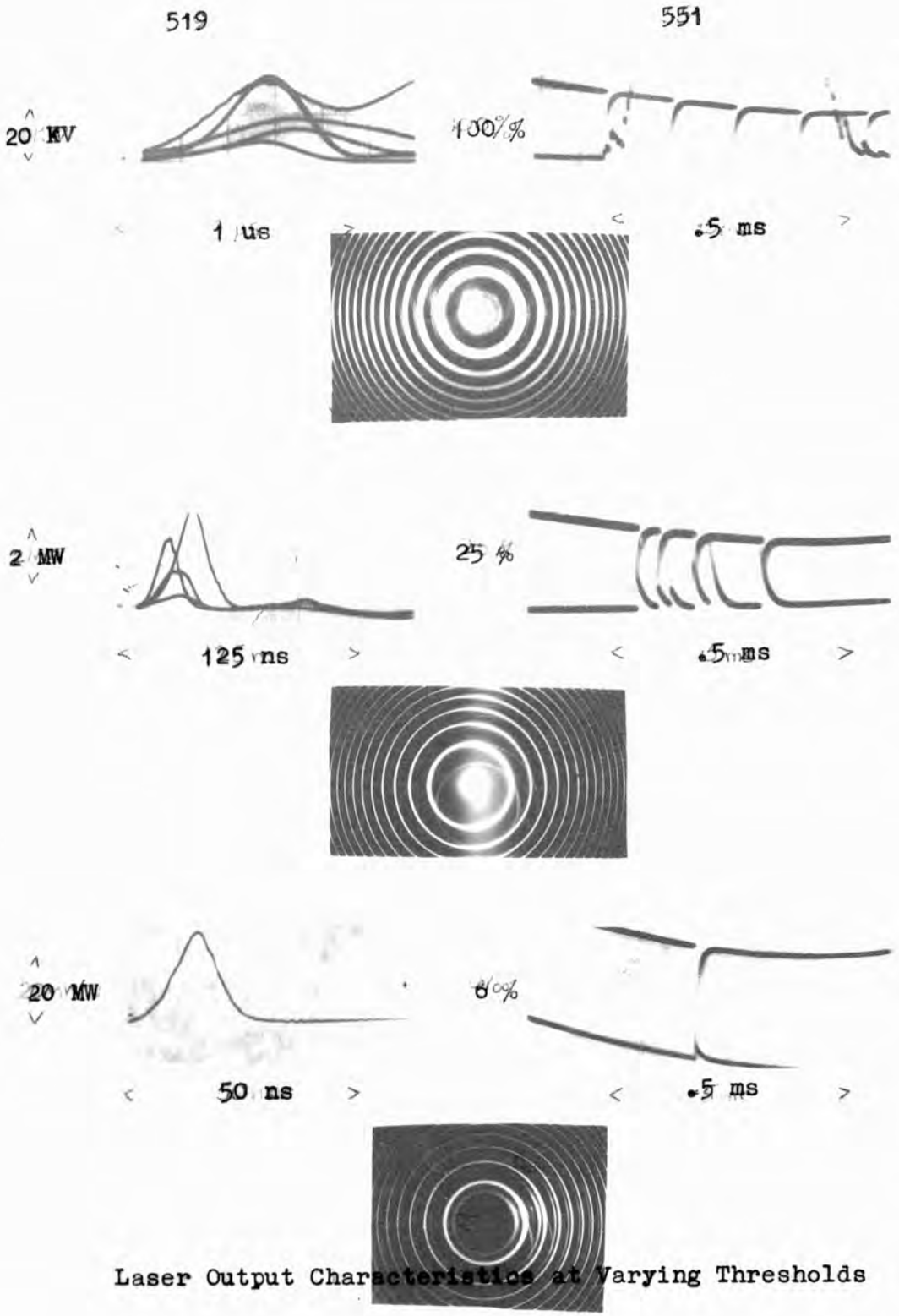

Laser Output Characteristics at Varying Thresholds

pulsing occurred. The depleted population inversion resulting from the emission of one of the pulses was easily reinstated by the remaining pump energy to give rise to further pulse emission. The corresponding Fabry-Perot photograph shows a considerable line broadening. This effect was due to thermal heating of the ruby from the discharge which resulted in a slight displacement in frequency of the gain profile for the ruby. Consequently each successive pulse, which always emitted at a frequency corresponding to the maximum of the gain profile, had a slightly displaced frequency from its neighbour.

As the dye concentration was increased the lasing threshold was raised. Consequently a greater population inversion built-up in the ruby before bleaching, with the subsequent emission of a powerful light pulse. Further pulses were emitted when the remaining pump energy had produced enough inversion together with the residual inversion left by the first pulse to again meet the threshold requirements. Obviously the number of output pulses were fewer than in the former case because of the greater demand made on the flash tube energy. At high dye concentrations, the extremely high inversion produced an output pulse of such power that stimulated scattering processes were induced in the Q-switch. From the measured shift shown on the Fabry-Perot photograph it was deduced that this induced non-linear effect was stimulated Brillouin scattering (see theoretical Chapter III). For even higher absorption in the Q-switch a limit was reached beyond which the lasing action could not be initiated. The gain resulting from the population inversion was then insufficient to counteract the losses of the dye.

The photographs in Plate 5.5 show the characteristics for lasing at threshold. For low thresholds, i.e. low dye concentrations and low flash light energy, the situation was tantamount to that discussed

previously for low dye concentration and high flash light energy, except that under the present conditions the number of spikes were fewer since the input energy was lower. For higher threshold conditions a single powerful pulse was produced having a well defined frequency. In this situation the state of inversion in the ruby rod was such that after depletion there was insufficient residual inversion and flash light energy to generate another light pulse. This situation satisfies the optimum conditions for lasing. As the threshold was now raised, increasingly powerful single pulse outputs were obtained until, again at very high powers, stimulated scattering was initiated in the Q-switch.

CHAPTER VI

EXCITED STATE ABSORPTION IN SATURABLE ABSORBERS

6.1 INTRODUCTION AND THEORETICAL CONSIDERATIONS

It was shown earlier in the theoretical section on saturable absorbers that, at high electric field intensities, there occurs, in organic dye solutions, an intensity dependent reduction of the absorptions coefficient. It is because of this phenomenon that dyes are used for the Q-switching of lasers. In those dyes suitable for Q-switching it is the transition from the ground state (0) to the first excited state (1) which is responsible for the absorption. The absorption coefficient is reduced when the laser intensity is such that the population of state (1) approaches that of state (0). There is however a residual absorption due to the transition from (1) to the second excited singlet state (2)[42,147]. This process is known as excited state absorption. The subsequent spontaneous transition (2) to (0) results in a blue fluorescence[43]. This fluorescence was first observed by the author when conducting some totally independent experiments. More rigorous investigations into this effect were made at a later date, the results of which are submitted in this chapter and were also recently published[40].

As a theoretical model we can consider the dye molecules as having a ground state (0) and two excited singlet states (1 and 2) where the energy gap between levels (0) and (1) and between levels (1) and (2) are equal. Let the dye be illuminated with photons of energy $h\nu$ equal to the energy of these gaps.

Then the population of molecules in the ground, first and second states are given by the following rate equations: (see Plate 6.1).

Plate 6.1

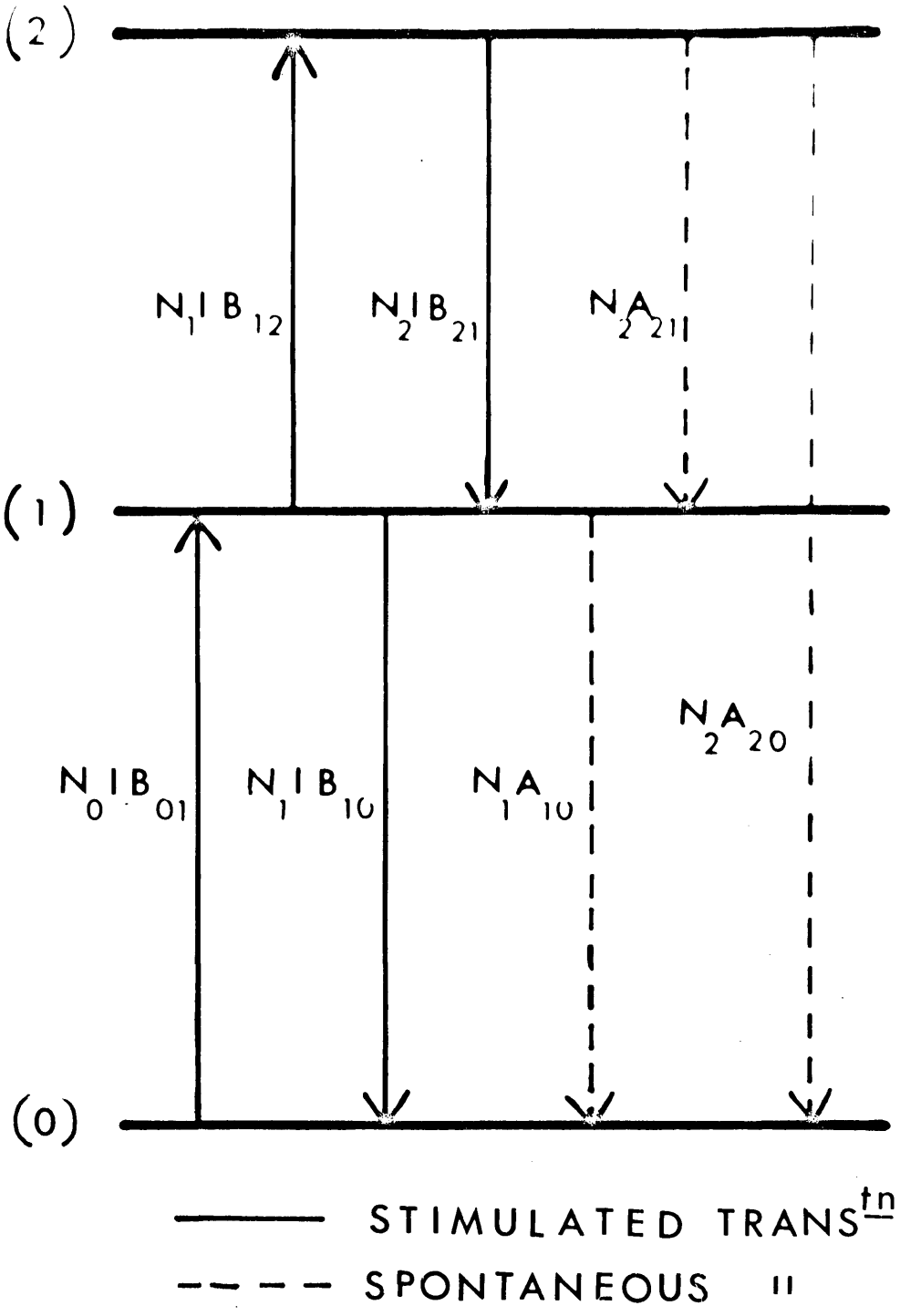

Energy Level Diagram Showing Excited State Absorption

$$\frac{dN_0}{dt} = - N_0 B_{01} I + N_2 A_{20} + N_1 (B_{10} I + A_{10})$$

$$\frac{dN_1}{dt} = N_0 B_{01} I + N_2(A_{21} - A_{20} + B_{21} I) - N_1(A_{10} + B_{12} I + B_{10} I)$$

$$\frac{dN_2}{dt} = N_1 B_{12} I - N_2(A_{21} + B_{21} I)$$

where $N = N_0 + N_1 + N_2$ = total number of molecules/cc.

A_{mn} and B_{mn} are the Einstein coefficients: A_{mn} is the spontaneous transition probability and is equal to $\frac{1}{T_{mn}}$, the reciprocal of the life-time of a molecule in a particular state. B_{mn} is the stimulated transition probability per photon and has the property $B_{mn} = B_{nm}$. In more common notation B_{mn} is an absorption cross-section given by σ_{mn}. I is the optical intensity in photons/unit surface area/second.

Since the pertinent relaxation rates in the process we are describing are fast relative to the laser pulse duration, a steady state situation prevails. Hence, from the above equations, the equilibrium population of state (2) is:

$$N_2 = I^2 \sigma_1 \sigma_2 N \left\{ I\sigma_2 (3I\,\sigma_1 + T_1^{-1} + T_{20}^{-1}) + (2I\,\sigma_1 + T_1^{-1})\, T_2^{-1} \right\}^{-1} ,$$

where σ_1 , σ_2 are absorption cross sections for transitions (0) → (1) and (1) → (2) respectively. T_1 , T_2 are the total lifetimes of levels (1) and (2) respectively. T_{20} is the lifetime characterising the transition (2) → (0).

When I is very small :

$$N_2 = I^2 \sigma_1 \sigma_2 T_1 T_2 N ,$$

thus the response is square law. When I is very large:

$$N_2 = \tfrac{1}{3} N ,$$

and there are equal populations of the three states.

Now the lifetime of state (2) for the dyes used[43,148] was about 10^{-13}secs, whilst that of state (1) was greater than or approximately equal to 10^{-10}secs. (See references 149,150). Also the low excited-state absorption for these dyes indicate[43] that $\sigma_2 \ll \sigma_1$. Thus the transition (0) → (1) saturates at a very much lower power than (1)→ (2) and:

$$N_2 = I^2 \sigma_1\sigma_2 \, N(3I^2\sigma_1\sigma_2 + 2I\,\sigma_1\,T_2^{-1} + T_1^{-1}\,T_2^{-1})^{-1} .$$

Now for $I\,\sigma_2 \ll T_2^{-1}$, i.e. for powers insufficient to saturate the transitions (1) → (2) :

$$N_2 = \frac{I^2\,\sigma_1\sigma_2\,N}{(2I\,\sigma_1 + T_1^{-1})T_2^{-1}} .$$

Let $$\sigma_1^{-1}\,T_1^{-1} = I_c ,$$

then:

$$N_2 = \sigma_2 N T_2\, I_c \frac{I^2/I_c^2}{1 + 2I/I_c} .$$

Since the number of fluorescent transitions (2) → (0) is proportional to N_2 :

$$\text{fluorescence} \propto \frac{I^2/I_c^2}{1 + 2I/I_c} .$$

6.2 EXPERIMENTAL DETAILS

A Q-switched ruby laser with an output of up to 200 MW and a pulse duration of about 15 nsecs was used to excite a dye polution. This solution was contained in a short cell which was misaligned with respect to the ruby beam. The light intensity incident on this cell was controlled by varying the concentration of a solution of copper sulphate placed in the path of the ruby laser light. The transmission curve for copper acetate is shown in Plate 6.2. This intensity was monitored using a calibrated beam splitter and photodiode connected to a Tektronix 454 oscilloscope. The blue fluorescence was detected by a Mullard 56 AVP photomultiplier connected to the same oscilloscope via a delay line. Scattered ruby laser light and red fluorescence was eliminated by use of

Plate 6.2

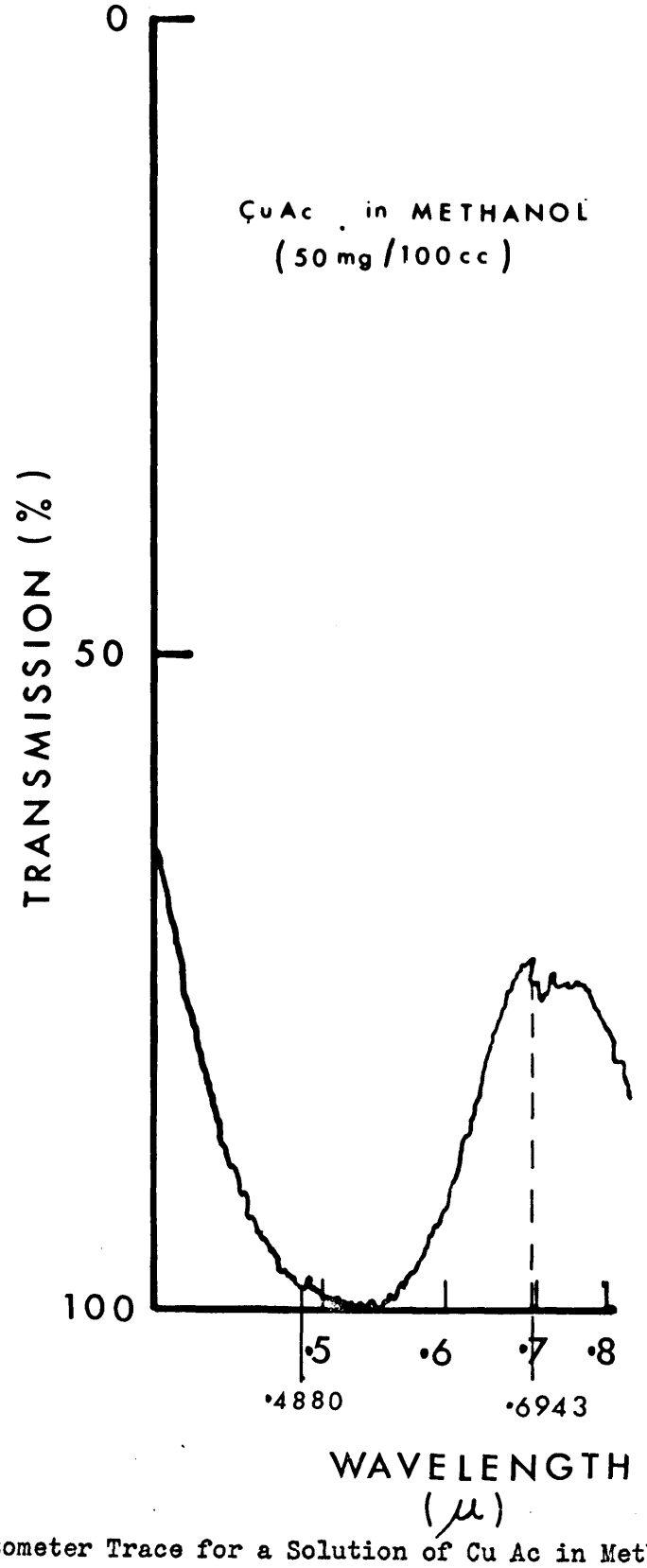

Spectrophotometer Trace for a Solution of Cu Ac in Methanol

Jena B.G.18 green filters. Noise due to the flashlight from the ruby cavity was minimised by use of a Wratten 29 filter placed after the copper acetate attenuation. Two photon absorption in this filter caused a small amount of blue fluorescence. This gave a negligible signal on the photomultiplier providing the distance of the dye cell from the filter was sufficiently long. It was necessary to use dilute dye solutions contained in a narrow cell in order to minimise intensity variations due to absorption of the ruby beam. The thin misaligned cell also eliminated the possibility of stimulated non-linear effects.

Spectrum analysis of the blue fluorescence was made using a diffraction grating which was scanned by a 56 AVP photomultiplier .

6.3 RESULTS AND DISCUSSION

Measurements of fluorescence as a function of incident intensity were first obtained for the standard two photon absorber Rhodamine G. The square law curve (see Plate 6.3) obtained from these results was used as a norm for comparing with the anomalous results obtained from the other dyes.

The other dyes used in this investigation were chloroaluminium-phalocyanine (CA P)[43], cryptocyanine and vanadium-phthalocyanine (Vn OPc). Curves A and B of Plate 6.4 show the dependence of fluorescence on incident laser intensity for solutions of CAP in chloronaphthalene and in methanol respectively.

At low inputs the fluorescence of both solutions follows the expected square law dependence on input intensity. With an increase of intensity this dependence changes and tends towards a linear law as predicted by the theoretical law (the nonlinear breakdown of the law at still higher powers is attributed to chemical decomposition of the solution). This

Plate 6.3

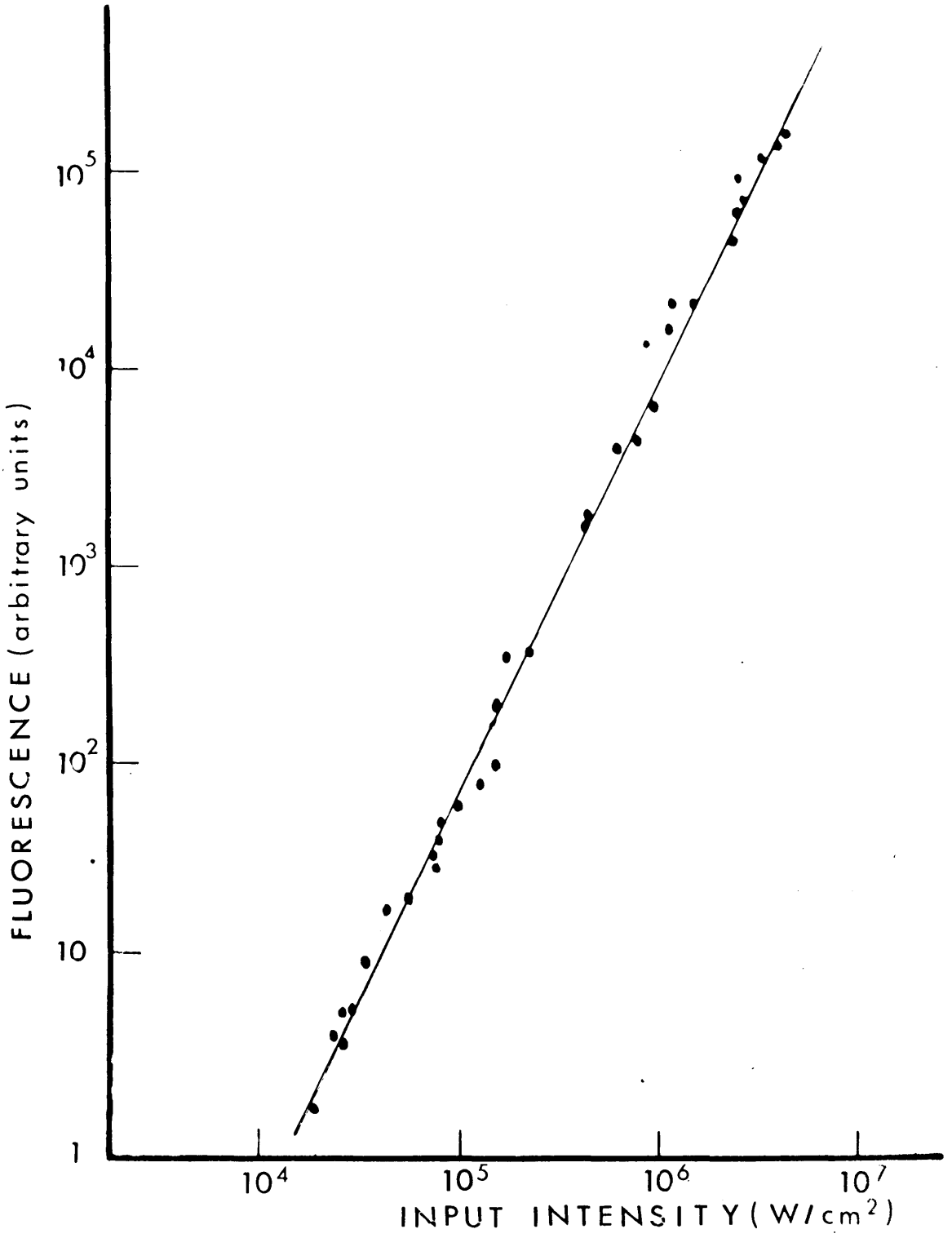

Two-Photon Absorption of Ruby Laser Light in RhodammeG

Plate 6.4

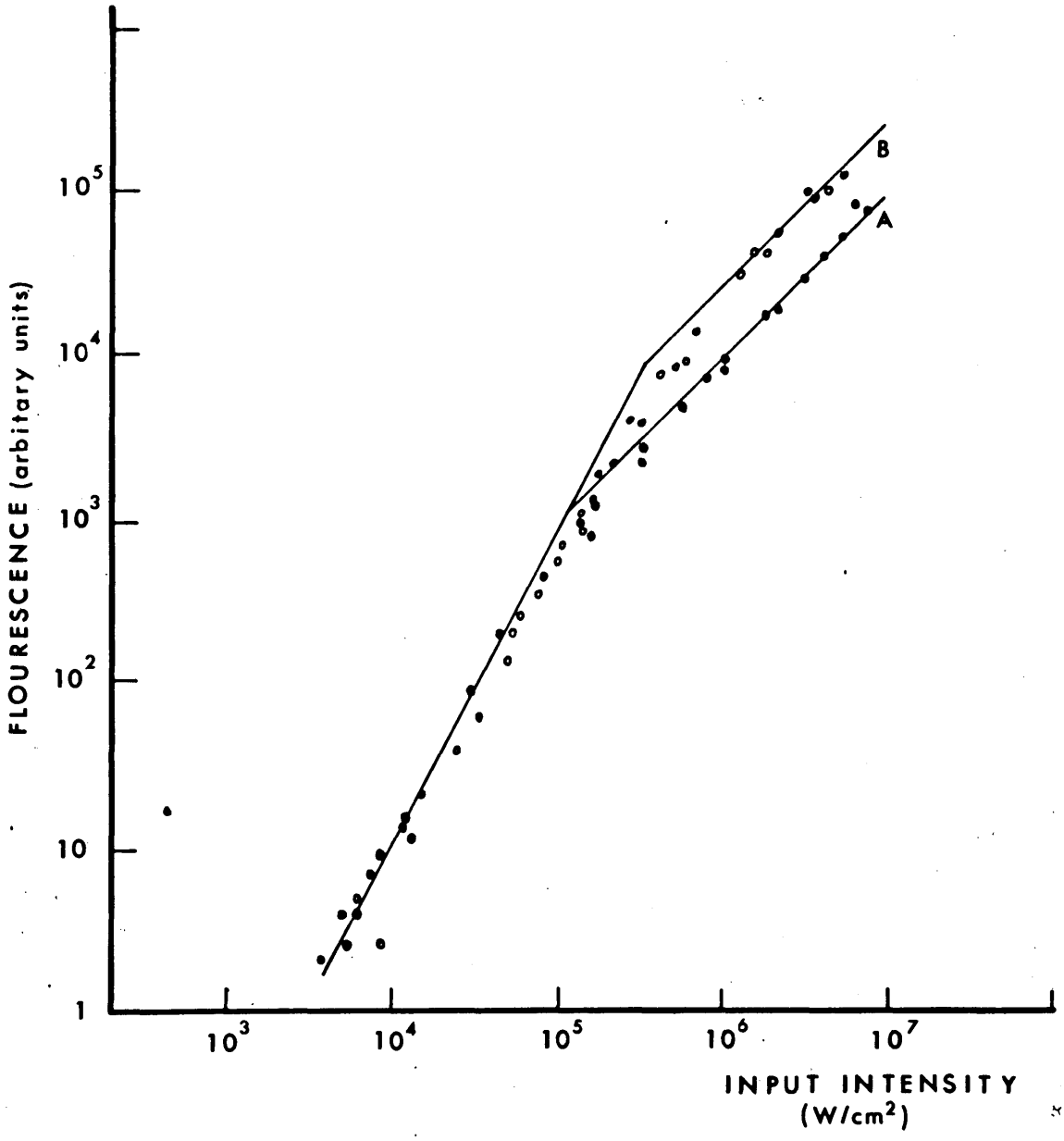

Excited State Absorption of CAP in
Chloronaphthalene (curve A) in Methanol (curve B)

corresponded to a saturation of the first excited singlet state of the dye. The characteristic intensity I_c at which this occurred was about 10^5 W cm^{-2} in the case of chloronaphthalene solution and about 3×10^5W cm^{-2} for the methanol solution. The different powers I_c for the two solutions are due to the different positions of the peaks of their absorption spectra. The peak of the spectrum of the solution in chloronaphthalene is much closer to the ruby wavelength than that of the solution in methanol. Consequently the absorption cross-section σ_1 is much greater, and I_c much smaller, in this case.

The dependence of fluorescence on input intensity for a solution of cryptocyanine in methanol (Plate 6.5) has the same features as that for CAP in chloronaphthalene. However, although the absorption cross-section for cryptocyanine in methanol ($\sigma_1 = 8{\cdot}1 \times 10^{-16}$ cm^2) is greater than that chloronaphthalene[149,150] ($\sigma_1 = 3 \times 10^{-16}$ cm^2), I_c is greater than that for CAP in chloronaphthalene ($\sigma_1 = 3 \times 10^{-16}$ cm^2) (references 149,150). I_c is greater for the cryptocyanine solution be over an order of magnitude ($I_c \sim 2{\cdot}5 \times 10^6$ W cm^{-2}). This is a result of the very much shorter lifetime of the first excited state of cryptocyanine ($T_1 \sim 10^{-10}$sec). For CAP[149,150], $T_1 \sim 5\ 10^{-9}$ sec. Thus theoretically:

$$\frac{I_c(\text{Cryptocyanine})}{I_c(\text{CAP})} \sim 25 \ .$$

This was confirmed experimentally.

The dependence of fluorescence on input intensity for the Vn OPc in nitrobenzene (Plate 6.6) is similar to that of other solutions. In this case saturation occurred at about $2{\cdot}5 \times 10^5$ W cm^{-2} as expected from the values $\sigma_1 = 4{\cdot}1\ \ 10^{-16}$ cm^2 and $T_1 \simeq 2\ \ 10^{-9}$ secs. These values of I_c confirm the results obtained by other workers using transmission and single photon fluorescence measurements[149-151].

Plate 6.5

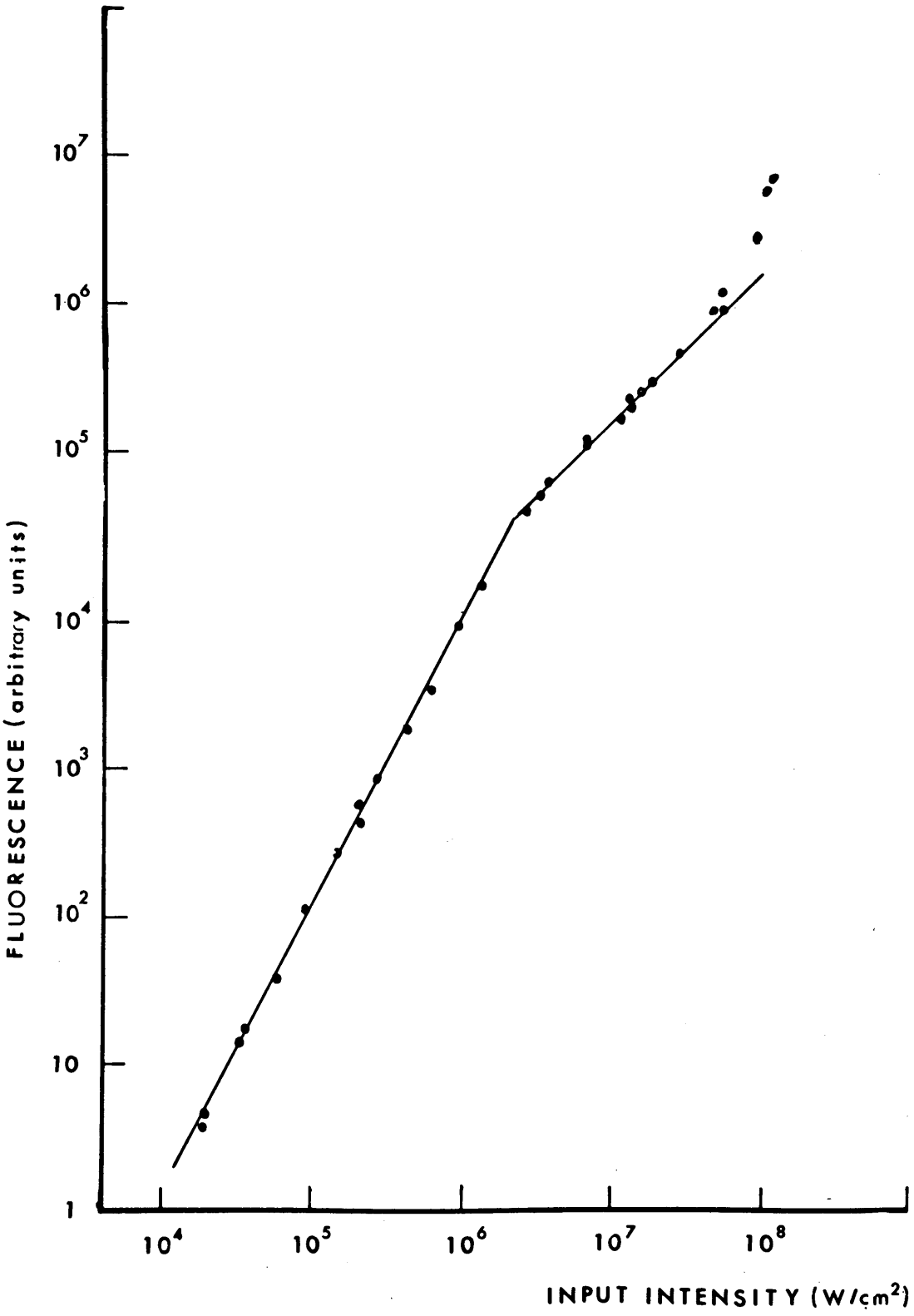

Excited State Absorption in Cryptocyanine in Methanol

Plate 6.6

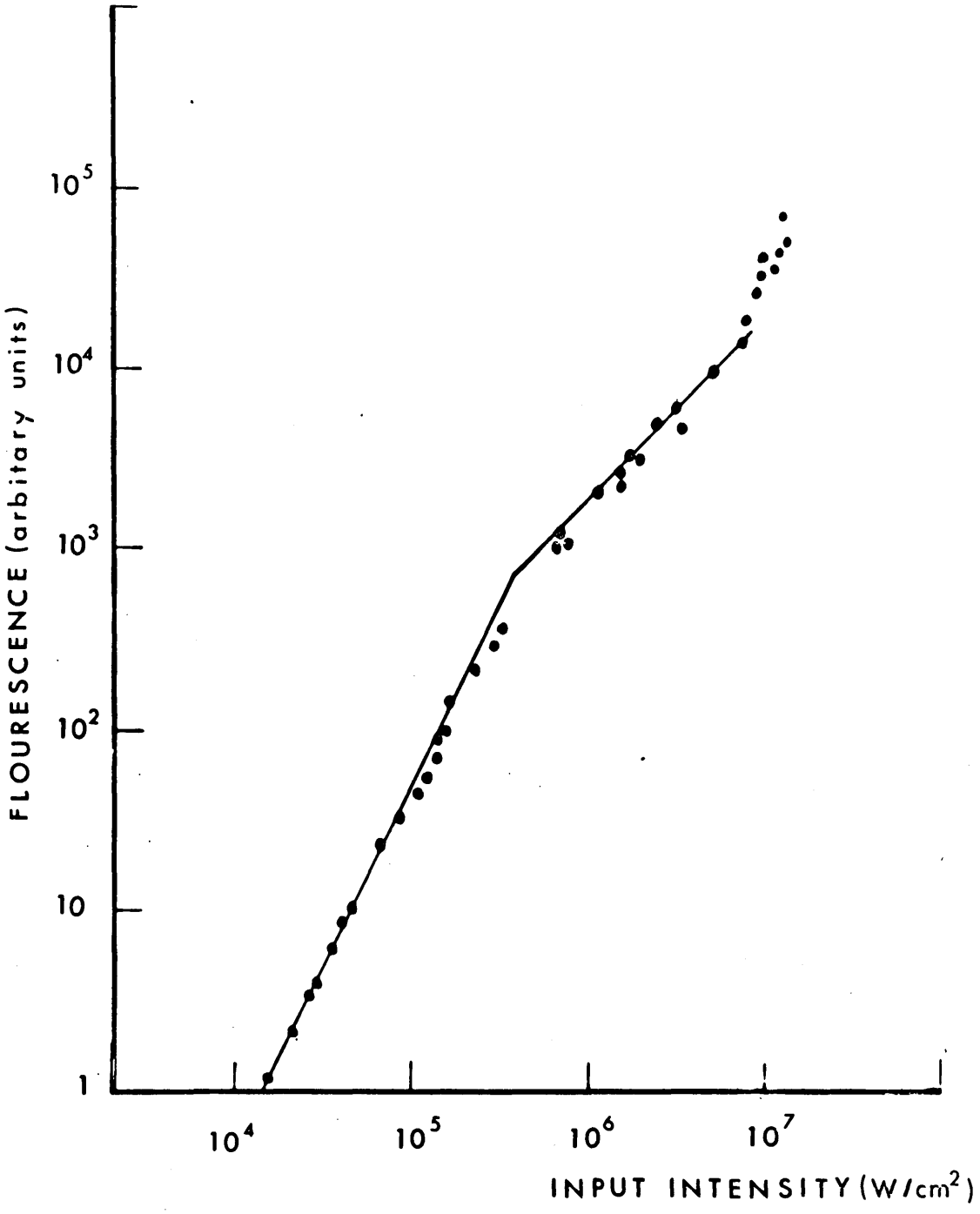

Excited State Absorption From Vn OPc in Nitrobenzene

The spectrum of the blue fluorescence was in all cases a fairly broad band (width about 800 Å). The peak of the emission was about 4000 Å for CAP[43] and at somewhat longer wavelength, about 4600 Å in the case of cryptocyanine (Plate 6.7). The true spectrum of Vn OPc could not be determined because of absorption of wavelengths less than 4400 Å by the nitrobenzene solvent.

A small amount of blue fluorescence was observed from the solvents chloronaphthalene and nitrobenzene. This followed a square-law dependence on input power (Plate 6.8). These solvents have no absorption at the ruby frequency, but have a considerable absorption at twice this frequency (Plate 6.9). This fluorescence was therefore attributed to two-photon absorption (see theoretical Chapter III).

At very high intensities chemical breakdown of the solvents occurred, accompanied by a marked increase in fluorescence as seen on the graphs. A change in the fluorescence mechanism at these intensities was also suggested by the marked increase in the relaxation time of the fluorescence (Plate 6.8). This reached about 50 nsec, whereas at low intensities it was considerably shorter than the laser pulse duration (~ 15 nsec.).

Plate 6.7

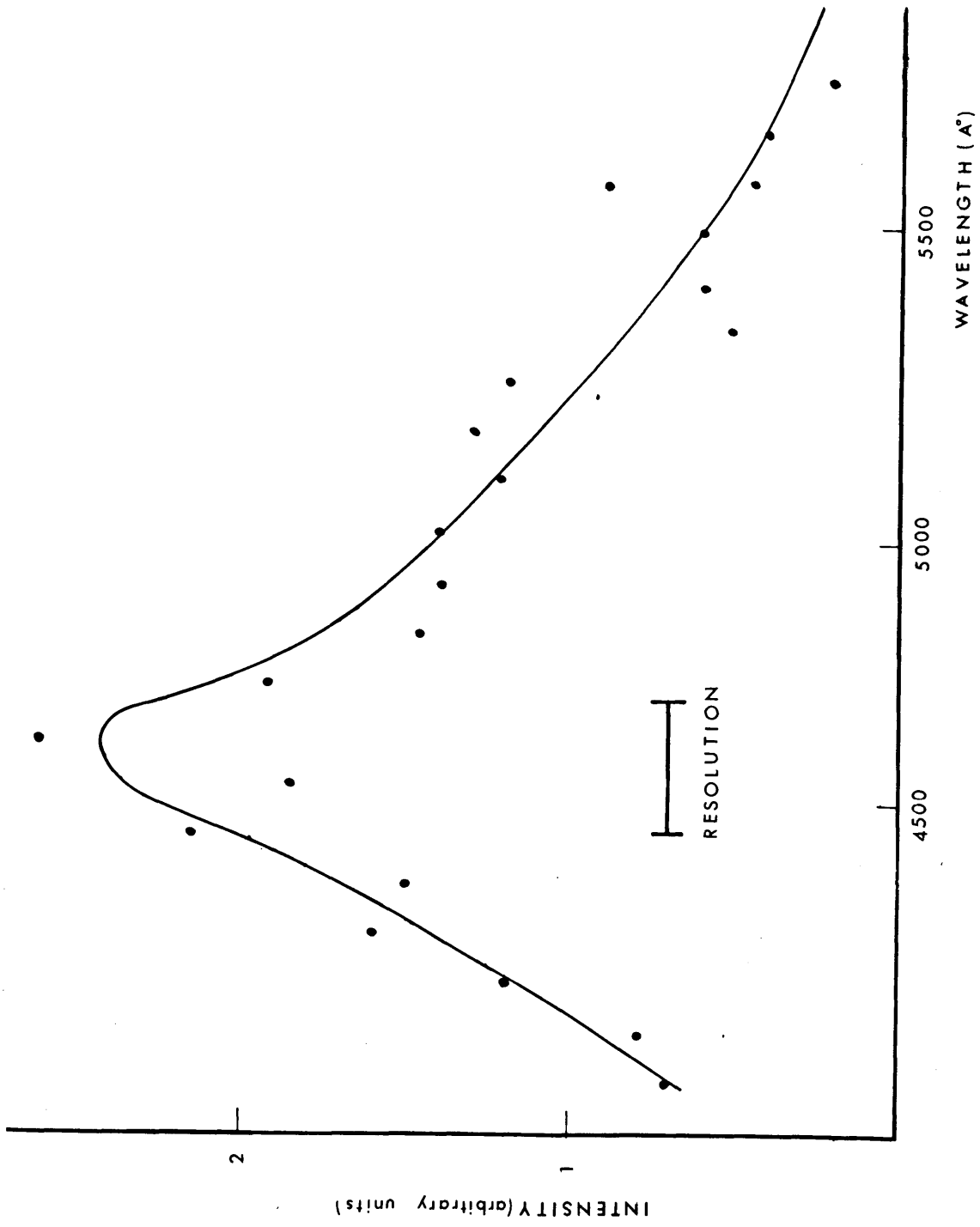

Variation of Fluorescence from Excited State Absorption with Wavelength for Cryptocyanine in Methanol

Plate 6.8

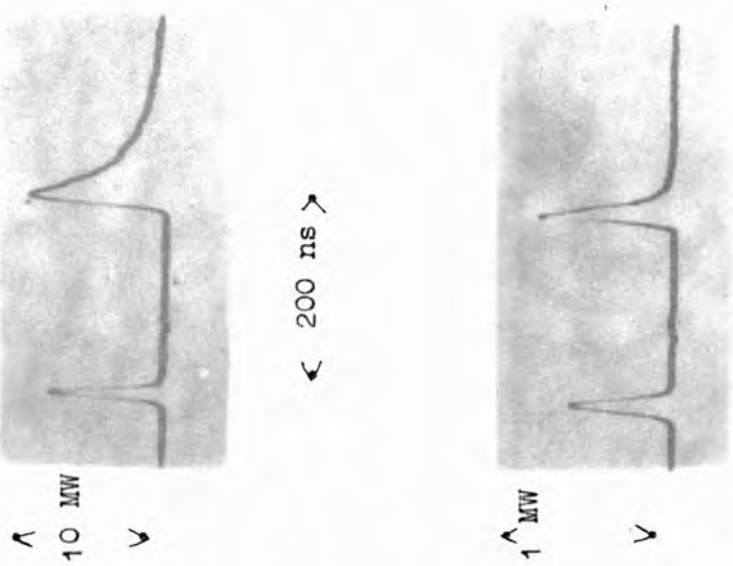

Chemical Breakdown of Solvents

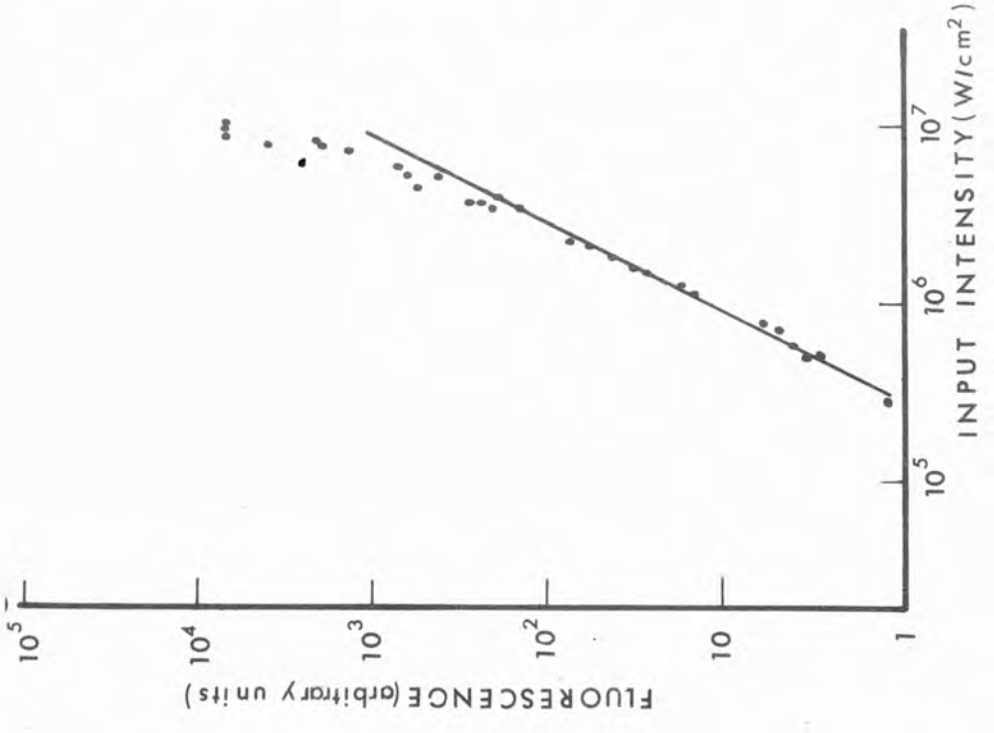

Two Photon Absorption from Chloronaphthalene

Plate 6.9

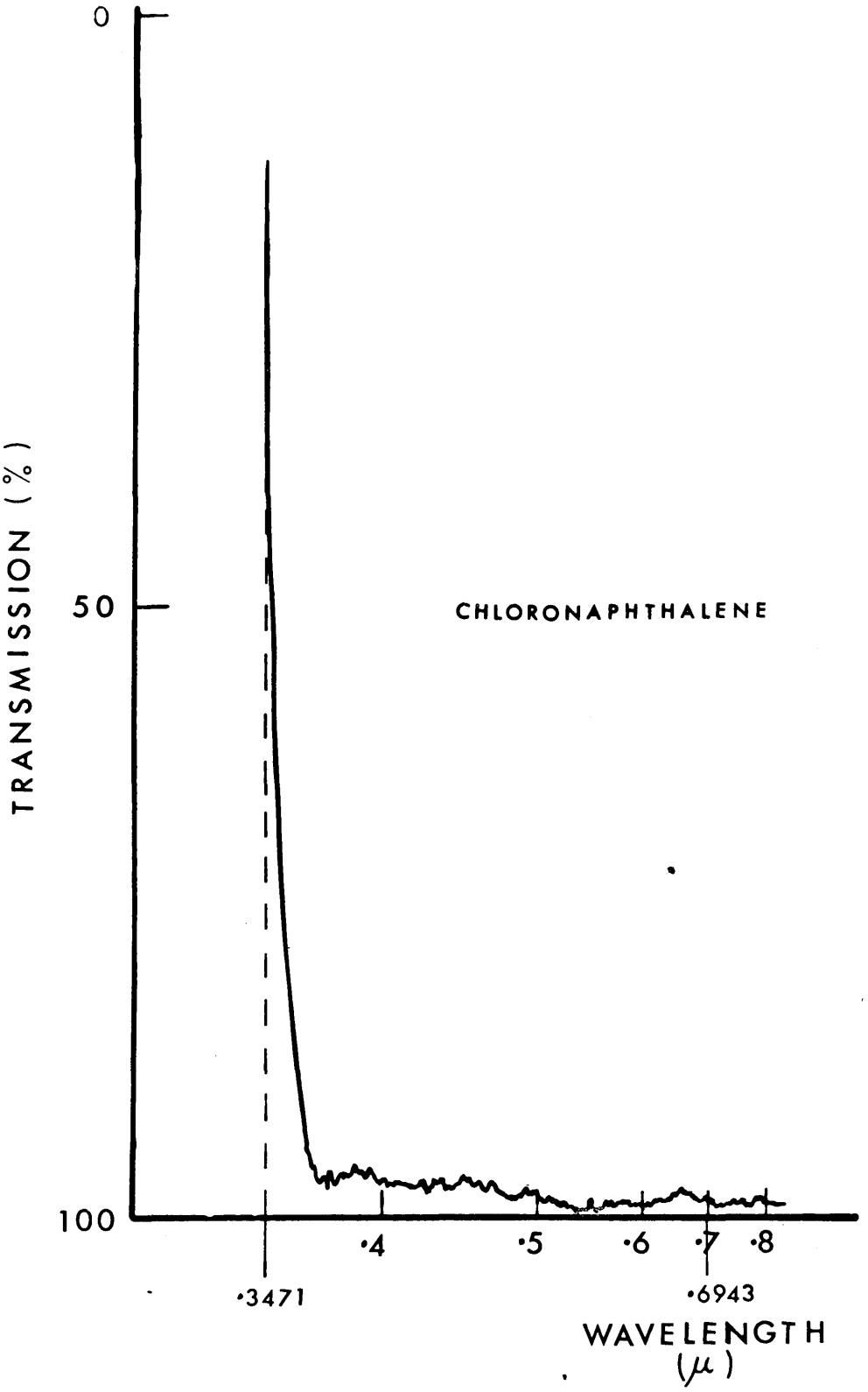

Spectrophotometer trace of Choronaphthalene

C H A P T E R VII

QUALITATIVE ASPECTS OF SELF-FOCUSING AND DE-FOCUSING

7.1 INTRODUCTION

The general theoretical outline of self-trapping and de-focusing was considered earlier in the theoretical chapter. Generally these phenomena arise from an intensity dependent change n of refractive index in the medium given by:

$$n = n_0 + n\,|A|^2$$

In a medium for which $n < 0$, de-focusing will occur and conversely, for a medium in which $n > 0$, self-focusing and self-trapping dominates.

The general features of self-trapping of laser light are shown in Plate 7.1, Fig.(a). Such self-trapping was obtained by focusing the 200 MW output from a ruby laser through a 10 cm focal length lens into a glass cell containing water. All photographs in Plate 7.1 are approximately to scale, and were taken at 90^0 to the direction of propagation of the laser beam. As seen from Fig. (a), the laser beam came to a focus at the centre of the cell and then continued forward in the form of a long thin pencil of light. Near the focal region there appears to be breakdown and shock wave formation. This was attributed to the high electric fields in the region which were in the order of 10^7 V/cm. Termination of the self-trapped beam was probably governed by dissipative processes such as multi-photon absorption and thermal heating[123]. The former process converts the coherent forward propagating laser radiation into fluorescence radiating radially and with a different frequency. The latter process results in a decrease in refractive index in the filament since for water $\partial n/\partial T < 0$. Both processes could lower the laser light flux to such an extent that the filament could no longer sustain itself.

Plate 7.1

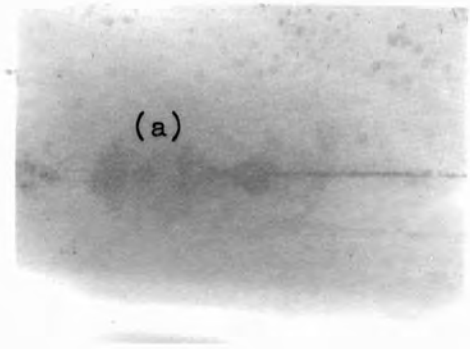

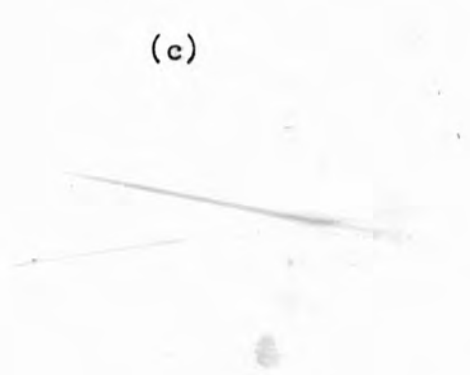

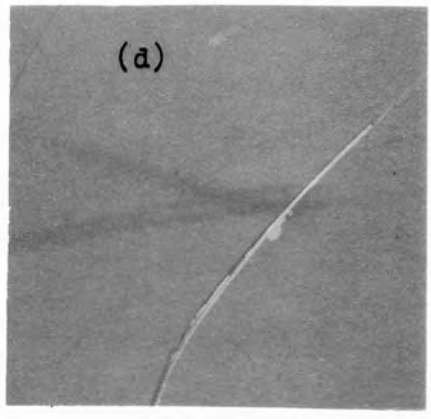

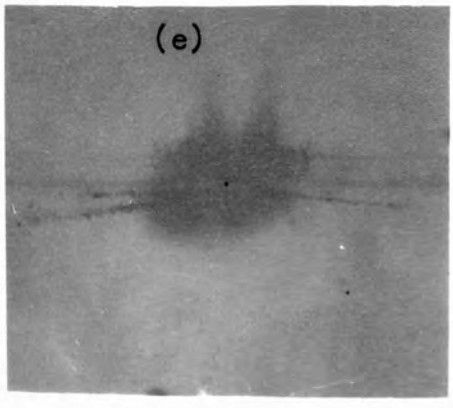

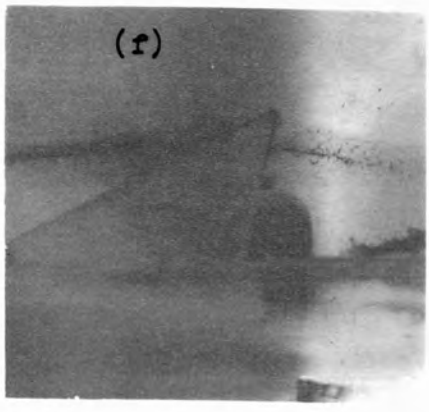

Phenomena Arising from Self-trapped Laser Light

7.2 INTERACTION OF SELF-TRAPPED LASER BEAMS

The experimental arrangement for producing two interacting highly intense laser beams is shown in Plate 7.2. The 200 MW, 20 nsec output from the Q-switched ruby laser was divided into two by a prism and then subsequently focused and directed into a glass cell containing water, so that the laser beams crossed each other a short distance (~ 3 cm) after their focal points.

The results of the investigation are shown in Plate 7.1 (Figs (b), (c) & (d)). The results shown in Fig.(b) were obtained from laser beam interactions in high purity distilled water. It is seen that the structural formation is rather inconsistent and there appears to be considerable laser scatter off a large number of discrete centres along the beam. These observations are in strong contrast with those obtained using water that had stood in the laboratory for a few days. These differences can be attributed to laser scattering off the oxygen content of the two types of water.

It seems feasible that the water that had stood for a considerable time had gradually become de-oxygenized. However, for water of the other kind, the oxygen content would have been relatively high, and consequently light scatter from these discrete scattering centres would be substantially greater.

When the two powerful laser beams, of the same frequency, were crossed, a spatially variable and temporally constant change in the index of refraction occurred. This produced a scattering of the laser beams with the scattered radiation for each of the initial beams being directed along the other beam. The first reported observations of this phenomenon were made by the author and co-workers in 1967[152]. Subsequently, in a theoretical note by Chaban[157], an explanation has been given of the

Plate 7.2

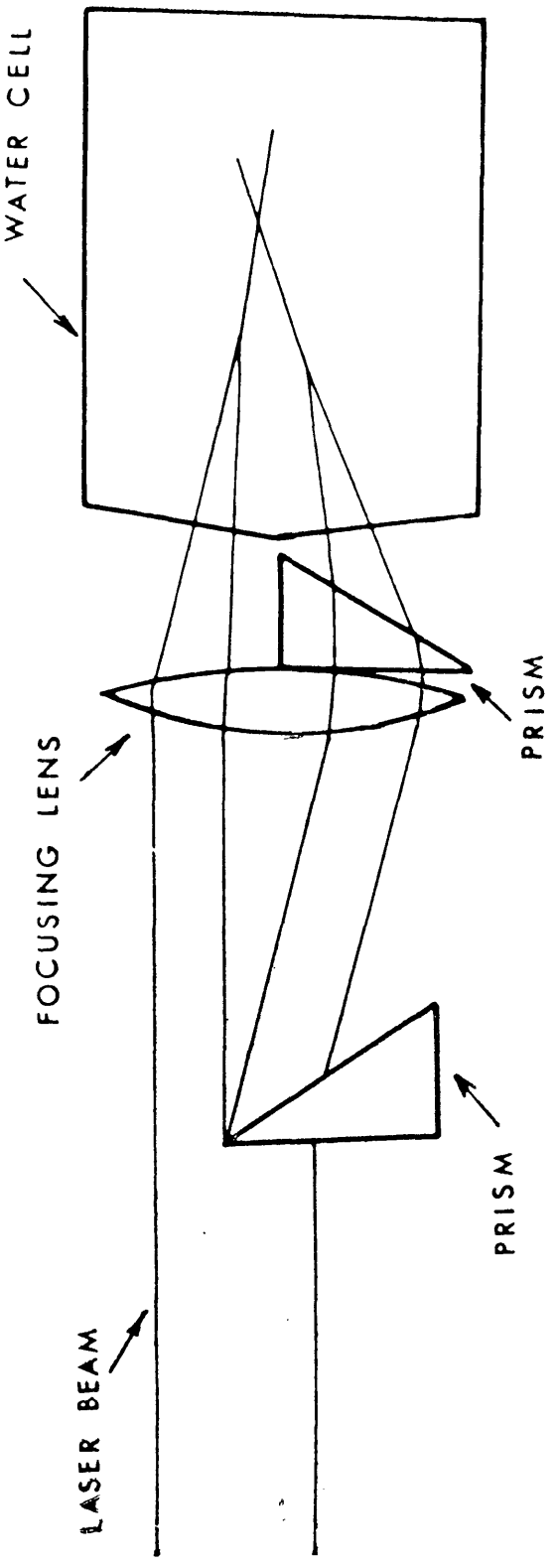

Experimental Arrangement

mechanism by which this scattering process arises. One can consider that the two crossed oscillating electric fields produce a phase grating in the form of a Moire fringe pattern. This grating results from intensity dependent refractive index changes (such processes have been discussed in detail in Chapter III, Sections 3.10 - 3.16)

From the theoretical development of Chapter III, Sections 3.10 - 3.16 it is inferred that two electric fields, of the same frequency incident upon each other at an angle of θ, and consequently having different wave vectors k_1 and k_2, produce a refractive index modulation of the form:

$$\Delta n = n A_1 A_2^* e^{j(k_1 - k_2)\cdot r}$$

where r is a position vector; now since $|k_1| = |k_2|$ and from conservation of momentum considerations (Chapter III, Section 3.17) we have:

$$k_1 - k_2 = 2 |k_1| \sin \frac{\theta}{2} .$$

Hence the refractive index modulation has a wavelength $2 |k_1| \sin \frac{\theta}{2}$.

It is therefore easy to see that both electric waves defined by (ω, k_1) and (ω, k_2) will satisfy the Bragg condition for reflection off this grating, and that the subsequent reflected beams will be directed along the forward path of their neighbour. The experimental results are shown in Plate 7.1, Figs.(c) & (d). It is noticed that in these photographs the more intense beam appears to lose more energy than the other beam. This is as expected, since a proportionally higher amount of light was reflected from the powerful beam into the weaker beam, than that reflected from the weaker into the stronger beam. It seems probable that the intensity dependent refractive index arose from electrostriction and Kerr effects since these are the dominant effects existing in non-absorbing liquids (see Chapter III, Sections 3.10 - 3.16).

7.3 SELF-BENDING OF ASYMMETRICAL LIGHT BEAMS

First reports of the self-bending of asymmetric light beams and of a self-trapped filament were made by the author and co-worker in 1967[152]. These observations have subsequently been confirmed both experimentally[153] and theoretically[154].

A study of the geometrical layout of the optical components shown in Plate 7.2, shows fairly clearly that a certain degree of asymmetry was produced in the electric field distribution of the laser beams in the liquid. This effect was particularly pronounced for the lower beam, where the field flux was considerably higher on the lower edge in a region at and before the focus (see Plate 7.1, Fig.(c) and also the enclosed publication[152] where the region is shown more clearly.

The intensity dependent refractive index changes are then much higher in this region than in the remainder of the focusing light cone. Consequently a refractive index gradient was set up across the beam. This gradient produced a general bending of the highly intense light beam emerging from the focal region in a direction in which the refraction was maximal (see Fig.(c) in conjunction with the photograph in the enclosed publication). This phenomenon is in agreement with the theoretical conclusion derived later by Kaplan[154]. In his paper Kaplan derives an equation for the self-bending of the form:

$$\varphi = \frac{16\,\pi^2 n\,P}{\lambda_o\, n_o^2\, c\, a}$$

where n is the nonlinear intensity dependent refractive index, P is the total power of the laser beam, λ_o the wavelength of the incident light, n_o the normal refractive index, c the velocity of light, a is a mean cross-sectional diameter of the laser beam and φ is the angle of bending.

From the photograph in the publication the angle φ , between the direction of the 'filament type' light beam emerging from the focus, and the axis of the focal cone, is $\sim 4^{o}$. The laser power in this beam was $\sim$ 100 MW and a value for a at the bending region was $\sim 0{\cdot}05$ cm. Substituting these values into Kaplan's equation gives a value for the intensity dependent refractive index of $n \sim 0{\cdot}85 \times 10^{-13}$ c.g.s.e.s.u. This is in fair agreement with the value derived by Chiao et al[12]: of $n \sim 2 \times 10^{-13}$ c.g.s.e.s.u.

Another very striking feature in the asymmetrical lower beam was the presence of a parasitic, fine, self-trapped filament that was initially directed in an upward direction relative to the main beam, and then subsequently bent down, in a direction in which the refraction was maximal: Figs.(c) and (d). It seems likely that this filament was formed in the intense regions of the lower part of the focusing cone, the filamentary formation being governed by the laser power threshold condition $P_{cr} = \lambda_o^2 c(1{\cdot}22)^2/64\, n_2$ (See Chapter III, Section 3.18). This filament then propagated through the focal region and on emergence suffered refraction due to the background refractive index gradient. The resulting bent filament, once beyond the influence of the index gradient propagated in a straight line for a further 4 or 5 cms.

7.4 REFLECTION AND REFRACTION OF SELF-TRAPPED LASER LIGHT

(a) Reflection of Self-Trapped Laser Light

In the experimental apparatus shown in Plate 7.2, the upper laser beam was masked off and the glass cell half filled with water. By judicious adjustment of the prisms, the lower light beam was totally internally reflected from the water-air interface (Plate 7.1, Fig.(e). At the interface there was a considerable disruption of the liquid causing explosions of the water, and the reflected light retained its filamentry

structure. An interesting consequence of high intensity light interaction at an interface is the bending of the boundary surface. Since a medium with a larger refractive index corresponds to a large field energy density (note that this refractive index is enhanced by the second order intensity dependent effects in a highly intense light beam) a light-pressure force is directed towards the medium with the smaller optical density. In a paper by Kats et al[155] where this phenomenon was theoretically considered, they showed that light outputs from standard pulsed laser systems could produce surface bending with a radius of curvature of $\sim$ 12 cm. Thus a light beam travelling through a liquid towards an air interface would see a concave surface and after subsequent total internal reflection would therefore become focused. From the photograph Fig.(e) it is difficult to ascertain whether self-focusing or trapping occurred before the boundary interaction region, or whether these effects derived from such a liquid curvature. However, it can be safely concluded that the resulting self-trapping suffered no loss due to the total internal reflection.

(b) Refraction of Self-Trapped Laser Light

In this experiment, a self-trapped light beam was directed through a prism immersed in water. The result is shown in Plate 7.1, Fig.(f). At the liquid-glass interface, there was again an explosion resulting in a shock wave due, in all probability, to the radiation pressure at the interface. The passage of the filament through the prism was characterised by a trail of small bubbles. From the photograph it is seen that the filament still retained its structure after emerging from the prism. It can therefore be concluded that the loss mechanism in the prism that produced the filamentary damage, was not sufficient to deplete the laser power below that required to sustain self-trapping. The threshold power for self-trapping is typically of the order of 1 $\sim$ 10 mW.

It seems likely that this damage was caused by stimulated Brillouin scattering (see Chapter III, Section 3.11). In such a process, the generated acoustic wave (typical power ~ 1 kilowatt), could produce high local stresses or, by its damping, result in local heating of the medium. A necessary threshold power for the onset of S.B.S. is typically 10^4 MW/cm^2. It is therefore seen from above that only about 0·1% of the power need travel in the forward direction to sustain self-trapping. This requirement is easily met under these conditions since, even at powers much greater than the threshold power for S.B.S., only 80 or 90% of the forward travelling light is scattered in the forward direction.

It should be mentioned at this point that damage of a similar nature occurred in two or three of the ruby rods used during the course of the experiment comprising this thesis. It seems very likely that this damage resulted from the same effect; a conclusion that is supported by the results of a paper published by Gibson on Ruby laser damage[34].

7.5 DE-FOCUSING OF CONTINUOUS LASER LIGHT

In these investigations, the continuous laser light output, of power ~ 1 watt, from an argon ion laser (see Chapter IV, Section 4.2) was directed into a quartz cell of length 9 cm and containing nitrobenzene. The subsequent thermal heating produced a decrease in refractive index in the vicinity of the laser beam (See Chapter III, Sections 3.12 and 18 which resulted in de-focusing of the argon light.

The results of this experiment are shown in Plates 7.3 and 7.4. The photographs show the cross-section of the laser beam and were taken from scattered light off a white card placed in the argon beam at a distance of about three metres from the de-focusing liquid.

Plate 7.3

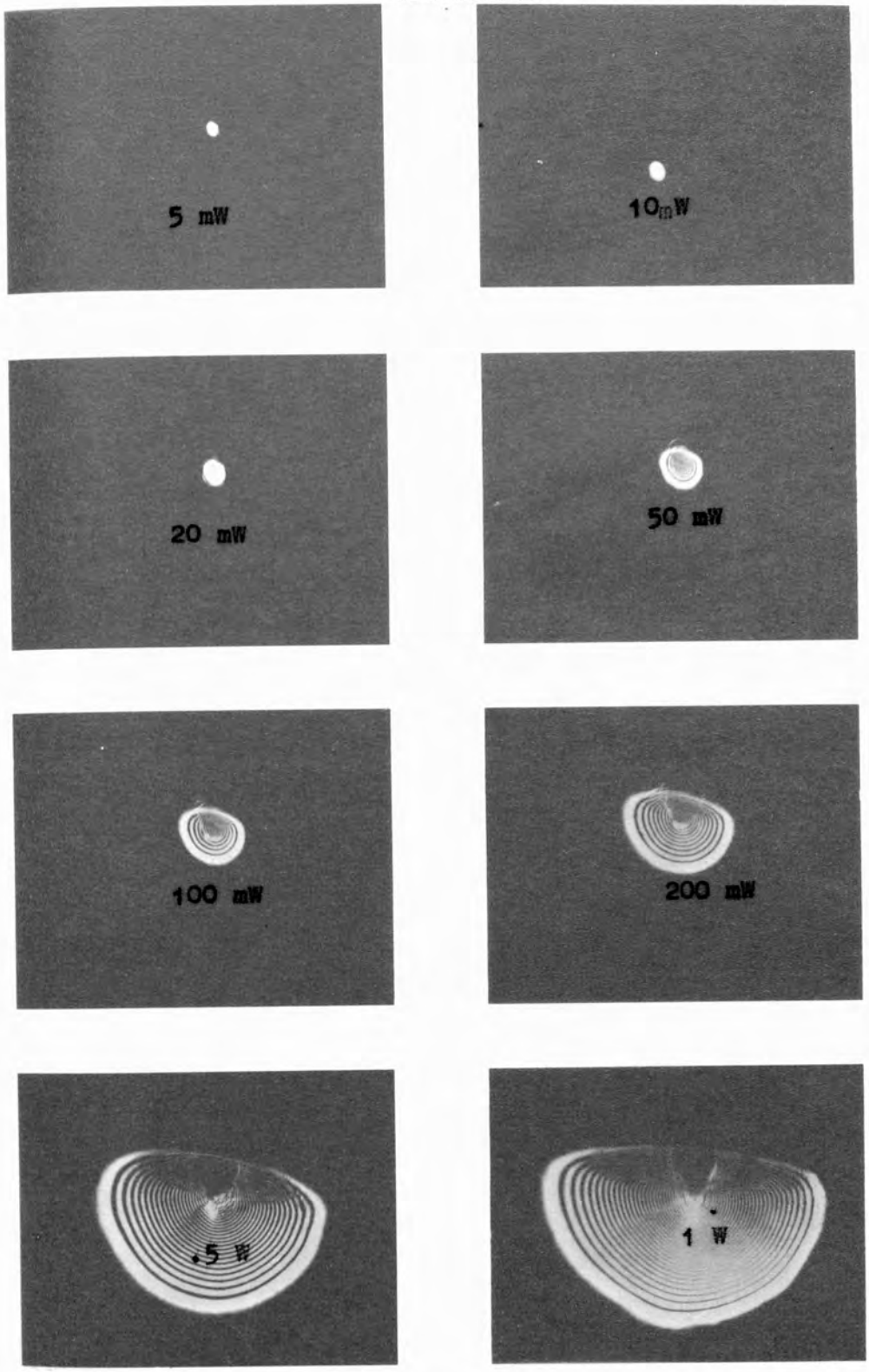

< 1 >

Variation of Argon Laser Light De- focusing with Laser Power

Plate 7.4

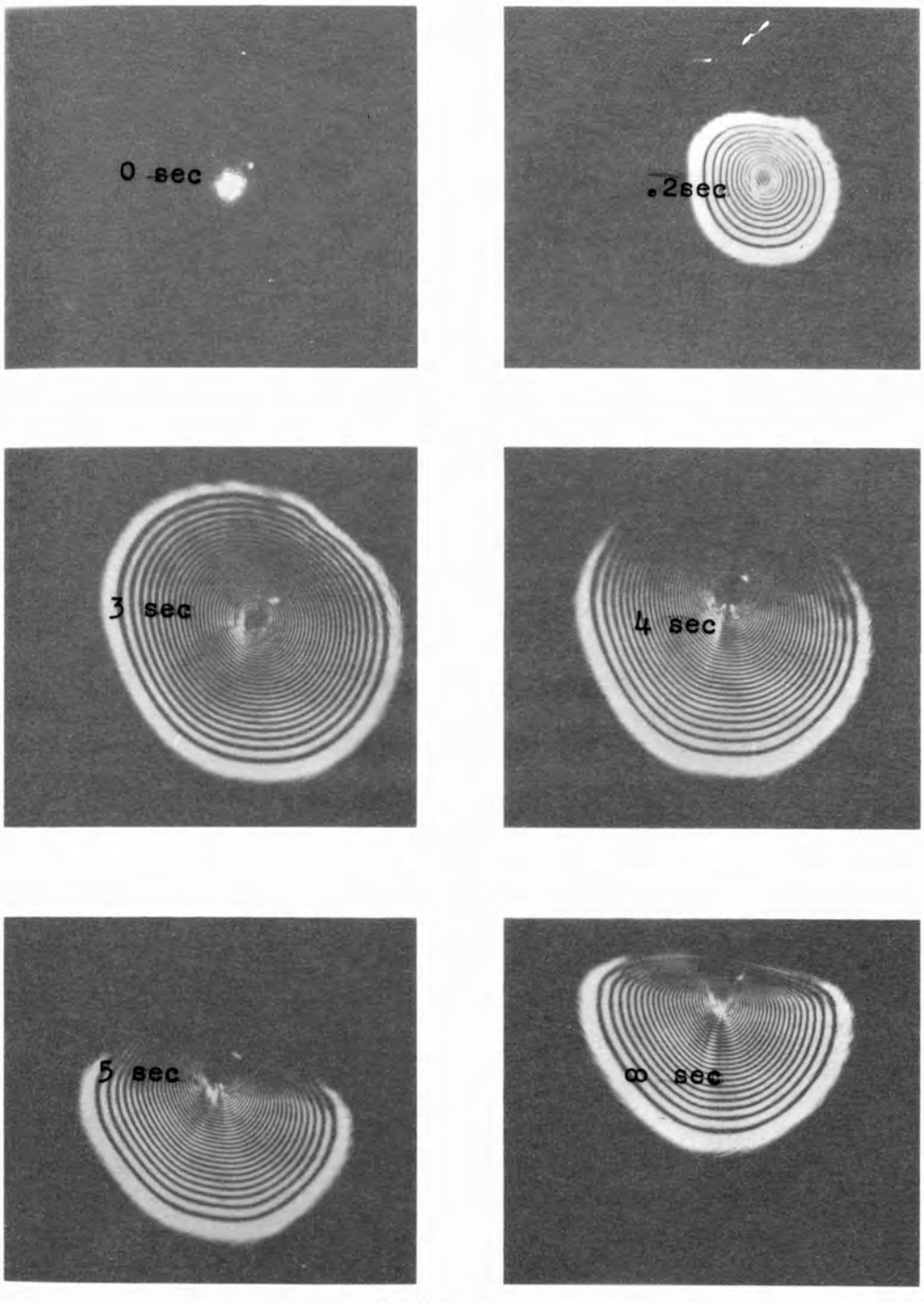

< 1 >

Variation of De-focusing of Argon Laser Light with Time

The spectacular structure in both these sets of photographs was associated with a multiple striation observed in the length of the laser beam when it passed through and emerged from the cell containing nitrobenzene. Both these effects were attributed to interference of the laser beam[17]. In explanation consider the intensity profile of the laser beam. Since this profile was approximately Gaussian in shape, an intensity dependent refractive index gradient was induced across the laser beam such that the refractive index was lowest at the centre, (since $\partial n/\partial t < 0$). Consequently light rays propagating off axially in the central region of the beam experienced an outward refraction greater than that experienced by rays in the facinity of the periphery of the laser beam. The subsequent crossing of the coherent light rays at all points across and along the laser beam produced the interference patterns shown in the photographs.

The photographs of Plate 7.3 show the increase in de-focusing with increasing laser power, and those of Plate 7.4 show the variation of de-focusing with time. The asymmetry occurring in most of the interference patterns is attributed to convection effects. From Plate 7.4 it is seen that for times < 3 secs after the laser was admitted to the liquid, the pattern is symmetrical; convection effects had insufficient time to become apparent. At times > 3 secs there was a general upsurge of relatively hot liquid from an area in the liquid corresponding to the centre of the beam. The temperature gradient in the upward direction was subsequently reduced, resulting in a decrease in the relative divergence of light rays in this region. Hence, as seen from the photographs the fringe separation associated with this area is smaller. It is finally noted from Plate 7.3 that convection effects only become really apparent for laser powers ≥ 50 mW.

Theoretical analyses of the de-focusing phenomena given by Akmanov et al[17] show that the increase in divergence $(\theta - \theta_o)$, of the light beam due to de-focusing is such that:

$$\theta - \theta_o = \frac{\left(\frac{\partial n}{\partial T}\right) P}{\pi\, n_o\, a\, \lambda} \left(1 - \exp(-\alpha\, \ell)\right),$$

where P is the light power, ℓ the length of liquid traversed, a the initial radius of the laser beam, θ_o the initial divergence of the laser; α and λ are the coefficients of absorption and thermal conductivity respectively. It should be noted that this theory does not take into account the effect of convection.

It is seen from the equation that $\theta \propto P$. This relation has been experimentally confirmed. A plot of the mean diameters of the de-focused laser cross-sections (which were proportional to θ) (Plate 7.3) against their associated laser powers gave the expected straight line. However for high laser powers there was a slight decrease in the gradient; this was attributed to the contribution of convection that was not taken into consideration in the theory.

From measurements of the de-focusing properties of liquids, one may also determine values for $(\partial n/\partial T)$; a parameter that is frequently used in certain aspects of non-linear optics, e.g. stimulated thermal Rayleigh and entropy scattering. The ease with which measurements may be taken makes this method for the evaluation of $(\partial n/\partial t)$ a relatively simple and short process.

CHAPTER VIII

INVESTIGATION OF THE RESIDUAL POPULATION CHARACTERISTICS OF RUBY USING STIMULATED BRILLOUIN SCATTERING

8.1 INTRODUCTION AND THEORETICAL OUTLINE

When a Q-switched laser emits a giant pulse of radiation, the inversion population of the active medium is depleted. The amount of residual population inversion depends on the original magnitude of the inversion and so on the output power of the giant pulse.

A comprehensive theoretical treatise of this problem has been given by Lengyel[130], the salient features of which will be briefly summarised here. The characteristics of giant pulse emission are generally described by the differential equations:

$$\frac{d\varphi}{dt} = \left(\frac{n}{n_p} - 1\right)\varphi \qquad , \qquad \frac{dn}{dt} = -\frac{2n\varphi}{n_p}$$

where $\varphi = \Phi/N_0$ and $n = N/N_0$. Φ is the photon density, N the population inversion, N_0 the total number of molecules/cc, $n_p = \gamma/\alpha_0 \ell$ where γ is the fractional photon loss per single passage in the cavity, α_0 is the absorption in the active medium and ℓ is the length of the medium.

Eliminating time from the equations and integrating:

$$\varphi = \varphi_i + \tfrac{1}{2}\left[n_p \log \frac{n}{n_i} - (n - n_i)\right] ,$$

where suffix i refers to initial conditions. The final population is determined by substituting $n = n_f$ and noting that φ_i and φ_f are negligibly small. Then:

$$n_p \log(n_f/n_i) = n_f - n_i .$$

A numerical solution to this equation is shown in Plate 8.1.

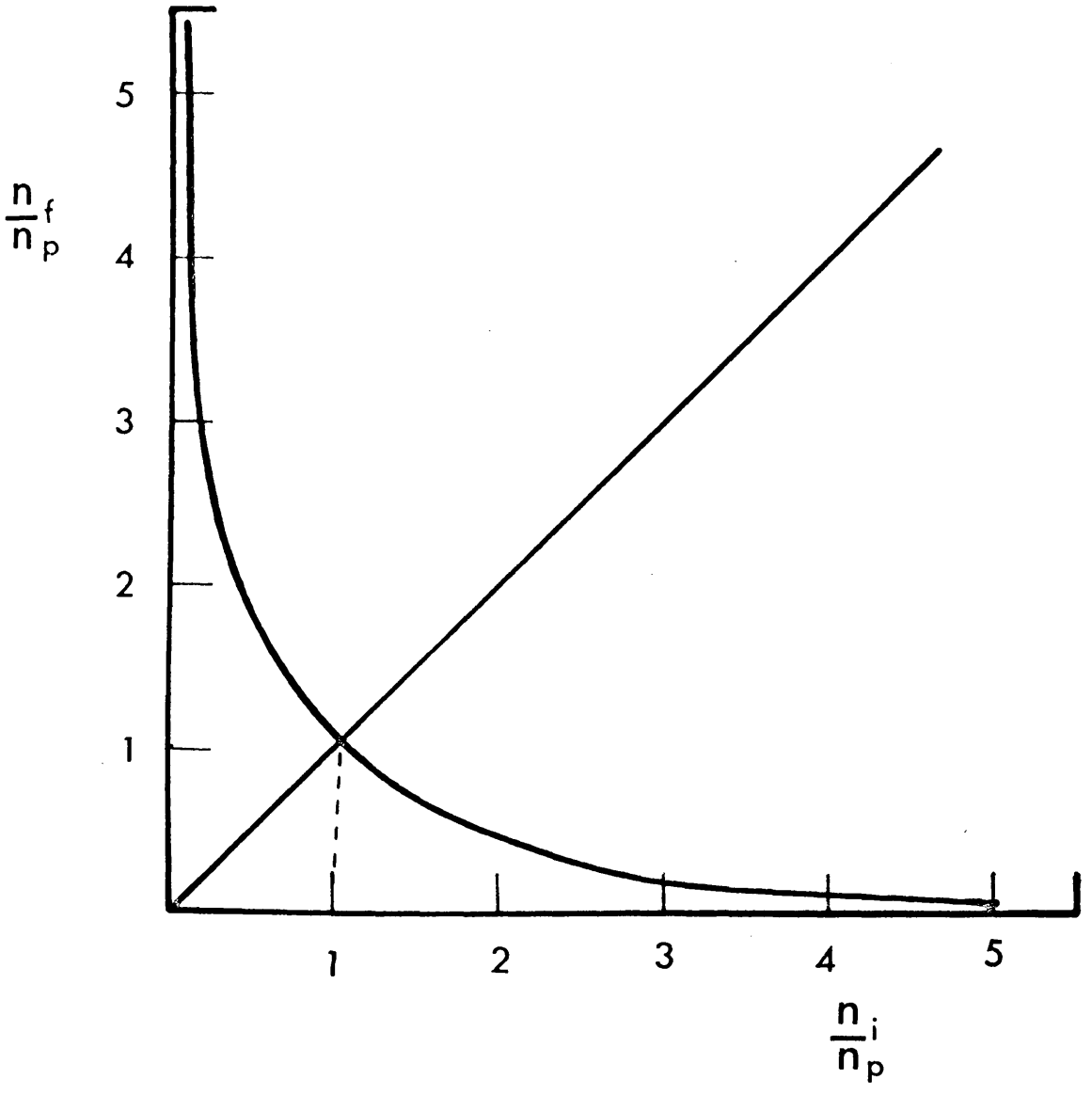

FIG. 4.6.

Theortical Curve of Initial to Final Population Inversion of a Ruby Rod during Lasing

The linear curve arises from the trivial solution $n_f = n_i$. It is seen that for high initial populations n_i, the residual population inversion n_f, will be small. This will correspond to a high power single pulse laser emission. As n_i is decreased n_p will increase. Hence for small values of n_i such that $\frac{n_i}{n_p} \ll 1$, there is a high probability, due to the relatively high residual inversion n_f, that the laser output will consist of several pulses all of which will, of course, have a much lower power than for the previous case.

The threshold for the onset of lasing action corresponds to $\frac{n_i}{n_p} = 1$. For values below this the equality $\frac{n_i}{n_f} = \frac{n_f}{n_p}$ exists. This expression is meaningful in the sense that, below the lasing threshold, there is no laser emission and so there will be no depletion of the initial population inversion. Note that values on the curve for $\frac{n_f}{n_p} > \frac{n_i}{n_p}$ are of course inadmissable.

Experimental investigations conducted by the author have, in a qualitative manner, confirmed the general features of this theory. The results of this investigation are presented in this chapter.

8.2 EXPERIMENTAL DETAILS

The experimental arrangement for such an investigation is shown in Plate 8.2. The laser output from the ruby system was directed through a short focal length lens and came to a focus inside a glass cell containing ether. The high light flux at this focal point was sufficient to generate stimulated Brillouin scattering in the liquid. The resulting scattered light beam was, by the very nature of the stimulating effect, highly collimated, powerful, Stoke-shifted in frequency and directed back along the exact path of the incident laser beam (see theoretical section on S.B.S.). It should be noted that the cell was placed at a sufficient distance from the cavity to prevent overlap between the forward and

Plate 8.2

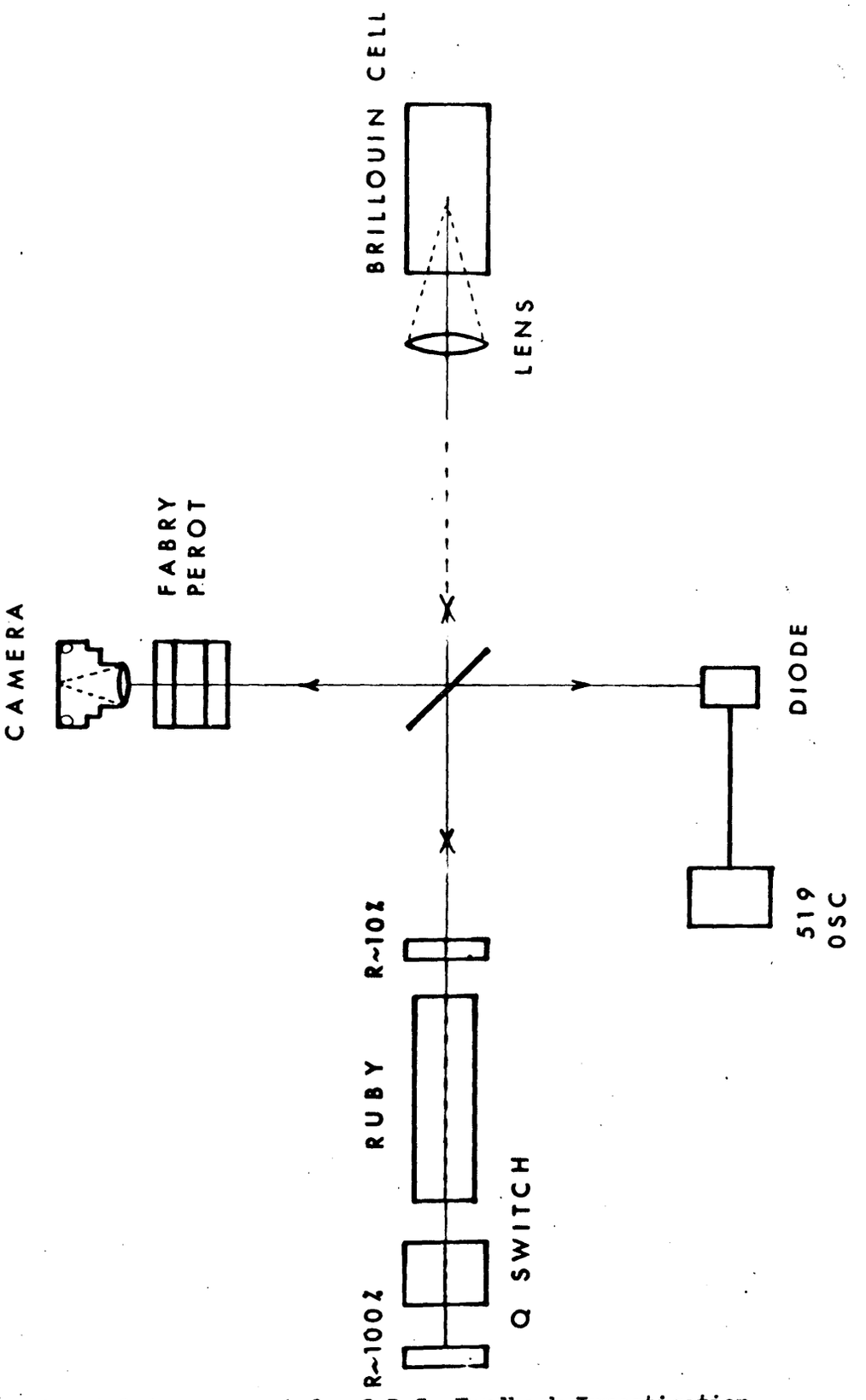

Experimantal Arrangement for S.B.S. Feedback Investigation

backward travelling light pulses at the ruby rod. Hence clear discrimination was made between each successive pulse. The stimulated back scattered light then travelled through the ruby cavity, where it experienced some degree of amplification, depending on the state of inversion in the active medium; and emerged from this system in the direction of the original laser output. As in the case of the original laser emission, this new output could generate another frequency shifted wave in the cell, which again could experience amplification by travelling through the ruby. Assuming there was sufficient residual population inversion, this process could be repeated any number of times. In practice, when the inversion fell to a level such that the resulting amplification of the light pulse was less than its attenuation by the saturable absorber, the power of the pulse dropped and continued to do so for each subsequent circuit of the system. Eventually the power would be too low to initiate stimulated scattering and the process would cease.

Each successive Brillouin pulse was recorded, by way of a beam splitter and an E.M.I.9648 photo-diode, on a 519 oscilloscope and a 551 oscilloscope with integrating circuit (not shown in diagram). This method of detection has been fully discussed in Chapter IV, section 4.1). As a reminder it need only be added that the slow sweep rate of the 551 oscilloscope with integrator was used to determine the number of pulses originally emitted from the laser; (in this experiment, in order to avoid confusion between more than one laser pulse and the Brillouin shifted pulses, the system was controlled by judicious choice of dye concentration and input energy, to give a single pulse). The fast sweep rate of the 519 oscilloscope was used to detect effects over a much shorter time scale, i.e. the multiple Brillouin pulses.

In addition the Brillouin light pulses, together with original laser emission, were frequency analysed using a Fabry-Perot system with a resolution of $\sim 0{\cdot}01\ cm^{-1}$ (for more details see Chapter IV, Section 4.3). The laser output power from the ruby system was controlled by the dye concentration of the saturable absorber Q-switch, and by the input energy to the flash tube.

8.3 RESULTS AND DISCUSSION

The results of this experimental investigation are shown in Plates 8.3 and 8.4. The integrated oscilloscope traces in both these plates are from the 551 oscilloscope and show that the laser output was always a single pulse.

The results of Plate 8.3 show the variation in the number of stimulated Brillouin pulses with laser power. From the traces of the oscilloscope (519) it is seen that for low laser powers the number of stimulated pulses is greater than for high powers. This is in direct accordance with the graph shown in Plate 8.1, for at low laser powers the initial population inversion is small. This corresponds to a relatively high residual inversion with the consequence that there is sufficient gain in the ruby to amplify any stimulated Brillouin pulses. As seen from the top 519 oscilloscope trace, at low laser powers, four small Brillouin pulses were generated, three of which were amplified and the fourth of which experienced a loss due to the depleted inversion. The second and third traces show that, with an increase in laser power, the number of Brillouin pulses decreases by one and there is considerable attenuation on the last pulse. The power of the Brillouin pulses has also increased. At such laser powers the population inversion remaining after the laser emission was only sufficient to amplify one stimulated pulse. For even higher laser powers only two pulses were generated.

Plate 8.3

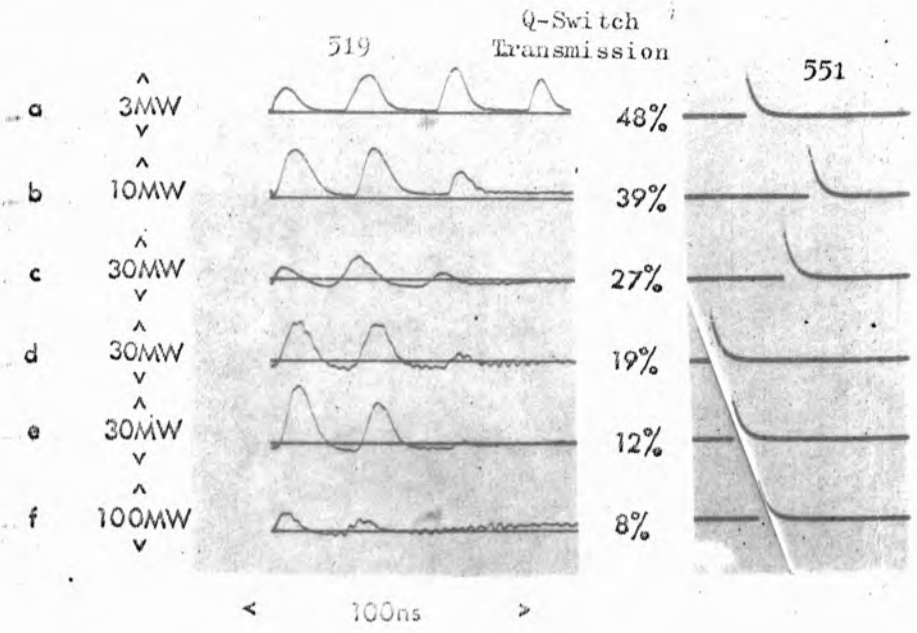

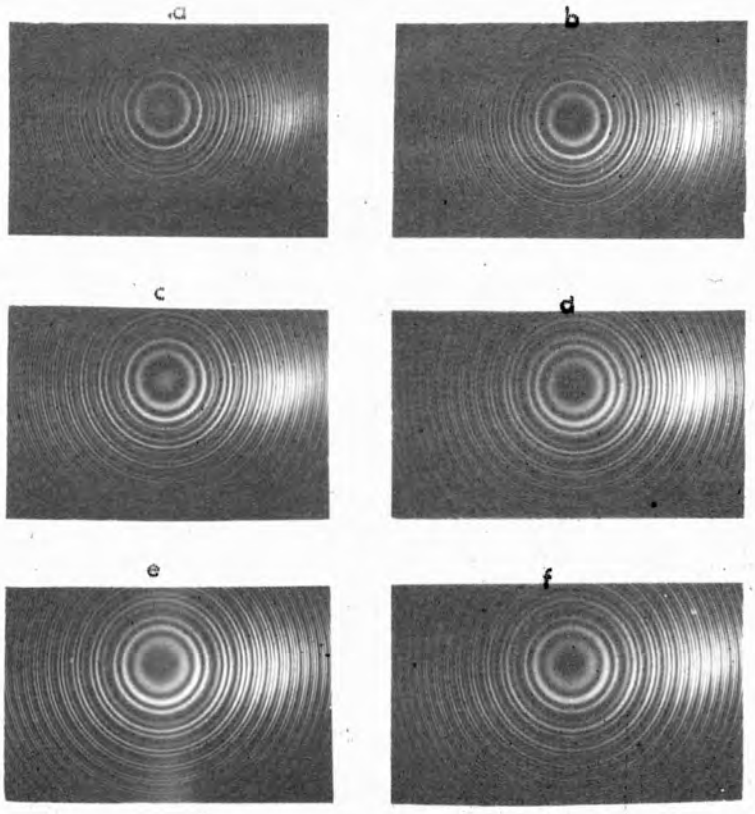

Pulse and Spectral Analysis of the S.B.S. Feedback Investigation

Plate 8.4

519

Q-switch
Transmission

551

< 500ns >

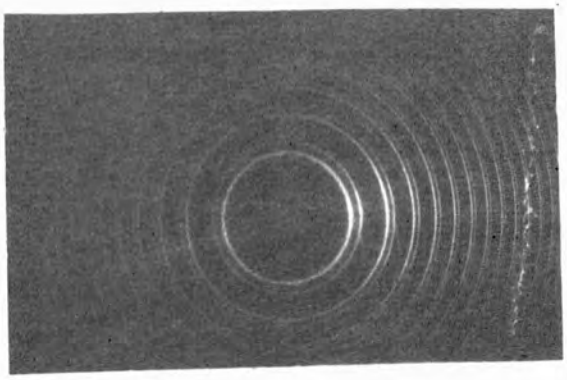

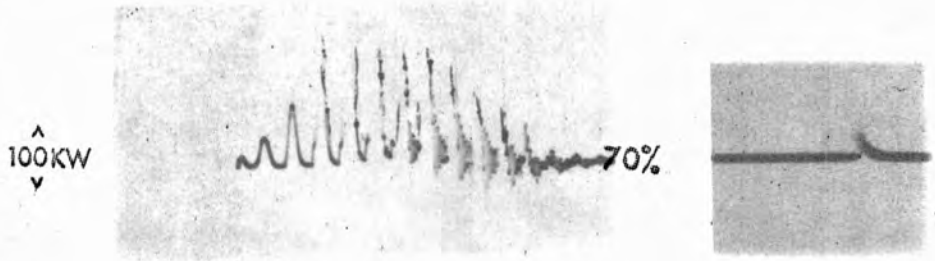

< 500ns >

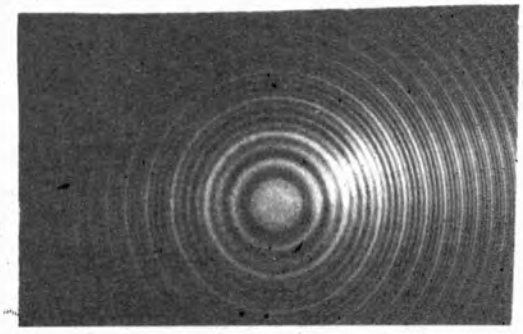

Pulse and Spectral Analysis of the S.B.S. Feedback Investigation

The Fabry-Perot patterns corresponding to these traces are also shown in Plate 8.3 (read across the plate and down). As was expected for a large number of Brillouin pulses there were a corresponding large number of frequency shifts, the inverse situation being true for a small number of pulses. The photographs of oscilloscope traces and corresponding Fabry-Perot rings shown in Plate 8.4, summarise quite dramatically the effects we have been discussing. For at extremely high laser output powers (see top traces and Fabry-Perot) only the primary pulse had sufficient power to generate a stimulated pulse. At low powers (bottom traces and Fabry-Perot) a whole series of low power Brillouin pulses were generated.

It should be noted that in these experiments no limitations were imposed on the possible number of Brillouin shifted pulses by the line-width of the ruby since this line-width was $\sim 10 - 15\ cm^{-1}$ whereas a typical Brillouin shift was $\sim 0{\cdot}04\ cm^{-1}$. The mechanism by which the inversion in the ruby was depleted is rather debatable (see Chapter V, Section 5.2). In a similar experiment published in a letter by T.A. Wiggins et al[156], the authors purport to show, by comparing the results of unshifted and shifted frequency feedback into the laser cavity, that a 'hole-burning' mechanism takes place in the frequency gain profile of the ruby. This however seems in direct contradition to the conclusions of Chapter V, Section 5.2).

CHAPTER IX

BRAGG REFLECTION OF LASER LIGHT FROM AN INDUCED PHASE GRATING IN A Q-SWITCHING LIQUID

9.1 INTRODUCTION

When highly intense laser light passes through a liquid intensity dependent non-linear refractive index changes are induced in this liquid. The mechanisms by which this refractive index modulation are induced has already been discussed in considerable detail in the theoretical chapter.

A saturable absorber used as a Q-switch will, like any other liquid, experience such perturbations[143] (see Chapter V, Section 5.5). The imaginary part of this index change will produce an intensity dependent absorption coefficient and the real part will produce an intensity dependent real refractive index change. In addition to these electronic polorizability non-linear effects, it is probable that there will also exist a thermally absorptive bulk refractive index modulation due to absorption of the laser light (see theoretical Chapter III, Section 3.13). Hence a typical standing wave set up in the laser cavity, by the circuital propagation of the laser light, should in principle induce both an amplitude grating, due to the bleaching mechanism, and a phase grating, due to real refractive index changes.

In the following investigations such an induced structure was successfully detected for the first time.

Preliminary experiments were conducted to prove the actual existence of such an effect by comparing the intensity of the laser light entering and leaving the Q-switch cell in both the forward and backward directions.

A more sophisticated technique was then employed, incorporating a frequency doubled probing beam which was Bragg reflected off the induced structure within the cell. This experiment successfully showed, that a probe light beam could directly detect light induced non-linear perturbations in a liquid material. The rather special problem of induced structure in a saturable absorber, to be discussed in this chapter (see also enclosed publication[144]) is therefore only one of the many non-linear effects that can be investigated by using the probing technique.

9.2 PRELIMINARY INVESTIGATION OF THE NON-LINEAR STRUCTURE

The experimental system is shown schematically in Plate 9.1. Two beam splitters were placed at the back end of the ruby cavity, one at either side of the Q-switch cell. Laser light reflected off the beam splitters was recorded by way of two diodes on two 519 oscilloscopes. The 519 oscilloscopes were coupled in such a way that the signal received by one triggered the other. Using delay cable, the signal to the latter oscilloscope was retarded long enough to allow ample time for triggering. Hence one could be sure of recording the same laser pulse on the two oscilloscopes.

The beam splitters were positioned in the same direction and both at an angle of 45° to the incident light. Hence light travelling out from the ruby, in the backward direction, was detected by way of the beam splitters represented in Plate 9.1 as continuous lines. For light detection in the forward direction, the beam splitters were both rotated through 90°. Hence, by using this system one was able to measure the ratios of the light reflected from the beam splitters for both directions of the laser light. From such ratios an estimate of the reflectivity of the grating could be deduced.

Plate 9.1

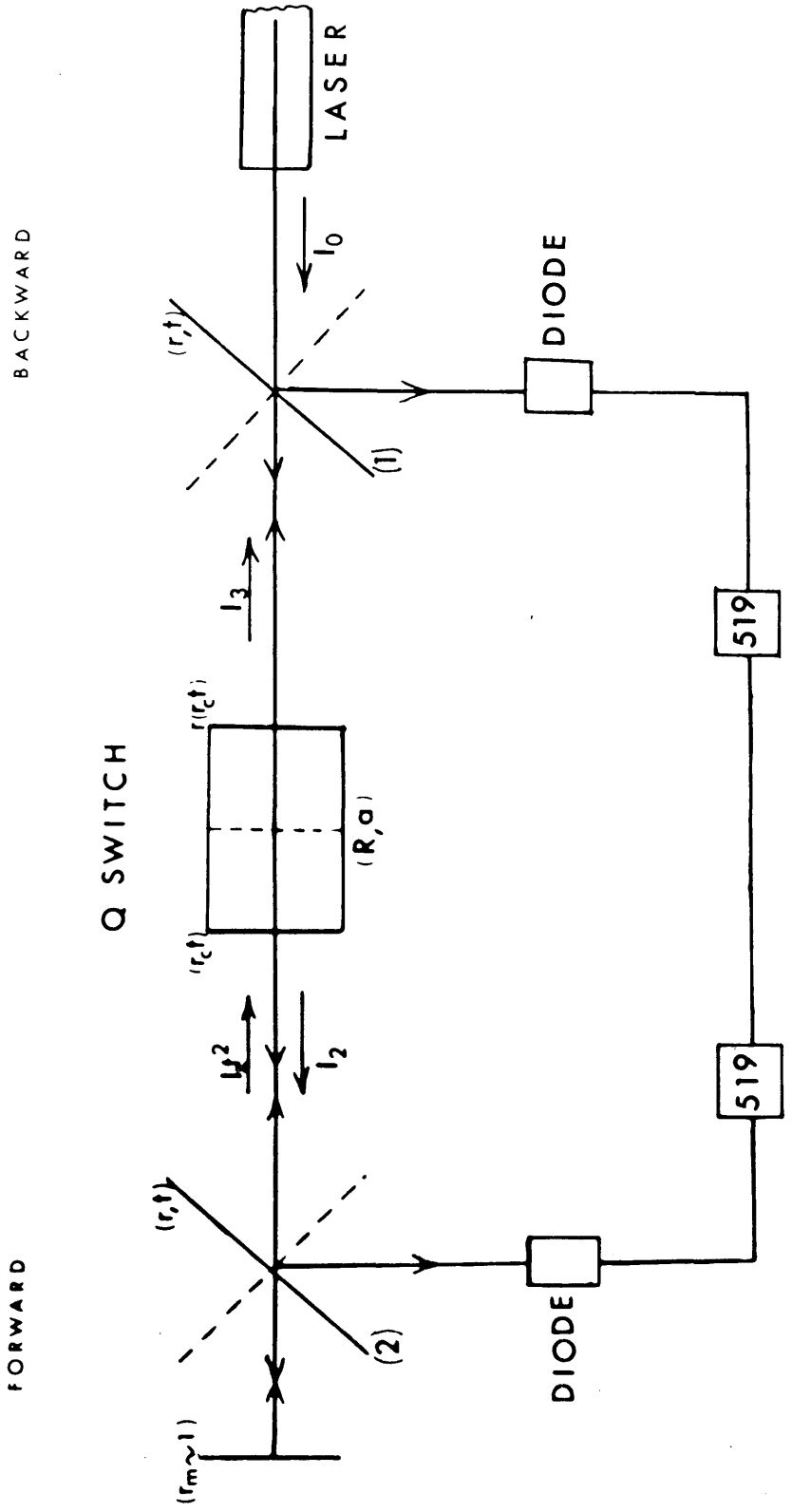

Experimental System for Preliminary Investigation
of the Induced Structure

Calculation of Reflectivity

Consider the passage of a pulse of laser light through the Q-switch as shown in Plate 9.1. The notation is standard, hence r and t refer to the reflectivity and transmissivity of all optical components. (r_c, t_c refers to the air glass interface of the Q-switch cell.) The effects from the glass-liquid interface are small and so have been ignored. R is the reflectivity of the grating and $a(= 1 - \alpha)$ is a measure of the absorption, where α is the absorption coefficient. I_0, I_2 and I_3 are, respectively, the laser intensity entering the system, leaving the Q-switch cell in the backward direction and leaving the same cell in the forward direction.

From considering the passage of the beam of light round this system we can derive the approximate relations.

$$\frac{I_0}{I_2} = \frac{1 - t^2\, t_c^2\, a\, R}{t\, t_c^2\, a\, (1 - R)} \quad ; \quad \frac{I_2}{I_3} = \frac{1}{(t^2 t_c^2\, a - 1) + \left(\frac{1 - t^2 t_c^2\, a\, R}{1 - R}\right)}$$

Now define R_1 to be the ratio of recorded signals from beam splitters 1 and 2 respectively for light travelling in the backward direction and R_2 as the ratio of signals from the beam splitters 2 and 1 for light travelling in the forward direction (for this recording the beam splitters are turned through 90^0 with respect to their previous positions). Hence:

$$R_1 = \frac{I_0}{I_2}\left(\frac{a}{b}\right)_1 \quad \text{and} \quad R_2 = \frac{I_2 t}{I_3}\left(\frac{b}{a}\right)_2 ,$$

where $(a/b)1$ and $(b/a)2$ are each the ratio of the sensitivities of the two oscilloscopes together with their diodes, for the forward and backward beam directions respectively. As these ratios are difficult to assess it is preferable to eliminate them by taking two sets of results; keeping these sensitivity ratios constant.

Hence for $\alpha = 0$; $a = 1$ and $R = 0$, then:

$$R_1 = \frac{1}{t\, t_c^2}\left(\frac{a}{b}\right)_1 = X_1 \quad \text{say} \quad \text{and} \quad R_2 = \frac{1}{t\, t_c^2}\left(\frac{b}{a}\right)_2 = Y_1 \quad \text{say.}$$

These are the signals for no dye in the Q-switch.

For a finite quantity of dye in the Q-switch, giving an absorption α , the signals will be:

$$R_1 = X_1 t\, t_c^2\, \frac{I_0}{I_2} = X_2 \quad \text{say} \quad \text{and} \quad R_2 = Y_1\, t^2 t_c^2\, \frac{I_2}{I_3} = Y_2 \quad \text{say} \ ,$$

where the values of $(a/b)1$ and $(b/a)2$ are determined from the previous expression in terms of the signals X_1 and Y_1. Now, by substituting in the original expressions for the ratios I_0/I_2 and I_2/I_3 and re-arranging, we find an expression for the reflectivity from the Q-switch of the form:

$$R = \frac{t^2 t_c^2\,(Y - X)}{(t^2 t_c^2 - X)(t^2 t_c^2 + Y)} \ ,$$

where $X = X_2/X_1$ and $Y = Y_2/Y_1$.

It must be emphasised that this calculation is only approximately valid since (a) the absorption has been assumed to be constant which is certainly not true for a bleachable dye and (b) the reflectivity of the phase grating has been considered to arise from a single boundary at the centre of the Q-switch cell.

The results of the experiment are shown in Plate 9.2. The top set of results are for zero absorption and the bottom set of results are for a finite absorption in the Q-switch. In both sets, the top rows of traces are signals from light travelling in the backward direction where the first trace of each row is from the beam splitter (1). The remaining two rows in the sets are from the forward travelling wave with the first traces now deriving from the second beam splitter (2).

Plate 9.2

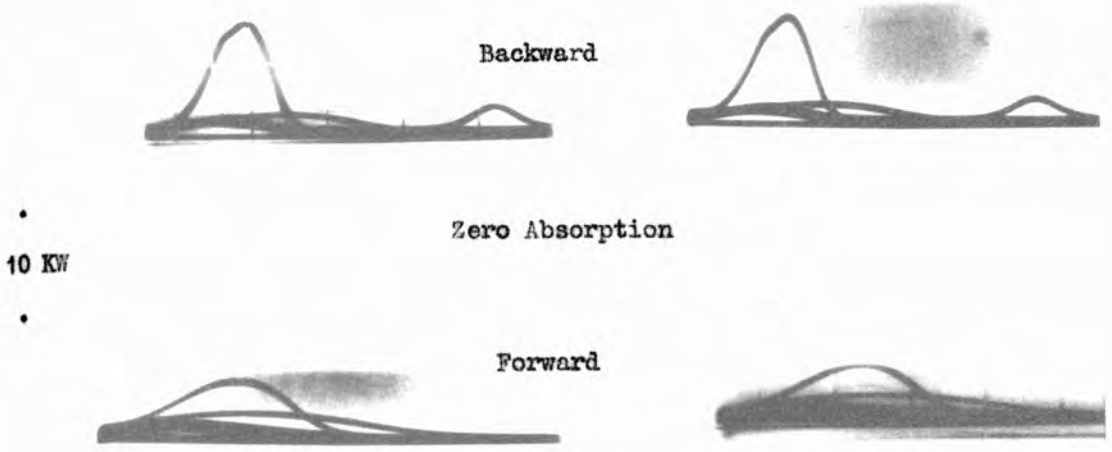

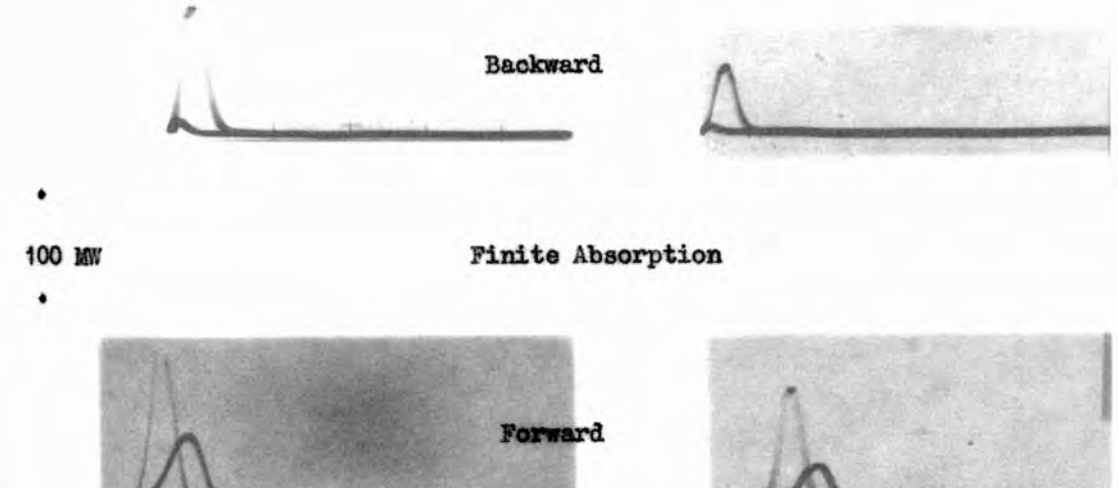

Oscilloscope Traces of Laser Light Signals for Determining the Reflectivity of a Q-Switching liquid

By adjusting the sensitivity of the instruments, the zero absorption set of traces were arranged to be approximately equal. The results obtained for a finite absorption in the Q-switch, using the same instrument sensitivities, show decidedly different ratios for the forward and backward travelling beams, indicating that a reflectivity exists in the Q-switch.

Measurements from these traces of the intensity ratios appearing in the reflectivity equation were substituted, together with experimentally determined values of transmissivity for the optical components, into the equation to yield a value of reflectivity of $R \sim 15 \sim 20\%$.

9.3 BRAGG REFLECTION PROBE INVESTIGATION OF THE INDUCED GRATING

(i) Experimental Arrangement

The experimental arrangement is shown in Plate 9.3. The Q-switch cell was in the shape of a regular hexagon having one inch square sides of Spectrosil-B glass flat to $\lambda/10$. With such a geometrical arrangement the probe light entering the cell face normally, experienced a minimal loss and also satisfied the Bragg angular condition of 60^{o} imposed by the wavelengths of the induced standing wave structure and the frequency doubled probe light. A standard Q-switching solution of cryptocyanine in isopropyl alcohol was used to produce a giant pulse of laser radiation having a typical output power of 30 MW and a time duration of 20 nsec. The spectral composition of the laser output was recorded on a Fabry-Perot and the pulse shape of the output was monitored on a 519 oscilloscope.

The giant pulse from the ruby passed through a frequency doubling crystal of ammonium di-hydrogen phosphate (A.D.P.) which was correctly orientated to give a maximum conversion efficiency of about 3%. (A

Plate. 9.3

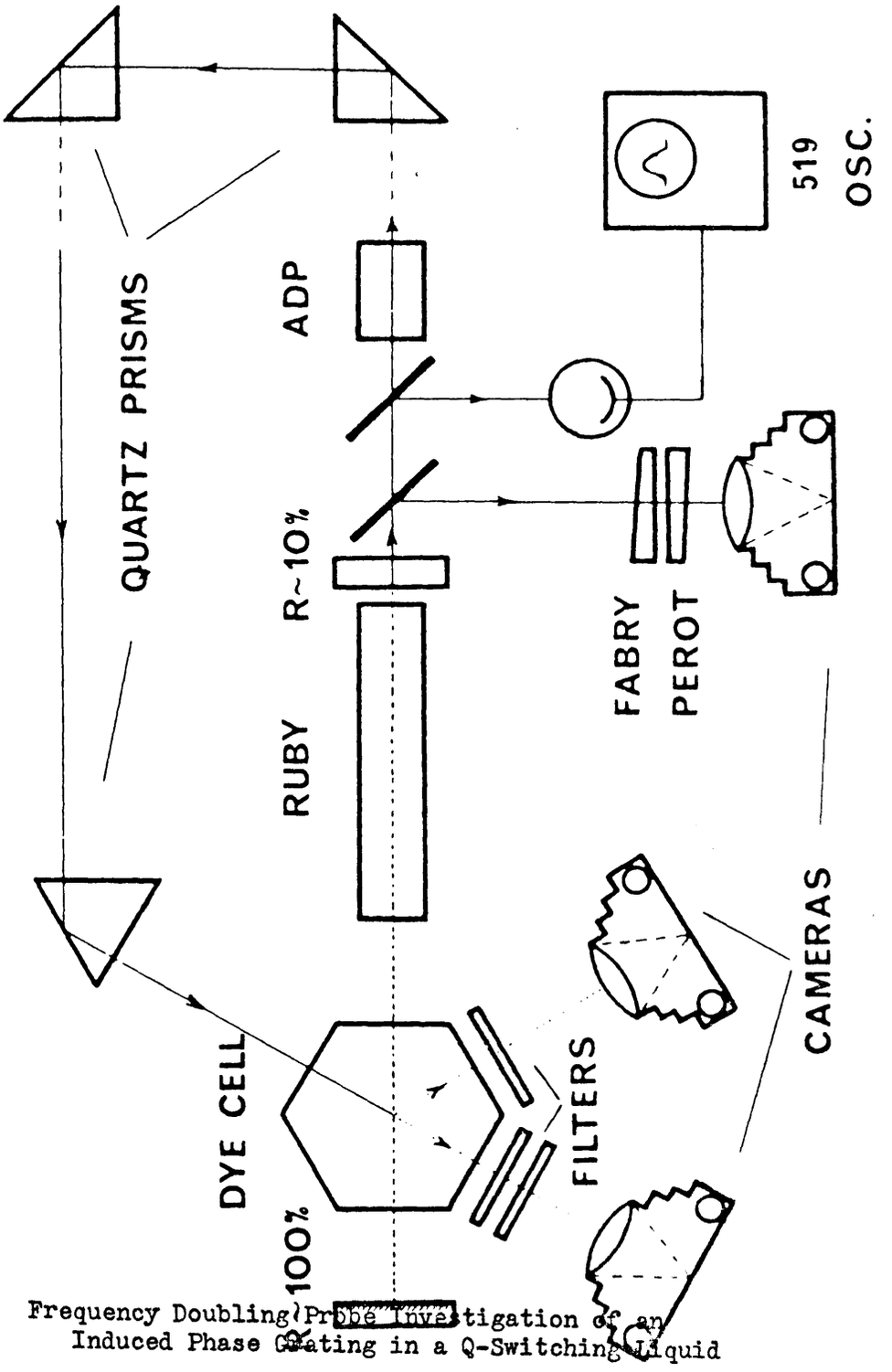

Frequency Doubling Probe Investigation of an Induced Phase Grating in a Q-Switching Liquid

description of frequency doubling techniques will be given at the end of this sub-section.) The output from the crystal was then directed, by means of a series of prisms, back into the Q-switch cell at an angle appropriate for Bragg reflection off the induced structure.

The optical path length of the frequency doubling probe light was made variable by movement of the back prism arrangement in a direction along the ruby axis. The consequent variable delay in the probe light entering the Q-switch cell facilitated a temporal analysis of the structural decay induced within the saturable absorber.

The direction of the probe light incident on the structure was sensitively controlled by small angular movements of the deflecting prism which was mounted on a rotating table having a micrometer adjustment. This table was held by a ratchet fixture to a movable arm of a kinematic spectrometer table (see Chapter IV, Section 4.4), the centre table of which held the Q-switch cell. By this means crude alignment adjustments were made by rotating the movable arm about the Q-switch cell.

The frequency doubled transmitted and reflected output from the structure was recorded separately on two plate cameras focused on infinity. Red light from the fundamental laser output and the flash tube were minimised using Wratten 18A filters, which were placed over the entrance windows of the cameras.

(ii) Frequency Doubling Techniques

In the theoretical chapter of this thesis it was shown (see section of phase matching), that phase matching is achieved when the velocities of the frequency doubled light and the fundamental light are equal. The most frequently employed technique for obtaining this condition is to use anisotropic crystals.

Such crystals support in general two waves with different propagation characteristics at any frequencies - the ordinary and the extraordinary waves. These waves have different refractive indices and it is often possible, by using a selection of the ordinary and extraordinary waves at the various frequencies involved, to achieve phase matching.

Maker[3] and Giordmaine[4] first demonstrated this principle, using a uniaxial crystal of K.D.P. (having essentially the same properties as the A.D.P. crystal used by the author). The refractive index surface for the ordinary ruby laser frequency and for the extraordinary frequency doubled component are shown in Plate 9.4, Fig.(b). It is seen that, at the angle θ_0 to the optic axis z phase matching is achieved, since the phase velocities for the ordinary and extraordinary waves are equal.

In this experiment the K.D.P. crystal was mounted on a kinematically designed table supplied with a micrometer adjustment to give measurable angular adjustments of $\sim \pm 3$ minutes. The crystal was arranged on the table so that the vertically plane polorized laser light passed through the crystal as an ordinary ray.

Frequency doubled light was visually observed using a zinc sulphide screen placed behind the crystal (the emergent ruby light being minimised by using filters) which fluoresced under blue light irradiation. Measurements taken showed that the peak output of the blue light could be determined to about ± 3 minutes. The conversion efficiency was measured by dividing the laser output into two, sending one beam through the crystal and the other beam round a delay path. Both pulses were then recorded via a photo-diode on a 519 oscilloscope. The results are shown in Plate 9.4, Figs.(c) & (d), where Fig.(c) was a calibration result taken without the frequency doubling crystal so that the ratio between

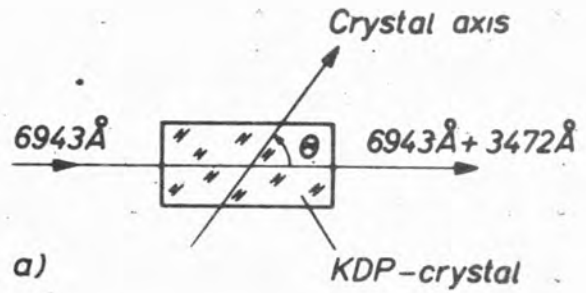

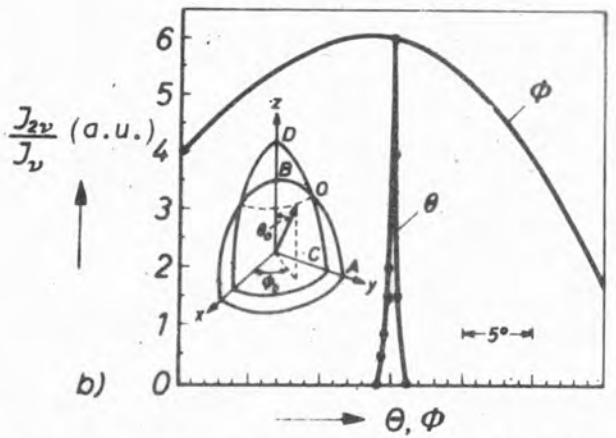

Frequency doubling and Phase Matching in KDP

Plate 9.4

the signals from the two laser-beams was known. The lower trace shows the results with the crystal in place together with sufficient filtering to minimise the emergent red laser light, the frequency doubled pulse and the fundamental pulse corresponding to the pulse traces on the left and right respectively. Measurements of the pulse heights of the lower trace relative to the calibration pulse heights, together with a knowledge of the spectral sensitivity of the photodiode gave an estimated conversion efficiency of about three percent.

(iii) Results and Discussion

Typical results of the investigation are shown in Plate 9.5. The upper set of results (i) represent successive exposures of the transmitted and reflected beams taken at angular intervals of 6 minutes, covering the angle for Bragg reflection. The transmitted light (second row of set (i)) was attenuated two-hundredfold. The reflected light exhibits a critical dependence on the angle of incidence, the intensity falling to half-value for a deviation of $\pm\overline{10}'$. These results correspond to an incident beam divergence of 5 mrad and about 1% of the light is reflected.

In addition to the magnitude of the amplitude of the induced grating, the amount of reflected light is governed by other processes. One such process could be the filamentary formation of the light within the Q-switch (see theoretical section on self-trapping). For such a process the effective interaction region for the probe light would be considerably reduced. Another important process is attributed to the divergence of the incident beam. For a highly collimated beam, the reflection should be noticeably higher than for a divergent beam, since the light flux at the critical angle would be correspondingly greater. In addition the angular tolerance for Bragg reflection should be reduced as the divergence of the probe beam is reduced. This is shown in the lower

Plate 9.5

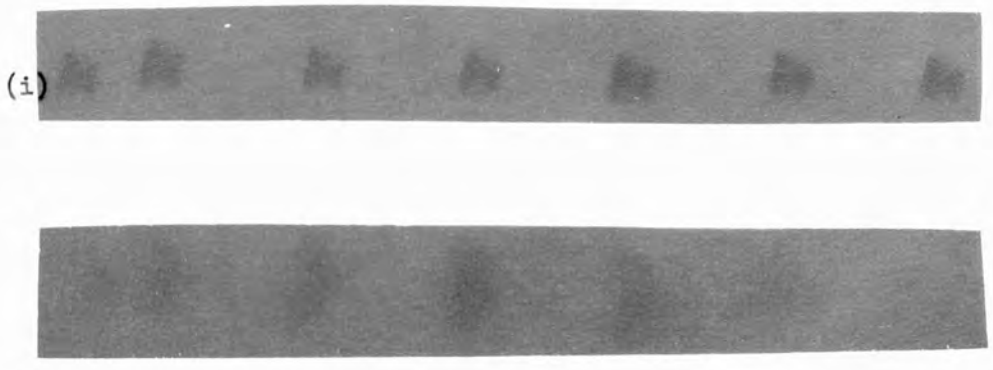

Angle Run of Bragg Reflected Light from an Induced Grating

set of recordings (ii) of Plate 9.5 which correspond to a beam divergence of the central region of the frequency doubled laser profile of about 2 mrad. The reduction in divergence was achieved simply by restricting the outer regions of the laser light, using two small aperture stops, one positioned at either end of the optical path. The exposures now represent increments of 2' in the angle of incidence. The reflectivity of the grating increased to 3%, and the intensity fell to half-value at $\pm 4'$.

To eliminate the possibility that the phenomenon resulted from spurious reflections, the A.D.P. crystal was removed, and a photograph was taken under identical conditions but without the ultra-violet filter. The resulting plate showed a diffuse fogging due to scattered light, but no evidence of a well- defined reflected beam.

Experiments were also conducted to investigate the effect on the reflectivity when introducing delays of up to 30 nsec into the probing beam. It was found that the relative intensity of the reflected light was not diminished, even for a maximum delay (for which the overlap of the probing pulse and the fundamental pulse was less than 20%). The implication of this result was that the processes governing the decay of the ordered structure in the liquid were probably due to absorptive heating. Hence the modulations formed a phase grating rather than an amplitude grating, and depended on the bulk properties of the material rather than the localized induced electronic polarizability which is much faster and gives rise to saturable absorbtion and an associated real refractive index charge.

Analysis of the spectral composition of the light on the Fabry-Perot showed that Bragg reflection took place for power levels well below the threshold for the stimulated Brillouin effect, as well as above it, indicating the ability of this method to probe acoustic modulations in addition to the thermal effects.

To date, most other experimental techniques for investigating non-linear phenomena in liquids depend on comparing the characteristics of the inducing incident and emergent light beams entering and leaving the medium. Analysis of the structure within the medium is inferred from such characteristics. However in this new probing technique no such inference is required since the structure is directly investigated. This probe method has also the distinct advantage of both direct temporal and spatial analysis of the induced non-linearity. From such temporal measurements, values for the relaxation times of the various effects in the liquid can, in principle, be determined.

However, it was realised that for such quantitative investigations certain modifications were required of the existing system, the most important of which were to use photo-tube detectors and to replace the frequency doubled probe source by a continuous laser probe. Some of the advantages of such a modified system are:

(a) A continuous laser output has a much lower beam divergence than a pulsed system.

(b) The induced structure could be probed during its complete build-up and decay period.

(c) Relaxation measurements were calculated directly from an oscilloscope trace recording of the Bragg reflected signal into a photomultiplier.

(d) The whole system was readily movable so that spatial analysis of the induced structure was made comparatively easy.

(e) A continuous laser gives a constant but tunable output power so only a recording of the Bragg reflected light was required, (and not the transmitted light).

From collaboration with Dr J. Katzenstein at Culham Laboratory such an argon laser system was used for further probe experiments. This series of experiments will be discussed in the next chapter.

CHAPTER X

BRAGG REFLECTION FROM A PHASE GRATING INDUCED BY NON-LINEAR OPTICAL EFFECTS IN LIQUIDS

PART I

10.1 INTRODUCTION AND SOME THEORETICAL CONSIDERATION

In the series of experiments to be described the output from a continuous argon laser was used to probe, at the Bragg angle, the intensity dependent refractive index modulations induced in a series of liquids by the high light flux from a ruby laser (see Chapter III, Section 3.17). Such a Bragg reflection is illustrated in Plate 10.1, where the ruby laser light, travelling in both the forward and backward directions producea a standing wave in the liquid, and so induces a refractive index modulation, which gives rise to a maximum reflectivity of the argon probe light (wavelength 4880 Å) at the Bragg angle:

$$\theta_o = \cos^{-1} \frac{\lambda_a}{\lambda_r} \cdot \frac{n_r}{n_a} = 45{\cdot}5^{o} \quad ,$$

where the suffixes a and r refer to argon and ruby respectively.

The results obtained from these investigations will be shown to be in good agreement with several of the theoretical conclusions of Chapter III, Sections 10.11-10.17. In addition, values for the thermal relaxation time for some liquids are determined.

Before discussing further the experimental results, consideration must first be given to some of the theoretical conclusions of Chapter III, Sections 10.11-10.17. The validity of these conclusions can only be experimentally tested provided certain simplifications are made to the related theory. Such modifications will be discussed in the next section.

Plate 10.1

Fig.1 Illustrative diagram showing Bragg reflection of a continuous argon beam from a periodic structure induced in a liquid by the standing wave of a ruby laser beam.

(i) Dependence of Reflectivity on Ruby Laser Power

The reflectivity of the induced refractive index modulation, as seen earlier (Chapter III, Section 3.17), is governed by the equation:

$$R = \frac{P_4(0)}{P_s(0)} = \left(\frac{k_1 L}{n_0 \sin\theta}\right)^2 |n_a|^2 \qquad \ldots (10.1)$$

where n_a is the amplitude of the intensity dependent refractive index modulation and is dependent on the amplitude of the laser light. Expressions for n_a arising from electric field induced bulk changes of the material were derived in Chapter III, Sections 3.11-3.15 (see also Chapter III, section 16). Now in all these expression for n_a :

$$n_a \propto A_1(z)A_2(z) , \qquad \ldots (10.2)$$

Where the dependence of electric field amplitude on z arises from normal absorption and stimulated gain, described by the gain equations (see Chapter III, Section 3.11):

$$\frac{dA_1}{dz} = - g k_1 |A_2|^2 A_1(z) - \alpha A_1(z) \qquad \ldots (10.3)$$

$$\frac{dA_2}{dz} = - g k_2 |A_1|^2 A_2(z) + \alpha A_2(z) \qquad \ldots (10.4)$$

where the first equation represents the pump wave travelling in the forward (+ z) direction, and the second equation represents the backward travelling wave (-z direction). Hence the forward wave experiences a loss and the backward wave experiences a gain.

Under the conditions that $A_2 \ll A_1$ such that $g k_1 |A_2|^2 \ll \alpha$ then equation (10.3) may be written as:

$$A_1(z) = A_1(0)\, e^{-\alpha z} . \qquad \ldots (10.5)$$

Substituting this expression into equation (10.4), using the approximation of expanding the exponential factor in a power series to the first order in z (this is justified providing $\alpha \ll z$ which is generally true), and finally integrating (remembering that the boundary conditions

for A_2 are applied at $z = \ell$, as reference is now made to a wave travelling in the -z direction), then:

$$A_2(z) = A_2(\ell)\ e^{(z-\ell)[gk_2|A_1(0)|^2\{(z-\ell)\alpha - 1\} + \alpha]} . \qquad \ldots (10.6)$$

Now from equations (10.1) and (10.2) it is seen that:

$$R \propto |A_1(z)|^2\ |A_2(z)|^2 . \qquad \ldots (10.7)$$

Hence the reflectivity of the induced structure expressed in terms of the boundary values of the laser light intensity entering the probe cell in the forward and backward directions is:

$$R \propto I_1(0)I_2(\ell)\ e^{g\frac{8\pi k_2 I_1(0)}{c}[(z-\ell)\{(z-\ell)\alpha - 1\}] - 2\alpha\ell} \qquad \ldots (10.8)$$

At this point let us consider the validity of the approximation made in deriving equation (10.5). As an example consider the induced refractive index change resulting from S.T.R. effect. The gain g is given by equation (3.65). Substituting this expression into the gain term of equation (10.3), and expressing the light amplitude in terms of intensity, the condition for which the approximation is valid is expressed as:

$$k_1\left(\frac{\gamma\beta c\alpha}{8\pi\rho_0 c_p n}\ \frac{1}{\Gamma_R + \Gamma_L}\right)\left(\frac{4\pi I_2(z)}{c}\right) \ll \alpha \qquad \ldots (10.9)$$

For a light absorbing solution of copper acetate in methanol with an absorption coefficient $\alpha \sim 0{\cdot}15\ \text{cm}^{-1}$, then:

$$I_2(z) \ll 35\ \text{MW/cm} .$$

This condition is easily fulfilled in experiment and so the approximation is justified.

Now the reflectivity expression above (equation (10.8) may be re-expressed in the more practical form:

$$\boxed{R \propto I_1(0)\ I_2(\ell)} \qquad \ldots (10.10)$$

providing:

$$g\frac{8\pi k^2}{c} \cdot I_1(0)[(z-\ell)\{(z-\ell)\,\alpha - 1\}] \ll 1 \qquad \ldots (10.11)$$

Hence, for the methanol solution contained in a cell of length $\ell = 4$ cm in which the induced structure is probed at the centre of the cell, such that $z = 2$; then the condition imposed on the input ruby laser intensity $I_1(0)$ will be for equation (10.11):

$$I_1(0) \ll 70 \text{ MW/cm}^2 .$$

(ii) Spatial Dependence of Reflectivity

From re-arrangement of equation (10.8) the reflectivity equation may be expressed as

$$R \propto I_1(0)\, I_2(\ell)\, e^{g\frac{8\pi k_2 I_1(0)}{c}(\ell - z) - 2\alpha\ell} . \qquad \ldots (10.12)$$

Therefore it is seen that the reflectivity varies exponentially with z and tends to a maximum as z tends to zero, i.e. maximum gain occurs near the front wall of the cell. Note that the exponential term $(z-\ell)^2\alpha$ in equation 10·8 has been neglected since in practice α is small.

(iii) Temporal Dependence of Reflectivity

Each of the intensity dependent non-linear effects discussed in Chapter III, Sections 3.11 to 3.17) has a characteristic relaxation time. These have the following orders of magnitude.

Electrostriction - 10^{-9} to 10^{-10} sec

Kerr effect - 10^{-11} to 10^{-12} sec

Thermal effect - 10^{-7} to 10^{-8} sec.

The length of the ruby pulse (~ 15 nsec) and the resolution of the instrument (~ 7 nsec) only allowed investigation of the thermal relaxation.

Hence for two light waves of frequencies, ω_1 and ω_2 travelling

in the forward and backward direction respectively through an absorptive liquid then the intensity dependent temperature modulation induced within the liquid can be shown, from equation (3.38) of Chapter III (where only the absorptive term is considered), to vary in time such that:

$$\frac{\partial T}{\partial t} + \left(\frac{\lambda k^2}{\rho_o c_v} - j\omega\right) T = \frac{1}{4\pi} \frac{n c \alpha}{\rho_o c_v} A_1 A_2^* \qquad \ldots (10.13)$$

where $\tau = (\rho_o c_v / \lambda k^2)$ and all other notation is defined in Chapter III, Section 3.19.

Now the small amplitude temperature modulations are related to the refractive index modulation by the expression:

$$T = \frac{\partial T}{\partial n} \cdot n_a ,$$

where n_a is the amplitude of the index modulation. The reflectivity of the probe light probing this structure which is proportional to $|n_a|^2$ (see equation 10.1) is then proportional to T^2. Hence from the solution of equation 10.13 together with these considerations a time dependent expression for the reflectivity is obtained such that:

$$R = e^{-2t/\tau} \left(\int \sqrt{I_1(t)\, I_2(t)} \; e^{t/\tau} \; dt \right)^2 \qquad \ldots (10.14)$$

Thus the thermal relaxation time τ of a liquid may be determined from measurements of the reflectivity of the induced grating as a function of time.

(iv) Dependence of Reflectivity on Concentration

In absorbing liquids the magnitude of the Bragg reflected light will depend on the absorption coefficient of the liquid. In such liquids the dominant non-linear contribution (for $\omega = 0$ $(= \omega_1 - \omega_2)$, i.e. forward and backward light waves of the same frequency) is that of absorptive heating (see next section).

For $\omega \sim 0$, the amplitude of the refractive index modulation is: (see Chapter III, Sections 3.13 and 3.16)

$$n_a = \frac{\gamma \beta c}{8\pi \rho_o c_p} \cdot \frac{\alpha}{\Gamma_R + \Gamma_L} A_1 A_2 \qquad \ldots (10.15)$$

Thus it is clearly seen from equation (10.1) that:

$$R \propto (\alpha)^2 \qquad \ldots (10.16)$$

(v) Modification of the Reflectivity Equation

The reflectivity equation given by equation (10.1) and originally derived in Chapter III, Section 3.17) is only strictly valid for a probe beam of approximately the same diameter as that of the ruby induced structure. However, since the diameter of the argon probe beam used in experiments was $\sim 1/5$ that of the ruby beam (and so of the induced structure), certain modifications must be made to the equation. Consider the illustration showing the probe beam (diameter y) entering the structure (diameter x) at an angle θ. Then the reflectivity equation is strictly valid for an elemental interaction region of area $\sim y^2$.

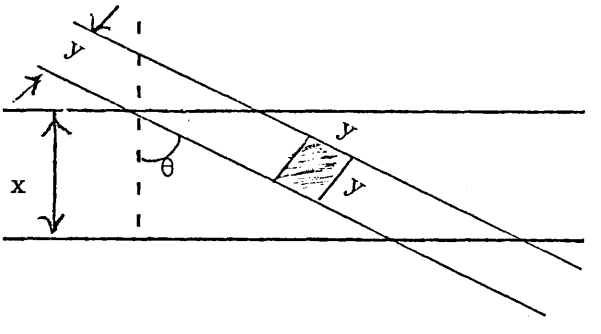

The approximation may be made of summing the reflectivities from all these elemental areas over the whole length $\ell (\approx x/\cos\theta)$ of the interaction region and ignoring the mutual interference effects of each of these elements. This approximation is valid (within the limits of accuracy of the related theory) when it is considered that such factors as the cross-sectional intensity distribution and the divergence of the ruby beam, inducing the structure, were disregarded in deriving the reflectivity equation.

Hence the reflectivity equation given by equation (10.1) may be re-written as:

$$R = \frac{x}{y \cos\theta}\left(\frac{k_1 y}{n_o \sin\theta}\right)^2 |n_a|^2 \quad . \qquad \ldots (10.17)$$

Substituting numerical values for x, y, and θ, then:

$$R = \frac{\sqrt{2}}{10}\left(\frac{k_1}{n_o}\right)^2 |n_a|^2 \qquad \ldots (10.18)$$

10.2 DISCRIMINATION OF CONTRIBUTIONS TO THE INDUCED NON-LINEAR REFRACTIVE INDEX MODULATIONS

In experiments in which the induced structure is established by a non-propagating standing light wave, i.e. $\omega_1 = \omega_2$, the contributions to the amplitude of the structure will come from all intensity dependent bulk changes of the material (see Chapter III, Sections 3.11-3.15, see also Section 3.16) for summary of relevant effects). It is therefore necessary to know the relative magnitude of each of these effects in order to discriminate between them.

Consider first the effects that do not depend on the absorption qualities of the media. Those effects are S.B.S., S.R.W., S.E.S, plus their associated in-phase components. By substituting values for the constants appearing in the expressions related to these effects (Chapter III, Section 3.16), it was found for $\omega(= \omega_1 - \omega_2) \approx 0$, that, for a general cross-section of liquids, these effects produced refractive index changes of the same order of magnitude, with the possible exception of the Kerr contribution (S.R.W. plus the in-phase component) which was slightly smaller. Typically, for a laser light power of $\sim$ 100 MW, the induced refractive index change is of the order of $10^{-6} \sim 10^{-7}$ c.g.s. e.s.u.

Consider now the thermally absorptive contribution, in an absorptive medium, induced by the standing light wave, i.e. S.T.R.S. plus the in-phase component (see Chapter III, Section 3.16). A numerical comparison of the induced refractive index change resulting from this effect with

any of those previously discussed shows that the absorptive effect is of the order of 100 to 1000 times greater. Typically, for a solution of Cu Ac in methanol having an absorption coefficient $\alpha \sim 0{\cdot}15\ cm^{-1}$, the absorptive effect is $\sim 5 \times 10^2$ times greater than the electrostrictive contribution, i.e. S.B.S. plus in-phase component. Therefore, for laser light power of $\sim$ 100 MW, the induced index change associated with absorptive heating is $\approx 10^{-4} \sim 10^{-5}$ c.g.s. e.s.u.

It is therefore evident that, for an absorptive medium, the thermal absorptive effect is by far the most dominant and so other contributing effects may be justifiably neglected. However, for a non-absorptive medium, where the contributions are all of the same order of magnitude, discrimination between these effects is far more difficult. Nevertheless, the presence of an effect can at least be detected.

The Kerr contribution, for example, can be detected when there is a difference in the refractive index induced by laser light when its polarization is parallel with, as compared with perpendicular to, that of the probe light. By Havelock's law[158]:

$$n_{\parallel} - n = 2(n_{\perp} - n) \ .$$

Therefore, the refractive index change for parallel polarization for light beams should be twice that for perpendicular polarizations. In practice the index change is detected by Bragg reflection of probe light off the induced structure. Since the reflectivity of this structure is proportional to the square of the index change, the Havelock ratio will be recorded as a ratio of 1:4 for a liquid in which the Kerr contribution is dominant. The ratio will be less for liquids in which more than one effect is present.

The presence of electrocaloric effect (entropy scattering and the in-phase component) can be detected by changing the temperature of

the liquid. As seen from Chapter III, Section 3.16, the refractive index change is proportional to temperature and so the reflectivity off the structure is proportional to the square of the temperature (Chapter III, Section 17). Hence a change in temperature by only a few degrees should make the effect detectable.

Finally it must be emphasised that the contribution of all these effects have been considered for $\omega \approx 0$ when the grating has been induced by a forward and backward travelling light wave of the same frequency. Under such conditions the contributions from effects such as that of electrostriction are extremely small compared to their peak values occurring at a displaced frequency such that $\omega \neq 0$, e.g. for the S.B.S. and the in-phase component, a maximum induced index amplitude occurs for $\omega \sim \omega_B$ (= vk). Under these conditions the magnitude of the phase grating is comparable with that induced by absorptive heating, and the effect may be identified by spectral analyses using a Fabry-Perot.

P A R T II

10.3 GENERAL DESCRIPTION OF EXPERIMENTAL ARRANGEMENT

The experimental arrangement is schematically illustrated in Plate 10.2.

The high power laser output had a pulse duration of $\sim$ 15 nsec and propagated in a single longitudinal mode. An aperture was used to reduce the divergence of the beam, and the resultant transmitted power densities were up to 100 MW/cm^2.

The light output passed through a quartz cell (cell 1) containing the liquid under investigation, and was re-directed back along its path through the cell in the opposite direction in one of two ways, either (a) by a non-frequency shifted reflection from a dielectric mirror accurately positioned normal to the incident radiation, or, (b) by a frequency shifted feedback of stimulated back-scattered light from a liquid contained in cell 2. A short focal length lens was used to produce the high radiation power fluxes ($\sim 10^4$ MW/cm^2) required to produce such stimulated scattering.

The forward and backward travelling waves through cell 1, produced a non-linear intensity dependent refractive index modulation within the liquid. This refractive index grating was probed using the continuous output from an argon ion laser (for full description of laser, see Chapter IV, Section 4.2). Maximum output powers of $\sim$ 1 W were obtained in a single line for the wavelengths 4880 Å and 5100 Å. The output, which was continuously recorded on a power meter during experimental investigations, was directed into the probe cell (cell 1) at the Bragg angle by fine adjustment of the mirror, M_i. The subsequent reflected argon laser light from the induced structure within the cell was directed into a photomultiplier P, from which the signal was finally recorded on to a Tektronix 454 oscilloscope.

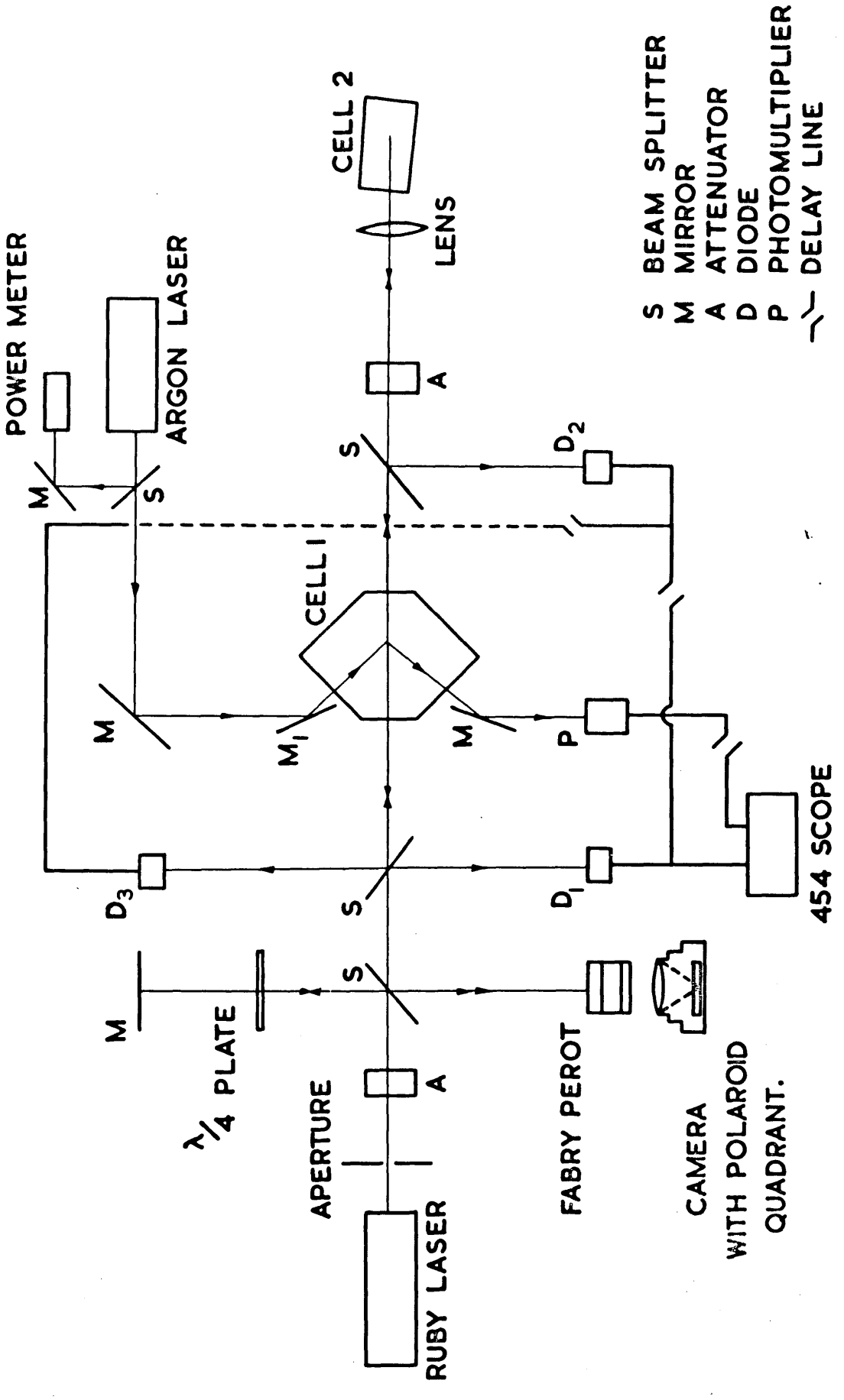

Fig.2 Experimental arrangement
CLM-P224

In addition to this recording, the oscilloscope also recorded the ruby laser radiation signals on the photo-diode detectors, D_1 , D_2 , and D_3 . Hence D_1 and D_2 measured the incident ruby beam power in each direction while P and D_3 simultaneously measured the amplitude of the refractive index modulation in the cell and the amplification which it caused in the beackward beam. By use of the appropriate cable delay lines, all four signals from the detectors were simultaneously displayed on a single trace of the 454 oscilloscope.

A Fabry-Perot was used for spectral analysis of the light in both the forward and the backward direction. Discrimination between these two beams was achieved using the ' $\lambda/4$ and polaroid quadrant' technique described in Chapter IV, Section 4.3. This system directly recorded the spectral composition of the laser output and of the amplified backward travelling wave.

The intensities of the ruby laser beam was controlled (and feed-back into the laser minimised) by means of $CuSo_4$ attenuators.

10.4 EXPERIMENTAL DETAILS

(i) Control and Description of Optical Components of the System

A single longitudinal mode output from the ruby was obtained using two narrow Q-switching cells, placed one at each end of the ruby and both containing a solution of cryptocyanine in methanol, in conjunction with a Fabry-Perot etalon serving as the exit mirror for the laser cavity (see Chapter IV. Section 4.1, and Chapter V, Section 5.5, for details).

The amplifier cell (cell 1) was mounted on a small movable 'trolley' which rested (by means of three ball bearings fixed to its underside) on the centre table of the kinematic optical table described in Chapter IV, Section 4.4; see also Plate 4.5). Two of the ball bearings sat in a

V-shaped groove and the remaining bearing rested on the surface of the table. Therefore, such a kinematically designed system only allowed one degree of movement of the trolley along the length of the groove. This arrangement was required for spatial analysis of the induced structure within the cell. Thus with the centre table accurately aligned, so that the length of the groove was parallel with the ruby beam direction, the cell-trolley arrangement could be moved along this length and the induced structure (within the liquid contained in the cell) could be probed by the argon beam, at any required position. With such a system the walls of the cell always retained the same angle with the incident laser beams and so the precise Bragg angle was perturbed by a minimal amount.

The Bragg angle of 45.5° between the ruby and argon laser beams permitted the very simple geometry of cell 1, and allowed the argon beam to enter the cell at normal incidence (see Plate 10.2). The walls of the cell, through which the ruby laser passed, were of high quality quartz and flat to $\lambda/10$. Thereby, phase distortion, resulting in a distorted refractive index modulation within the liquid, was minimised. The quartz flats were separated by a distance of about 10 cm.

The argon probe beam was directed into the cell by the mirror M_1. This mirror was assembled in a mount fixed to a horizontally rotating table possessing very sensitive angular adjustment, which was in turn rigidly fixed to a movable arm of the kinematic spectrometer table (see Plate 4.5).

Accurate alignment of the probe beam was achieved in the following manner. A horizontal bar, crossing above the scattering cell, was supported by a vertical column mounted on a movable arm of the spectrometer table. This bar had a small adjustable table fixed to its under-

side at the point where it crossed the vertical axis of the spectrometer table. A small piece of beam splitter, mounted on the underside of this table in a plane containing the vertical axis of the system, was immersed in the liquid of the scattering cell. Rotation of the moveable arm thus allowed measurement of the angle between the beams within the liquid in the cell.

The continuous output from a helium neon laser, in position, behind the ruby system, for general alignment(see Chapter IV, Section 4.6) was used to represent the ruby laser output. The movable arm was first positioned and the mirror adjusted to reflect this helium-neon laser output in a direction back along its incident path. Hence the mirror in this position simulated the induced grating. The movable arm was then turned (about the central axis of the 'kinematic table'), in a clockwise direction through the calculated Bragg angle of incidence. Thus the argon probe light would, if incident at the Bragg angle, be normally reflected off the mirror in its new position. Adjustment of mirror M_1, using the horizontially rotating table and movable arm, was made to meet this requirement. Precise interaction of the two laser beams was obtained by turning the moveable arm (that held the beam splitter), back to its original position and observing, on the mirror, the reflection points of the two beams; any vertical displacement between these points was corrected by a slight adjustment of either of the two deflecting mirrors for the incident argon probe beam. Finally the exit mirror, which was also mounted on a movable arm, was positioned to receive the Bragg reflected light from the 'beam splitter' and direct it into a photo-multiplier.

By using such an alignment procedure, the Bragg angle was located to within ± 3 minutes. The oscillator cell (cell 2) usually contained the same liquid as the amplifier cell (cell 1). Therefore the stimulated,

frequency shifted, backward travelling wave from cell 2 experienced maximum amplification on passing through cell 1. However, by using a series of different liquids in cell 2, the frequency of the stimulated light could be varied. By measuring the amplification experienced by each of these frequency components traversing the amplifier cell (containing the liquid under investigation), the gain-frequency profile for this liquid could be determined[95,30] (see Chapter III, Sections 3.11-3.16) for theoretical profiles for stimulated scattering). Alternatively the profile could be determined by measuring the magnitude of the Bragg reflected probe light off the induced structure, produced by each of the frequency shifted light beams. In practice, however, it is found that the frequency shifts produced in this way are too large to scan the gain-frequency profiles in any detail[95]. In fact the only process that could be adequately investigated by these methods was that of the stimulated Rayleigh wing. Zero frequency shifted feedback of laser light into the amplifier cell was produced by reflecting the incident light off a dielectric mirror which replaced the oscillator cell.

As stated earlier a $CuSo_4$ attenuator was used to prevent feedback of high amplitude laser radiation into the laser cavity. Thereby, the mode structure of the initial ruby laser output recorded on the Fabry-Perot system was well defined, and clearly discriminated from any subsequent weak frequency shifted feedback components which entered the laser system.

(ii) Control and Description of Laser Light Detection

The electronic circuit of the detection system is shown in Plate 10.3 (see Plate 10.2 for key to symbols). Laser light from both the ruby and the argon systems was detected by probing the beams with beam splitters. The reflected signals from the ruby beam were detected on three photo-diodes (D_1, D_2, and D_3) type E.M.I. 9648b. The diodes

Plate 10.3

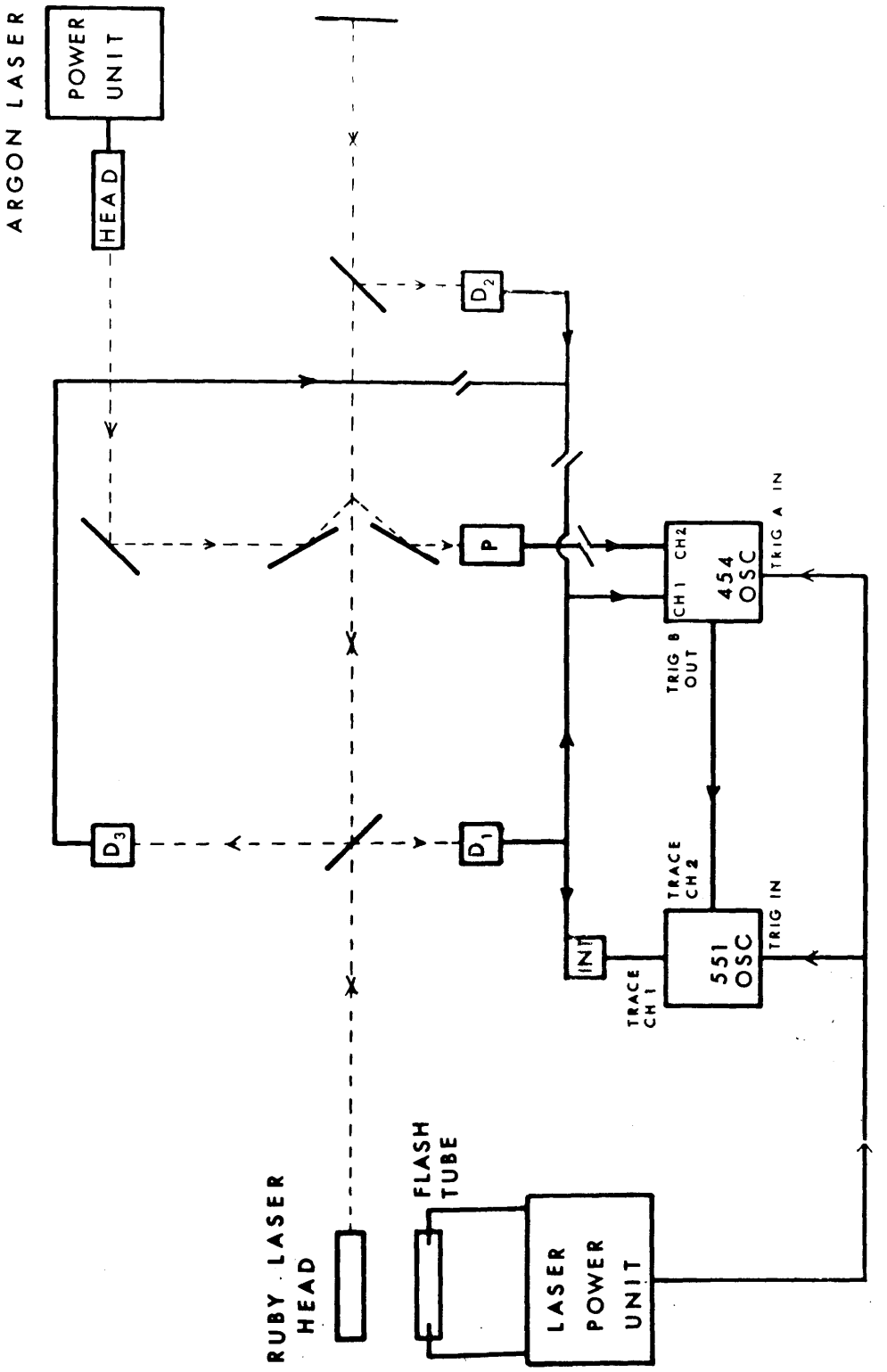
ARGON LASER
POWER UNIT
HEAD
D2
P
D3
D1
CH1 CH2
454 OSC
TRIG A IN
TRIG B OUT
TRACE CH2
TRIG IN
IN
TRACE CH1
551 OSC
FLASH TUBE
LASER POWER UNIT
RUBY LASER HEAD

D_1 , D_2 and D_3 recorded the laser power entering the probe cell in the forward direction and entering and leaving the cell in the backward direction respectively. The Bragg reflected argon laser signal was detected on a 56 A.V.P. photo-multiplier. Recordings of the signals from these detectors were made on a Tektronix 454 oscilloscope.

The 454 oscilloscope was used in a double triggering mode of operation. In this way the 454 was initially triggered (trig.A) by the triggering signal from the laser unit. After a set time delay (which was adjustable), trigger B automatically switched into operation, ready to record signals from the photo-tubes. This double triggering delay technique ensured that electronic noise from the laser triggering unit occurred during delay time before triggering B. Therefore the subsequent oscilloscope display, from the B triggering recorded only the signals from the photo-tubes.

Signals from the powerful ruby laser light and from the weak Bragg reflected argon light were recorded separately on Channels 1 and 2 of the oscilloscope, since the sensitivity requirements on the 454 needed for displaying the signals from the two laser beams were totally different. This separate recording of the argon signal was also advantageous when conducting experiments in which the ruby signal was constant but the argon signal variable (due to a variable induced grating).

By using the necessary lengths of delay cable, the signals from all four photo-tubes were displayed simultaneously and consequtively on one tract of the 454 oscilloscope (see Plate 10.4, Fig.(b) where the photo-multiplier trace is not recorded. The pulse signal from D_1 , displayed as the first pulse on the 454 was also recorded on the lower trace of a Tektronix 551 oscilloscope by means of the trig.B out control on the 454. The 551 was initially triggered by the ruby laser triggering unit and the upper trace recorded the total output from the ruby laser. From a

direct comparison of the two traces one could determine what pulse of the output recorded on D_1 was recorded on the 454. In practice the ruby laser system was arranged to give a single pulse output. However, due to the occassional presence of additional small parisitic pulses, it was essential to know which pulse triggered the 454, in order to correlate its associated power with the power of the induced Bragg reflected argon signal. Throughout the experiments the argon laser power was recorded on a power meter.

(iii) Calibration of the Ruby Laser Output

The calibration procedure was conducted in a similar way to that described in Chapter V, Section 5 6. In the present experimental arrangement (see Plate 10.2) the calorimeter was inserted after the second beam splitter and before the probe cell.

The results are shown in Plate 10.4, Fig.(a). As there was no backward travelling beam, the beam discriminator only transmitted light through two poloroid quadrants corresponding to the forward beam components. The 551 oscilloscope trace shows that the ruby laser emitted a single pulse which was recorded on the 454 oscilloscope.

The 454 calibrated trace illustrated in Plate 10.4, Fig.(b), shows the signals from the three photo-diodes D_1, D_2 and D_3 when the calorimeter was removed. The liquids contained in the attenuators and probe cell were non-absorbing and the back reflector was a dielectric mirror (reflectivity $\sim$ 100%). The power of the recorded D_1 signal was determined from the previous calibration and the powers of signals D_2 and D_3 were determined from an estimate of the losses suffered by the light in passing through the various optical components. Note that the dis-proportionate size of the D_2 and D_3 traces relative to the D_1 trace was due to differences in filtering.

Plate 10.4

D_1 pulse

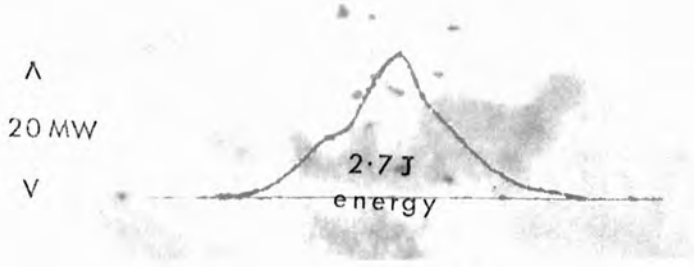

< 20 ns >

(a)

(b)

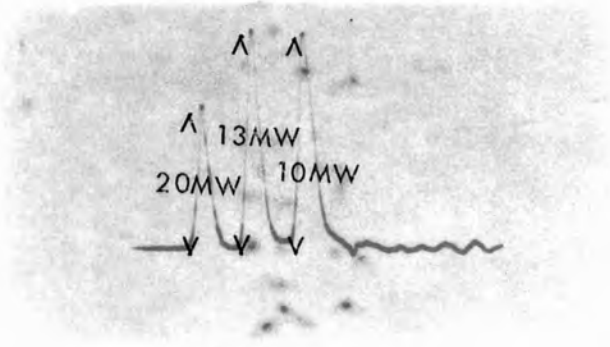

< 200ns >

Calibration

PART III

Results and Discussion

The majority of the results presented in the following sections were obtained using an absorptive liquid with an unshifted frequency feedback. Under such conditions the absorptive heating effect was dominant; (this will be experimentally confirmed in a later section).

These results should be regarded as representative of the kind of information, and the accuracy of measurements, which can be obtained by using this experimental technique in the investigation of all intensity dependent non-linear refractive index effects.

10.5 ANGULAR DEPENDENCE OF THE REFLECTIVITY

Using a solution of copper acetate in methanol with an absorption coefficient $\alpha = 0{\cdot}15\ \text{cm}^{-1}$, the angle giving the maximum Bragg reflection was measured to be $45{\cdot}5 \pm 0{\cdot}1^{\circ}$ and was equal to the theoretical value given by:

$$\cos^{-1} \frac{\lambda_a}{\lambda_r} \frac{n_r}{n_a} .$$

While the angle could only be measured absolutely to $\pm 0{\cdot}1^{\circ}$, small incremental adjustments could be made much more accurately (see section 10.4 of this Chapter). The results shown in Plate 10.5 are those for an angle run across the optimum Bragg angle. The reflectivity curve was plotted from the 454 oscilloscope recordings of the laser light signals shown in the plate. Note that the extreme right-hand signal is that of the Bragg reflected probe light. From these results it is seen that the width at half height is $\sim$ six minutes.

This may be compared with the theoretical value obtained from equation (3.83 of Chapter III, Section 17):-

Plate 10.5

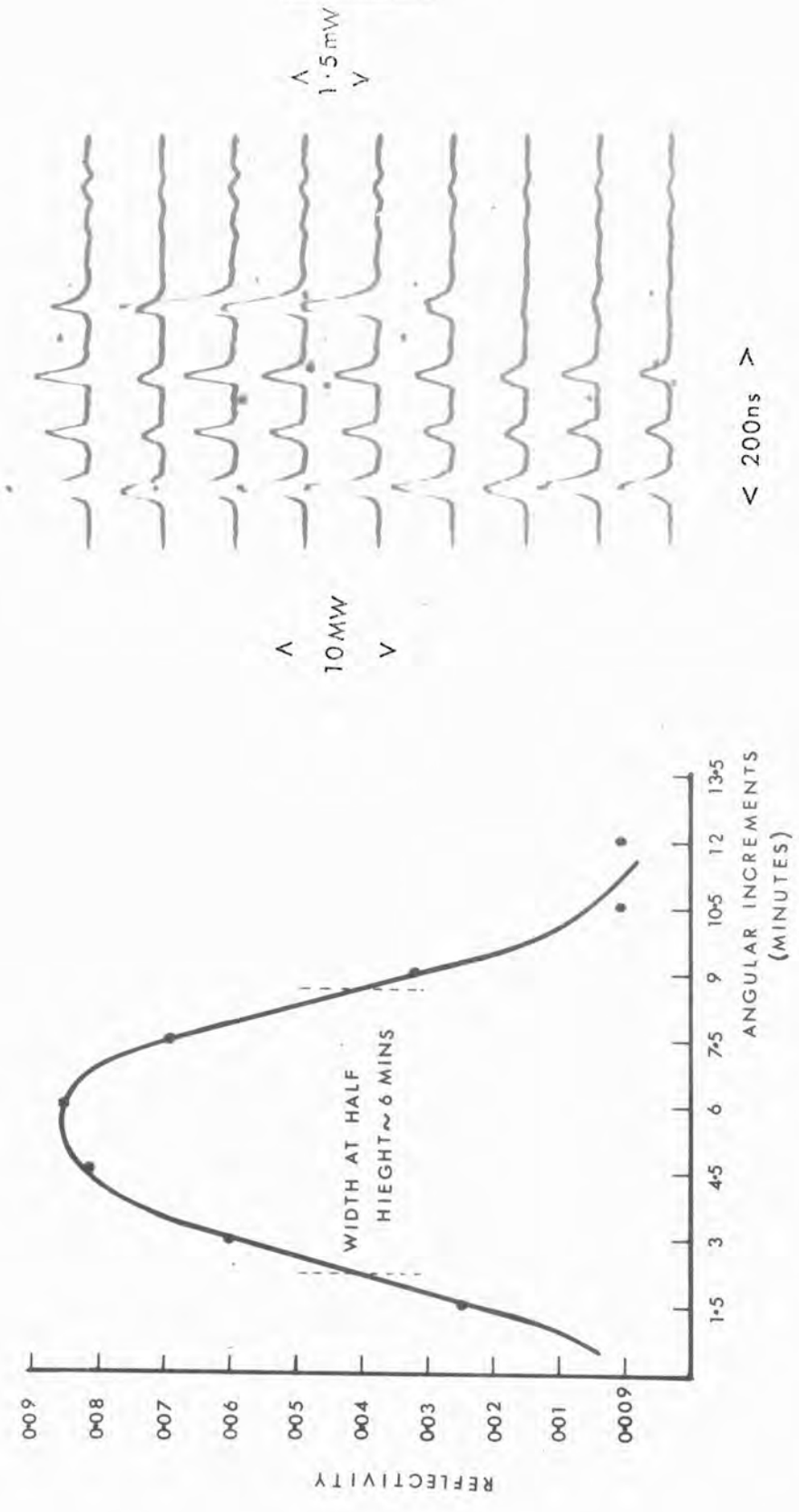

Angular Dependence of Reflectivity

$$\frac{1}{2} = \sin^2 \frac{\left(\frac{\Delta\theta}{\sin\theta} \cdot \frac{ky}{2}\right)}{\left(\frac{\Delta\theta}{\sin\theta} \cdot \frac{ky}{2}\right)^2}$$

where the interaction length L is for each element of interaction considered, equal to y, the diameter of the argon beam (see Section 1(v) of this Chapter). Hence:

$$\Delta\theta = \frac{2{\cdot}78 \sin\theta}{ky} \quad ,$$

where $k \approx 2k_1$, the incident ruby wave vector, $y \approx 0.1$ cm, and $\theta \sim 45^\circ$. Therefore $\Delta\theta \sim 15$ seconds.

The discrepancy between the theoretical and experimental values is attributed to the divergence of the argon probe beam which was of the order of six minutes. It is noted that this discrepancy could not have arisen from multi-frequency modulations produced by a multi-mode output from the ruby since, for an angular width at half height of approximately six minutes, a wavelength spread for the ruby output of ~ 6 Å would be required. This possibility could not have existed anyway, since the ruby output was controlled to give a single longitudinal mode.

10.6 DISCRIMINATING CHARACTERISTICS OF CONTRIBUTIONS TO THE INDUCED PHASE GRATING

(i) Electrostriction

The results in Plate 10.6 show the general features of the electrostrictive effect. The results were obtained using pure methanol contained in cell (1) and an unshifted frequency feedback (see Plate 10.2). The ruby laser was operated at power levels corresponding approximately to the power threshold for inducing S.B.S. within the Q-switch cryptocyanine-methanol solution. Hence the laser output was unshifted in frequency for power levels below the S.B.S. threshold, and for power

Plate 10.6

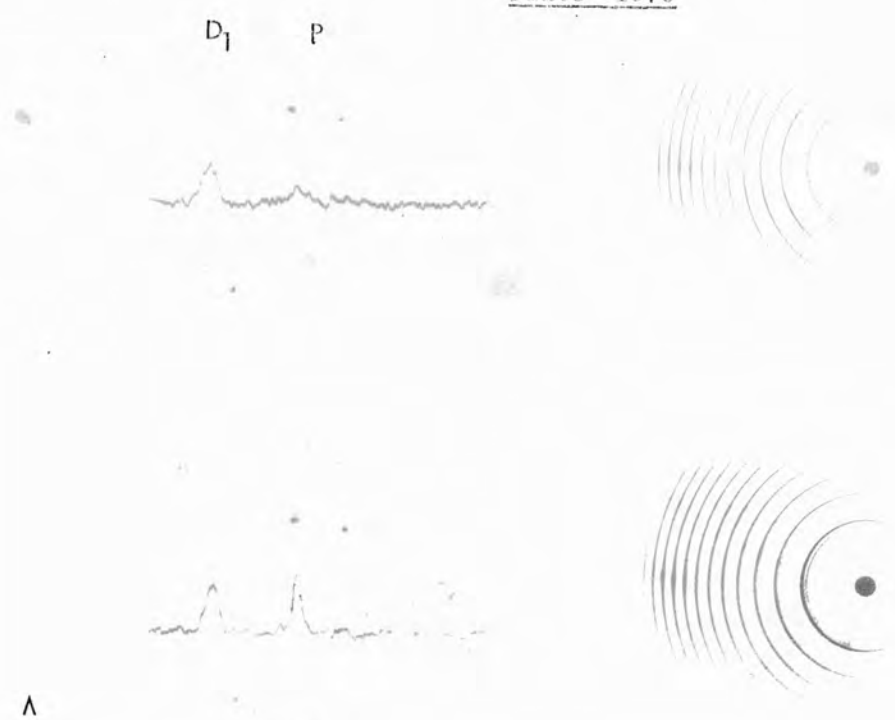

Electrostriction

levels above this threshold, one or more additional frequency shifted components were present.

Note that the Fabry-Perot recordings of the ruby output (see Plate 10.6) were taken without the forward-backward beam discrimination (see Chapter IV, Section 4.3).

The top set of results shown in Plate 10.6 were taken for power levels below the S.B.S. power threshold. The phase-grating produced in the methanol was therefore induced by the forward and backward travelling laser light of a single frequency. As expected, (see Plate 10.6) the reflection was negligibly small since, for $\omega\,(=\omega_1 - \omega_2) \approx 0$, the electrostrictive effect is off-resonance (see Chapter III, Section 3.16).

For power levels above the S.B.S. threshold the amplitude of the grating increased considerably, resulting in a relatively large Bragg reflected signal (see the remaining sets of results of Plate 10.6). Under such conditions, $\omega\,(=\omega_1 - \omega_2) \approx \omega_B$, which was the Brillouin shift for the Q-switching liquid. Since the probe liquid was the same as that for the Q-switch, the inducing light components of frequency ω_1 and $\omega_1 - \omega_B$ were on resonance to give a maximum refractive index modulation (see Chapter III, Section 3.16) in the probe cell.

(ii) Kerr Effect

The Kerr effect was investigated with an unshifted frequency feedback. From Chapter III. Section 3.16 it is seen that, for these conditions ($\omega \approx 0$), this effect is a maximum.

In Section 10.2 of this chapter, it was shown by Havelock's Law that, for the Kerr effect, the Bragg reflected light from a refractive index change induced by laser light. with its polorization parallel to that of the probe light, was four times greater than that obtained for

Plate 10.7

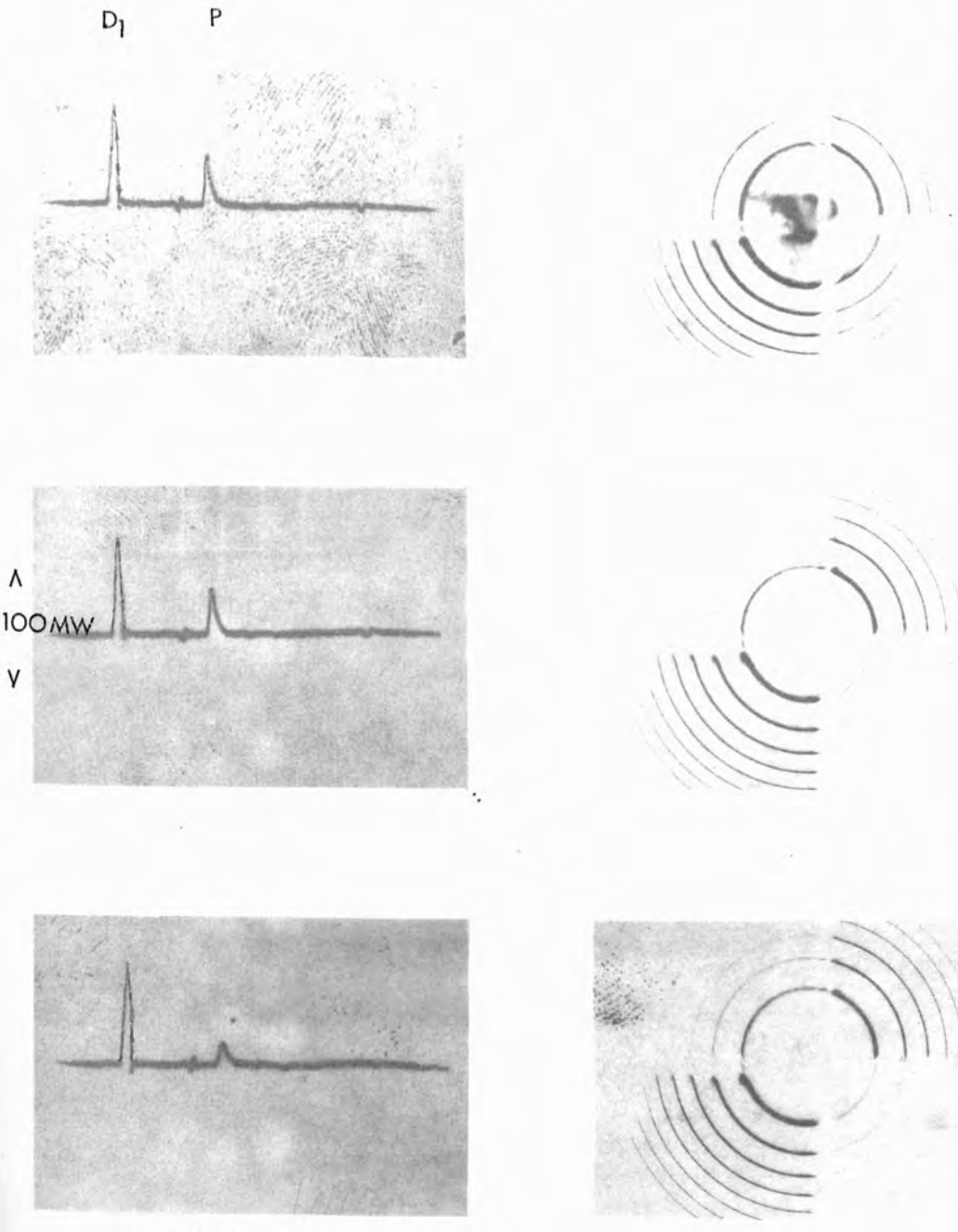

Kerr Effect

laser light with its polorization perpendicular to the probe light. The results are shown in Plate 10.7.

Tho polorization of the ruby light was rotated through 90^{o}, to be perpendicular to the probe beam, by passing the laser light through a crystalline quartz disc of width $\sim$ 4 mm (inserted before the probe cell containing methanol), in a direction along the optic axis. To normalize reflection and absorption losses of the laser light, this optical rotator was replaced by a fused quartz disc of similar dimensions when requiring laser light of undeviated polorization, i.e. parallel to the polorization of the probe beam.

The top set of results of Plate 10.7 show the Bragg reflected signal obtained without a quartz component. It is seen from the next set of results, obtained using the fused quartz component, that the light losses were in fact quite small. The lower set of results show the marked change in the Bragg reflected signal when the ruby polorization was set perpendicular to that of the probe light (by inserting the crystalline quartz disc). Note that the Fabry-Perot recordings were taken to ensure that no stimulated frequency shifted components were present, which would have confused the interpretation of results.

The measured ratio of the two Bragg reflected signals, for the two polorization settings, gave a ratio of $\sim \frac{1}{2}$ in contrast to the theoretical value of $\frac{1}{4}$. This suggests that, in addition to the Kerr effect, there were also present other non-linear contributions, such as the electrostrictive and electrocaloric effects. It should be noted that the induced reflection, resulting from these effects, was extremely small; experimental estimates showed that, for all the non-polar liquids studied, the absorptive heating effect (which was obtained by adding a small quantity of soluble absorber to the liquid) gave a reflection of $\sim 10^{4}$

times greater than that arising from these other effects for an unshifted frequency feedback. These results are in agreement with the theoretical estimate of Section 2 of this Chapter.

(iii) Absorptive Heating - Absolute Measurement of Reflectivity

The results of absorptive heating investigations are shown in Plate 10.8 for a solution of CuAc in methanol having an absorption coefficient $\alpha = 0{\cdot}15\ \text{cm}^{-1}$. The Fabry-Perot recordings again confirm that no frequency shifted components were present.

The upper set of recordings were taken for pure methanol and the lower set for a CuAc-methanol absorptive solution.

It is clearly seen from a direct comparison of the oscilloscope traces that the Bragg reflected signal (P), due to absorptive heating, was far greater than that due to any residual non-linear effects in the pure methanol, i.e. electrostriction etc. etc.

The photo-diode signals D_2 and D_3 show the gain experienced by the backward travelling laser light. Again, from a comparison of the two traces, the effect is quite noticeable.

The output laser power from the argon probe beam was 1 W and the Bragg reflected light power recorded on the trace was 1·5 mW. This gives an experimentally determined reflectivity for the phase grating of $R \sim 0{\cdot}15\%$. This may be compared with the theoretical value given by equation (10.18):

$$R = \frac{\sqrt{2}}{10}\left(\frac{k_1}{n_o}\right)^2 \left(\frac{\delta' \beta c \alpha}{8\pi \rho_o c_p} \frac{1}{\Gamma_R + \Gamma_L}\right)^2 I_1 I_2 ,$$

where the thermal absorptive contribution to the refractive index (see Chapter III, Section 3.16) for $\omega \approx 0$ has been substituted into this equation.

Plate 10.8

Absorptive Heating

Hence for laser light entering the methanol solution in the forward and backward direction, of beam diameter ~ ·5 cm and powers of 4 MW and 1·3 MW respectively, and with a linewidth of ~ 600 MH, the theoretically determined reflectivity for the phase grating was R ~ 0·2%. The good agreement between the experimental and theoretical values for the reflectivity should not be regarded as a true measure of the limit of accuracy of the theory (or the experiment) since considerably greater errors certainly exist in the theory, arising from (a) a disregard of the intensity profile of the ruby laser light, (b) estimating the interaction length, of the probe light with the induced structure, and neglecting mutual interference effects (see Section 10.1(v)).

10.7 DEPENDENCE OF REFLECTIVITY ON RUBY LASER POWER

It was shown in the introductory section of this chapter (see Section 10.1(i)) that the relationship between the reflectivity of the phase grating and the intensity of the laser beams inducing the grating may be approximated to the expression:-

$$R \propto I_1(0)\, I_2(\ell)$$

providing :

$$I_2 < I_1 \ll 70 \text{ MW/cm}^2.$$

This relationship has been experimentally confirmed for absorbing media of (a) CuAc in methanol (b) cryptocyanine in methanol.

(i) CuAc in Methanol

A solution of CuAc in methanol of absorption coefficient $\alpha = 0{\cdot}15 \text{ cm}^{-1}$ was contained in a quartz cell of length 4 cm. The backward travelling light was unshifted in frequency and attenuated by the attenuator A (Plate 10.2) such that $I_2(\ell) = 0{\cdot}33\, I_1(0)$. The reflectivity relationship may now be re-expressed as, reflectivity, $R \propto I_1^2(0)$. The results shown in Plate 10.9 are in good agreement with this theoretically predicted square law dependence of reflectivity on laser intensity.

Plate 10.9

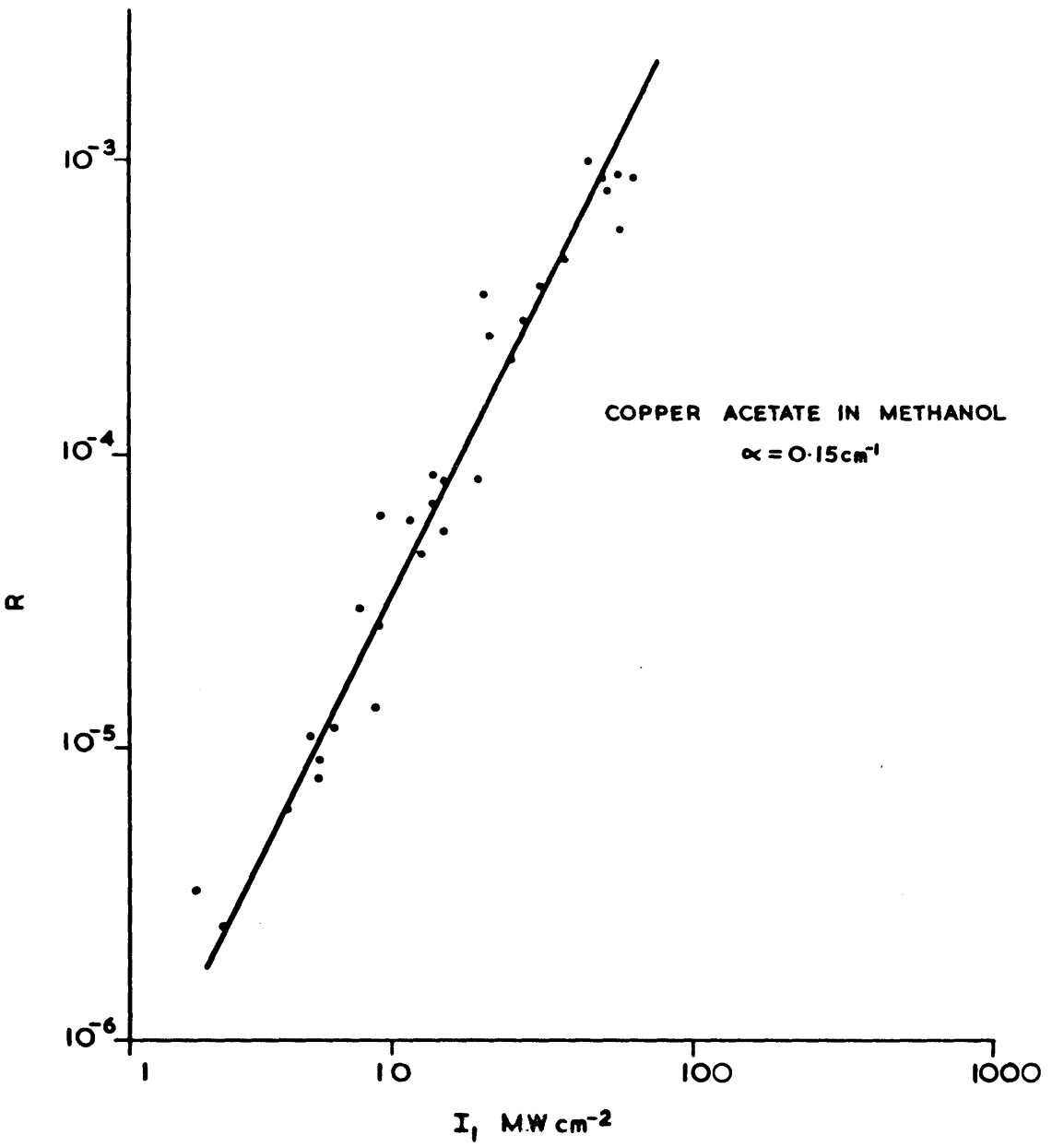

Fig.3

Reflectivity (R) of the phase grating as a function of the intensity (I_1) of the forward-going beam with $I_2 \propto I_1$. The line shows the theoretical square law.

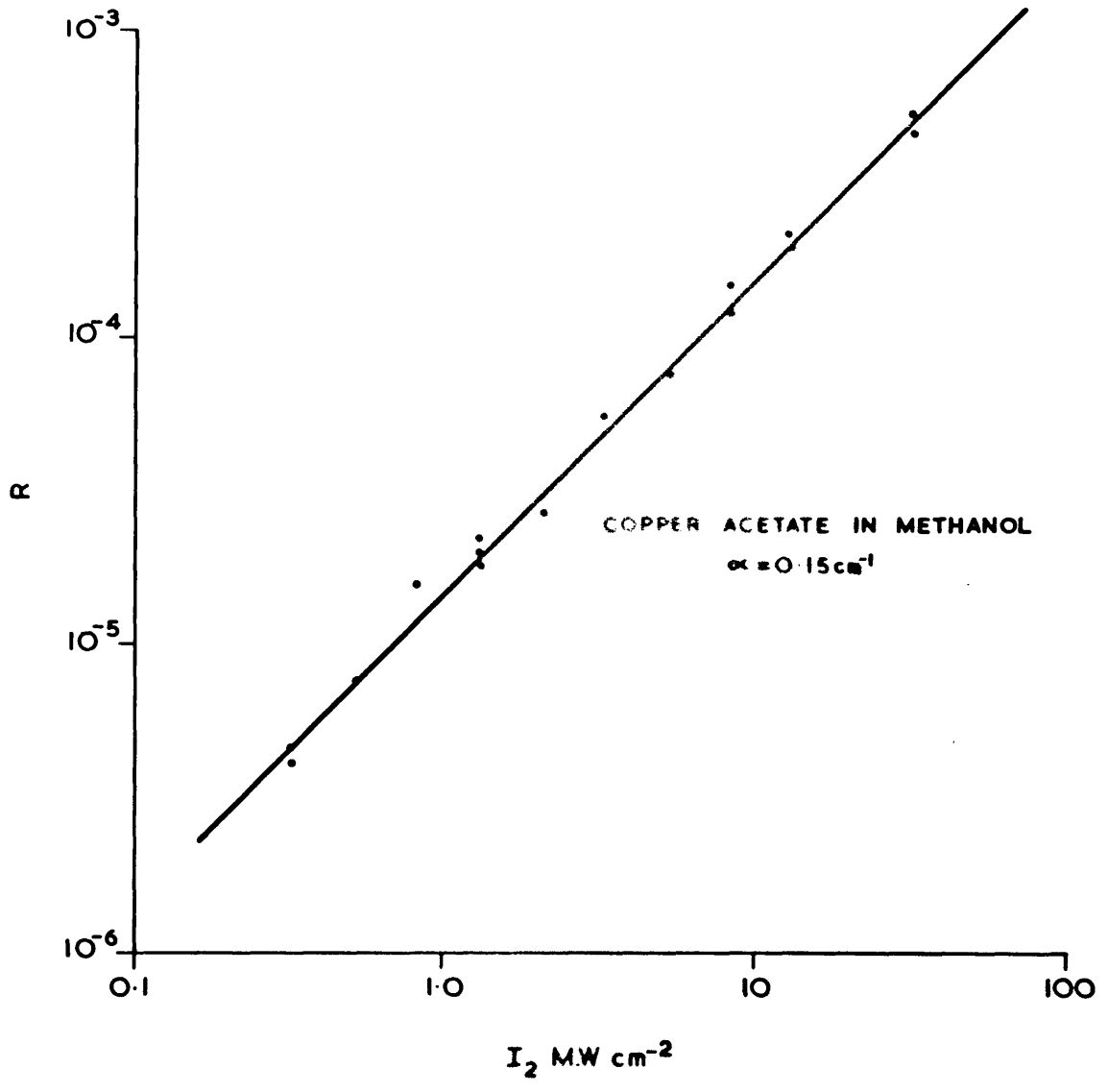

Fig.4
Reflectivity (R) of the phase grating as a function of the intensity (I_2) of the backward-going beam with I_1 constant at 71 MW cm^{-2}. The line shows the theoretical linear law.

It was expected, however, that the upper region of this curve would generally steepen (the points on the curve being too high by a factor of about 3) since the condition under which the reflectivity expression was valid was for $I_1(0) \ll 70$ MW cm^2. The lack of evidence of this steepening can, in all probability, be accounted for by an incorrect estimate in locating the position of the interacting region. For example for an incorrect estimate of 0·5 cm such that the interacting region was at $z = 2{\cdot}5$ cm, (instead of $z = 2$ cm) the intensity limit imposed on $I_1(0)$ would be raised to $\sim$ 100 MW. Hence the points on the curve corresponding to high intensities such as $I_1(0) \sim 70$ MW would be too low by a factor < 2. This factor falls within the limits of accuracy of the curve. The errors in the curve are ascribed mainly to variation of the divergence of the ruby light due to lack of transverse mode control.

Plate 10.10 shows that the reflectivity was proportional to $I_2(\ell)$ when $I_1(0)$ was kept constant. These results were obtained under identical conditions to those of the previous experiment with the exception that the absorption coefficient of the back attenuator was varied by controlled amounts in order to vary $I_2(\ell)$.

The two results discussed above confirm the theoretical relationships of reflectivity dependence on laser intensity.

(ii) Cryptocyanine in Methanol

The results in Plate 10.11 were obtained for a bleachable solution of cryptocyanine in methanol of absorption coefficient $\alpha = 0{\cdot}36$ cm^{-1}.

It is seen that, unlike the corresponding curve plotted for CuAc in methanol (see Plate 10.9), the square law dependence breaks down for ruby laser intensities $\gtrsim$ 10 MW.

Plate 10.11

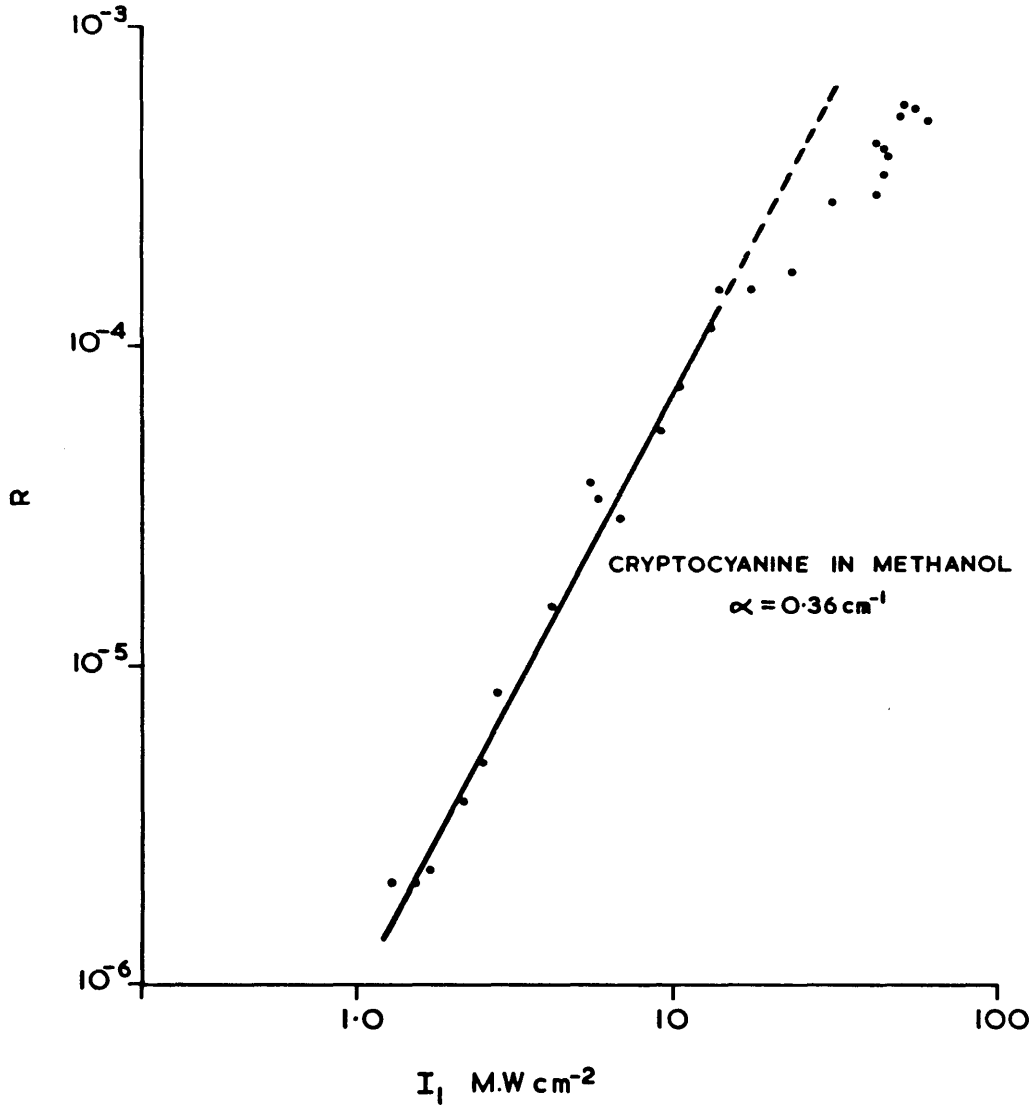

Fig.5
Reflectivity of phase grating as a function of I_1 for a saturable absorber.

This anomaly, it is believed, results from saturation of the cryptocyanine dye. For laser powers below dye saturation requirements there existed preferential, intensity dependent bleaching (see Chapter III, Section 3.8; Chapter V, Section 5.5 and Chapter 9, Section 9.1), which resulted in higher light absorption at the nodes than at the anti-nodes, thus producing a phase grating. However, for laser intensities in excess of that required to saturate the dye, there was a tendency towards uniform bleaching, resulting in a refractive index modulation of smaller amplitude.

This explanation is confirmed by the results of Chapter VI, where it was shown by a totally different experimental procedure, that the laser power threshold for bleaching of cryptocyanine was in fact 10 MW.

10.8 DEPENDENCE OF REFLECTIVITY ON ARGON LASER POWER

To ensure that the argon light was acting solely as a probe and not contributing significantly to the non-linear effects, the dependence of reflected power on incident argon power was investigated. For solutions not absorbing at the argon wavelength, e.g. CuAc in methanol, the expected linear dependence was observed (Plate 10.12). However, for solutions having even a slight absorption at the argon wavelength, e.g. nitrobenzene, thermal de-focusing (see Chapter VII) of the argon beam greatly reduced the Bragg reflection.

10.9 DEPENDENCE OF REFLECTIVITY ON ABSORBER CONCENTRATION

For an absorbing liquid, the reflectivity is proportional to the square of the concentration (see Section 10.1 (iv) of this chapter). Experimental measurement of the reflectivity as a function of the absorption coefficient α is complicated by the fact that variations of α affects the values $I_1(z)$ and $I_2(z)$. This can only be corrected for

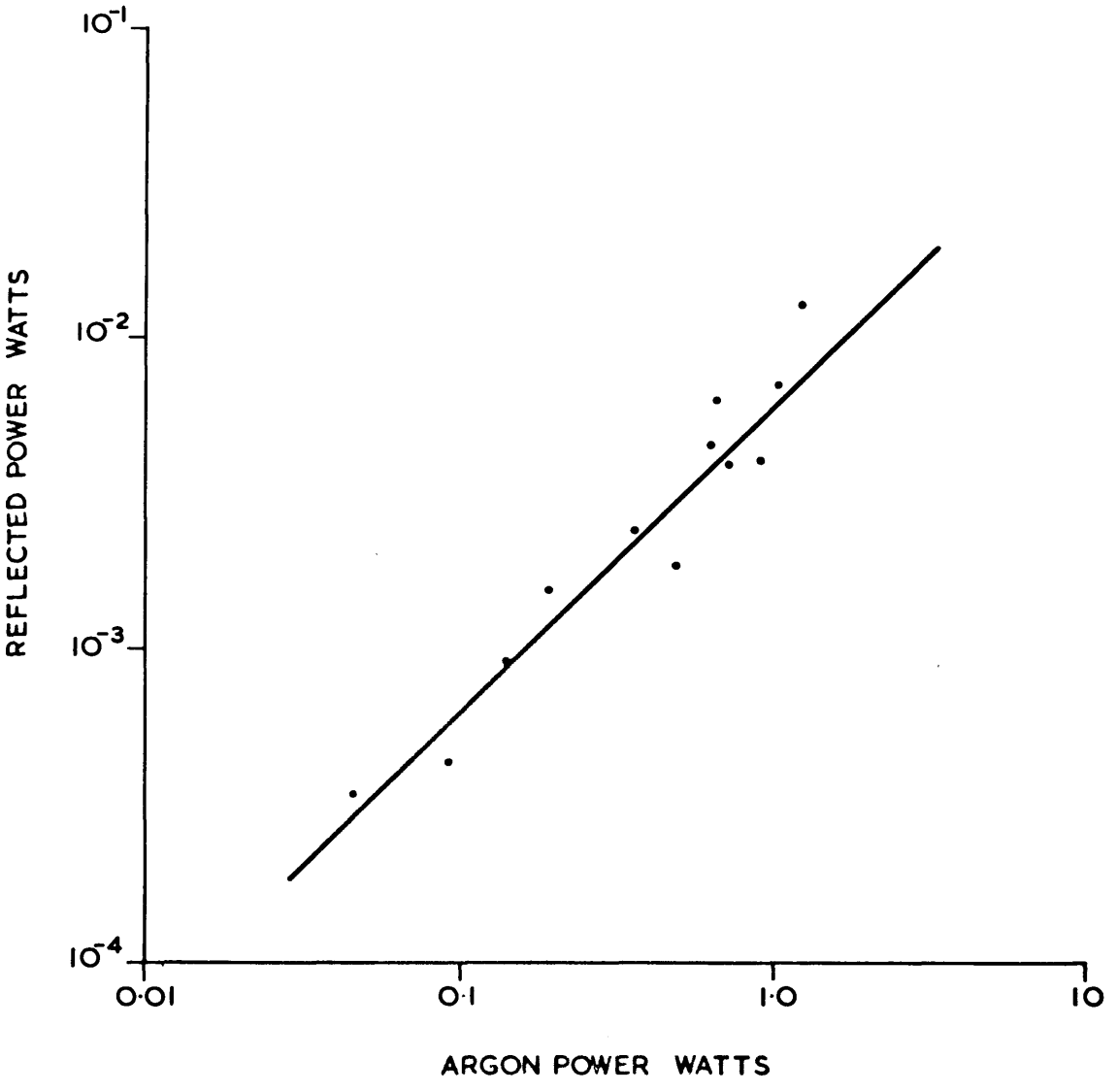

Fig.6
Reflected power as a function of incident argon laser power.

CLM-P224

as long as the non-linear effect in the cell has a negligible effect on the ruby beam, a condition that requires a short cell.

In these investigations such a thin cell (width $\sim \frac{1}{2}$ cm) containing the absorbing solution of CuAc-methanol under test, was immersed in pure methanol contained in the probe cell (1) (see Plate 10.2). In this way, the Bragg angle for the incident probe light was unaltered (assuming that the walls of the thin cell were parallel and that the CuAc solute had a negligible effect on changing the normal refraction index of the methanol). The results of the measurements of reflectivity of the phase grating as a function of varying absorption coefficient, are shown in Plate 10.13. Throughout the experiment the laser intensity was kept constant, corrections being made for the effect of linear absorption of the laser light passing through the cell in both directions. The theoretically predicted square law dependence of reflectivity on concentration is well confirmed by the experimental curve shown in Plate 10.13.

10.10 SPATIAL DEPENDENCE OF REFLECTIVITY

In this investigation the standard solution of CuAc in methanol, absorption coefficient $\alpha = 0{\cdot}15$ cm^{-1}, was contained in the probe cell (1) (see Plate 10.2). Spatial probing of the structure along the direction of the ruby laser light was facilitated by moving the cell in this direction (see section 10.4 of this chapter for experimental details).

It was shown earlier that the theoretical spatial dependence of reflectivity on z obeys the relation (Section 10.1(ii))

$$R \propto e^{g \frac{8\pi k_2}{c} I_1(0)(\ell - z)}.$$

The experimental plot shown in Plate 10.14 of $\ell n R$ against $(\ell - z)$ for $I_1(0)$ and $I_2(\ell)$ kept constant, confirm this result. The errors are again mainly attributed to lack of transverse mode control.

Plate 10.13

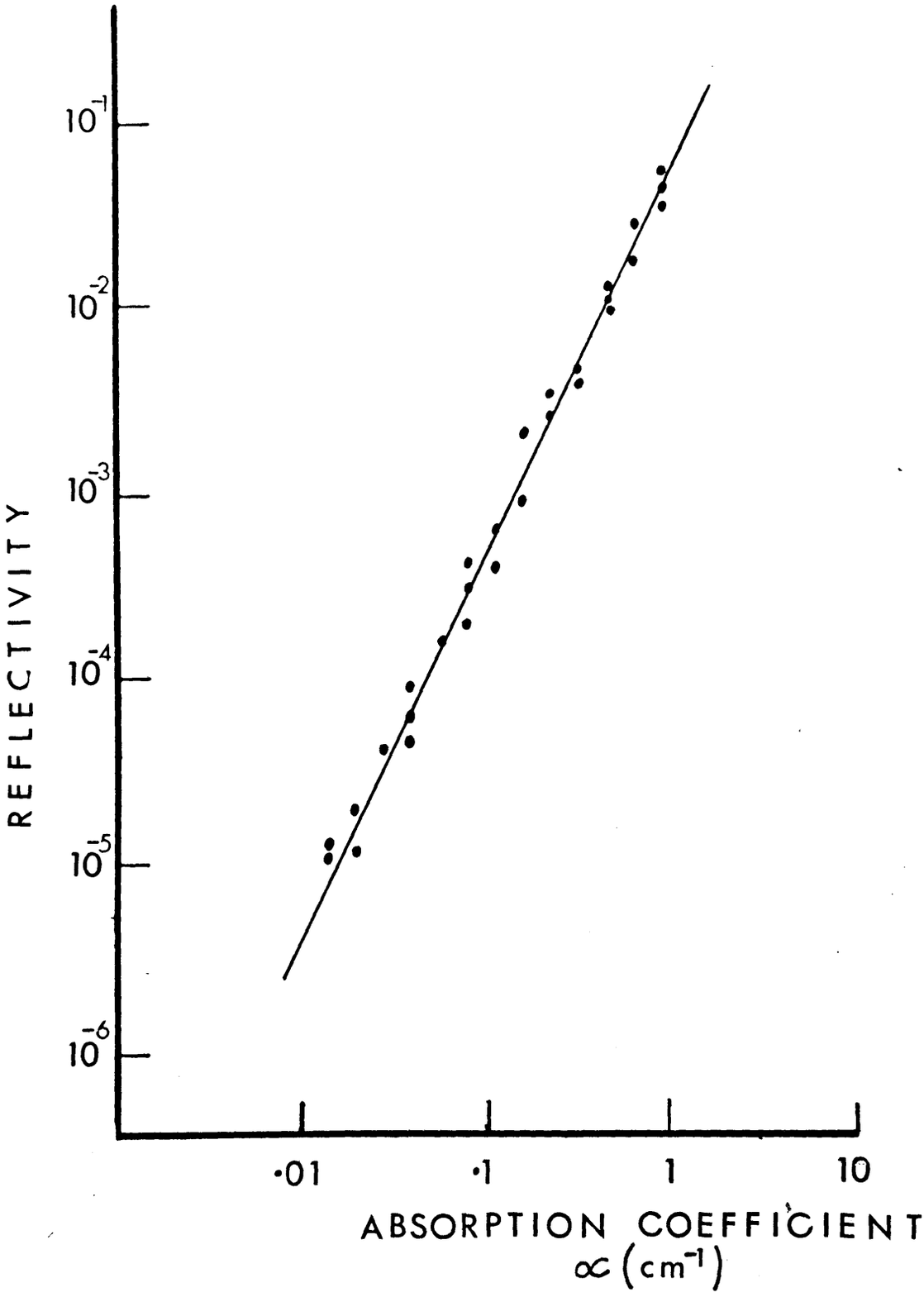
REFLECTIVITY
10^{-1}
10^{-2}
10^{-3}
10^{-4}
10^{-5}
10^{-6}
·01
·1
1
10
ABSORPTION COEFFICIENT
α (cm^{-1})

Plate 10.14

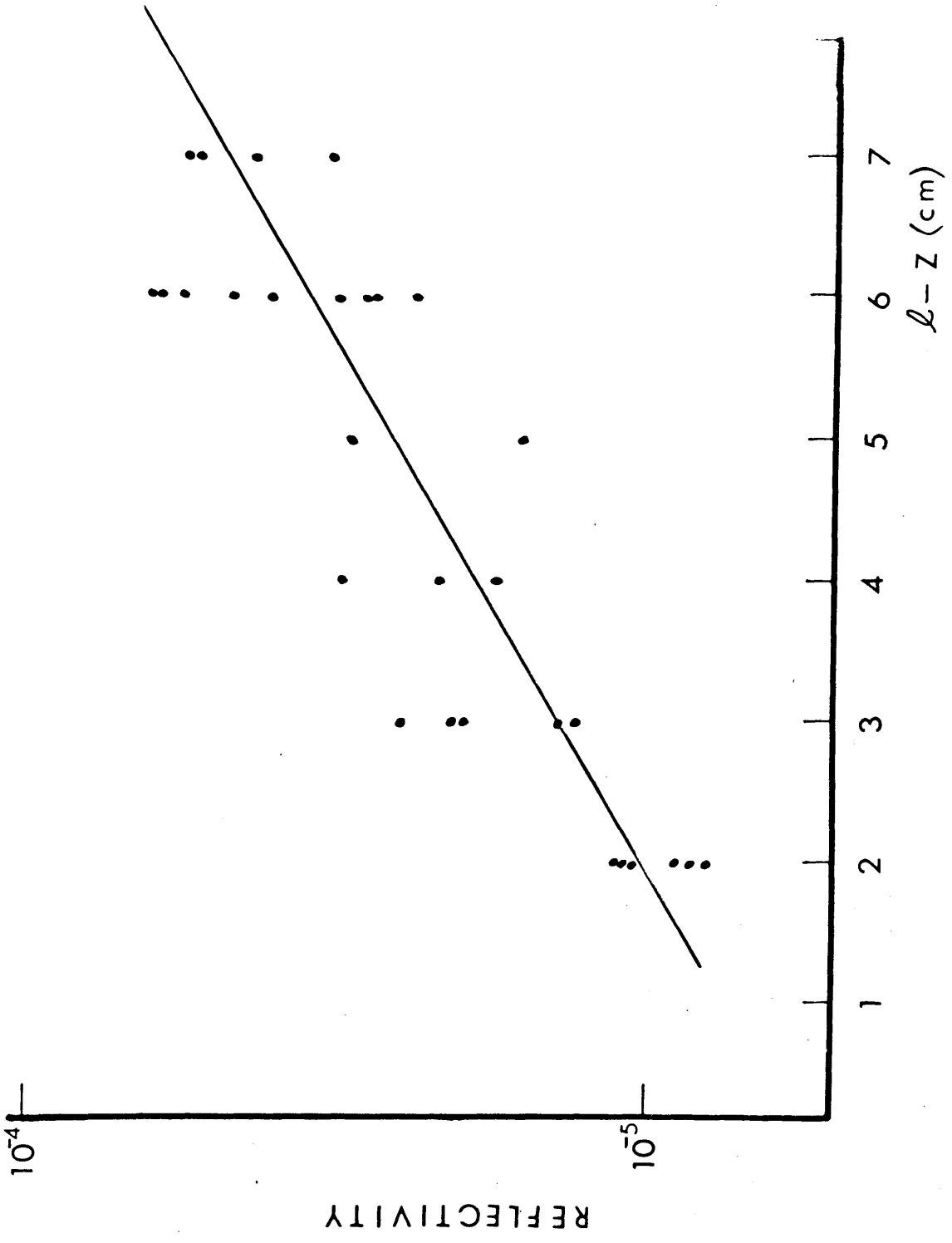

From the gradient of the slope a value for the gain coefficient may be determined. Hence for $I_1(0) \sim 45$ MW/cm^2 then $g(k_2/c) \approx (0{\cdot}3 \pm 0{\cdot}1) \times 10^{-3}$ cm/MW. This is in agreement with the theoretical value determined by equation (3.65) of Chapter III, Section 3.13 which gives a value for gain such that $g(k_2/c) = 0{\cdot}27 \times 10^{-3}$ cm/MW. (Note that in the gain equation 3.65 the effect of the laser linewidth is considered, i.e. Γ_R is replaced by $\Gamma_R + \Gamma_L$).

10.11 THERMAL RELAXATION TIMES OF LIQUIDS

From Section 10.1(iii) of this chapter it was shown that, due to the relatively long rise time of the detecting instruments, only temporal analyses could be made of induced refractive index modulations arising from the effect of absorptive heating. The results shown in Plate 10.15 (three lower traces) show the pronounced thermal relaxation arising from such an effect for absorptive solutions of CuAc in methanol, acetone and water respectively. The upper trace is that for electrostriction induced in methanol. Because of the fast relaxation time of the electrostrictive effect, this trace serves as a measure of the relatively long rise-time of the detecting instruments, i.e. photomultiplier and 454 oscilloscope.

Taking the rise-time into consideration then the observed reflectivity, R_0, off the induced structure, recorded on the photomultiplier is given by the expression:

$$R_0 \quad \alpha \; e^{-t/\tau_1} \int R \; e^{t/\tau_1} \; dt \; ,$$

where τ_1 is the rise-time of the instruments. A value for τ_1 was determined numerically by finding the best fit of the above expression, for various values of τ_1, to the oscilloscope recording of the electrostrictive effect.

Plate 10.15

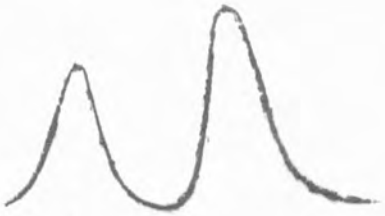

(a) Electrostriction

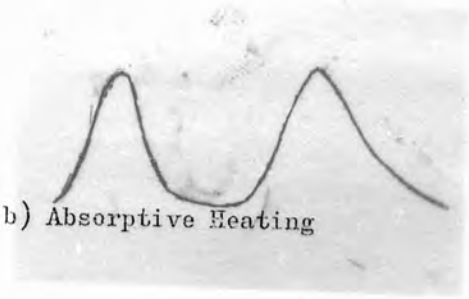

(b) Absorptive Heating

A

50 MW

V

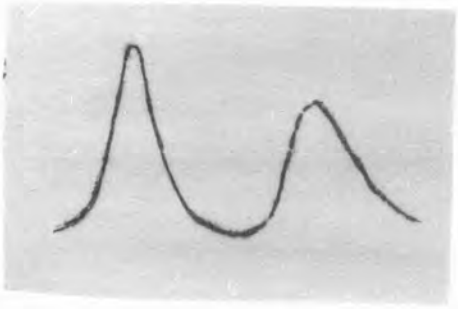

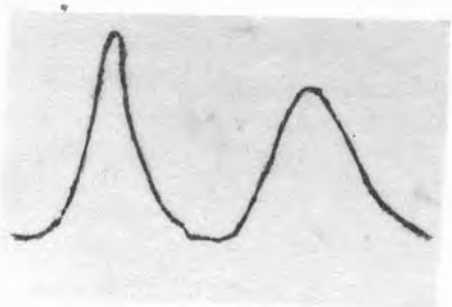

< 50ns >

D_1 P

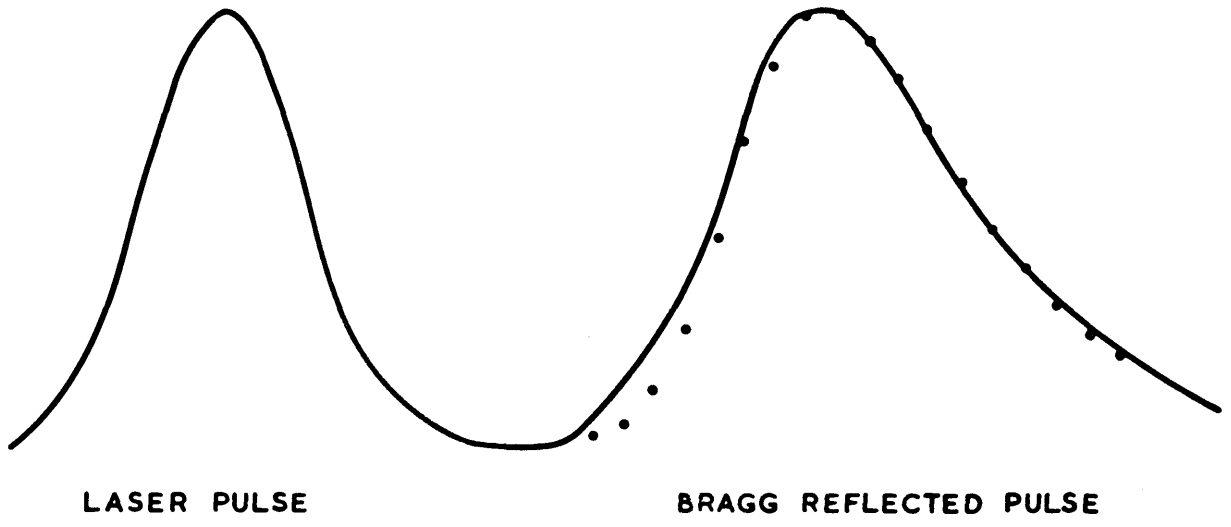

THERMAL

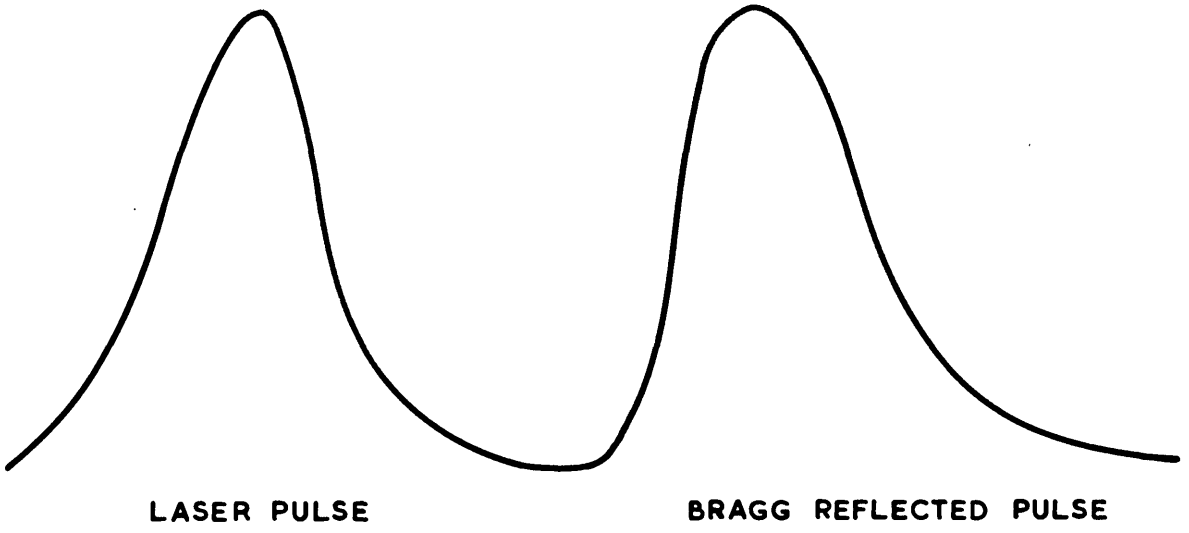

ELECTROSTRICTIVE

Fig.7 Time profile of the ruby laser pulse and the resulting Bragg reflected pulse in the thermal and electrostrictive cases. The points marked are those calculated given the theoretical relaxation time.

CLM-P224

Hence the reflectivity for the thermal decay process defined earlier (equation (10.4) will be modified when the instrumental rise-time is taken into consideration such that the observed reflectivity will be expressed as:

$$R_0 \propto e^{-t/\tau_1} \left[\int e^{-2t/\tau} \left(\int \sqrt{I_1(t)\, I_2(t)}\, e^{-t/\tau}\, dt \right)^2 dt \right] .$$

A value for τ the thermal relaxation time of the liquid is obtained in a similar way to that described above. Plate 10.16 shows the results of such calculations, for the thermal process in methanol, where the dots show the best theoretical fit to the experimental curve. Numerical calculations have been performed to determine the relaxation time. By this method the relaxation times of the liquid in methanol, acetone and water, (see Plate 10.15) have been determined[159] and shown to be in good agreement with theoretical values[160].

It is forseen that for future investigations of the relaxation times of other non-linear effects, e.g. lifetime of the phonons generated by the stimulated Brillouin effect, better detector resolution and shorter laser pulses will be required.

REFERENCES

(1) BLOEMBERGEN, N. and PERSHAN, P.S. Phys. Rev., vol.128, p.606, (1962)

(2) ARMSTRONG, J.A., BLOEMBERGEN, N., DUCUING, J. and PERSHAN, P.S., Phys. Rev., vol.127, p.1918, (1962)

(3) MAKER, P.D., TERHUNE, R.W., NISENOFF, M. and SAVAGE, C.M. Phys. Rev. Letters, vol.8, p.21, (1962)

(4) GIORDMAINE, J.A., Phys. Rev. Letters, vol.8, p.19, (1962)

(5) BASS, M., FRANKEN, P.A., WARD, J.F. and WEINREACH, G., Phys. Rev. Letters, vol.9, p.446, (1962).

(6) SMITH, A.W. and BRESLAU, N., J. Appl. Phys., vol.34, p.2105, (1963).

(7) MINCK, R.W., TERHUNE, R.W., and WANG, C.C. Applied Optics, vol.5, p.1595, (1966).

(8) HARRIS, S., Proc. I.E.E.E., vol.57, p.2096, (1969).

(9) KROLL, N., Phys. Rev., vol.127, p.1207, (1962).

(10) AKHMANOV, S.A., KOVRIGIN, A.I., PISKARSKAS, A.S., FADEEV, V.V. and KHOKLOV, R.V., J.E.T.P. Letters, vol.2, p.191, (1965).

(11) AKHMANOV, S.A., SUKHORUKOV, A.P. and KHOKHLOV, R.V., Sov. Phys - Usp., vol.93, p.609, (1968).

(12) CHIAO, R.Y., GARMIRE, E., and TOWNES, C.H., Phys. Rev. Letters, vol.13, p.479, (1964).

(13) KELLEY, P.L., Phys. Rev. Letters, vol.15, p.1005, (1965).

(14) GARMIRE, E., CHIAO, R.Y., and TOWNES, C.H., Phys. Rev. Letters, vol.16, p.347, (1966)

(15) AKHMANOV, S.A., SUKHORUKOV, A.P. and KHOKHLOV, R.V., Soviet Phys.- JETP, vol.23, p.1025, (1966).

(16) CALLEN, W.R., HUTH, B.G. and PANTELL, R.H., Appl. Phys. Letters, vol.11, p.103, (1967).

(17) AKHMANOV, S.A., KRINDACH, D.P., SUKHORUKOV, A.P. and KHOKHLOV, R.V. JETP Letters, vol.6, p.38, (1967)

(18) SHIMIZU, F., Phys. Rev. Letters, vol.19, p.8, (1967).

(19) BREWER, R.G., Phys. Rev. Letters, vol.19, p.8, (1967).

(20) BLOEMBERGEN, N., Am. J. Phys., vol.35, p.989, (1967).

(21) DENARIEZ, M. and BRET, G., Phys. Rev., vol.171, p.160, (1968).

(22) MAKER, P.D. and TERHUNE, R.W., Phys. Rev., vol.137, p.A801, (1965)

(23) BLOEMBERGEN, N. Non-Linear Optics, Benjamin, N.Y. (1965).

(24) LEVINE, A. Lasers, vol.2, Edward Arnold (publishers), (1968).

(25) FABELINSKII, I. and STARUNOV, V., Appl. Optics, 6, p.1793, (1967)

(26) GOLDBLATT, N.R. and LITOVITZ, T.A., J. Acous. Soc. America, vol.41, p.5, (1967).

(27) BAROCCHI, F., MARCINI, M. and VALLAURI, R., Il Nuova Cimento, vol.ILB, N.2, p.3669, (1967)

(28) ALCOCK, A.J. and DeMICHELIS, C., App. Phys. Letters, vol.11, p.6, (1967).

(29) POHL, D., Phys. Letters, vol.24A, p.239, (1967).

(30) POHL, D., MAIER, M. and KAISER, W., Phys. Rev. Letters, vol.20, p.366, (1968)

(31) WINTERLING, G. and HEINICKE, W., Phys. Letters, vol.27A, p.329, (1968)

(32) TIKHONOV, E.A. and SHPAK, M.T., JETP Letters, vol.8, p.173, (1968)

(33) LAUBEREAU, A., ENGLISCH, W. and KAISER, W., I.E.E.E. J. Quantum Electronics, vol.QE-5, p.410, (1969)

(34) GIBSON, A., Brit. J. App. Phys., series 2, vol.1, p.933, (1968)

(35) BELIKOVA, T.P., SAVCHENKO, A.N. and SVIRIDENKOV, E.A., Sov. Phys-JETP, vol.27, p.19, (1968).

(36) BONCH-BRUEVICH, A.M. and KHODOVO, V.A., Sov. Phys.-Usp., vol.85, p.1, (1965).

(37) KEY, P., HARRISON, R., LITTLE, V. and KATZENSTEIN, J. (Submitted for publication in IEEE J. Quantum Electronics.)

(38) GIORDMAINE, J. and HOWE, J., Phys. Rev. Lett., vol.11, p.207, (1963).

(39) ABELLA, I., Phys. Rev. Letters, vol.9, p.453, (1962).

(40) HARRISON, R., KEY, P., and LITTLE, V., British J. App. Phys., vol.3, p.758, (1970).

(41) REGENSBURGER, P. and PANIZZA, E. Phys. Rev. Letters, vol.18, p.113, (1967).

(42) GIULIANO, C. and HESS, L., IEEE J. Quantum Electronics, vol.QE-3, p.358, (1967)

(43) GIBBS, W., Appl. Phys. Letters, vol.11, p.113, (1967).

(44) BRILLOUIN, L., Ann. Phys., (Paris), vol.17, p.88, (1922)

(45) EINSTEIN, A., Ann. Phys., vol.38, p.1275, (1910)

(46) MASII, D., STARANOV, V., TIGANOFF, E. and FABELINSKI, I., Sov. Phys.-JETP, vol.22, p.6, (1966)

(47) LANDAU, L. and PLACZEK, G.,m Physik. Z. Sowjetunion, vol.5, p.172, (1934)

(48) FRENKEL, J., Kinetic Theory of Liquids. Clarenden Press, Oxford, (1946).

(49) GROSS, E., Nature, vol.126, p.201, (1930) also
J. de Phys., vol.6, p.457, (1935)
vol.7, p.113, (1936)

(50) STARUNOV, V., Sov. Phys.-Doklady, vol.8, p.1206, (1964)

(51) STARUNOV, V., Opt. Spektrosk, vol.18, p.165, (1963)

(52) ZAITSEV, G. and STARUNOV, V., Opt. Spektrosk, vol.22, p.221, (1965)

(53) PRORVIN, A., Opt. Spektrosk, vol.5, p.380, (1968)

(54) STARUNOV, V., TIGANOFF, E. and FABELINSKI, I., Sov. Phys.-JETP Letters, vol.5, p.260, (1967)

(55) STEGMAN, G. and STOICHEFF, B., Phys. Rev. Letters, vol.21, p.202, (1968).

(56) FABELINSKI, I., SABIROV, L., and STARUNOV, V., Phys. Letters, vol.29A, p.414, (1969)

(57) RAMAN, C., Ind. J. Phys., vol.2, p.387, (1928).

(58) RAMAN, C. and KRISHNAN, K., Nature, vol.121, p.501, (1928)

(59) LOUDON, R., Advan. Phys. vol.13, p.423, (1964)

(60) McLEAN, T. (Private communication)

(61) MANLEY, J. and ROWE, H., Proc. I.R.E., vol.44, p.904, (1956)

(62) GARRETT, G. and KAISER, W, Phys. Rev. Letters, vol.7, p.229, (1961)

(63) BLOEMBERGEN, N., Proc. Int. Sch. Phys. Enrico Fermi, Course XXXI (Accademic Press, New York, 1964)

(64) BLOEMBERGEN, N. and SHEN, Y., Phys. Rev., vol.133, p.A37, (1964)

(65) GARMINE, E., PANDARESE, F. and TOWNES, C., Phys. Rev. Letters, vol.11, p.160, (1963)

(66) WOODBURY, E. and NG, W., Proc. I.R.E., vol.50, p.2367, (1962)

(67) ECKHARDT, G., HELLWARTH, R., McCLUNG, F., SCHARTZ, S., WEINER, D. and WOODBURY, E., Phys. Rev. Letters, vol.9, p.455, (1962).

(68) TERHUNE, R., Bull. Am. Phys. Soc., vol.8, p.359, (1963).

(69) CHIAO, R., GARMIRE, E., TOWNES, C. and STOICHEFF, B., Proc. Int. Sch. Phys. Enrico Fermi, Course XXXI, (Academic Press, N.Y. 1964)

(70) LOUDON, R., Proc. Phys. Soc., vol.82, p.393, (1963)

(71) GROB, K., Z. Phys., vol.201, p.59, (1967).

(72) BLOEMBERGEN, N. and SHEN, Y., Phys. Rev. Letters, vol.12, p.504, (1964) also vol.13, p.720, (1964).

(73) SHEN, Y., Phys. Rev., vol.138, p.A1741, (1965).

(74) ALEKSANDROV. E., BONCH-BRUEVICH, A., KOSTIN, N. and KHODOVOI, V. Sov, Phys. - J.E.T.P., vol.22, p.986, (1966).

(75) MASTERS, J.I., WARD, J., and HARTOUNI, E., Rev. Sci. Instr., vol.34, p.365, (1963).

(76) SOFFER, B., J. Appl. Phys., vol.35, p.2551, (1964).

(77) SOROKIN, P.P., LUZZI, J.J., LANKARD, J.R., and PETTIT, G.D., I.B.M. J. Res. & Development, vol.8, p.182, (1964).

(78) KAFALAS, P., MASTERS, J.I., and MURRAY, E.M.E., J. Appl. Phys., vol.35, p.2349, (1964).

(79) BRETT, G., and GIRES, F., Appl. Phys. Letters, vol.4, p.175, (1964).

(80) HERMAN, R., and GRAY, M. Phys. Rev. Letters, vol.19, p.824, (1967).

(81) FOLTZ, N., CHO, C., RANK, D., and WIGGINS, T., Phys. Rev., vol.165., p.396, (1968).

(82) STARANOV, V., Sov. Phys - Dokl., vol.13, p.217, (1968)

(83) HERMAN, R., Phys. Rev., vol.164, p.200, (1967)

(84) MASH, D., MOROZOV, V., STARUNOV, V. and FABELINSKI, I., J.E.T.P. Letters, vol.2, p.25, (1965).

(85) CHO, C., FOLTZ, N., RANK, D., WIGGINS, T., Phys. Rev. Letters, vol.18, p.107, (1967).

(86) BLOEMBERGEN, N. and LALLEMAND, P., Phys. Rev. Letters, vol.16, p.81, (1966)

(87) SHEN, Y., and SHAKAM, Y., Phys. Rev., vol.163, p.224, (1967)

(88) ABRAHAM, M. and BECKER, R., 'Electricity and Magnetism', (Blackie & Son, 1932)

(89) LANDAU, L. and LIFSHITZ, E. 'Electrodynamics of Continuous Media, (Pergamon Press, 1965).

(90) STARUNOV, V. Phys. Letters, vol.26A, p.428, (1968).

(91) AKHMANOV, S. and KHOKHLOV, V., Sov. Phys - Usp., vol.11, p.394, (1968).

(92) CUMMINS, H. and GAMMON, R., J. Chem. Phys., vol.44, p.2785, (1966)

(93) HUNT, F., 'American Institute of Physics Handbook' (McGraw-Hill Book Company, Inc., New York, 1957).

(94) MOUNTAIN, R., Rev. Modern Phys., vol.38, p.205, (1966)

(95) DENARIEZ, M. and BRET, G. Phys. Rev., vol.171, p.160, (1968)

(96) CHIAO, R., TOWNES, C. and STOICHEFF, B., Phys. Rev. Letters, vol.12, p.592, (1964).

(97) KROLL, N., J. Appl. Phys., vol.36, p.34, (1965).

(98) GROBB, K., Z. Physik, vol.201, p.59, (1967).

(99) GARMIRE. E., and TOWNES, C., Appl. Phys. Letters, vol.5, p.84, (1964)

(100) MACH, D., MOROZOV. V., STARUNOV, V., and FABELINSKII, I., J.E.T.P. Letters, vol.2, p.349, (1965)

(101) TANG, C., J. Appl. Phys., vol.37, p.2945, (1966)

(102) MAIER, M., Phys. Rev., vol.166, p.113, (1968)

(103) BAROCCHI, F., J. Appl. Phys., vol.46, p.2867, (1969)

(104) ZLATIN, S., KRIVOKHIZHA, S., and FABELINSKII, I., Sov. Phys. - J.E.T.P., vol.29, p.638, (1969)

(105) SHEN, Y., Phys. Letters, vol.20, p.378, (1966)

(106) POHL, D., REINHOLD, I. and KAISER, W. Phys. Rev. Letters, vol.20, p.1141, (1968).

(107) RANK, D., CHO, C., FOLTZ, N., WIGGINS, T., Phys. Rev. Letters, vol.19, p.828, (1967).

(108) CHO, C., FOLTZ, N., RANK, D., and WIGGINS, T., Phys. Rev., vol.175, p.271, (1968)

(109) WIGGINS, T., CHO, C., DIETZ, D. and FOLTZ, N., Phys. Rev. Letters, vol.20, p.831, (1968).

(110) GRAY, M. and HERMAN, R., Phys. Rev., vol.181, p.374, (1969)

(111) LETOKHOV, V., and PAVLIK, B., Sov. Phys.-Tech. Phys., vol.13, p.251, (1968)

(112) ZAITSEV, G., KYZYLASOV, Yu., STARUNOV, V., and FABELINSKII, I., J.E.T.P. Letters, vol.6, p.255, (1967).

(113) MASH, D., MOROZOV, V., STARUNOV, V., and FABELINSKII, I. Sov. Phys.-JETP, vol.28, p.1085, (1969)

(114) BESPALOV, V. and KUBAREV, A., J.E.T.P. Letters, vol.6, p.31, (1967)

(115) QUATE, C.F., WILKINSON, C., and WINSLOW, D., Proc. I.E.E.E., vol.53, p.1604, (1965)

(116) ASKARYAN, G., Sov. Phys.-JETP, vol.15, p.1088, (1962)

(117) TALANOV, V., Izv. vuzov (Radiofizika), vol.7, p.564, (1964)

(118) CHIAO, R., GARMIRE, E., and TOWNES, C., Phys. Rev. Letters, vol.14, p.1056, (1965)

(119) PILIPETSKII, N., and RUSTAMOV, A., J.E.T.P. Letters, vol.2, p.55, (1965)

(120) HAUCHECORNE, G., and MAYER, G., Compt. Rendus, vol.261, p.4014, (1965)

(121) WANG, C., Phys. Rev. Letters, vol.16, p.344, (1966),

(122) SACCHI, C., and TOWNES, C. Phys. Rev., vol.174, p.439, (1968)

(123) CHIAO, R., JOHNSON, M., KRINSKY, S., SMITH, H., TOWNES, C., and GARMIRE, E., I.E.E.E. J. of Quant. Electronics, vol.2, p.467, (1966)

(124) BREWER, R. and LIFSITZ, J. Phys. Letters, vol.23, p.79, (1966)

(125) AKHMANOV, S., KRINDACH, D., SUKHORUKOV, A., and KHOKHLOV, R., J.E.T.P. Letters, vol.6, p.38, (1967)

(126) CALLEN, W., HUTH, B., and PANTELL, R., Appl. Phys. Letters, vol.11, p.103, (1967).

(127) KEY, P., HAYWARD, G., HARRISON, R., and LITTLE, V., J. Sci. Instr. vol.2, p.374, (1969)

(128) BATEMAN, D., Royal Aircraft Establishment, Tech. Report no.66349.

(129) LEVINE, A., 'Lasers', vol.1, (Edward Arnold (publishers) 1966)

(130 LANGYEL, B., 'Introduction to Laser Physics' (John Wiley & Sons, Inc., New York, 1966)

(131) HEAVENS, O., 'Optical Masers', (London, Methuen & Co. Ltd., 1964).

(132) HUGHES, T., Nature, vol.195, p.325, (1962).

(133) KISLUIK, P., and WALSH, D., Bull. Am. Phys. Soc., vol.7, p.330, (1962)

(134) HAKEN, H., and SAUERMANN, H., Z. Physik, vol.173, p.261, (1963)

(135) TANG, C., STATZ, H., and deMARS, G., J. Appl. Phys., vol.34, p.2289, (1963)

(136) BENNETT, W. Jr., Phys. Rev., vol.126, p.580, (1962)

(137) BOERSCH, H., and EICHLER, H., Zeits. f. Angew. Physik, vol.22, p.378, (1967)

(138) DeMARIA, A., STETSER, D., GLENN, W. Jr., Science, vol.156, p.1557, (1967)

(139) DeMARIA, A., GLENN, W., BRIENZA, M., and MACK, M., Proc. I.E.E.E. vol.57, p.2, (1969)

(140) HARGROVE, L., FORK, R., POLLACK, A., Appl. Phys. Letters, vol.5, p.4, (1964)

(141) MOCKER, H., Appl. Phys. Letters, vol.7, p.270, (1965)

(142) DeMARIA, A., STETSER, D. and HEYNAU, H., Appl. Phys. Letters, vol.8, p.174, (1966)

(143) KATZENSTEIN, J., MAGYAR, G., and SELDON, A., Opto-Electronics, vol.1, p.13, (1969)

(144) HARRISON, R., KEY, P., LITTLE, V., MAGYAR, G. and KATZENSTEIN, J. Appl. Phys. Letters, vol.13, p.253, (1968)

(145) BAKER, J., and PETERS, C., Appl. Opt., vol.1, p.674, (1962)

(146) SKINNER, J.G. and GEUSIC, J.E., 47th Annual Meeting Optical Society of America; Quantum Electronics, (P. Grivet and N. Bloembergen, eds.), Columbia University Press, New York, vol.III, p.1437, (1964)

(147) HERCHER M., CHU, W., and STOCKMAN, D., IEEE J. Quantum Electron. QE-4, p.954, (1968)

(148) KASHA, M., Disc. Faraday Soc., vol.9, p.14, (1950)

(149) GIRES, F., IEEE J. Quantum Electronic, vol.QE-2, p.624, (1966)

(150) SELDEN, A., British J. Appl. Phys., vol.18, p.743, (1967)

(151) ARMSTRONG, J., J. Appl. Phys., vol.36, p.471, (1965)

(152) LITTLE, V., KEY, P., HARRISON, R., Nature, vol.216, p.257, (1967)

(153) BRODIN, M., and KAMUZ, A., J.E.T.P. Letters, vol.9, p.351, (1969)

(154) KAPLAN, A., J.E.T.P. Letters, vol.9, p.33, (1969)

(155) KATS, A., and KONTOROVICK, V., J.E.T.P. Letters, vol.9, p.112, (1969)

(156) WIGGINS, T., WICK, R., RANK, D., and GUENTHER, A., Appl. Opt. vol.4, p.1203, (1965)

(157) CHABAN, A., Opt. and Spect., vol.24, p.429, (1968)

(158) DITCHBURN, R. 'Light' (1952)

(159) KEY, P. 'The Scattering of Light from Light Induced Structures in Liquids. (Ph.D. Thesis, 1970)

(160) SELDON, A. (Private communications)

A C K N O W L E D G E M E N T S

I wish to express my deep gratitude for the constant guidance and encouragement of Dr V.I. Little who supervised this project.

My thanks are also due to Dr G. Magyar and Dr J. Katzenstein for much stimulating discussion and to J. Hayward for his invaluable technical assistance.

The experimental work was carried out at both Royal Holloway College and Culham Laboratory. I wish to thank those principally involved in this contract, Prof. S. Tolansky and Dr V. Little of Royal Holloway College, and Dr J. Katzenstein and Mr B. Tozer of Culham Laboratory. I am also indepted to the Science Research Council for their financial support of this project.

My warm thanks are expressed to my parents for their help and constant encouragement and to Miss M. Mendelssohn and A. Seldon and in particularly to P. Key, with whom I collaborated, for many interesting and entertaining discussions.

I am most grateful to Mrs I. Godwin for the great care and interest taken by her in the preparation of this manuscript.

Journal of Scientific Instruments (Journal of Physics E)
1969 Series 2 Volume 2

A high precision spectrometer table

P Key, G Hayward, R G Harrison and V I Little
Department of Physics, Royal Holloway College
(University of London), Egham, Surrey
MS *received 3 January 1969*

Abstract In this note a novel form of spectrometer table is described. It has easily demountable arms and an incremental accuracy to 10^{-5} radian.

Notes on experimental technique and apparatus

A versatile spectrometer table with removable arms has been designed by using kinematic principles. Such design allows various optical systems to be set up and positioned with considerable accuracy and with the minimum of effort. A table of this kind has been used successfully by the authors (Harrison *et al.* 1968) in an experiment in which laser light was Bragg-reflected from a laser-induced structure in a liquid.

The design is shown in figure 1. The movable arm has two ball bearings rigidly fixed to its underside. These rest in a

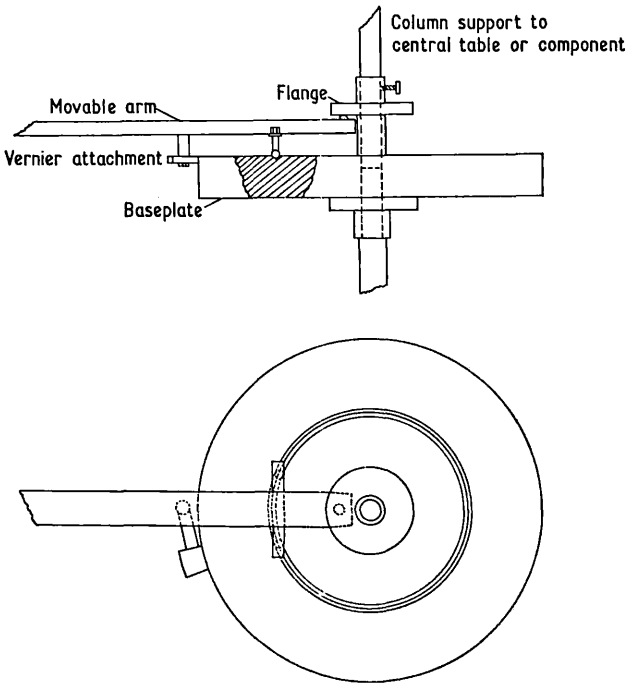

Figure 1

circular groove of V-shaped cross section, cut in the baseplate. A third ball bearing fixed to the upper face of the arm and positioned at its end makes contact with the underside of a flange machined parallel to the baseplate. Thus five points of contact are made between the arm and the fixed part of the instrument leaving one degree of freedom, i.e. rotation about a central axis. When the balls are correctly located, as shown in the diagram, the system is in neutral equilibrium provided the centre of mass of the arm lies outside the V-groove circle. A number of arms may be positioned simultaneously, and arms may easily be interchanged.

Angular displacements of an arm may be estimated with the help of a vernier scale attached to the arm and a circular scale engraved on the baseplate. A micrometer screw may be adapted to the system and used to achieve more precise adjustments.

The accuracy with which the groove and the flange have been machined sets an upper limit to the precision with which changes in the angular position of an arm may be made. For the system described, machining tolerances of the order 1 in 10^4 imply that a displacement of the order 10^{-1} radian will be subject to angular errors no greater than 10^{-5} radian, assuming of course that the machining errors are distributed and not localized over a narrow angular range.

References

Harrison R G Key P Y Little V I Magyar G and Katzenstein J 1968 *Appl. Phys. Lett.* **13** 253–5

Fluorescence due to excited state absorption in saturable absorbers

R. G. HARRISON, P. Y. KEY and V. I. LITTLE

Royal Holloway College, University of London

MS. received 5th November 1969, in revised form 26th January 1970

Abstract. Blue fluorescence has been observed from saturable absorbers excited by ruby laser light. The intensity dependence of this fluorescence showed that it was a result of excited-state absorption to the second singlet state. This intensity dependence also indicated the power density required to saturate the first excited singlet state for each dye. A similar fluorescence due to two photon absorption was observed in certain solvents.

1. Introduction

The use of an organic dye solution for the Q-switching of a laser depends on the intensity dependent reduction of the absorption coefficient of the dye at the laser frequency (Szabo and Stein 1965). In those dyes found suitable for Q-switching it is the transition from the ground state (0) to the first excited singlet state (1) which is responsible for this adsorption. The absorption coefficient is reduced when the laser intensity is such that the population of state (1) approaches that of state (0). There is, however, a residual absorption due to the transition from (1) to the second excited singlet state (2) (Guiliano and Hess 1967, Hercher *et al.* 1968). The subsequent spontaneous transition (2) to (0) results in the blue fluorescence (Gibbs 1967) studied in this experiment.

The equilibrium population of state (2) for the three-level system described, may be easily shown to follow the equation

$$N_2=I^2\sigma_1\sigma_2N\{I\sigma_2(3I\sigma_1+T_1^{-1}+T_{20}^{-1})+(2I\sigma_1+T_1^{-1})\,T_2^{-1}\}^{-1}$$

where σ_1, σ_2 are cross sections for transitions (0) $\rightarrow$(1) and (1) $\rightarrow$(2) respectively. T_1, T_2 are the total lifetimes of levels (1) and (2) respectively. T_{20} is the lifetime characterizing the transition (2) $\rightarrow$(0).

When I is very small

$$N_2=I^2\sigma_1\sigma_2T_1T_2N$$

thus the response is square law.

When I is very large

$$N_2=\tfrac{1}{3}N$$

and there are equal populations of the three states.

Now the lifetime of state (2) for the dyes used was about 10^{-13} s (Kasha 1950 and Gibbs 1967) whilst that of state (1) is greater than or approximately equal to 10^{-10} s (Gires 1966 and Selden 1967).

Also the low excited-state absorption of these dyes indicates $\sigma_2\ll\sigma_1$ (Gibbs 1967, Guiliano and Hess 1967). Thus the transition (0) $\rightarrow$(1) saturates at a very much lower power than (1) $\rightarrow$(2) and

$$N_2=I^2\sigma_1\sigma_2N(3I^2\sigma_1\sigma_2+2I\sigma_1T_2^{-1}+T_1^{-1}T_2^{-1})^{-1}.$$

Now for $I\sigma_2\ll T_2^{-1}$ i.e., for powers insufficient to saturate the transition (1) $\rightarrow$(2).

$$N_2=\frac{I^2\sigma_1\sigma_2N}{(2I\sigma_1+T_1^{-1})\,T_2^{-1}}.$$

Let $\sigma_1^{-1}T_1^{-1}=I_c$ then

$$N_2=\sigma_2 N T_2 I_c \frac{I^2/I_c^2}{1+2I/I_c}.$$

Since the number of fluorescent transitions (2) $\rightarrow$(0) is proportional to N_2

$$\text{fluorescence} \propto \frac{I^2/I_c^2}{1+2I/I_c}.$$

2. Experimental details

A Q-switched ruby laser with an output of up to 200 MW and a pulse duration of about 15 nanoseconds was used to excite a dye solution. This solution was contained in a short cell which was misaligned with respect to the ruby beam. The light intensity incident on this cell was controlled by varying the concentration of a solution of copper sulphate placed in the path of the ruby laser light. This intensity was monitored using a calibrated beam splitter and photodiode connected to a Tektronix 454 oscilloscope. The blue fluorescence was detected by a Mullard 56 AVP photomultiplier connected to the same oscilloscope via a delay line. Scattered ruby laser light and red fluoresence was eliminated by use of Jena BG 18 green filters. Noise due to the flashlight from the ruby cavity was minimized by use of a Wratten 29 filter placed after the copper sulphate attenuator. Two-photon absorption (Garrett and Kaiser 1961, Bloembergen 1967) in this filter caused a small amount of blue fluorescence. This gave a negligible signal on the photomultiplier providing the distance of the dye cell from the filter was sufficiently long.

It was necessary to use dilute dye solutions contained in a narrow cell in order to minimize intensity variations due to absorption of the ruby beam. The thin misaligned cell also eliminated the possibility of stimulated non-linear effects (Bloembergen 1967, Minck *et al.* 1966).

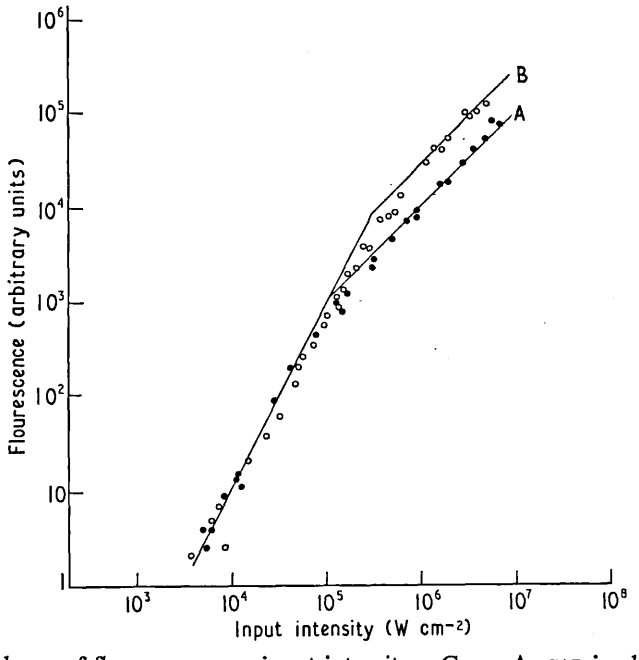

Figure 1. Dependence of fluorescence on input intensity. Curve A, CAP in chloronaphthalene; curve B, CAP in methanol. (In each figure I_c is the value of input intensity at the intersection of the theoretical lines representing fluorescence $\propto I^2$ and fluorescence $\propto I$.)

3. Results

The intensity of the blue fluorescence was measured as a function of the incident intensity, for the dyes chloroaluminiumphthalocyanine (CAP) (Gibbs 1967), cryptocyanine and vanadium–phthalocyanine (VnOPc).

Curves A and B of figure 1 show the dependence of fluorescence on incident intensity for solutions of CAP in chloronaphthalene and in methanol respectively.

At low inputs the fluorescence of both solutions follows the expected square law dependence on input intensity. With an increase of intensity this dependence changes and tends

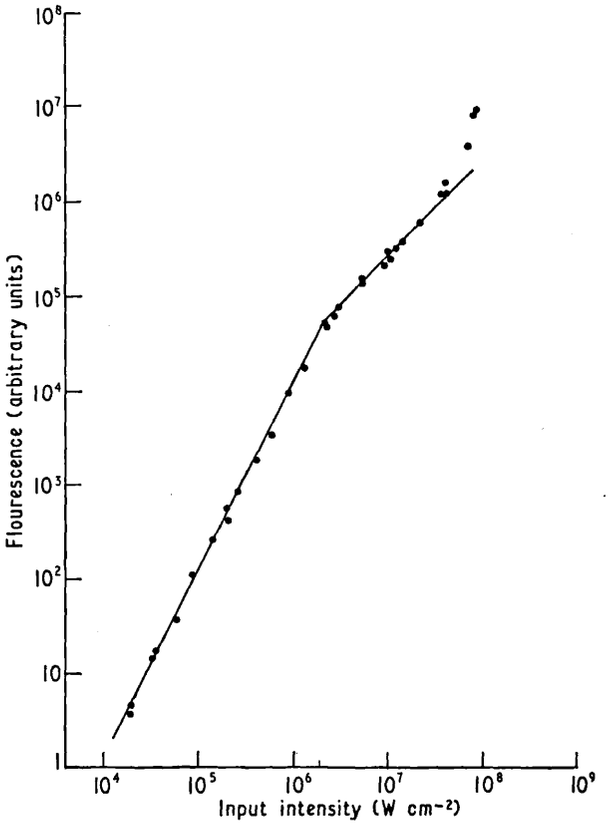

Figure 2. Dependence of fluorescence on input intensity for cryptocyanine in methanol.

towards a linear law as predicted by the theoretical law. (The non-linear breakdown of this law at still higher powers is attributed to chemical decomposition of the solution.) This corresponds to saturation of the first excited singlet state of the dye. The characteristic intensity I_c at which this occurs is about 10^5 W cm^{-2} in the case of the chloronaphthalene solution and about 3×10^5 W cm^{-2} for the methanol solution. The different powers I_c, for the two solutions are due to the different positions of the peaks of their absorption spectra. The peak of the spectrum of the solution in chloronaphthalene is much closer to the ruby wavelength (6943 Å) than that of the solution in methanol. Consequently the absorption cross section σ_1 is much greater and I_c much smaller in this case.

The dependence of fluorescence on input intensity for a solution of cryptocyanine in methanol (figure 2) has the same features as that for CAP in chloronaphthalene. However, although the absorption cross section for cryptocyanine in methanol ($\sigma_1 = 8{\cdot}1 \times 10^{-16}$ cm^2) is greater than that for CAP in chloronaphthalene ($\sigma_1 = 3 \times 10^{-16}$ cm^2) (Gires 1966, Selden 1967), I_c is greater for the cryptocyanine solution by over an order of magnitude

($I_c \sim 2{\cdot}5 \times 10^6$ W cm^{-2}). This is a result of the very much shorter lifetimes of the first excited state of cryptocyanine ($T_1 \sim 10^{-10}$ s). For CAP, $T_1 \sim 5 \times 10^{-9}$ s (Gires 1966, Selden 1967).

Thus theoretically

$$\frac{I_c(\text{cryptocyanine})}{I_c(\text{CAP})} \sim 25.$$

This is confirmed experimentally.

The dependence of fluorescence on input intensity for the VnOPc in nitrobenzene (figure 3) is similar to that of the other solutions. In this case saturation occurs at about $2{\cdot}5 \times 10^5$ W cm^{-2} as expected from the values $\sigma_1 = 4{\cdot}1 \times 10^{-16}$ cm^2 and $T_1 \sim 2 \times 10^{-9}$ s (Gires 1966). These values of I_c confirm the results obtained by other workers using transmission and single-photon fluorescence measurements (Armstrong 1965, Gires 1966 and Giuliano and Hess 1967).

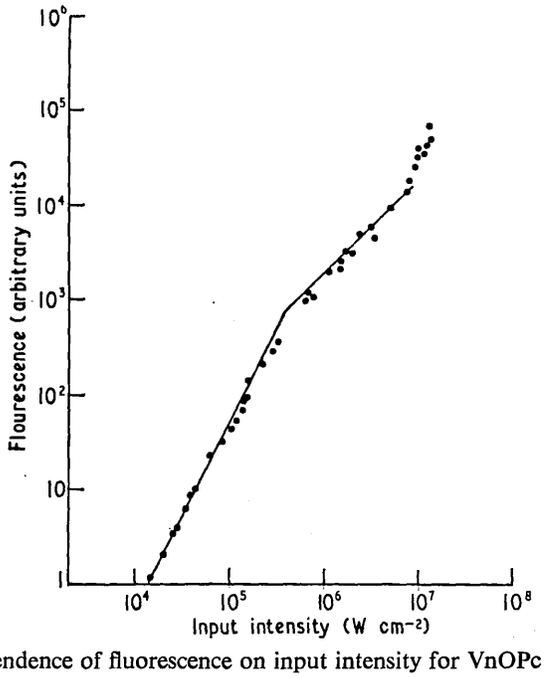

Figure 3. Dependence of fluorescence on input intensity for VnOPc in nitrobenzene.

The spectrum of the blue fluorescence was in all cases a fairly broad band (width about 800 Å). The peak of this emission was at about 4000 Å for CAP (Gibbs 1967) and at a somewhat longer wavelength about 4700 Å in the case of cryptocyanine. The true spectrum for VnOPc could not be determined because of absorption of wavelengths less than 4400 Å by the nitrobenzene solvent.

A small amount of blue fluorescence was observed from the solvents chloronaphthalene and nitrobenzene. This followed a square-law dependence on input power. These solvents have no absorption at the ruby frequency, but have a considerable absorption at twice this frequency. We therefore attribute this fluorescence to two-photon absorption (Giordmaine and Howe 1963). At very high intensities chemical breakdown of the solvents occurred. This was accompanied by a marked increase in fluorescence as seen on the graphs. A change in the fluorescence mechanism at these intensities was also suggested by the marked increase of the relaxation time of the fluorescence. This reached about 50 ns whereas at low intensities it was considerably shorter than the laser pulse duration (~15 ns).

References

ARMSTRONG, J. A. 1965, *J. appl. Phys.*, **36**, 471–3.
BLOEMBERGEN, N., 1967, *Am. J. Phys.*, **35**, 989–1023.
GARRETT, G. B. C., and KAISER, W., 1961, *Phys. Rev. Lett.*, **7**, 229.
GIBBS, W. E. K., 1967, *Appl. Phys. Lett.*, **11**, 113–5.
GIORDMAINE, J. A., and HOWE, J. A., 1963, *Phys. Rev. Lett.*, **11**, 207–9.
GIRES, F., 1966, *IEEE J. quantum Electron.*, **QE-2**, 624–6.
GIULIANO, C. R., and HESS, L. D., 1967, *IEEE J. Quantum Electron.*, **QE-3**, 358–67.
HERCHER, M., CHU, W., and STOCKMAN, D. L., 1968, *IEEE J. Quantum Electron.*, **QE-4**, 954–68.
KASHA, M., 1950, *Disc. Faraday Soc.*, **9**, 14.
MINCK, R. W., TERHUNE, R. W., and WANG, C. C., 1966, *Appl. Optics*, **5**, 1595–612.
SELDEN, A. C., 1967, *Br. J. appl. Phys.*, **18**, 743–8.
SPAETH, M. L., and SOOY, W. R., 1968, *J. Chem. Phys.*, **48**, 2315–23.
SZABO, A., and STEIN, R. A., 1965, *J. appl. Phys.*, **36**, 1562–6.

(*Reprinted from Nature, Vol. 216, No. 5112, pp. 257–258, October 21, 1967*)

Interaction of Self-trapped Light Beams

PRELIMINARY experiments have been carried out on the interaction of two self-trapped light beams in water. The 200 MW, 20 nsec output from a Q-switched ruby laser* was split by prisms and focused into a glass cell containing water to form two self-trapped beams (Fig. 1). Photographs were taken using the light scattered sideways from these beams.

Two types of scattering from self-trapped beams were observed; type A occurred when high purity water was used; type B was only produced in water which had been allowed to stand in an uncovered cell. When type A scattering was observed, the beams were characterized by fineness, short length, sharp cut-off and a tendency to scatter from a large number of discrete centres along the beam (Fig. 2). When type B scattering was observed, the beams were much longer than those associated with type A and the scattered light was much more diffuse, so that it was not always clear whether self-trapping had occurred (Fig. 3).

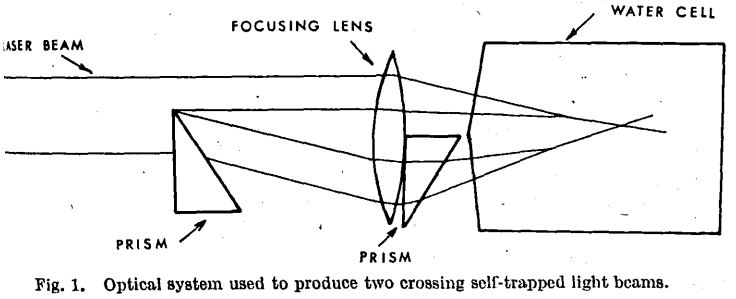

Fig. 1. Optical system used to produce two crossing self-trapped light beams.

* Ruby laser Bradley type *LH* 351, delivering 200 MW in 20 nsec distributed among a number of transverse modes (between 1 and 8). Beam divergence, 8 milliradians.

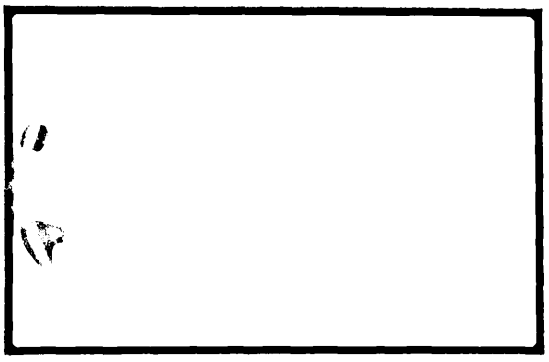

Fig. 2. Interaction of two crossing "type A" self-trapped beams. (×1.)

The apparatus used introduced distortion into the lower focused beam. The higher and lower edges of this beam were more intense than the centre, particularly the lower edge where self-trapping appeared to occur before the focal point was reached. Beyond the focal point two self-trapped beams were observed. The stronger beam travelled straight out from the end of the cone while the weaker appeared to be a continuation of the self-trapped lower edge of the cone. The weaker beam, after splitting from the stronger at the focus, bent and continued parallel with it.

Using the optical system shown in Fig. 1, the interaction of the two crossing light beams was observed. In the case of type A scattering, interaction was shown as an intense spot at the cross-over point (Fig. 2), but no significant effect on the beams could be observed because their scattering was not uniform. In the case of type B scattering, however, a considerable reduction in the intensity of the

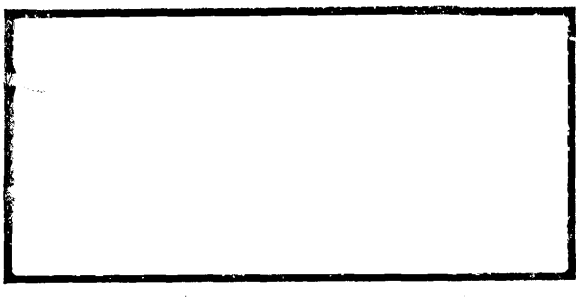

Fig. 3. Interaction of two crossing "type B" self-trapped beams. (×1.)

upper beam was always observed (Fig. 3). It is possible that this upper beam was not self-trapped, in which case interaction was between a high intensity light beam and self-trapped light. A considerable amount of energy was lost by the upper beam. This could have been reflected into the liquid or back along the pipe by the reflexion coefficient of the cross-over point, or could have been converted into shock energy. Whatever the mechanism, it is notable that the loss occurred only from the upper beam.

V. I. Little
P. Y. Key
R. G. Harrison

Department of Physics,
Royal Holloway College,
University of London.

Received June 12, 1967.

Printed in Great Britain by Fisher, Knight & Co., Ltd., St. Albans.

Reprinted from

Volume 13, Number 8 APPLIED PHYSICS LETTERS 15 October 1968

BRAGG REFLECTION OF LASER LIGHT FROM A PHASE GRATING IN A Q-SWITCHING LIQUID

R. G. Harrison, P. Key, V. I. Little, and *G. Magyar*
Royal Holloway College, Englefield Green, Surrey, England

J. Katzenstein
U.K.A.E.A. Culham Laboratories, Abingdon, Berkshire, England
(Received 9 August 1968)

It is postulated that in a saturable dye absorber used for giant pulse laser switching a phase grating is formed. To prove this experimentally a frequency doubled part of the laser beam was reflected from this "Lippman plate" at the Bragg angle.

In the last few years many experimental and theoretical papers have been published on the phenomenon of laser Q-switching by saturable absorbers. Its principal features, like the relatively low power needed for saturation, mode-locking, etc., have been explained in terms of "spectral hole burning," i.e., the saturation of only a portion of the homogeneously broadened absorption line (see, e.g., Schwartz and Tan[1]). In this letter we propose an alternative explanation based upon the idea of a phase grating in the liquid, what we have called the Lippman plate mechanism[2] or what can also be described as spatial hole burning in the dye that forms the saturable absorber. Experimental evidence is cited to support this hypothesis: we report the first observation of Bragg reflected light from a phase grating created by the laser light in a Q-switching liquid.

The Lippman plate mechanism may be described as follows. The phenomenon of saturable absorption must be accompanied by an intensity-dependent variation of refractive index since these effects arise from the imaginary and real terms respectively of the nonlinear susceptibility.[3] If laser action commences in a single cavity mode, the resulting standing wave produces a periodic distribution of high and low electric fields, with a corresponding periodicity in the refractive index. The spatial period is half the wavelength of the mode. The situation can be described in the Mathieu–Hill equation:

$$\frac{d^2u}{dz^2} + \frac{\omega^2}{c^2}(n^2 - 2\delta n^2 \cos 2kz)u = 0 ,$$

where δn represents the intensity-dependent part of the refractive index and the cosine term stands for its spatial modulation. A medium with a periodically varying refractive index, a so-called Lippman plate, has a strong selective reflectivity for light of the same periodicity. Starting from the above equation, the reflectivity has been computed for various numbers of layers and depths of modulation.[4] It can be shown[5] that in a typical dye cell, for a few percent reflectivity the variation of refractive index required is $\delta n \sim 10^{-5}$. This value can be realized by the postulated nonlinear mechanism. Also, during the giant pulse there can be sufficient thermal energy deposited in the liquid to produce a similar variation of the refractive index.[5] The formation of such a Lippman plate effectively removes the absorption of the dye cell for those modes of the cavity whose periodicity closely matches that of the spatially varying refractive index. Thus, provided there is no mode-selective element present and the cell is sufficiently short in comparison with the total length of the resonator, this spatial hole burning facilitates mode-locking of the laser. The spatially selective bleaching also explains the relatively low power required for saturation.

The experimental arrangement is shown schematically in Fig. 1. The ruby laser was Q-switched using cryptocyanine in isopropyl alcohol. The Q-switch cell was in the shape of a regular hexagon having one inch square sides of Spectrosil-B glass, flat to $\lambda/10$. The fundamental light (typical power 30 MW) was frequency doubled with an efficiency of 3% in an ADP crystal, delayed around an adjustable optical path, and passed again through the cell at approximely 60° to the cavity radiation. The unique angle for Bragg reflection in this case is given by $2d \cos\theta = \lambda$, where $2d$ is the fundamental wavelength and λ is the second harmonic wavelength in the liquid. After adequate filtering of the red light, the transmitted and reflected frequency doubled beams were photographed using two cameras focused on infinity. The pulse shape and the spectral

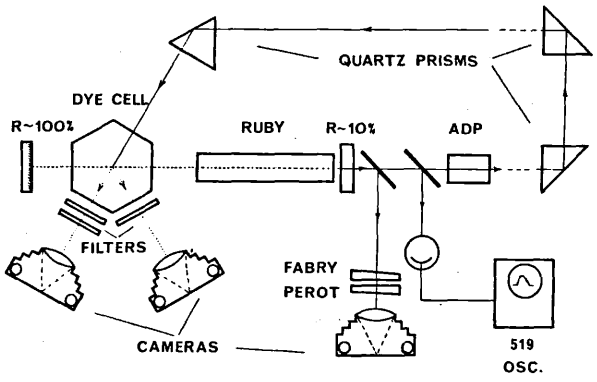

Fig. 1. Experimental arrangement for the observation of the Bragg-reflected second harmonic beam from the "Lippman plate" in a Q-switching dye.

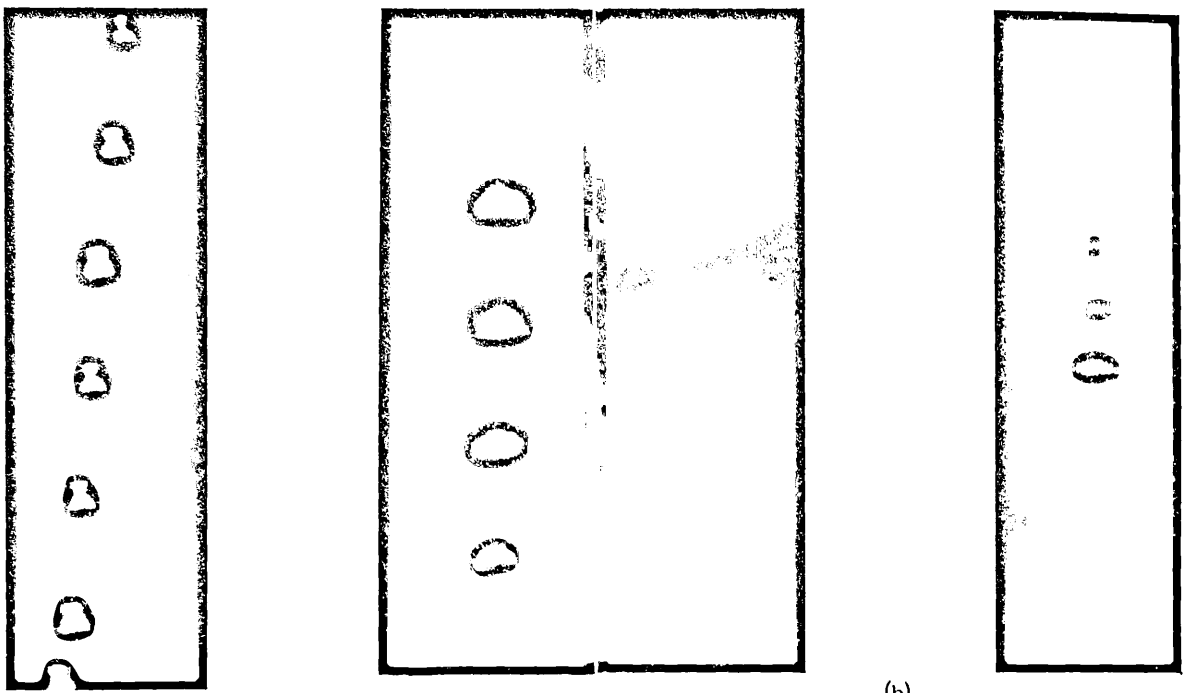

(a) (b)

Fig. 2. (a) Comparison of the transmitted and reflected beams. Exposures represent 6′ angular intervals. Transmitted beam is attenuated by ~ 200. Beam divergence: ~ 5 mrad. (b) Same with beam divergence reduced to ~ 2 mrad. Angular intervals of 2′.

composition were separately monitored.

Typical results are shown in Fig. 2. Figure 2(a) represents successive exposures of the transmitted and reflected beams taken at angular intervals of 6′, covering the angle for Bragg reflection. The transmitted light (left) is attenuated two-hundred-fold. The reflected light exhibits a critical dependence on angle of incidence, the intensity falling to half-value for a deviation of ±10′. Figure 2(a) corresponds to an incident beam divergence of 5 mrad, and about 1% of the beam is reflected. The amount of light reflected will be related to a number of factors, e.g., the amplitude of the induced periodic structure, filamentary processes, beam divergence, etc. Figure 2(b) shows the effect of restricting the incident beam by means of stops in the central portion to a divergence of 2 mrad. The exposures now represent increments of 2′ in the angle of incidence. 3% of the light is now reflected, and the intensity falls to half-value at ± 4′.

To eliminate the possibility that the phenomenon results from a spurious reflection, the ADP crystal was removed, and a photograph was taken under identical conditions but without the ultraviolet filter. The resulting plate showed a diffuse fogging due to scattered light, but no evidence of a well-defined reflected beam.

The effect of introducing delays of up to 30 nsec into the probing beam was also investigated. It was found that the relative intensity of the reflected light was not diminished, even for maximum delay (for which the overlap of the probing pulse and the fundamental pulse was less than 20%). The implication of this result was that the processes governing the decay of the ordered structure in the liquid were probably thermal. There was also an indication that the reflected intensity had a maximum for a delay time of 15 nsec. This could be explained by an integration of the thermal contribution to the amplitude of the structures in the liquid during the giant pulse.

Analysis of the spectral composition of the light showed that Bragg reflection took place for power levels well below the threshold for the stimulated Brillouin effect, as well as above it. We conclude from this that an ordered structure analogous to a Lippman plate was formed in the liquid in the Q-switching cell of the giant pulse laser.

This technique should prove valuable in the measurement of relaxation times and associated phenomena in liquids. Further experiments are in progress involving longer delay times and differing liquid temperatures. A further experiment is planned in which the dye cell will be probed continuously with a beam from a high power gas laser, the Bragg reflection being detected photoelectrically. Such an experiment would give more detailed information of the evolution of the processes taking place.

Three of us, Little, Harrison, and Key, wish to acknowledge the assistance of the Science Research Council in financing this experiment.

[1]S. E. Schwartz and T. Y. Tan, Appl. Phys. Letters 10, 4 (1967).
[2]G. Lippman, Compt. Rend. 112, 274 (1891).
[3]N. Bloembergen, Am. J. Phys. 35, 989 (1967).
[4]M. Iwata, R. Makabe, and S. Katsube, Japan. J. Appl. Phys., Suppl. 1, 4, 347 (1965).
[5]J. Katzenstein, G. Magyar, and A. C. Selden, Opt. Electron. (to be published).

CLM-P224

United Kingdom Atomic Energy Authority

RESEARCH GROUP

Preprint

BRAGG REFLECTION FROM A PHASE GRATING INDUCED BY NON-LINEAR OPTICAL EFFECTS IN LIQUIDS

P. Y. KEY
R. G. HARRISON
V. I. LITTLE
J. KATZENSTEIN

Culham Laboratory
Abingdon Berkshire

1969

CLM - P 224

BRAGG REFLECTION FROM A PHASE GRATING INDUCED BY NON-LINEAR OPTICAL EFFECTS IN LIQUIDS

by

P.Y. KEY*
R.G. HARRISON*
V.I. LITTLE*
J. KATZENSTEIN

(To be submitted for publication in IEEE Journal of Quantum Electronics)

ABSTRACT

Bragg reflection of light from a phase grating has been used as a technique for the investigation of non-linear optical phenomena. A continuous argon ion laser was used to probe the structure induced in a liquid by the non-linear interaction of a high intensity ruby laser beam with that liquid. This arrangement had the advantage of allowing direct space and time resolved measurements of the induced effects.

*Royal Holloway College (London University), Egham, Surrey, England.

U.K.A.E.A. Research Group,
Culham Laboratory,
Abingdon,
Berks.

October, 1969 (MEJ)

C O N T E N T S

1. INTRODUCTION

The strong electric field of the light output of a ruby laser affects the refractive index of a medium through which it passes in a number of ways. The most significant of these are:-

1. Electrostriction
2. Kerr effect
3. Thermal effects - in absorbing media.

When the light is reflected back along its own path, large oscillating fields exist at the antinodes of the resulting standing wave. As the above effects are dependent on the square of the field a spatially periodic variation of refractive index is set up proportional to the mean square of the local field (Fig.1). If the frequency of the back-reflected light is slightly shifted, the nodes and antinodes will propagate through the medium. The distortion associated with each of the above effects also has a characteristic velocity of propagation. (Electrostriction gives acoustic phonons - the Kerr effect gives optical phonons - the thermal fluctuations decay but do not propagate.) When the velocity of propagation of the nodes of the field matches that of the distortion of the medium, the effect on the medium has a resonant maximum. (It is this situation which, at sufficiently high laser powers, can give rise to the stimulated scattering associated with each of the interactions, i.e. electrostriction gives stimulated Brillouin scattering[1,2], the Kerr effect gives stimulated Rayleigh Wing[3,4] and stimulated Raman scattering[5], the thermal effect gives stimulated thermal Rayleigh scattering[6,7]). Thus by choosing the appropriate feedback frequency we can select the form of interaction we wish to investigate.

The refractive index variation set up in this way, by the ruby laser light, acts as a phase grating[8,9,10] upon a probing argon laser beam traversing the medium. Each layer of high and low index reflects a small portion of the incident argon light. When these portions add in phase, a maximum overall reflectivity is reached. The condition for this is the Bragg condition:

$$\theta_o = \cos^{-1} \frac{\lambda_a}{\lambda_r} \cdot \frac{n_r}{n_a} = 45{\cdot}5^o$$

where θ_o is the angle between the two beams, and suffices a and r refer to the argon and ruby wavelengths respectively. At this angle, providing the reflectivity is small

$$\text{reflectivity} = \left(\frac{\pi N \delta}{2\cos^2\theta} \right)^2 \qquad \text{(see Appendix)}$$

where N = number of modulations crossed

$\delta = \frac{\Delta n_a}{2n_{ao}}$

Δn_a = difference between maximum and minimum refractive index (for argon light) induced by the standing wave.

n_{ao} = refractive index of the undisturbed medium for argon light.

When $\Delta n \sim 2 \times 10^{-6}$ and length of interaction region $\sim$ 1 cm

reflectivity $\sim$ 1%.

The angular width at half reflectivity is

$$\frac{4 \times 1{\cdot}39}{\pi N \tan\theta_o} \qquad \text{(see Appendix)}$$

For 1 cm interaction length

$$\text{angular width} \sim 5 \times 10^{-5} \text{ radians} \sim 10 \text{ seconds.}$$

2. EXPERIMENTAL

Fig.2 shows the experimental arrangement. Single longitudinal mode output of the ruby laser was achieved by the use of two narrow dye cells for Q-switching and a resonant reflector as the output mirror. An aperture was used to cut down the divergence of the beam, and power densities of up to 100 MW/cm^2 were transmitted. The pulse duration was of the order of 15 nsec.

The argon laser gave 1 W output at 4880 Å with a beam divergence of 1 mrad. Accurate adjustment of the Bragg angle between the argon light and ruby induced structure was achieved by sensitive control of mirror M_1. A Fabry-Perot interferometer was used to check the single mode output of the ruby laser and to measure the frequency shift of the backward-going beam. These beams were distinguished by the use of the $\lambda/4$ plate and polaroid quadrant[7], as shown in the diagram. The reflected beam could either be shifted or unshifted in frequency. An unshifted frequency was obtained simply by the use of a mirror normal to the ruby beam. A shifted frequency was generated by stimulated back-scattering of light focussed into cell (2), as shown in the diagram. The frequency shift was determined by the liquid contained in cell (2).

An advantage of this set up was that the detectors D_1, D_2 measured the incident ruby beam in each direction while P and D_3 simultaneously measured the amplitude of the refractive index modulation in the cell and the amplification which it caused in the backward beam. This was achieved by the use of cable delay lines allowing simultaneous display of four pulses on a single trace of a Tectronix 454 oscilloscope.

The intensities of the beams were controlled (and feed-back into the laser minimised) by the use of $CuSO_4$ attenuators. The Bragg angle of $45{\cdot}5^{o}$ between the ruby and argon laser beams permits the very simple geometry of cell (1) and normal incidence of the argon beam as shown. Spatial resolution could be directly achieved by longitudinal movement of the cell along the ruby beam.

3. RESULTS

The experimental investigations were carried out mainly in absorbing media using unshifted frequency feedback. The thermal effect was therefore dominant.

(a) Angular Dependence

Using a solution of copper acetate in methanol with absorption coefficient $\alpha = 0{\cdot}15\ cm^{-1}$ the angle giving maximum Bragg reflection was measured to be $45{\cdot}5 \pm 0{\cdot}1^{o}$, and was equal to the theoretical value given by $\cos^{-1} \frac{\lambda_a}{\lambda_r} \cdot \frac{n_r}{n_a}$. While the angle could only be measured absolutely to $\pm\ 0{\cdot}1^{o}$, small incremental adjustments could be made much more accurately[11]. The angular width at half reflectivity was found to be ~ 5 minutes corresponding to the divergence of the argon laser beam.

(b) Magnitude of Reflectivity

The refractive index modulation due to thermal effects is given by[12]

$$\Delta n = \gamma \frac{p}{2\ell\chi(n_r k_r)^2} \left(\frac{\partial n}{\partial T} \right)$$

where γ is a numerical factor such that $0{\cdot}5 < \gamma < 1$ and P is the power per unit area absorbed in the medium of length ℓ and thermal conductivity χ.

Hence with the same solution as in (a), with an intensity of 23 MW/cm^2 and $\ell \sim 4$ cm

$$\Delta n \sim 4 \times 10^{-6}$$

Now reflectivity $= \left(\frac{\pi N \delta}{2 \cos^2 \theta} \right)^2 \sim 4\%$ for argon light incident at the Bragg angle. However, the theoretical angular width at half reflectivity of the Bragg is of the order of 10 seconds for a non-divergent beam (see Introduction), whereas the divergence of the argon laser beam was about 5'. Hence only about 3% of the argon beam was available for reflection, and thus resultant reflectivity ~ 0·1%. This estimate was experimentally confirmed.

(c) Dependence of Reflectivity on Ruby Laser Power

The change in refractive index at any point is proportional to the mean square of the local field. Let $\underline{E_1}$ and $\underline{E_2}$ be the electric vectors of the forward- and backward- going beams respectively.

Now

$$E_1 = A_1 \sin(kz-\omega t)$$

$$E_2 = A_2 \sin(-kz-\omega t).$$

The local field $E = E_1 + E_2$

$$= A_1 \sin(kz-\omega t) + A_2 \sin(-kz-\omega t)$$

$$\bar{E}^2 = \tfrac{1}{2}A_1^2 + \tfrac{1}{2}A_2^2 + \frac{A_1 A_2}{2} \cos 2kz$$

therefore the difference between maxima and minima of the mean square of the local field $= A_1 A_2$.

Hence the difference between the maxima and minima of the refractive index $\delta n \propto A_1 A_2$.

Now reflectivity of grating $\propto (\delta n)^2$ (see Introduction)

$\propto I_1 I_2$ where I_1, I_2 are the intensities of the forward- and backward- going beams respectively. Fig.3

shows the dependence of reflectivity of a solution of copper acetate in methanol ($\alpha = 0{\cdot}15\ cm^{-1}$) on I_1 when $I_2 = 0{\cdot}33\ I_1$. In this case reflectivity $\propto I_1^2$ as is confirmed by the graph. We ascribe the errors mainly to variation of the divergence of the ruby light due to lack of transverse mode control.

Fig.4 shows that the reflectivity is proportional to I_2 when I_1 is kept constant. These two results confirm the theoretical relationship.

Further power dependence investigations were made in the case of a saturable absorber (cryptocynanine in methanol). As was expected, the I_1^2 dependence breaks down at about 10 MW/cm^2 owing to the bleaching of the dye[13,14,15] (Fig.5).

(d) Dependence of Reflected Power on Incident Argon Laser Power

To ensure that the argon light was acting solely as a probe and not contributing significantly to the non-linear effects, the dependence of reflected power on the incident argon power was investigated. For solutions not absorbing at the argon wavelength, e.g. copper acetate in methanol, the expected linear dependence was observed (Fig.6). However, for solutions having even a slight absorption at the argon wavelength, e.g. nitrobenzene, thermal de-focusing[16] of the argon beam greatly reduced the Bragg reflection.

(e) Dependence of the Reflectivity on Concentration

The reflectivity of the grating was also investigated as a function of the absorption coefficient. As expected, different solutes in the same solvent gave equal reflectivities when the absorption coefficients of the solutions were equal.

The measurement of the reflection as a function of the absorption coefficient α was complicated by the fact that variation of α affects the values of E_1 and E_2. This can only be corrected for as long as the non-linear effect in the cell has a negligible effect on the ruby beam, a condition that requires a much shorter cell than that used in this experiment.

(f) Time Resolution

Each of the non-linear effects mentioned earlier has a characteristic relaxation time[17]. These have the following orders of magnitude:

Electrostriction - 10^{-9} to 10^{-10} sec

Kerr effect - 10^{-11} to 10^{-12} sec

Thermal effect - 10^{-7} to 10^{-8} sec.

The length of the ruby pulse (~ 15 nsec) and the resolution of the instruments (~ 7 nsec) only allowed investigation of the thermal relaxation.

Fig.7 shows the time profile of the ruby laser pulse and the resulting Bragg reflected pulse in the thermal and the electrostrictive cases. The relaxation time of the effect of electrostriction is very fast (compared with the pulse profile and instrument resolution). Hence the profile of this pulse provides a measure of the resolution of the instruments, (7 nsec). The relaxation time of a thermal grating is calculated from the bulk properties of the medium by the formula[7]

$$\tau = \frac{c\rho}{\chi(2k_r n_r)^2}$$

where c = specific heat at constant pressure and ρ = density. This gives a value of 16·5 nsec for methanol. The points marked on Fig.7

are the theoretical points given this relaxation time and the resolution time of the instruments. There is good agreement for this value of relaxation time and significant misfit if it is varied by more than 2 nsec.

Similar agreement was obtained in the case of a number of other liquids.

This technique can be used more generally for investigation of any non-linear optical effect dependent on E^2. In particular short pulses and better detector resolution will allow direct measurement of the lifetimes of the phonons generated by the stimulated Brillouin effect.

REFERENCES

1. R.Y. Chiao., C.G. Townes and B.P. Stoicheff, "Stimulated Brillouin scattering and coherent generation of intense hypersonic waves", Phys. Rev. Letters, vol.12, pp.592-595, May 1964.

2. K. Grob, "On the theory of stimulated Brillouin scattering in liquids", Z. Physk, vol.201, pp.59-68, April 1967.

3. D.I. Marsh, V.V. Morozov, V.S. Starinov and I.L. Fabelinskii, "Stimulated scattering of light of the Rayleigh Line Wing", JETP Letters, vol.2, pp.25-27, July 1965.

4. V.S. Starinov, "The theory of the stimulated Rayleigh Wing Scattering", Sov. Phys. Dokl., vol.13, pp.217-219, September 1968.

5. N. Bolembergen, "The stimulated Raman effect", Am. J. Phys, vol.35, pp.989-1023, November 1967.

6. R.M. Herman and M.A. Grey, "Theoretical predictions of the stimulated thermal Rayleigh scattering in liquids", Phys. Rev. Letters, vol.19, pp.824-828, October 1967.

7. D.H. Rank, C.W. Cho, N.D. Foltz and T.A. Wiggins "Stimulated thermal Rayleigh scattering", Phys. Rev. Letters, vol.19, pp.828-830, October 1967.

8. R.G. Harrison, P.Y. Key, V.I. Little, G. Magyer and J. Katzenstein, "Bragg reflection of laser light from a phase grating in a Q-switching liquid", Appl. Phys. Letters, vol.13, pp.253-255, October 15, 1968.

9. J. Walder and C.L. Tang, "Photoelastic amplification of light and generation of hypersound by the stimulated Brillouin process", Phys. Rev. Letters, vol.19, pp.623-626, Spetember 1967.

10. H. Boersch and H. Eichler, "Beugung an einen mit stehenden Lichtwellen gepumpten Rubin", Z. Angew. Phys. vol.22, pp.378-379, 1967.

11. P.Y. Key, R.G. Harrison, G. Hayward and V.I. Little, "A high precision spectrometer table", J. Sci. Instr., series 2, vol.2, pp.374-375, April 1969.

12. V.S. Letokhov and B.D. Pavlik "Theory of the resonant feedback laser", Sov. Phys. -Tech. Phys. vol.13, pp.251-259, August 1968.

13. F. Gires, "Experimental studies of saturable optical absorption", IEEE J. Quantum Electronics, vol.QE-2, pp.624-626, Spetember, 1966.

14. C.R. Guiliano and L.D. Hess, "Nonlinear absorption of light", IEEE J. Quantum Electronics, vol.QE-3, pp.358-367, August 1967.

15. R.G. Harrison, P.Y. Key and V.I. Little "Fluorescence due to excited state absorption in saturable absorbers", Brit. J. Appl. Phys., to be published.

16. S.A. Akhlmanov, D.P. Krindach, A.P. Sukhorukov and R.V. Khokhlov, "Nonlinear defocusing of laser beams", JETP Letters, vol.6, pp.38-42, July 1967.

17. M. Denariez and G. Bret, "Investigation of Rayleigh Wing and Brillouin stimulated scattering in liquids", Phys. Rev. vol.171, pp.160-171, July 1968.

APPENDIX

Let θ = angle of incidence at a refractive index boundary

θ' = angle of refraction at a refractive index boundary

A_i = amplitude of wave incident on boundary

δA_r = amplitude of wave reflected from boundary

δn = very small change of refractive index at boundary

then $$\frac{\delta A_r}{A_i} = \frac{-\sin(\theta-\theta')}{\sin(\theta+\theta')} \sim \frac{-\delta n}{2n_{ao}\cos^2\theta}$$ for parallel polarisation

in limit $\delta n \to 0$ $$\frac{1}{A_i} \cdot \frac{dA_r}{dn} = \frac{-1}{2n_{ao}\cos^2\theta}$$

Now let

n_{ao} = undisturbed refractive index for argon light

n_{ro} = undisturbed refractive index for ruby light

Δn_a = difference between max and min refractive index for argon light

λ_a = wavelength of argon light in vacuo

λ_r = wavelength of ruby light in vacuo

$$k_a = \frac{2\pi}{\lambda_a}$$

$$k_r = \frac{2\pi}{\lambda_r}$$

z = distance along ruby beam direction

then $$n_a = n_{ao} + \frac{\Delta n_a}{2} \sin 2k_r n_{ro} z$$

$$\frac{dn_a}{dz} = \frac{\Delta n_a}{2} \, 2k_r n_{ro} \cos(2k_r n_{ro} z)$$

$\therefore$ $$\frac{1}{A_i} \cdot \frac{dA_r}{dz} = \frac{-\Delta n_a \cdot k_r n_{ro} \cos(2k_r n_{ro} z)}{2n_{ao} \cdot \cos^2\theta} \cdot$$

Now light reflected from boundary at z has phase lag of $2n_{ao}k_a z\cos\theta$ at $z = 0$

$$\therefore \quad \frac{1}{A_i}\frac{dA_{ro}}{dz} = \frac{-\Delta n_a \cdot k_r n_{ro}}{2n_{ao}\cdot\cos^2\theta}\cdot\cos(2k_r n_{ro} z)\cdot e^{i2n_{ao}k_a z\cos\theta}$$

where A_{ro} is the amplitude at $z = 0$ of the wave reflected from a depth z of grating. Then total amplitude, A_R, of wave at $z = 0$ reflected from grating of depth L is given by

$$\frac{A_R}{A_I} = \int_0^L \frac{1}{A_i}\cdot\frac{A_{ro}}{dz}\cdot dz = \frac{-\Delta n_a k_r n_{ro}}{2\cos^2\theta\, n_{ao}}\int_0^L \cos(2k_r n_{ro} z)e^{i2n_{ao}k_a z\cos\theta}dz$$

assuming $A_i \sim \text{const} = A_r$ i.e. total reflectivity $\ll 1$ where L = total length of modulations probed.

Now let $\quad 2k_r n_{ro} = k$

$$2k_a n_{ao}\cos\theta = k'$$

$$\left(\frac{A_R}{A_I}\right) = \frac{-k\,\Delta n_a}{4\cos^2\theta n_{ao}}\int_0^L \cos kz\, e^{ik'z}dz$$

$$\left(\frac{A_R}{A_I}\right) = \frac{-k\Delta n_a}{8\cos^2\theta n_{ao}}\left[\frac{\sin(k'+k)L}{k'+k} + \frac{\sin(k'-k)L}{k'-k} + i\left[\frac{1-\cos(k'+k)L}{k'+k} + \frac{1-\cos(k'-k)L}{k'-k}\right]\right]$$

for $k' \sim k$ terms with $k'-k$ denominator $\gg$ terms with $k'+k$ denominator

$$\therefore \quad \left|\frac{A_R}{A_I}\right|^2 = \left(\frac{k\Delta_{na}}{8\cos^2\theta n_{ao}}\right)^2\left[\frac{\sin^2(k'-k)L+(1-\cos(k'-k)L)^2}{(k'-k)^2}\right]$$

$$= \left(\frac{k\,\Delta n_a\, L}{8\cos^2\theta n_{ao}}\right)^2\left[\frac{\sin\left(\frac{k'-k}{2}\right)L}{\left(\frac{k'-k}{2}\right)L}\right]^2$$

This has maximum when $k' = k$

i.e. when $\cos\theta = \frac{\lambda_a}{\lambda_r} \cdot \frac{n_{ro}}{n_{ao}}$

then $\frac{I_R}{I_I} = \left|\frac{A_R}{A_I}\right|^2 = \left(\frac{k \Delta n_a L}{8 \cos^2 \theta n_{ao}}\right)^2$

where I_R, I_I are the reflected and incident intensities

$$\boxed{\text{reflectivity} = \frac{I_R}{I_I} = \left(\frac{\pi N \delta}{2 \cos^2\theta}\right)^2}$$

where $N = \frac{2n_{ro}L}{\lambda r}$

$$\delta = \frac{\Delta n_a}{2n_{ao}}$$

At half reflectivity $\frac{\sin\left(\frac{k'-k}{2}\right)L}{\left(\frac{k'-k}{2}\right)L} = \frac{1}{\sqrt{2}}$

now $k'-k = 2k_a n_{ao} \cos\theta - 2k_r n_{ro}$

let $\theta = \theta_o + \delta\theta$ where $\theta_o = \cos^{-1}\frac{k_r n_{ro}}{k_a n_{ao}}$

$$k' - k = -\delta\theta \sqrt{k_a^2 n_{ao}^2 - k_r^2 n_{ro}^2}$$

$$\therefore \frac{\sin\left(\frac{\delta\theta}{2}\sqrt{k_a^2 n_{ao}^2 - k_r^2 n_{ro}^2} \cdot L\right)}{\frac{\delta\theta}{2}\sqrt{k_a^2 n_{ao}^2 - k_r^2 n_{ro}^2} \cdot L} = \frac{1}{\sqrt{2}}$$

$$\therefore \frac{\delta\theta}{2}\sqrt{k_a^2 n_{ao}^2 - k_r^2 n_{ro}^2} \cdot L = \pm 1{\cdot}39 \text{ radians}$$

$$\therefore \delta\theta = \pm \frac{2 \times 1{\cdot}39}{\pi N \sqrt{\left(\frac{k_a n_{ao}}{k_r n_{ro}}\right)^2 - 1}}$$

$$\therefore \boxed{\text{angular width at half reflectivity} = \frac{4 \times 1{\cdot}39}{\pi N \tan\theta_o}}$$

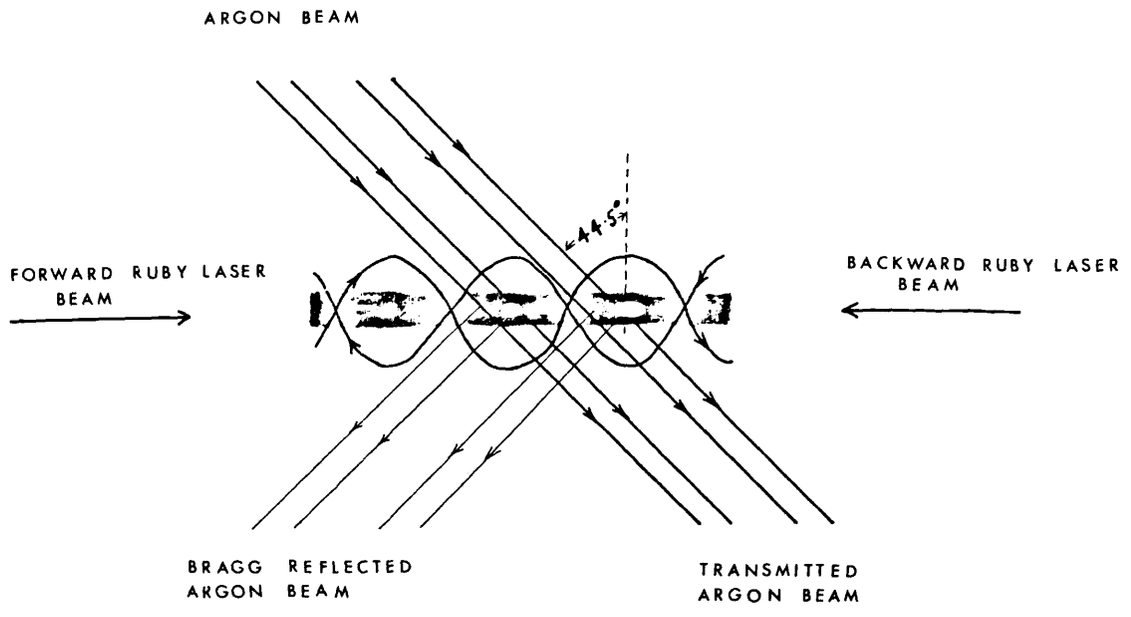

Fig.1 Illustrative diagram showing Bragg reflection of a continuous argon beam from a periodic structure induced in a liquid by the standing wave of a ruby laser beam.

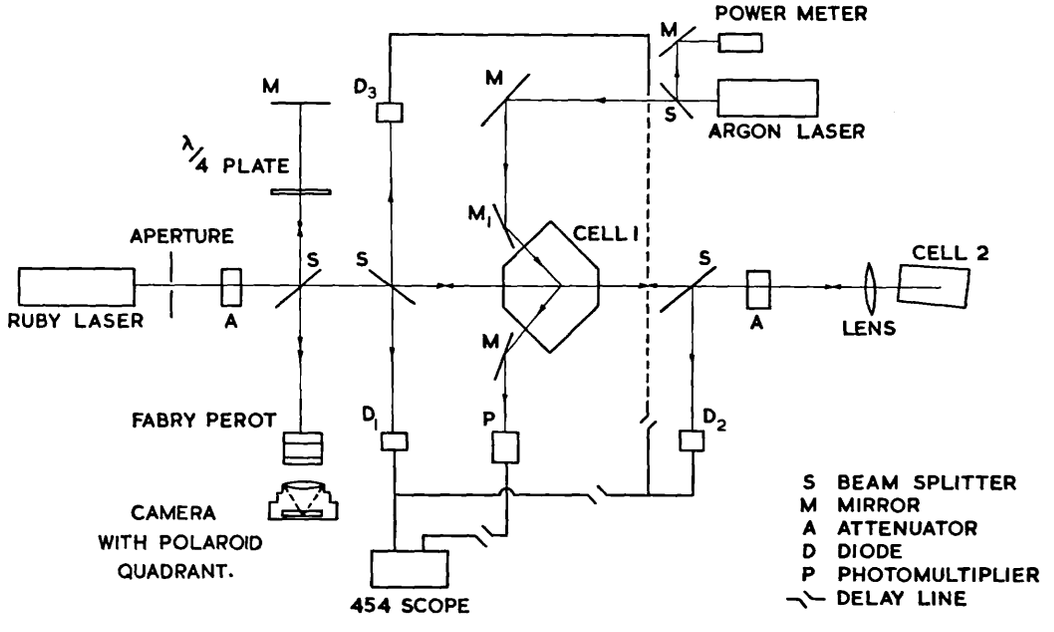

Fig.2 Experimental arrangement

CLM-P224

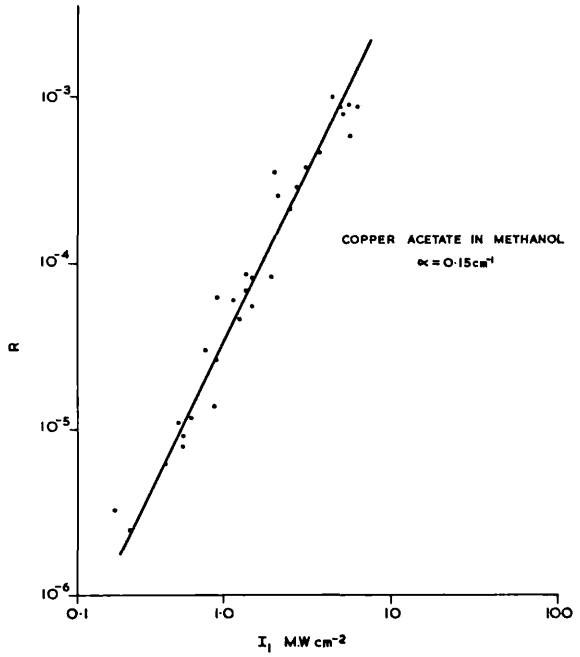

Fig.3
Reflectivity (R) of the phase grating as a function of the intensity (I_1) of the forward-going beam with $I_2 \propto I_1$. The line shows the theoretical square law.

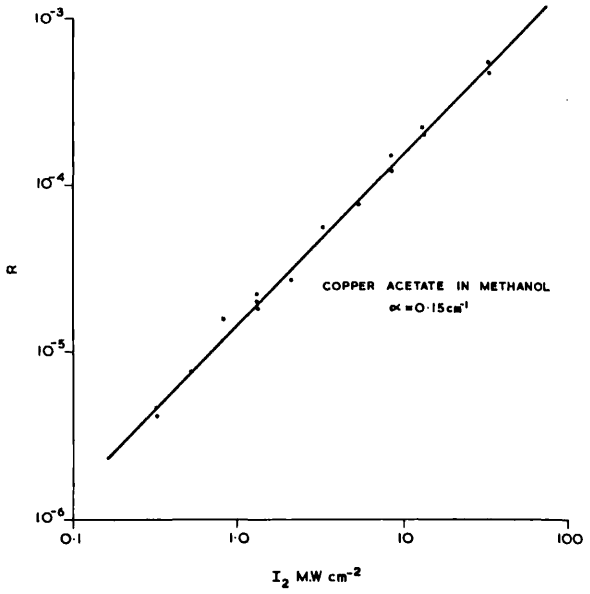

Fig.4
Reflectivity (R) of the phase grating as a function of the intensity (I_2) of the backward-going beam with I_1 constant at 71 MW cm^{-2}. The line shows the theoretical linear law.

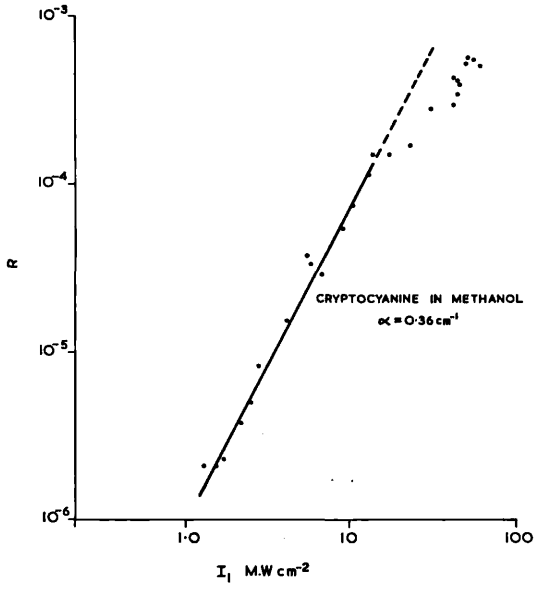

Fig.5
Reflectivity of phase grating as a function of I_1 for a saturable absorber.

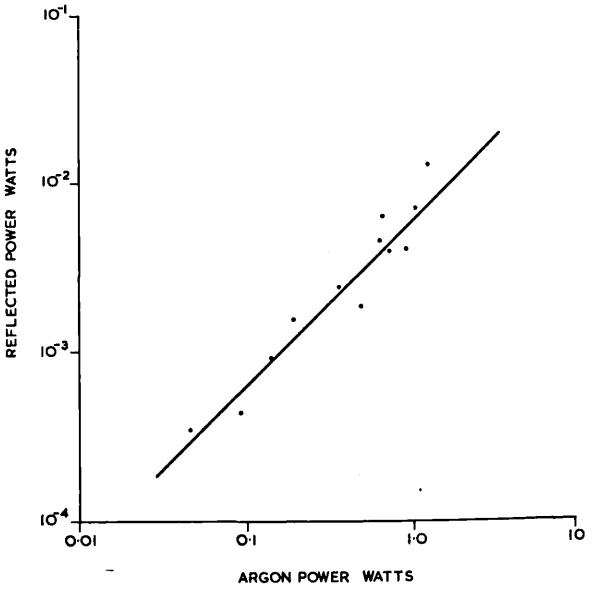

Fig.6
Reflected power as a function of incident argon laser power.

CLM-P224

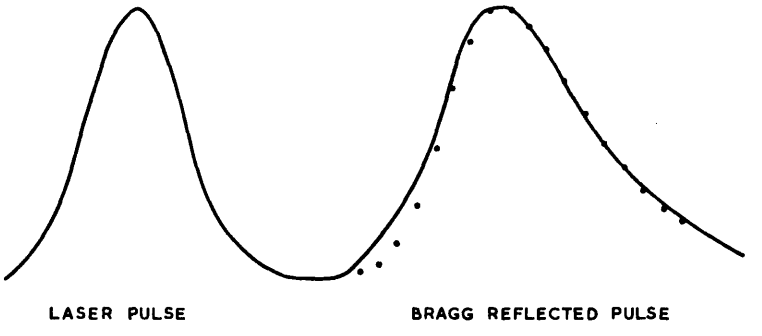

THERMAL

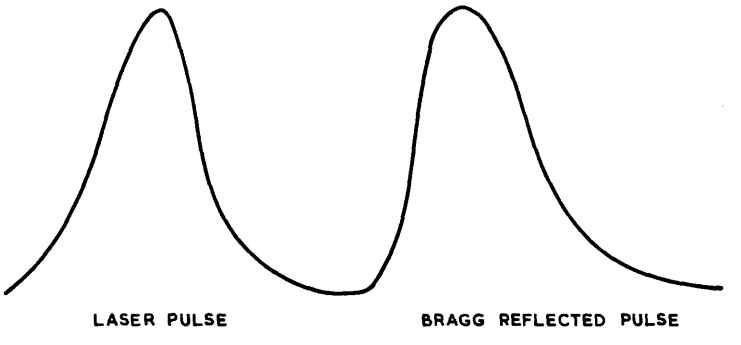

ELECTROSTRICTIVE

Fig.7 Time profile of the ruby laser pulse and the resulting Bragg reflected pulse in the thermal and electrostrictive cases. The points marked are those calculated given the theoretical relaxation time.

CLM-P224